UNIVERSIDADE FEDERAL DO RIO GRANDE
PÓS-GRADUAÇÃO EM OCEANOGRAFIA BIOLÓGICA

PROPRIEDADES ÓPTICAS DAS FLORAÇÕES DO FITOPLÂNCTON NA QUEBRA DE PLATAFORMA ARGENTINA

AMABILE FERREIRA

Tese apresentada ao Programa de Pós-graduação em Oceanografia Biológica da Fundação Universidade Federal do Rio Grande, como requisito parcial à obtenção do título de DOUTOR.

Orientador: Dr. Carlos Alberto Eiras Garcia
Co-Orientador: Dr. Dariusz Stramski

Rio Grande
Março/2013

Aos meus pais.

“Somewhere, something

incredible is waiting to be known.”

Carl Sagan

Agradecimentos

À FURG, por ter me acolhido por 7 anos e me formado mestre e doutora.

Ao Pato, por tudo proporcionado para meu doutorado, pela orientação e os momentos felizes.

Ao Grupo de Oceanografia de Altas Latitudes, por me acolher como integrante. Tenho muito orgulho de ter sido GOAL.

Ao CNPq, pela bolsa de doutorado por 3 anos.

À CAPES, pela bolsa sanduíche no exterior por 1 ano.

Ao SCRIPPS *Institution of Oceanography* e ao *Marine Physical Laboratory* por me receberem para o doutorado sanduíche.

Ao Dr. Dariusz Stramski, pela consideração e orientação.

À Marinha do Brasil, pelos embarques para coleta de dados e por ter me levado à Antártica.

À NASA, pela disponibilidade das imagens de satélite da cor do oceano e do programa SeaDAS para o processamento das mesmas.

À Profa. Virginia Maria Tavano, pela disponibilidade dos dados de pigmentos.

Aos coautores dos artigos: Dra. Ana Inês Dogliotti, Dra. Áurea Maria Ciotti, Dra. Virginia Maria Tavano, Dr. Carlos Rafael Borges Mendes, Dr. Márcio Silva de Souza.

À banca de avaliação: Dr. Milton Kampel, Dra. Clarisse Odebrecht, Dr. Maurício Magalhães Mata, Dra. Margareth Copertino, Dr. Márcio Silva de Souza.

Às grandes mentes da Bio-Óptica Marinha, por todo conhecimento gerado, pilar das nossas pesquisas atuais.

À Áurea, pela primeira vez que me disse que o fitoplâncton muda a cor dos oceanos e pelos ensinamentos e dedicação que se seguiram por 9 anos.

A todos os meus professores, gratidão eterna.

À Ella, Lolo, Tati e Caju pela amizade. À Caju também pela "amizade científica" e a Shezinha pela ajuda com os match-ups.

Aos companheiros de LEOC e FURG: Rodrigo, Fuji, Gabi, Ingrid, Ricardo, Piauí, Marina, Rafaiel, Cá, Amália, Márcio, Zé Luiz, Arnaldo, Paula, Rosane, Maurício, Ana, Jeane, Milton.

Aos meus pais, por tudo que fizeram pela minha educação e formação.

Ao Cesar, surpresa boa, meu amigo e amor.

À Nanda, luz da minha vida.

ÍNDICE

LISTA DE APÊNDICES

Apêndice 1: **Ferreira, A.,** Garcia, C. A. E., Dogliotti, A. I., e Tavano, V. M., Bio-optical characteristics of the Patagonian Shelf-break waters: Implications for ocean color algorithms. Artigo aceito para publicação no *Remote Sensing of Enviroment.*

Apêndice 2: **Ferreira, A.,** Stramski, D., Garcia, C. A. E., Ciotti, A. M., Tavano, V. M., e Mendes, C. R. B., Variability in light absorption and scattering of phytoplankton in Patagonian waters: Role of community size structure and pigment composition. Artigo publicado no *Journal of Geophysical Research.*

Apêndice 3: **Ferreira, A.,** Stramski D., Garcia, C. A. E., Mendes, C. R. B., Tavano, V. M., Bio-optical characteristics of the Patagonian Shelf-break waters: Discrimination of phytoplankton assemblages in Patagonian waters from their absorption spectra. Artigo em preparação para submissão.

LISTA DE SÍMBOLOS E ABREVIAÇÕES

$a(\lambda)$	coeficiente de absorção da luz, m^{-1}
$a_{det}(\lambda)$	coeficiente de absorção da luz pelos detritos, m^{-1}
$a_p(\lambda)$	coeficiente de absorção da luz pelo material particulado, m^{-1}
$a_{ph}(\lambda)$	coeficiente de absorção da luz pelo fitoplâncton, m^{-1}
$a^*_{ph}(\lambda)$	coeficiente específico de absorção da luz pelo fitoplâncton (ou seja, normalizado por Chl*a*), m^2 mg^{-1}
$a_{<ph>}(\lambda)$	$a_{ph}(\lambda)$ normalizado pelo valor médio de $a_{ph}(\lambda)$ entre 400 e 700 nm
$\int a_{ph}(\lambda)$	$a_{ph}(\lambda)$ normalizado pela soma de $a_{ph}(\lambda)$ entre 400 e 700 nm
Allo	pigmento aloxantina
AOPs	propriedades ópticas aparentes *(Apparent Optical Properties)*
APD	diferença percentual absoluta *(Absolute Percentage Difference)*
$b(\lambda)$	coeficiente de espalhamento da luz, m^{-1}
$b_b(\lambda)$	coeficiente de retro-espalhamento da luz, m^{-1}
$b_{bp}(\lambda)$	coeficiente de retro-espalhamento da luz pelas partículas, m^{-1}
$b^*_{bp}(\lambda)$	coeficiente específico de retro-espalhamento da luz pelas partículas (ou seja, normalizado por Chl*a*), m^2 mg^{-1}
$b^*_p(\lambda)$	coeficiente específico de espalhamento da luz pelo material particulado (ou seja, normalizado por Chl*a*), m^2 mg^{-1}
BMCF	profundidade da base do pico de fluorescência de clorofila-*a*
Buta	pigmento 19'-butanoiloxifucoxantina
$c(\lambda)$	coeficiente de atenuação da luz, m^{-1}
$c_p(\lambda)$	coeficiente de atenuação da luz pelas partículas, m^{-1}
Chl*a*	concentração de clorofila-*a*, mg m^{-3}
Chl*b*	clorofila-*b*

Chlc_1	clorofila-c_1
Chlc_3	clorofila-c_3
DPR	razão de pigmentos diagnósticos *(Diagnostic Pigment Ratios)*
$E_d(\lambda,z)$	irradiância descendente, W m^{-2} nm^{-1}
Fuco	pigmento fucoxantina
HCA	Análise Hierárquica de Cluster *(Hierarchical Cluster Analysis)*
HPLC	Cromatografia Líquida de Alta Eficiência
Hex	pigmento 19'-hexanoiloxifucoxantina
IOPs	propriedades ópticas inerentes *(Inherent Optical Properties)*
$K_{bio}(\lambda)$	coeficiente de atenuação difusa sem a atenuação da água para a radiância ascendente na coluna d'agua, m^{-1}
$K_d(\lambda)$	coeficiente de atenuação difusa para a irradiância descendente na coluna d'agua, m^{-1}
$K_u(\lambda)$	coeficiente de atenuação difusa para a radiância ascendente na coluna d'agua, m^{-1}
$K_u(\lambda)$	coeficiente de atenuação difusa da água para a radiância ascendente na coluna d'agua, m^{-1}
$L_u(\lambda,z)$	radiância emergente, W m^{-2} nm^{-1} sr^{-1}
$L_w(\lambda,z)$	radiância emergente que deixa a superfície da água, W m^{-2} nm^{-1} sr^{-1}
MAAs	*Mycosporine-like Amino Acids*
MCF	profundidade do pico de fluorescência de clorofila-*a*
modc	material orgânico dissolvido colorido
OC2v6	Algoritmo bio-ótico empírico que utiliza duas bandas de $R_{rs}(\lambda)$
OC3v6	Algoritmo bio-ótico empírico que utiliza três bandas de $R_{rs}(\lambda)$
OC4v6	Algoritmo bio-ótico empírico que utiliza quatro bandas de $R_{rs}(\lambda)$

P460 carotenoide desconhecido com absorbância máxima em 460 nm

PATEX *PATagonian EXperiment*

Peri pigmento peridinina

Pras pigmento prasinoxantina

QPA Quebra de plataforma Argentina

RPD Diferença Percentual Relativa *(Relative Percentage Difference)*

$R_{rs}(\lambda)$ reflectância do sensoriamento remoto (*Remote Sensing Reflectance*), sr^{-1}

S_f fator de tamanho celular do fitoplâncton

TChl*a* concentração total de clorofila-*a*, mg m^{-3}

z profundidade, m

Zea pigmento zeaxantina

β fator de correção da amplificação da absorbância no filtro GF/F

λ comprimento de onda, nm

$[Chla]_F$ concentração de clorofila-*a* total determinada por fluorimetria, mg m^{-3}

$[Chla]_{HPLC}$ concentração de clorofila-*a* total determinada por HPLC, mg m^{-3}

[Chlb] concentração de clorofila-*b*

[Hexa] concentração de 19'-hexanoiloxifucoxantina

$[micro\ Chla]_F$ concentração de clorofila-*a* do micro-fitoplâncton determinada por fluorimetria, mg m^{-3}

$[micro\ Chla]_{HPLC}$ concentração de clorofila-*a* do micro-fitoplâncton estimada por pigmentos diagnósticos, mg m^{-3}

$[nano\ Chla]_{F/HPLC}$ diferença entre $[Chla]_F$ e $[micro\ Chla]_F$ subtraído $[pico\ Chla]_{HPLC}$

$[nano\ Chla]_{HPLC}$ concentração de clorofila-*a* do nano-fitoplâncton estimada por pigmentos diagnósticos, mg m^{-3}

[pico Chla]$_{HPLC}$ concentração de clorofila-*a* do pico-fitoplâncton estimada por pigmentos diagnósticos, mg m^{-3}

[pico+nano Chl*a*]$_{F}$ concentração de clorofila-*a* da fração combinada do pico-fitoplâncton e nano-fitoplâncton determinada por fluorimetria, mg m^{-3}

[pico+nano Chla]$_{HPLC}$ fração combinada da concentração de clorofila-*a* do pico-fitoplâncton e nano-fitoplâncton estimada por pigmentos diagnósticos, mg m^{-3}

[PPC] soma das concentrações dos carotenóides fotoprotetores, mg m^{-3}

[PSC] soma das concentrações dos carotenóides fotossintéticos, mg m^{-3}

RESUMO

Imagens de satélite da cor do oceano detectam intensas florações do fitoplâncton durante primavera e verão ao longo da quebra de plataforma Argentina, mas são escassas as medidas ópticas *in situ* na região. O objetivo geral desta tese foi investigar a variabilidade das propriedades ópticas das florações do fitoplâncton na quebra de plataforma Argentina e arredores. Entre 2006 e 2009, seis cruzeiros foram conduzidos com diversas medidas biológicas e físicas, incluindo medicões bio-ópticas, dentre as quais algumas inéditas na região. As seguintes medidas foram consideradas: coeficientes spectrais de absorção da luz pelo material particulado, que inclui o fitoplâncton e detritos; coeficiente de atenuação da luz pelo material particulado a 660nm; irradiância descendente e radiância ascendente da luz com alta resolução espectral, a partir das quais se obtém os coeficientes da atenuação difusa e a reflectância do sensoriamento remoto *in situ*; reflectância do sensoriamento remoto medida por satélite; concentração de clorofila-*a* total e fracionada por classes de tamanho do fitoplâncton estimada pelo método fluorimétrico; concentrações de clorofila-*a* e pigmentos acessórios do fitoplâncton, obtidas por HPLC; abundância taxonômica relativa do fitoplâncton estimada por CHEMTAX; e fator de tamanho celular do fitoplâncton estimado pelos espectros de absorção da luz pelo fitoplâncton. Grande variabilidade foi observada nos coeficientes de absorção, atenuação (e espalhamento) e atenuação difusa da luz para uma dada concentração de clorofila-a e vice-versa. Grande parte dessa variabilidade pôde ser explicada por variações no tamanho celular do fitoplâncton e, portanto, ao efeito "pacote". A variabilidade nos espectros de reflectância do sensoriamento remoto (propriedade óptica aparente) medidos *in situ* revelou o fitoplâncton como componente dominante nas propriedades ópticas das florações na região. Porém, a variabilidade nos coeficientes específicos (i.e., normalizados por clorofila-a) de

absorção e espalhamento (propriedades ópticas inerentes), devido a variações no tamanho celular do fitoplâncton, influenciou o desempenho de modelos bio-ópticos para estimar concentração de clorofila-a por satélite. As principais situações de composição taxonômica do fitoplâncton que ocorrem durante as florações na região (dominância por diatomáceas, haptofíceas, e com contribuições destes grupos e de outros, sem dominância) foram refletidas de forma coerente nos comportamentos espectrais de absorção da luz pelo fitoplâncton, indicando o potencial em discriminar as assembleias das florações na região através de dados ópticos. Particularmente, a identificação de dominância de diatomáceas e haptofíceas, a partir de um comprimento de onda, e também pelo fator de tamanho celular do fitoplâncton, que pode ser estimado por satélite, indica o potencial em identificar a dominância de tais grupos taxonômicos por sensoriamento remoto na região.

Palavras-chave: quebra de plataforma Argentina; absorção da luz; espalhamento da luz; reflectância do sensoriamento remoto; pigmentos; taxonomia do fitoplâncton

ABSTRACT

Satellite images usually detect intense phytoplankton blooms during spring and summer along the Argentina shelf break. Because *in situ* optical measurements are scarce in the region, six cruises were conducted from 2006 to 2009 to measure several physical, biological, and optical properties. Some of the bio-optical properties were gathered for the first time in the region. The aim of this thesis was to characterize the optical properties of phytoplankton blooms along the Argentina shelf break e adjacent areas. For this purpose, the following measurements and data were considered: light absorption coefficients of particulate material that includes phytoplankton and detritus; light attenuation coefficient of particulate material at 660 nm; hyperspectral downwelling irradiance and upwelling radiance, from which one obtains the vertical attenuation coefficients for downwards irradiance and upwards radiance and *in situ* reflectance of remote sensing; total and size-fractionated chlorophyll-concentration, estimated by fluorimetric method; concentrations of chlorophyll-a and accessory pigments of phytoplankton obtained by HPLC; relative taxonomic abundance of phytoplankton estimated by CHEMTAX; a cell size parameter for phytoplankton estimated from the phytoplankton absorption spectra. Large variability was observed for absorption coefficients of phytoplankton, scattering of particles and the vertical attenuation coefficients for downwards irradiance for a given chlorophyll-a concentration. Such variability could be largely explained by variations in cell size of phytoplankton and therefore the "package" effect, as indicated by the cell size parameter. The characterization of the variability in the remote sensing reflectance (apparent optical property) measured *in situ* revealed phytoplankton as the dominant component on the optical properties of algal blooms in the region. Nevertheless, the variability in absorption and scattering coefficients (inherent optical properties) due to variations in

cell size of phytoplankton was shown to impact the performance of bio-optical models that relies on band reflectance ratios of remote sensing to retrieve chlorophyll-a from satellite. The main taxonomic composition of the phytoplankton blooms (dominance of diatoms, haptophytes, and mixed contributions of these and others groups, but with no dominance) was consistently reflected on the spectral shape of light absorption of phytoplankton. Our results indicate a potential to discriminate phytoplankton assemblages in the region through optical data. Particularly, the identification of diatoms or haptophytes using one wavelength or through a phytoplankton cell size parameter, which can be estimated from satellite, has a potential of identifying the dominance of such taxonomic groups from remote sensing in the region.

Key words: Patagonia shelf-break; light absorption; light scattering; remote sensing reflectance; pigments; phytoplankton taxonomy

APRESENTAÇÃO

Essa tese segue a formatação alternativa “Modelo com trabalhos em apêndice”, segundo o Guia de Teses da Coordenação de Curso da Pós-Graduação em Oceanografia Biológica, FURG. Assim, o documento é composto por uma Introdução com aspectos gerais sobre a região de estudo, breve esplanação e revisão bibliográfica sobre a Bio-óptica Marinha, justificativas, hipóteses e os objetivos gerais e específicos da tese; Material e Métodos em linhas gerais; Síntese dos Resultados, que sumariza separadamente os resultados dos três artigos resultantes da tese; Conclusões e Literatura Citada até então; Apêndice, que consiste nos três manuscritos resultantes da tese, os quais são referidos aqui como Artigos, para fins práticos. Especificamente, o Artigo 1 se encontra aprovado para publicação, o Artigo 2 publicado e o Artigo 3 em processo de submissão. As figuras citadas ao longo desta tese são encontradas nos Apêndices.

1. INTRODUÇÃO

1.1. A região da quebra de plataforma da Argentina

Na região próxima à quebra de plataforma Argentina (QPA), a transição entre as águas da Corrente das Malvinas e as águas de plataforma forma uma frente termo-halina que se estende entre 37 e 50º S (Guerrero *et al*., 1999; Acha *et al*., 2004). Intensas florações de fitoplâncton ocorrem ao longo da QPA, e imagens de satélite (sensoriamento remoto) da cor do oceano indicam essas ocorrências entre setembro e março (Garcia *et al*., 2004; Saraceno *et al*., 2005, Rivas *et al*., 2006, Romero *et al*., 2006, Signorini *et al.*, 2006), com forte ciclo anual (Garcia *et al*., 2004). A área com grande biomassa do fitoplâncton que margeia a QPA seria sustentada pelas águas águas ricas de origem subantártica em nutrientes (Romero *et al*., 2006; Garcia *et al*., 2008). Além disso, processos de ressurgência na QPA foram descritos recentemente devido à interação da Corrente das Malvinas com a topografia do talude (Matano e Palma, 2008; Matano *et al*., 2010; Piola *et al*., 2010). Um estudo global estimou que um maior aumento na concentração de clorofila-*a* durante o período estudado (1998–2003) ocorreu no mar da Região Patagônica (Gregg *et al.,* 2005). A frente da quebra de plataforma da região influencia a abundância de recursos pesqueiros e predadores de topo (Bertolotti *et al.,* 1996; Cousseau e Perrota, 2000; Copello *et al.,* 2011).

Estudos com imagens de satélite sugerem que uma das mais intensas florações de cocolitoforídeos no oceano global ocorre na Plataforma Argentina (Brown e Yoder, 1994; Brown e Podestá, 1997). Séries temporais de imagens de satélite mais atuais de concentração de clorofila-*a*, Chl*a*, e de calcita evidenciaram a dominância do grupo sobre a assinatura espectral de reflectância na região entre dezembro e fevereiro (Signorini *et al*., 2006). Expedições recentes constataram *in situ* florações de

cocolitoforídeos na Plataforma Argentina Sul (Garcia *et al.,* 2011; Souza *et al.,* 2012) e Região Frontal Sub-Antártica (Balch *et al.,* 2011). Os cocolitoforídeos apresentam um papel fundamental no ciclo do carbono, entre o oceano e a atmosfera, pois suas células sintetizam carapaças de carbonato de cálcio, a partir dos íons bicarbonato da água (Holligan *et al*., 1993). A senescência destas florações cíclicas anuais resulta em altas taxas de sedimentação de carbono (aprisionado nas carapaças como $CaCO_3$), cuja parte é acumulada no fundo oceânico, constituindo uma forma de sequestro de CO_2 atmosférico (Holligan *et al*., 1993) dentro do ciclo global do carbono. Por fim, estas células promovem um alto grau de retro-espalhamento da luz, causando erros na aplicação de algoritmos empíricos aplicados ao sensoriamento remoto para estimativa de Chl*a* a partir de dados de reflectância (Gordon *et al*., 2001).

Além dos aspectos específicos referentes às florações dos cocolitoforídeos em períodos determinados do ano na região, os altos valores de biomassa associados a diatomáceas e dinoflagelados (Carreto *et al.*, 2008; Garcia *et al*, 2008; Comin, 2009; de Souza, 2012) durante toda a primavera e verão austral, bem como de produtividade primária comparáveis com máximos sazonais de produtividade em correntes de contorno leste (Carreto *et al.*, 2008; Garcia *et al*, 2008; Lutz *et al.*, 2010), evidenciam o papel importante da região com respeito aos ciclos biogeoquímicos. Em estudos anteriores, a plataforma e o talude da Patagônia foram definidos como áreas de intensa absorção de CO_2 atmosférico pelos oceanos no hemisfério sul devido, em parte, à alta produtividade fitoplanctônica (Takahashi *et al*., 2002; Bianchi *et al.*, 2009).

Apesar da importância ecológica e biogeoquímica da região, poucos estudos *in situ* têm sido conduzidos com o objetivo de fornecer informações sobre o fitoplâncton, especificamente na região da QPA (e.g. Carreto *et al.,* 2008). Recentemente, Schloss

et al. (2007) avaliaram a influência da estrutura da comunidade planctônica sobre a dinâmica do carbono nas águas superficiais da plataforma na região da Patagônia, mas poucos pontos foram amostrados na área oceânica ou do talude. Os autores verificaram relação inversa entre biomassa do fitoplâncton e a diferença de pressão parcial do CO_2 entre a água e a atmosfera, quando as assembleias do fitoplâncton foram dominadas por diatomáceas, não sendo o caso onde pequenos flagelados (≤ 5 μm) foram os organismos mais abundantes. Medições bio-ópticas têm sido raramente realizadas nas águas da Patagônia (Ferreira *et al.*, 2009;. Lutz *et al.*, 2010; *Garcia et al.,* 2011).

Em função dos antecedentes científicos apontados, e a importância ecológica e biogeoquímica da região, assim como das teleconexões entre regiões subantártica e costeira do Brasil, o Grupo de Oceanografia de Altas Latitudes (GOAL) propos o projeto PATEX - Processos físicos e bio-geoquímicos na quebra de plataforma da Patagônia, no âmbito do CNPq/Programa Antártico Brasileiro, e uma série de cruzeiros, denominada PATEX (*PATagonian EXperiment*), foi conduzida na região entre 2004 e 2009 durante primavera e verão para coleta de dados físicos, bioquímicos, ópticos e biológicos a fim de caracterizar tais florações e os fatores ambientais atuantes. O presente trabalho teve como objetivo caracterizar a variabilidade das propriedades bio-ópticas relacionando-as com as observadas florações de fitoplâncton nas águas da quebra de plataforma da Argentina e áreas adjacentes, com base em seis cruzeiros da série PATEX (2006 a 2009).

1.2. Bio-óptica

1.2.1. Propriedades ópticas e constituintes ópticos da água do mar

Segundo Preisendorfer (1961), as propriedades ópticas dos oceanos podem ser divididas em i) *propriedades ópticas inerentes*, *IOPs*[1] (*Inherent Optical Properties*), pois suas características dependem exclusivamente da concentração e composição dos componentes do meio, e ii) *propriedades ópticas aparentes*, *AOPs*, que dependem também da distribuição geométrica do campo da luz radiante que interage com as *IOPs*. As principais *IOPs* são os coeficientes de absorção e espalhamento da luz, enquanto as principais *AOPs* consistem na radiância, irradiância, reflectância da superfície (ou cor do oceano) e os coeficientes de atenuação difusa da luz. As magnitudes destas propriedades dependem do comprimento de onda, λ, que nos estudos bio-ópticos se restringem essencialmente à faixa espectral da luz visível, entre 400 a 700 nm.

A teoria que quantifica os coeficientes de absorção, $a(\lambda)$ e espalhamento, $b(\lambda)$, da luz, comumente expressos em m^{-1}, assume um feixe de luz paralelo que passa por uma camada fina de água. O coeficiente de espalhamento é subdividido em dois: para frente e para trás (retro). Para aplicações de sensoriamento remoto, considera-se o coeficiente de retro-espalhamento, $b_b(\lambda)$, que fornece informações sobre os constituintes ópticos da água do mar, pois a luz incide sobre a superfície do mar retro-espalhando energia radiante de volta para a superfície. O coeficiente de atenuação da

[1] Grande parte das abreviações apresentadas no corpo da tese são referentes aos termos em inglês, a fim de evitar o uso de duas diferentes abreviações para um mesmo termo contido no corpo da tese em português e nos artigos submetidos ou aceitos em inglês (Ver Lista de Símbolos e Abreviações). O termo em inglês considerado como base para tal abreviação é devidamente informado no texto em português.

luz, $c(\lambda)$, é a soma dos coeficientes de absorção e espalhamento. Os principais componentes que determinam as *IOPs* nos oceanos são i) a própria água; ii) as partículas, que incluem o fitoplâncton e o material não-vivo (ou detritos[2]), podendo ser orgânico e inorgânico; e iii) o material orgânico dissolvido colorido (*modc*). Os coeficientes de absorção da luz são determinados pela água, partículas e *modc*. A água do mar e as partículas também determinam os coeficientes de espalhamento além dos de absorção, enquanto o espalhamento pela *modc* é considerado desprezível (Mobley, 1994). Os coeficientes de absorção e espalhamento da água são conhecidos e variam pouco (Pope e Fry, 1997). O fitoplâncton contribui com a variabilidade óptica de um corpo d'água principalmente com a absorção da luz e, em menor grau, com seu espalhamento. Os detritos inorgânicos desempenham maior importância sobre o espalhamento da luz em comparação com a absorção. No espectro do visível, a absorção da luz pela *modc*, detritos e organismos heterotróficos decai exponencialmente com o comprimento de onda (Bricaud *et al.,* 1981), enquanto o espectro de absorção da luz pelo fitoplâncton reflete o comportamento dos pigmentos fotossintéticos e fotoprotetores.

Em bio-óptica, as águas dos oceanos são classificadas em termos das contribuições dos constituintes ópticos relativas ao fitoplâncton (Morel e Prieur, 1977). Águas do Caso 1 são aquelas nas quais o fitoplâncton é o principal e dominante agente atenuador da luz, e os demais componentes, dissolvidos e particulados, covariam com sua biomassa. Águas do Caso 2 são significativamente influenciadas também por constituintes não-algais (*modc* e partículas), incluindo partículas minerais, que não covariam com o fitoplâncton. Geralmente, regiões costeiras são classificadas como águas de Caso 2.

[2] Nos estudos de bio-óptica marinha, as partículas tanto orgânicas quanto inorgânicas são geralmente denominadas como detritos.

Os coeficientes de absorção e espalhamento dos constituintes óticos (*IOPs*) se relacionam com a reflectância do sensoriamento remoto (*AOPs*), $R_{rs}(\lambda)$ (*Remote Sensing Reflectance*), através da forma simplificada da Teoria de Transferência Radiativa (Gordon *et al.,* 1988 e referências inclusas):

$$R_{rs}(\lambda) = L_w(\lambda) / E_d(\lambda) \sim f\ b_b(\lambda) / [a(\lambda) + b_b(\lambda)], \quad \text{(Eq. 1)}$$

onde $L_w(\lambda,z)$ é a radiância emergente da água em W m^{-2} nm^{-1} sr^{-1}, $E_d(\lambda,z)$ é a irradiância descendente em W m^{-2} nm^{-1}, f é o fator de proporcionalidade que depende da distribuição geométrica do campo de luz, sem dimensão. Assim, a reflectância é, de certa forma, diretamente proporcional ao coeficiente de retro-espalhamento e inversamente correlacionada ao coeficiente de absorção.

O coeficiente de atenuação difusa para a irradiância descendente na coluna d'agua (*AOP*), $K_d(\lambda)$, descreve o decaimento de $E_d(\lambda,z)$ ao longo da coluna de água. Ele é definido como o coeficiente da regressão linear entre $\ln[E_d(\lambda,z)]$ e a profundidade, e também pode ser descrito como função das *IOPs* (Sathyendranath e Platt, 1988):

$$K_d(\lambda) = [a(\lambda) + b_b(\lambda)] / \mu, \quad \text{(Eq. 2)}$$

onde μ é o coseno médio da distribuição da luz perfeitamente difusa após refratada pela superfície do mar.

As *AOPs* e *IOPs* têm sido amplamente analisadas para águas de Caso 1 e geralmente parametrizadas como função da Chl*a* (índice de biomassa do fitoplâncton). Dentro de várias ordens de magnitude, essas relações são robustas (e.g., Morel, 1988, Morel e Maritorena, 2001; Morel *et al.*, 2007), sendo que para uma dada Chl*a*, a variabilidade nas *AOPs* e *IOPs* são decorrentes de variações i) nas características ópticas do fitoplâncton (detalhadas mais adiante) e ii) na proporção entre o material não-algal (dissolvido e particulado) e a Chl*a*. Em águas de Caso 1 com alta biomassa do fitoplâncton, a variabilidade nas propriedades ópticas pode ser grande de acordo

com o estágio das florações e disponibilidade de nutrientes (Morel *et al.,* 2006). As relações empíricas entre Chl*a* e *AOPs* e *IOPs* são geralmente mais ruidosas em águas de Caso 2 comparadas às relações de águas de Caso I com baixa biomassa algal, (O'Reilly *et al.,* 1998).

A fim de investigar se a variabilidade bio-óptica em águas de Caso 1 com alta Chl*a* tende a ser maior que a verificada nas águas de Caso 1 com com menor Chl*a* (e melhor documentada), faz-se necessário análises com dados mais diversificados, incluindo aqueles de zonas de ressurgência (Morel *et al.,* 2006). Em contribuição a esta investigação, este estudo analisou as relações entre a concentração de clorofila-*a* e os coeficientes de absorção da luz pelo i) material particulado, $a_p(\lambda)$, e ii) fitoplâncton, $a_{ph}(\lambda)$, iii) coeficientes de atenuação pelo material particulado, $c_p(\lambda)$ e iv) coeficientes de atenuação difusa, $K_d(\lambda)$, nas florações do fitoplâncton na quebra de plataforma Argentina. Também investigou-se a variabilidade dos espectros de reflectância do sensoriamento remoto, $R_{rs}(\lambda)$, durante essas florações.

1.2.2. Modelos bio-ópticos

Estimativas de Chl*a* através de dados de satélite da cor do oceano são geralmente baseadas em algoritmos (ou modelos) bio-ópticos empíricos que consistem em relações estatisticamente significantes entre a Chl*a* e a radiância emergente da água do mar normalizada, ou a reflectância de sensoriamento remoto, $R_{rs}(\lambda)$. Esses modelos são construídos a partir de dados correspondentes de Chl*a* superficial e $R_{rs}(\lambda)$, ambos medidos *in situ*, em diversas regiões dos oceanos (Werdell e Bailey, 2005). No geral, esses modelos consistem em polinômios que descrevem a dependência da Chl*a* com razões de $R_{rs}(\lambda)$ nas porções azul e verde espectrais (ver O'Reilly *et al.,* 1998). Estes

modelos assumem que i) a Chl*a* é primariamente o fator responsável pela variabilidade espectral de $R_{rs}(\lambda)$ e, portanto, que ii) o fitoplâncton é o componente dominante em relação aos demais componentes óticos, e iii) que, se estes existirem, eles covariam com o fitoplâncton. Obviamente, tais modelos geralmente não são adequados para águas de Caso 2.

Como já visto porém, a $R_{rs}(\lambda)$ (*AOP*) é diretamente proporcional à razão entre os coeficientes de retro-espalhamento e absorção (*IOPs*) de todos os componentes opticamente ativos presentes na água. Mesmo para águas do Caso 1, variações na proporção entre os componentes não-algais e o fitoplâncton e/ou nas propriedades ópticas do fitoplâncton, em comparação às propriedades associadas ao conjunto de dados dos quais as relações estatísticas entre Chl*a* e $R_{rs}(\lambda)$ foram estabelecidas, afetarão a estimativa da Chl*a* a partir dos modelos óticos empíricos (Brown *et al.,* 2008; Loisel *et al.,* 2010; Szeto *et al.,* 2011).

Assim, o conhecimento dos processos que causam variações no comportamento espectral dos componentes óticos e a quantificação da variabilidade nas *IOPs* contribui para melhorar as estimativas de Chl*a* através de imagens de satélite de $R_{rs}(\lambda)$ (IOCCG, 2006; Lee *et al.,* 2010). Diferenças regionais nas propriedades ópticas são relacionadas a diferenças ecológicas e biogeoquímicas, o que enfatiza a importância de conjunto de dados regionais (Szeto *et al.,* 2011). Também, algoritmos semi-analíticos (IOCCG, 2006), que se baseiam na relação teórica entre *AOPs* e *IOPs*, têm o potencial de melhorar as estimativas da Chl*a* a partir da $R_{rs}(\lambda)$. Esses algoritimos também estimam outros produtos, como as próprias *IOPs* associadas a cada componente óptico presente na água do mar.

O presente estudo avaliou o desempenho de modelos bio-ópticos empíricos, que são rotineiramente aplicados a imagens de satélite para derivar Chl*a*, durante as

florações do fitoplâncton na quebra de plataforma Argentina. Dados de $R_{rs}(\lambda)$ medidos *in situ* e de satélite foram considerados nestas análises. Também investigou-se a hipótese de que variações nos coeficientes de absorção da luz pelo fitoplâncton e espalhamento pelas partículas normalizados por Chl*a*, contribuem para os erros nas estimativas de Chl*a* a partir desses modelos aplicados a dados *in situ* de $R_{rs}(\lambda)$. O desempenho de modelos bio-ópticos semi-analíticos também foram avaliados, utilizando-se dados de $R_{rs}(\lambda)$ medidas por satélite.

1.2.3. Absorção da luz pelo fitoplâcton

Em geral, as propriedades de absorção da luz pelo fitoplâncton são bem caracterizadas através de medições laboratoriais e de campo. O coeficiente de absorção do fitoplâncton, $a_{ph}(\lambda)$, tem aplicações oceanográficas diversas, incluindo a propagação da luz (e.g., Atlas e Bannister, 1980; Sathyendranath e Platt, 1988), estrutura térmica (e.g., Lewis *et al.,* 1983; Stramska e Dickey, 1993) nas primeiras camadas dos oceanos, produção primária (Morel, 1991; Marra *et al.,* 2007) e fisiologia do fitoplâncton (Stramski e Reynolds, 1993; Bouman *et al.,* 2003). Devido a variabilidade na reflectância dos oceanos ser determinada em grande parte pelas variações em $a_{ph}(\lambda)$ nas águas superficiais, particularmente nas águas de Caso 1, este coeficiente também é essencial em aplicações do uso de observações de satélite da cor do oceano (Morel e Bricaud, 1981; Roesler e Perry, 1995; Sathyendranath *et al.*, 2001).

Variações em $a_{ph}(\lambda)$ resultam de mudanças na concentração do fitoplâncton e/ou propriedades ópticas de células individuais (e.g. Morel e Bricaud, 1981; Stramski *et al.,* 2001). Particularmente, a variabilidade observada em torno do comportamento

médio das relações estatísticas entre Chl*a* e $a_{ph}(\lambda)$ está relacionada ao efeito 'pacote' (*package effect*) celular (Duysens, 1956; Morel e Bricaud, 1981) e a composição de pigmentos nas células do fitoplâncton (Stuart *et al.*, 1998; Ciotti *et al*., 1999).

Uma tendência comum em comunidades do fitoplâncton é o aumento do efeito 'pacote' conforme o tamanho celular aumenta. Este efeito se refere ao decréscimo na absorção de luz pelos pigmentos presentes nas células, comparado com a absorção potencial para a mesma concentração pigmentar em solução, devido a um auto-sombreamento dos mesmos (*self-shading*). Um aumento do efeito 'pacote' devido a menor eficiência de absorção de luz por unidade de pigmento ocorre tanto com o aumento do tamanho celular (essencialmente porque há maior concentração de pigmentos e menor relação superfície:volume em maiores células), quanto com o aumento da concentração interna dos pigmentos causado por respostas foto-adaptativas (e.g., Morel e Bricaud 1981; Kirk, 1994).

Outra tendência comum em um gradiente trófico é um decréscimo na contribuição relativa dos pigmentos acessórios do fitoplâncton (aqueles além da Chl*a*, que consistem em fotossintéticos e fotoprotetores), em relação à contribuição da Chl*a*. Geralmente, é admitido que o tamanho celular médio aumenta de áreas oligotróficas para eutróficas (e.g., Malone, 1980; Yentsch e Phinney, 1989; Chisholm, 1992), enquanto a razão entre concentração de pigmentos não-fotossintéticos e Chl*a* tende a diminuir (Bricaud *et al*., 1995; Ciotti *et al*., 1999). Assim, os coeficientes específicos de absorção do fitoplâncton (ou seja, normalizados por Chl*a*), $a^*_{ph}(\lambda)$, variam, essencialmente, devido a mudanças na composição dos pigmentos e ao efeito 'pacote'. Geralmente, $a^*_{ph}(\lambda)$ diminui com um aumento em Chl*a* e o tamanho celular dominante do fitoplâncton, enquanto aumenta com as razões entre as pigmentos acessórios e Chl*a* (Bricaud *et al.*, 2004 e referências inclusas).

Na mesma linha do trabalho de Sathyendranath *et al*. (1987), diversos outros estudos objetivaram separar o efeito da composição do pigmentos e do efeito 'pacote' sobre os espectros de $a_{ph}(\lambda)$ (Lohrenz *et al.*, 2003;. Toepel *et al.*, 2005;. Fishwick *et al.*, 2006; Chazottes *et al*., 2007; Wang *et al*., 2007; Matsuoka *et al.*, 2011). Em geral, a importância da composição do pigmentos sobre as variações em $a^*_{ph}(\lambda)$ é menor que do efeito do tamanho celular (e.g. Ciotti *et al.,* 2002). No entanto, a variabilidade sazonal da importância relativa de ambos os fatores pode ser observada em algumas regiões dos oceanos (e.g. Toepel *et al.*, 2005). Nosso estudo investigou a influência do efeito "pacote" e da composição de pigmentos na variabilidade dos espectros de absorção da luz pelo fitoplâncton associada às florações ao longo da quebra de plataforma Argentina.

Esforços significativos têm sido dedicados ao desenvolvimento de modelos ópticos, incluindo os que envolvem o sensoriamento remoto da cor do oceano, para derivar informações sobre o tamanho celular do fitoplâncton a partir dos espectros de absorção do fitoplâncton (ver revisão de Brewin *et al.*, 2011a). Alguns trabalhos mais recentes propuseram a discriminação do grupo taxonômico do fitoplâncton a partir dos espectros de reflectância para aplicações em imagens de satélite (ver revisão de Rudorff *et al.*, 2011).

1.2.4. Espalhamento da luz pelas partículas

O fitoplâncton atua também no espalhamento da luz nos oceanos (Morel e Ahn, 1991; Stramski e Kiefer, 1991) e domina a concentração de partículas em águas do Caso 1. O coeficiente de atenuação da luz pelas partículas, $c_p(\lambda)$, é uma medida óptica que permite a inferência da concentração das mesmas. Quando medido através de um

transmissômetro na porção vermelha do espectro (~ 650–660 nm), onde a absorção da luz pelas partículas é fração muito pequena de $c_p(\lambda)$, esse coeficiente é muito próximo do coeficiente de espalhamento da luz pelas partículas, $b_p(\lambda)$ (Loisel e Morel, 1998) que, por sua vez, depende da concentração, tamanho e composição do material (Stramski e Kiefer, 1991; Babin e Stramski, 2004).

Relações empíricas baseadas em medições *in situ* têm sido estabelecidas entre Chl*a* e $c_p(\lambda)$ (e.g. Voss, 1992; Loisel e Morel, 1998; Behrenfeld e Boss, 2006), o coeficiente de espalhamento pelas partículas, $b_p(\lambda)$ (e.g. Gordon e Morel, 1983; Loisel e Morel, 1998; Huot *et al.,* 2008) e o coeficiente de retro-espalhamento pelas partículas, $b_{bp}(\lambda)$ (e.g. Reynolds *et al.,* 2001; Stramska *et al.*, 2006; Huot *et al.,* 2008). Variações nos coeficientes específicos de espalhamento das partículas (ou seja, normalizados por Chl*a*), $b^*_p(\lambda)$, foram relacionadas ao estado fisiológico do fitoplâncton (Behrenfeld e Boss, 2003), e poucos estudos têm investigado o papel do tamanho celular do fitoplâncton sobre tais variações (e.g. Gernez *et al.,* 2011). A forte correlação entre os coeficientes de espalhamento e retroespalhamento indicam que as variações em $b^*_p(\lambda)$ podem ser assumidas também para o coeficiente específico de retro-espalhamento da luz pelas partículas (ou seja, normalizados por Chl*a*), $b^*_{bp}(\lambda)$ e, portanto, com aplicações para estimativa da biomassa e fisiologia do fitoplâncton (Westberry *et al.*, 2010), bem como a estrutura de tamanho (Loisel *et al.*, 2006) através de sensores a bordo de satélites.

A quantificação e compreensão das causas de variabilidade em ambas as propriedades de absorção e espalhamento da luz pelo fitoplâncton são, portanto, essenciais para melhorar a nossa capacidade de recuperar informações biologicamente relevantes através de dados *in situ* e de sensoriamento remoto. Este estudo pretende contribuir para essa compreensão nas águas da quebra de plataforma da Patagônia.

1.2.5. Discriminação de grupos taxonômicos do fitoplâncton através de medidas ópticas

Desde o lançamento do primeiro satélite da cor do oceano (Feldman *et al.*, 1989), o sensoriamento remoto tem realizado o monitoramento quase permanente da biomassa do fitoplâncton nos oceanos, indexada como concentração de clorofila-*a*. No entanto, a Chl*a* não é suficiente para elucidar a contribuição do fitoplâncton sobre os ciclos biogeoquímicos, porque os grupos de algas diferem em suas funções biogeoquímicas (ver revisão de Le Quéré *et al.,* 2005 e Nair *et al.,* 2008). Neste contexto, um tipo funcional de fitoplâncton representa um grupo de espécies que, independentemente da filogenia, têm características biogeoquímicas similares (Nair *et al.*, 2008).

Por exemplo, sílica, cálcio e nitrogênio são utilizados principalmente por diatomáceas, cocolitóforídeos e algumas cianobactérias (e.g. *Trichodesmium*), respectivamente. Dinoflagelados e haptófíceas são responsáveis por importante produção de dimetil sufeto (DMS) nos oceanos que contribui para a troca de enxofre entre o oceano e a atmosfera e para a formação de nuvens. O tamanho celular do fitoplâncton também tem clara importância ecológica, pois pode fornecer informações sobre a transferência de energia através da cadeia trófica. Devido a maiores razões superfície:volume celulares, o pico-fitoplâncton absorve nutrientes com alta eficiência sob condições tróficas limitadas e, portanto, é geralmente dominante em águas oligotróficas. Também, esse grupo sedimenta mais lentamente do que células maiores, e portanto seu papel no transporte de carbono de águas superficiais para profundas é limitado. Por sua vez, o micro-fitoplâncton é o principal agente em cadeias alimentares eficientes, no afundamento de partículas e consequente exportação de carbono pra o fundo oceânico.

Na última década, os estudos de sensoriamento remoto da cor do oceano então evoluiu para estudos com o objetivo de identificação dos grupos do fitoplâncton (ver revisão de Rudorff *et al.,* 2011), para potencialmente melhorar a nossa compreensão dos processos biogeoquímicos no oceano global. Algoritmos foram desenvolvidos tanto para o mapeamento da distribuição de grupos funcionais (Subramaniam *et al.,* 2002; Sathyendranath *et al.,* 2004; Alvain *et al.,* 2005; Raitsos *et al.,* 2008; Bracher *et al.,* 2008) e classes de tamanho celular (Ciotti *et al.,* 2002; Aiken *et al.,* 2006; Ciotti e Bricaud, 2006; Uitz *et al.,* 2006; Hirata *et al.,* 2008; Kostadinov *et al.,* 2009; Brewin *et al.,* 2010; Mouw e Yoder, 2010; Devred *et al.,* 2011) do fitoplâncton.

A possibilidade de acesso a informações sobre a estrutura das comunidades do fitoplâncton a partir do espaço se baseia no fato de que a reflectância nos oceanos é em grande parte determinada pelas propriedades de absorção da luz pelo fitoplâncton presente nas camadas superiores (e.g., Sathyendranath e Platt, 1989). Por sua vez, esses espectros de absorção são variáveis devido ao efeito "pacote" e a composição celular de pigmentos, como já mencionado anteriormente.

Alguns estudos têm tentado extrair informações da composição de pigmentos a partir de espectros de absorção da luz pelo fitoplâncton (Hoepffner e Sathyendranath, 1993; Stuart *et al.,* 1998; Moisan *et al.,* 2011). Porém, estes métodos são ainda um problema difícil de inversão, pela dificuldade em isolar o efeito da concentração de pigmentos daquele do efeito "pacote" sobre a variabilidade nos espectros de absorção de fitoplâncton. Melhorias nas estimativas de concentração de pigmentos a partir desses espectros foram alcançadas com análises estatísticas avançadas (Bricaud *et al.,* 2007; Chazottes *et al.,* 2006, 2007), que não parecem ser viáveis rotineiramente.

A possibilidade de identificação do grupo dominante do fitoplâncton diretamente de espectros de absorção de luz ou inversão a partir da reflectância tem sido mais

explorada (Subramaniam *et al.,* 1999; Staher e Cullen, 2003; Westberry *et al.,* 2005; Craig *et al.,* 2006; Lubac *et al.,* 2008; Mao *et al.,* 2010). Especificamente, análises estatísticas de agrupamento aplicadas sobre espectros de absorção do fitoplâncton e/ou de reflectância em conjunto com informações de composição taxonômica como referência têm sido testados como abordagens automatizadas para a identificação do grupo taxonômico dominante a partir dessas propriedades ópticas (Taylor *et al.,* 2011; Torrecilla *et al.,* 2011). Esses estudos confirmaram a vantagem do uso de dados hiperespectrais em comparação com multiespectrais (resolução atual dos sensores satelitais) e de aplicação de derivadas sobre os mesmos dados, com a finalidade de identificação de grupos fitoplanctônicos. No entanto, a aplicabilidade destas técnicas para detectar diferentes comunidades de fitoplâncton a partir de dados de satélite ainda é um grande desafio, principalmente por causa de características específicas regionais (Alvain *et al.,* 2008) e a escassez de dados *in situ* que são necessárias para validar essas técnicas (Platt *et al.,* 2006).

Nesta tese foi investigado se diferenças no comportamento espectral de absorção da luz pelo fitoplâncton podem ser utilizadas para discriminar dominância taxonômica nas águas da quebra de plataforma da Argentina.

1.3. Hipótese e Objetivos da Tese

Neste trabalho, partiu-se da seguinte hipótese: as variações na comunidade do fitoplâncton são refletidas nas propriedades e características ópticas das águas da quebra de plataforma Argentina. Para testá-la, uma série de cruzeiros foi realizado em diferentes épocas do ano, com aquisição de dados sobre i) propriedades ópticas

aparentes e inerentes da água do mar e ii) estrutura das comunidades do fitoplâncton durante as florações.

O objetivo geral desta tese foi, portanto, **estudar as propriedades ópticas durante as florações do fitoplâncton de primavera e verão ao longo da quebra de plataforma Argentina, de forma a contribuir para a aplicação do sensoriamento remoto da cor do oceano para a região.**

Os seguintes objetivos específicos foram definidos:

1) Investigar as relações entre a concentração de clorofila-*a* e as propriedades ópticas inerentes (coeficientes de absorção de luz e de atenuação de luz pelo material particulado, que inclui o fitoplâncton e detritos) e aparentes (coeficientes de atenuação difusa da luz), contribuindo para a documentação de propriedades ópticas em águas de alta biomassa fitoplanctônica, como recomendado por Morel *et al.* (2006);

2) Descrever a variabilidade hiperespectral da reflectância do sensoriamento remoto e avaliar as estimativas de concentração de clorofila-*a* e coeficientes de absorção do fitoplâncton através de modelos bio-ópticos empíricos e semi-analíticos utilizando-se dados de reflectância *in situ* e de satélite;

3) Investigar a relação entre os erros de estimativas da concentração de clorofila-*a* através de modelos bio-ópticos empíricos e os coeficientes específicos de absorção da luz pelo fitoplâncton e espalhamento pelas partículas (ambos normalizados por clorofila-*a*);

4) Caracterizar a variabilidade dos coeficientes de absorção da luz pelo fitoplâncton e espalhamento pelas partículas. Particularmente, investigar o efeito do tamanho dominante e composição de pigmentos do fitoplâncton sobre a variabilidade desses coeficientes como função da clorofila-*a*;

5) Investigar a possibilidade de classificar os espectros de absorção da luz pelo fitoplâncton de acordo com sua composição pigmentar e taxonômica;

6) Investigar assinaturas espectrais dos coeficientes absorção da luz pelo fitoplâncton e seu potencial como meio para identificar o grupo de fitoplâncton dominante.

Para fins práticos, os manuscritos científicos serão referidos aqui como Artigos. Os objetivos específicos 1, 2 e 3 foram desenvolvidos no Artigo 1 (aceito para publicação), o objetivo 4 foi desenvolvido no Artigo 2 (publicado) e os objetivos 5 e 6 no Artigo 3 (em preparação).

Vale ressaltar a co-autoria do artigo publicado: Garcia, C. A. E., V. M. T. Garcia, A. I. Dogliotti, **A. Ferreira**, S. I. Romero, A. Mannino, M. S. de Souza, e M. M. Mata (2011), Environmental conditions and bio-optical signature of a coccolithophorid bloom in the Patagonian shelf, *J. Geophys. Res.*, *116,* C03025, doi:10.1029/2010JC006595. Este trabalho consiste em um estudo das propriedades ópticas relacionadas à floração de cocolitoforídeos amostrada durante o cruzeiro PATEX 5, que se encontra citado ao longo da tese.

2. MATERIAL E MÉTODOS

2.1. Cruzeiros oceanográficos e coleta de dados

Os dados analisados neste estudo foram coletados durante seis cruzeiros ao longo da quebra de plataforma Argentina, QPA, e arredores. Três cruzeiros nomeados como PATEX 2, PATEX 4 e PATEX 6 foram realizados durante a primavera, especificamente nos períodos de 28 a 31 outubro de 2006, 16 a 21 outubro de 2007 e 14 a 18 Outubro 2008, respectivamente. Dois cruzeiros, PATEX 5 e PATEX 7, foram realizados durante o verão nos períodos de 4 a 07 de janeiro de 2008 e 5 a 8 de janeiro de 2009. O cruzeiro PATEX 3 ocorreu durante o início do outono, de 25 a 29 março de 2007. As localizações das estações (Figura 1 – Apêndice 1) estenderam-se desde a porção norte da QPA (PATEX 6) através das águas altamente produtivas ao longo do talude (PATEX 2, 3 e 4) e da plataforma sul (PATEX 5) e ao sul da Ilha das Malvinas (PATEX 7). Ao todo, 176 estações foram realizadas através de transectos meridionais e zonais ao longo da QPA e entorno durante os seis cruzeiros.

Em todas as estações, perfis verticais de fluorescência da clorofila-*a* e coeficiente de atenuação em 660 nm foram realizados através de sistema CTD / Rosette (SeaBird ® 911 +), com garrafas Niskin de 5 L acopladas para coleta de água. As amostras analisadas no presente estudo são provenientes de coletas em superfície, profundidade onde foi observado o pico de fluorescência de clorofila-*a* (*depth of maximum chlorophyll fluorescence*, *MCF*) e profundidade da base deste pico (*bottom of the maximum chlorophyll fluorescence, BMCF*). As seguintes medições são consideradas e discutidas: i) concentração total de clorofila-*a*, Chl*a*, ii) concentração fracionada de Chl*a* em classes de tamanho do fitoplâncton, iii) concentração de pigmentos do fitoplâncton, iv) coeficientes de absorção de luz espectral do material particulado, que

inclui o fitoplâncton e partículas não-algais, v) coeficiente de atenuação de partículas em 660 nm; vi) radiância de luz emergente da água e irradiância solar incidente sobre a água, a partir das quais se computam o coeficiente de atenuação difusa de luz e a reflectância da água do mar (ou do sensoriamento remoto). Destaca-se que a Chl*a* total foi determinada pelos métodos fluorométrico (F) e Cromatografia Líquida de Alta Resolução (HPLC), como descrito a seguir.

2.2. Determinação da concentração de clorofila-a por fluorimetria

Em cada estação, amostras discretas de água (0,5-1L) foram coletadas em superfície, *MCF* e *BMCF*. Os volumes foram filtrados em filtros de fibra de vidro (Whatman GF/F) com 25 mm de diâmetro para determinação da Chl*a* pelo método fluorimétrico, designada por $[Chla]_F$. Em superfície e *MCF*, amostras foram também préfiltradas através de filtros de membrana de policarbonato (20 μm de poro) e o material que passou pelos mesmos foi então filtrado em filtros GF/F para a determinação da fração de clorofila-*a* associada às células do fitoplâncton menores que 20 μm. Esta fração da Chl*a* representa a contribuição combinada de pico-fitoplâncton e nano-fitoplâncton, denominada por $[\text{pico + nano Chl}a]_F$. A diferença entre a $[Chla]_F$ e $[\text{pico + nano Chl}a]_F$ fornece a contribuição do micro-fitoplâncton (> 20 μm de tamanho), que é designada por $[\text{micro Chl}a]_F$. As razões $[\text{pico + nano Chl}a]_F/\text{Chl}a$ e $[\text{micro Chl}a]_F/\text{Chl}a$ indicam a contribuição relativa das respectivas frações de tamanho para a biomassa algal total, em termos de Chl*a*.

Imediatamente após a filtração, os filtros GF/F foram embrulhados em papel alumínio e mantidos em nitrogênio líquido. Em laboratório, os pigmentos do

fitoplâncton foram extraídos em acetona 90% e a determinação de Chl*a* (mg m^{-3}) foi feita em fluorímetro Turner Designs TD-700 (Welschemeyer, 1994).

No primeiro artigo, foram consideradas os valores de Chl*a* (i) de superfície, profundidade do pico de fluorescência (*MCF*), e base deste pico (*BMCF*) para análise em correspondência com os coeficientes de absorção da luz pelo material particulado (*N*=356) (ii) de todas as profundidades amostradas em correspondência ao coeficiente de atenuação em 660 nm medido ao longo da coluna d'água (*N*=790) e (iii) de superfície para correspondência com os coeficientes de atenuação difusa e a reflectância do sensoriamento remoto (*N*=176). Para (iii), o número de dados de Chl*a* de superfície foi reduzido para 116, em correspondência com o número de estações realizadas durante o dia. No segundo e terceiro artigos, foram considerados os valores de Chl*a* (i) de superfície e (ii) de *MCF* para correspondência com os dados de HPLC/CHEMTAX (ver adiante).

2.3. Determinação da concentração de pigmentos por HPLC

As concentrações dos pigmentos fitoplanctônicos além da Chl*a* foram obtidas pela técnica de Cromatografia Líquida de Alta Resolução, HPLC, para amostras coletadas em superfície e *MCF* durante os cruzeiros, PATEX 4, 5, 6, e 7. O procedimento para a coleta e armazenamento de amostras foi o mesmo que o descrito para determinação de Chl*a* por fluorimetria. de Souza (2012) descreveu em detalhes o procedimento de HPLC utilizado neste trabalho para determinação da concentração dos pigmentos fitoplanctônicos para nossas amostras, que também se encontram em Mendes *et al*. (2007) e de Souza *et al*. (2012). As análises dos pigmentos por HPLC e processamento dos dados foram realizadas na FCUL (Portugal), em cooperação entre

as professoras Dra. Vanda Brotas e Dra. Virginia M. Tavano, do Laboratório de Ecologia do Fitoplâncton e Microrganismos Marinho (FURG).

2.3.1. Pigmentos considerados na investigação da variabilidade dos coeficientes específicos de absorção do fitoplâncton

Um conjunto de concentrações de pigmentos detectados por HPLC foi considerado para análises apresentadas na Seção 3.2 e no Artigo 2, que inclui: (1) clorofila-*a* total, $[Chla]_{HPLC}$, que consiste na soma da monovinil clorofila-*a*, clorofilídeo-*a*, e epímeros e alômeros da clorofila-*a* (a divinil clorofila-*a* não foi detectada em nossas amostras); (2) clorofila-*b*, [Chlb]; and (3) 19'-hexanoiloxifucoxantina, [Hexa]; (4) carotenóides fotossintéticos, [PSC], que inclui [Hexa], fucoxantina, 19'- butanoiloxifucoxantina, e peridinina, e (5) carotenóides fotoprotetores, [PPC], que inclui diadinoxantina, alloxantina, e zeaxantina. As concentrações de outros pigmentos, que são geralmente muito baixas, não foram incluídas nessas análises.

Um carotenóide desconhecido que deslocou o pico principal de absorção do fitoplâncton na faixa espectral azul ao redor de 440 para 460 nm foi detectado em 37 amostras coletadas nos cruzeiros PATEX 2, 3, 4, e 6. Este pigmento foi nomeado aqui como P460 e a investigação do seu efeito sobre os espectros de absorção do fitoplâncton está apresentada na Seção 3.2. e no Artigo 2.

2.3.2. Determinação de razões de pigmentos diagnósticos do fitoplâncton

Embora 13 pigmentos além da clorofila-*a* tenham sido detectados em nossas

amostras através da técnica de HPLC, vários ocorrem geralmente em concentrações muito baixas e/ou que não são diagnósticos (ou biomarcadores) de grupos taxonômicos, enquanto outros co-variam com outros pigmentos, sendo redundantes (Vidussi *et al.,* 2001). Na Seção 3.3 e no Artigo 3, considerou-se conveniente utilizar as razões entre pigmentos diagnósticos e a concentração somada desses pigmentos como conjunto de dados que caracterizem a composição de pigmentos do fitoplâncton em nossas amostras (Torrecilla *et al.,* 2011). Oito pigmentos diagnósticos (Gieskes *et al.*, 1988; Prézelin *et al.,* 2000; Vidussi *et al.,* 2001), foram detectados e alguns já citados na Seção 2.3.1, cujas abreviações aqui apresentadas se referem ao nome do pigmento (não a sua concentração): 1) clorofila-*b* (Chl*b*); 2) 19'-hexanoiloxifucoxantina (Hex); 3) prasinoxantina (Pras); 4) 19'-butanoiloxifucoxantina (Buta); 5) fucoxantina (Fuco); 6) peridinina (Peri); 7) aloxantina (Allo); e 8) zeaxantina (Zea). Embora não sejam geralmente considerados como pigmentos diagnósticos, as 9) clorofila-c_1 (Chl*c1*) e 10) clorofila-c_3 (Chl*c3*), também foram inclusas, resultando em um conjunto de dados com 10 pigmentos diagnósticos. Chl*c1* e Chl*c3* foram consideradas porque podem, em certos casos, distinguir dois tipos de diatomáceas (Stauber e Jeffrey, 1988).

Stauber e Jeffrey (1988) verificaram que, enquanto a clorofila-c_2 estava presente em todas as diatomáceas testadas em seu estudo, 12% das mesmas continham Chl*c3* no lugar de Chl*c1*. Análises de microscopia revelaram a ocorrência de diatomáceas que contém clorofila-c_3 em várias amostras exclusivamente dos cruzeiros PATEX 4 e PATEX 7 (de Souza, 2012). Especificamente, as espécies *Thalassiothrix antarctica* e *Rhizosolenia crassa* estiveram presentes nos cruzeiros PATEX 4 e PATEX 7, respectivamente. As duas categorias de diatomáceas que diferem no tipo de clorofila-*c* presente, serão referidas aqui como diatomáceas-Chlc_1 e diatomáceas-Chlc_3.

Para cada amostra, as 10 razões de pigmentos diagnósticos foram computadas através da normalização da concentração de cada pigmento diagnóstico pela soma das concentrações dos 10 pigmentos diagnósticos (Uitz *et al.,* 2006). Esse conjunto de dados foi considerado nas análises apresentadas na Seção 3.3 e Artigo 3.

2.3.3. *Determinação das abundâncias relativas dos grupos taxonômicos do fitoplâncton*

As abundâncias relativas dos grupos fitoplanctônicos que contribuíram para a biomassa fitoplanctônica total, em termos de Chl*a*, foram obtidas através do programa de análise químio-taxonômica CHEMTAX 1.95 (Mackey *et al.,* 1996; Writght *et al.,* 1996). Este programa utiliza um processo interativo de factorização matricial para otimizar a associação entre os diferentes pigmentos fitoplanctônicos presentes e determinar a mais adequada composição de grupos taxonômicos. Para tanto, utiliza-se uma matriz de entrada com razões entre cada pigmento e a concentração total da clorofila-*a* representativas da região de interesse (Mackey *et al.,* 1996). Considerou-se como razões iniciais de pigmentos para as principais classes taxonômicas do fitoplâncton as apresentadas em estudos nas águas da plataforma da Patagônia (Carreto *et al.,* 2003; Zapata *et al.,* 2004; Souza *et al.,* 2011). A matriz de saída contém as frações de concentração de clorofila-*a* atribuída a cada grupo taxonômico, obtidas após o melhor ajuste aos dados com base na matriz de entrada (Mackey *et al.,* 1996).

Os cálculos incorporados no programa CHEMTAX estão detalhadamente descritos em Mackey *et al.* (1996) e os procedimentos especificamente adotados no presente trabalho estão descritos em Mendes *et al.* (2007), de Souza *et al.* (2012), e de

Souza (2012). Com base nos pigmentos detectados nas amostras e análise de microscopia, 6 grupos do fitoplâncton foram incluidos no software CHEMTAX para nossas amostras: (1) diatomáceas, (2) grupo-quimiotaxonômico, (3) dinoflagelados, (4) criptofíceas, (5) prasinofíceas, e (6) cianobactérias. O grupo-quimiotaxonômico inclui haptofíceas, dinoflagelados sem peridinina e outros organismos cuja composição pigmentar ainda não foi analisada completamente (de Souza, 2012). Análises de microscopia revelaram a dominância de haptofíceas sobre esse o grupo-quimiotaxonômico (Souza M. S. e Mendes, C. R. M., comunicação pessoal). Neste estudo, denominou-se esse grupo então como haptofíceas.

Diatomáceas-Chlc_1 e diatomáceas-Chlc_3 foram incluídas separadamente na matriz de entrada para os cruzeiros PATEX 4 e PATEX 7, nos quais as diatomáceas-Chlc_3 foram identificadas por microscopia, totalizando então 7 grupos. Os resultados da metodologia CHEMTAX serão mostrados de acordo com a presença de 7 grupos, ou seja, com discriminação entre diatomáceas-Chl*c1* e diatomáceas-Chl*c3*. Assim, somente as amostras dos cruzeiros PATEX 4 e PATEX 7 apresentarão diatomáceas-Chl*c3* além das diatomáceas-Chl*c1*. Para cada amostra, as contribuições relativas das 6 (ou 7) classes taxonômicas para a biomassa fitoplanctônica total foram então calculadas dividindo-se a fração da concentração de clorofila-*a* atribuída a cada classe pela concentração de clorofila-*a* total. Esse conjunto de dados foi considerado nas análises apresentadas na Seção 3.3 e Artigo 3.

2.4. Estimativa das frações de tamanho do fitoplâncton

A determinação da Chl*a* para a fração do fitoplâncton > 20 μm e a Chl*a* total por fluorimetria permitiu a estimativa da Chl*a* para as duas frações pico-fitoplâncton +

nano-fitoplâncton [pico + nano Chl*a*]$_F$ e [micro Chl*a*]$_F$ e, então, suas respectivas contribuições relativas para a biomassa total, em termos da Chl*a* total. Através da concentração de pigmentos fitoplanctônicos acessórios, é possível a estimativa da contribuição relativa de 3 classes de tamanho (pico-, nano- e micro-fitoplâncton) para a Chl*a* total.

Esta informação pode ser obtida a partir da concentração de pigmentos obtida por HPLC através do método proposto por Vidussi *et al.* (2001), com refinamentos apresentados por Uitz *et al.* (2006). Esse método se baseia no fato de que certos pigmentos acessórios servem como diagnósticos (ou biomarcadores) de grupos taxonômicos específicos do fitoplâncton, sendo que a estes taxa são atribuídas uma das três classes de tamanho: pico-, nano, ou micro-fitoplâncton. Esta atribuição é baseada em observações de campo que i) o micro-fitoplâncton inclui principalmente diatomáceas, ii) o nano-fitoplâncton inclui principalmente haptofíceas e iii) o pico-fitoplâncton inclui principalmente espécies procarióticas. Esta abordagem apresenta limitações porque vários grupos podem compartilhar certos pigmentos diagnósticos e alguns táxons incluem células que cobrem uma grande variedade de tamanho. Apesar destas limitações, este método tem fornecido informações úteis sobre composição baseada em pigmentos e estrutura de tamanho das comunidades do fitoplâncton (Bricaud *et al.*, 2004;. Uitz *et al*., 2006, 2008; Ras *et al*., 2008).

As concentrações de pigmentos diagnósticos determinadas para os cruzeiros PATEX 4 a 7 foram consideradas para estimar a Chl*a* associada às 3 classes de tamanho [pico Chla]$_{HPLC}$, [nano Chla]$_{HPLC}$ e [micro Chla]$_{HPLC}$ e então, a contribuição relativa de cada classe a biomassa total do fitoplâncton, em termos de Chl*a*. Encontrou-se fraca concordância entre as contribuições relativas de cada fração sobre a Chl*a* total obtidas a partir dos pigmentos diagnósticos e aquelas obtidas a partir da

separação física das frações maior e menor que 20 μm e subsequente medidas da Chl*a* de cada fração por fluorimetria (fracionamento/fluorimetria). Estas diferenças foram quantificadas através da inclinação da reta das seguintes relações lineares: (i) [pico + nano Chla]$_F$ *vs.* [Chla]$_F$ vs, (ii) [micro Chla]$_F$ *vs.* [Chla]$_F$, (iii) [pico + nano Chla]$_{HPLC}$ (ou seja, a soma de [pico Chla]$_{HPLC}$ e [nano Chla]$_{HPLC}$, já que ambas as frações não foram fisicamente separadas por fracionamento/fluorimetria) *vs.* [Chla]$_F$, e (iv) [micro Chla]$_{HPLC}$ *vs.* [Chla]$_F$ (Tabela 1; Artigo 2).

A contribuição de [micro Chla]$_{HPLC}$ estimada a partir de pigmentos diagnósticos foi significativamente maior do que a contribuição de [micro Chla]$_F$ obtida pelo fracionamento/fluorimetria. O oposto foi observado para a soma das contribuições pico-fitoplâncton e nano-fitoplâncton, para as quais o método dos pigmentos diagnósticos forneceu valores mais baixos em comparação com o fracionamento/fluorimetria (Tabela 1 – Apêndice 2).

Existem várias razões possíveis para as discrepâncias observadas, e algumas delas estão certamente relacionadas com as limitações do método baseado em pigmentos diagnósticos. Por exemplo, as estimativas relativamente elevadas de [micro Chla]$_{HPLC}$ podem ser explicadas pela fucoxantina ser assumida como pigmento diagnóstico de diatomáceas, que são geralmente maiores e pertencentes ao micro-fitoplâncton, enquanto diatomáceas também fazem parte do nano-fitoplâncton. O grupo das haptofíceas, pertencentes ao nano-fitoplâncton, também apresenta fucoxantina como pigmento acessório.

Assim, decidiu-se considerar as contribuições relativas das frações de tamanho do fitoplâncton obtidas através do fracionamento/fluorimetria, i.e., os dados de [pico + nano Chla]$_F$ e [micro Chla]$_F$, que foram obtidos em todos os seis cruzeiros PATEX. Ainda, para os quatro cruzeiros dos quais temos disponíveis os dados de HPLC,

dividimos a fração [pico + nano Chla]$_F$ em dois componentes: [pico Chla]$_{HPLC}$ e [nano Chla]$_{F/HPLC}$, o primeiro estimado a partir do método que se baseia em pigmentos diagnósticos, e o segundo através da diferença entre [Chla]$_F$ e [micro Chla]$_F$ somada a [pico Chla]$_{HPLC}$. Note que assumir as estimativas de [pico Chla]$_{HPLC}$ por pigmentos acessórios é coerente porque os pigmentos diagnósticos do pico-fitoplâncton estão presentes exclusivamente nesta faixa de tamanho da célula.

As contribuições relativas das frações de tamanho do fitoplâncton foram consideradas nas análises apresentadas na Seção 3.2 e Artigo 2.

2.5. Classificação da fração dominante de tamanho do fitoplâncton

A fração dominante de tamanho do fitoplâncton em uma amostra (de superfície e profundidade do pico de fluorescência da Chl*a*) foi definida como aquela com contribuição acima de 50% da biomassa algal total. Para tanto, foi considerada a contribuição relativa da Chl*a* de cada fração sobre a [Chla]$_F$, em percentagem. As frações pico-fitoplâncton e nano-fitoplâncton combinadas e micro-fitoplâncton estiveram disponíveis para os cruzeiros PATEX 2 e 3 através de fracionamento físico das amostras, enquanto essas três frações estiveram disponíveis separadamente para os cruzeiros PATEX 4, 5, 6, and 7, que incluiu a estimativa da fração pico-fitoplâncton através de pigmentos (Seção 2.4). Assumiu-se que o pico-fitoplâncton nunca foi dominante durante os cruzeiros PATEX 2 e 3 e, portanto, [pico+nano Chla]$_F$ foi considerado como [nano Chla]$_F$ para estes dois cruzeiros. Durante os demais, apenas 2 amostras foram dominadas pelo pico-fitoplâncton, enquanto 8 amostras não contiveram alguma fração de tamanho com contribuição maior que 50%. Assim, essas 10 amostras foram descartadas para nossas análises. A maioria das

amostras (189 amostras de 226) foram dominadas pelo nano-fitoplâncton, enquanto 45 foram dominadas pelo micro-fitoplâncton. A variabilidade dos coeficientes de absorção da luz pelo fitoplâncton, $a_{ph}(\lambda)$, e de espalhamento pelas partículas, $b_p(660)$, foram analisadas e discutidas na Seção 3.2 e no Artigo 2, comparando-se os dois grupos de dominância de tamanho do fitoplâncton, referidos como Grupo-N (*N-group*) e Grupo-M (*M-group*).

2.6. Determinação dos coeficientes de absorção do material particulado e fitoplâncton

Os espectros dos coeficientes de absorção da luz pelo material particulado, $a_p(\lambda)$ em m^{-1}, foram medidos através da técnica *Quantitative Filter Technique* (Mitchell *et al.*, 2000). Amostras de água (0,5 - 2 L) das mesmas profundidades de coleta para determinação da Chl*a* total (superfície, profundidade do pico de fluorescência da clorofila-*a* e base deste pico) foram filtradas através de filtros de vibra de vidro Whatman GF/F, de 25 mm de diâmetro. As medidas de absorbância foram realizadas entre 300-750 nm com resolução de 1 nm em um espectrofotômetro de feixe duplo (Cary Modelo 1E). Imediatamente após essas medidasos filtros foram imersos em metanol para extração dos pigmentos do fitoplâncton (Kishino *et al.,* 1985) para amostras dos cruzeiros PATEX 2 e 3 e descoloridos com solução de hipoclorito de sódio, NaClO, a 15% (Tassan e Ferrari, 1995) para os cruzeiros PATEX 4, 5, 6 e 7. A absorbância dos filtros extraídos ou descoloridos foi então medida, e corresponde ao material particulado não-algal (ou detritos), que inclui partículas orgânicas e inorgânicas, (Kishino *et al.*, 1985; Tassan e Ferrari, 1995; Mitchell *et al.,* 2000). Para os cálculos de $a_p(\lambda)$ e $a_{det}(\lambda)$ (absorção da luz pelos detritos, em m^{-1}), foi utilizado o

fator β determinado por Ferreira *et al.* (2009), que corrige o efeito de amplificação de absorbância pelo material contido no filtro em comparação ao mesmo material em suspensão, e a normalização pela área e volume filtrados. O espectro dos coeficientes de absorção do fitoplâncton, $a_{ph}(\lambda)$, foi obtido pela diferença entre $a_p(\lambda)$ e $a_{det}(\lambda)$. A fim de enfatizar as diferenças nos comportamentos (ou formas) espectrais, cada espectro de $a_{ph}(\lambda)$ foi normalizado pela soma dos valores espectrais de $a_{ph}(\lambda)$ entre 400 e 700 nm do próprio espectro. Os valores desse espectro normalizado serão indicados como $\int a_{ph}(\lambda)$, e as análises dos espectros de absorção da luz do fitoplâncton da Seção 3.3 e do Artigo 3 serão baseadas nesses valores normalizados.

2.7. Estimativa de um índice de tamanho celular do fitoplâncton

A fim de estimar um índice de tamanho celular, cada espectro de $a_{ph}(\lambda)$ foi normalizado pelo seu respectivo valor médio entre 400 e 700 nm (Ciotti *et al.,* 2002), sendo esse espectro normalizado referido como $a_{<ph>}(\lambda)$. Assumindo-se que a forma do espectro de absorção do fitoplâncton é principalmente definida pelo tamanho celular dominante, Ciotti *et al*. (2002) desenvolveram um modelo que reconstitui a forma de $a_{<ph>}(\lambda)$ através de uma combinação linear de dois espectros que representam espectros de absorção totalmente dominados i) pelas menores (pico-fitoplâncton) e ii) maiores células (micro-fitoplâncton). O algoritmo de Levenberg-Marquardt foi utilizado para ajustar o espectro de $a_{<ph>}(\lambda)$ a um modelo linear (ver Equação 3 em Ciotti *et al.* 2002), que estima um índice de tamanho celular, S_f, para um dado espectro de $a_{<ph>}(\lambda)$. Esse espectro pode então ser reconstruído a partir de S_f. Esse índice de tamanho celular indica o quanto cada espectro de $a_{<ph>}(\lambda)$ se aproxima dos espectros com total dominância pelos dois extremos de tamanho (pico- e micro-

fitoplâncton). Os valores de S_f são contínuos e variam entre 0 e 1, onde S_f tende a 0 quando as células grandes de fitoplâncton (> 20 μm) são dominantes, e tende a 1 quando células pequenas (< 2 μm) dominam uma amostra. Os valores intermediários representam todas as situações possíveis entre esses dois extremos. A qualidade do ajuste do modelo foi avaliada para cada espectro normalizado através do cálculo do coeficiente de determinação, R^2, entre todos os valores espectrais de cada espectro de $a_{<ph>}(\lambda)$ medido e todos os valores espectrais do espectro reconstruído pelo modelo.

2.8. Análise Hierárquica de Cluster apresentada no Artigo 3

Uma Análise Hierárquica de Cluster (*HCA*, *Hierarchical Cluster Analysis*), foi utilizada para classificar nossas amostras com base em três conjuntos de dados: i) as razões de pigmentos diagnósticos, *DPR* (*diagnostic pigment ratios*) ii) a contribuição relativa dos grupos taxonômicos do fitoplâncton derivados por CHEMTAX, e iii) os espectros de absorção da luz pelo fitoplâncton. A *HCA* tem sido aplicada em outros estudos com propósitos semelhantes a nossa análise, com conjuntos de dados selecionados com composição de pigmentos contrastantes (Torrecilla *et al.,* 2011) ou com grandes conjuntos de dados de pigmentos (Taylor *et al.,* 2011). A *HCA* é um método de agrupamento que constrói uma hierarquia de clusters (ou um dendrograma), onde os clusters em um nível estão unidos aos clusters do nível imediatamente superior, portanto, uma pré-definição de número de classes não é necessária. O número de clusters mais adequado é então definido por inspecção visual deste dendrograma.

A construção de um dendrograma envolve a medida de proximidade (ou distância) entre o par de observações e um critério de união (ou *linkage*) que especifica a

dissimilaridade dos grupos em função das distâncias entre os pares (*Hair et al.,* 2009). Neste estudo, a distância euclidiana e um algoritmo de *linkage* "objeto mais distante", que utiliza a maior distância entre os objetos em dois grupos, foram aplicados aos conjuntos de dados de *DPR* e de contribuição relativa dos grupos taxonômicos do fitoplâncton. A distância cosseno foi escolhida como mais adequada para aplicação sobre os espectros de $a_{ph}(\lambda)$, pois reflecte principalmente as diferenças nas formas espectrais (Torrecila *et al.,* 2011). Uma normalização anterior dos dados é necessária antes da aplicação da HCA. Para o nosso estudo, a *HCA* é adequada porque dois dendrogramas podem ser gerados a partir de dados independentes (i.e., *DPR*, contribuição relativa dos grupos taxonômicos do fitoplâncton e os espectros de absorção da luz pelo fitoplâncton) e serem posteriormente comparados (Torrecilla *et al.,* 2011). Isto é feito através do cálculo do índice cofenético (*CI*, *Cophenetic Index*), que representa a correlação entre duas matrizes cofenéticas (ou matrizes de similaridade) associadas a cada dendrograma gerado (Sokal e Rohlf, 1962).

2.9. Determinação do coeficiente de espalhamento do material particulado

O coeficiente de atenuação total, $c(\lambda)$ em m^{-1}, foi medido a 660 nm, $c(660)$, ao longo da coluna de água através do transmissômetro C-star (WETLabs, Inc.) com caminho ótico de 25 cm. O protocolo do cálculo de $c(660)$ é fornecido pelo fabricante (http://www.wetlabs.com/products/). As medidas tomadas em águas profundas (~ 1.000 m), porém distante do fundo do mar e, portanto, distante da região de ressuspensão de partículas, foram consideradas como estimativa da atenuação da água do mar livre de partículas (Loisel e Morel, 1998). O valor médio de todas as medições do coeficiente de atenuação total em grandes profundidades para cada cruzeiro foi

subtraído de todas as medições ao longo da coluna de água para remover os valores de atenuação da água do mar pura. Os valores resultantes representam o coeficiente de atenuação das partículas em 660 nm, $c_p(660)$, sob a suposição de que a contribuição do material dissolvido para a atenuação da luz neste comprimento de onda é desprezível. As medidas obtidas a 5 m de profundidade foram assumidas como o coeficiente de atenuação na superfície, o que é justificável para evitar ou minimizar a potencial contribuição intermitente de bolhas de ar injetadas na superfície pelo vento.

Devido ao coeficiente de atenuação de partículas ser a soma do coeficiente de espalhamento e absorção da luz pelas partículas, o coeficiente de absorção de partículas $a_p(660)$ foi subtraído de $c_p(660)$, obtendo-se assim o coeficiente de espalhamento das partículas em 660, $b_p(660)$. O cálculo $b_p(660) = c_p(660) - a_p(660)$ foi efetuado para superfície (considerando medidas de $c_p(660)$ ao redor de 5 m), profundidade de pico de fluorescência de clorofila-*a* e base deste pico, profundidades nas quais $a_p(\lambda)$ foi medido.

2.10. Coeficiente de atenuação difusa e reflectância de sensoriamento remoto

Medições radiométricas hiperespectrais (alta resolução espectral) foram obtidas ao longo da coluna d'água nas estações realizadas durante o dia (Figura 1.1) com um Radiômetro Perfilador Hiperespectral (HyperOCR, Satlantic, Inc.), que mede a radiância emergente da água (em direção à superfície do mar), $L_u(\lambda,z)$, e a irradiância solar descendente, $E_d(\lambda,z)$, entre 350-800 nm e com resolução espectral de 3,3 nm (137 bandas). A reflectância do sensoriamento remoto, $R_{rs}(\lambda)$ em sr^{-1}, é definida como a razão entre a radiância emergente da água logo acima da superfície (0^+), $L_w(\lambda)$, e $E_d(\lambda,0^+)$. Os valores de $L_u(\lambda,z)$ e $E_d(\lambda,z)$ medidos nos primeiros metros da coluna d'água são usados para estimar $L_u(\lambda)$ e $E_d(\lambda)$ logo abaixo da superfície (0^-) e então

propagar $L_u(\lambda,0^-)$ e $E_d(\lambda,0^-)$ através da interface água-ar para se obter o $L_w(\lambda)$ e $E_d(\lambda,0^+)$.

Os dados de $L_u(\lambda,z)$ e $E_d(\lambda,z)$ medidos ao longo da coluna d'água foram inicialmente processados com o software ProSoft 7.7.11, fornecido pelo fabricante Satlantic Inc. Os valores medidos no "escuro" e de calibração foram aplicados e os dados médios a cada 0,1 m foram obtidos ao longo da coluna d'água. A confiabilidade das medidas de $E_d(\lambda,z)$ e $L_u(\lambda,z)$ próximas à superfície é limitada devido às ondas, então dados cujas profundidades eram inferiores a 2 m foram descartados. A visualização dos perfis de $E_d(\lambda,z)$, $L_u(\lambda,z)$, Radiação Fotossinteticamente Ativa, PAR ($E_d(\lambda,z)$ integrada entre 400 a 700 nm) e o ângulo de inclinação de descida dos sensores foi importante para avaliar a qualidade dos dados e o intervalo de profundidade a ser considerado para extrapolar os valores de uma determinada profundidade até a superfície do mar. Os coeficientes de atenuação difusa de $E_d(\lambda,z)$, $K_d(\lambda,z)$, e de $L_u(\lambda,z)$, $K_u(\lambda,z)$, foram computados como a inclinação da reta obtida por regressão linear ajustada aos valores de $E_d(\lambda,z)$ e $L_u(\lambda,z)$ logtransformados, dentro do intervalo de profundidade selecionado, que geralmente variou entre 4 e 9 m., Os valores de $E_d(\lambda,0^-)$ e $L_u(\lambda,0^-)$, logo abaixo da superfície do mar, foram calculados utilizando-se $K_d(\lambda,z)$ e $K_u(\lambda,z)$, $E_d(\lambda,z)$ e $L_u(\lambda,z)$ medidos no intervalo de profundidade selecionado em cada perfil. A reflectância do sensoriamento remoto, $R_{rs}(\lambda)$, foi então calculada através da equação $R_{rs}(\lambda)=0{,}54L_u(\lambda,0^-)/1{,}04E_d(\lambda,0^-)$, onde 0,54 e 1,04 são os coeficientes de transferência para a interface do mar-ar para $L_u(\lambda)$ e $E_d(\lambda)$, respectivamente (Austin, 1974). A variabilidade de $K_d(\lambda)$ e $R_{rs}(\lambda)$ será descrita na Seção 3.1. e no Artigo 1. Note que o símbolo 'z' é omitido de $K_d(\lambda,z)$ para fins práticos.

2.11. Avaliação do desempenho de modelos bio-óticos empíricos

Investigou-se o desempenho de algoritmos (ou modelos) bio-óticos empíricos, que se baseiam na relação entre razões de $R_{rs}(\lambda)$ nas faixas azul e verde espectrais, e que são aplicados rotineiramente sobre imagens de satélite de reflectância pelas agências espaciais (e.g., NASA) para estimar a Chl*a* do espaço. Os modelos empíricos utilizados foram os OC2v6, OC4v6 e OC3v6 (as versões #6 são atualmente utilizadas (http://oceancolor.gsfc.nasa.gov/REPROCESSING/R2009/ocv6), sendo que os dois primeiros foram desenvolvidos para o sensor SeaWiFS e o último para o sensor MODIS. Os números 2, 3 e 4 indicam o número de bandas de $R_{rs}(\lambda)$ consideradas por cada modelo (indicadas posteriormente na Figura 1.7). A Chl*a* estimada foi obtida a partir de nossas medições de $R_{rs}(\lambda)$ *in situ* durante todos os cruzeiros através dos três modelos, e então comparada com a Chl*a* medida *in situ*. Comparações foram realizadas entre a Chl*a* medida *in situ* e a estimada a partir de medições de $R_{rs}(\lambda)$ por satélite através dos três modelos empíricos e do modelo semi-analítico Garver-Siegel-Maritorena, GSM, Maritorena *et al.,* 2002). Adicionalmente, comparou-se os coeficientes de absorção do fitoplâncton medidos *in situ* com os valores estimados pelos algoritmos semi-analíticos QAA (Lee *et al.,* 2002) e GSM (Maritorena *et al.,* 2002) através de dados satelitais. Os parâmetros estatísticos diferença percentual relativa média, *RPD* (*Relative Percentage Difference*), e a diferença percentual absoluta média, *APD* (*Absolute Percentage Difference*), foram utilizados para avaliar o desempenho dos algoritimos. As definições de *RPD* e *APD* estão apresentadas na Tabela 1.3. O coeficiente de determinação, R^2, inclinação e intercepto da reta obtidos a partir da análise de regressão linear sobre os valores logtransformados medidos *in situ* e estimados pelos diferentes algoritmos também foram considerados para avaliar seus desempenhos.

2.12. *Comparação entre dados medidos in situ e estimados por satélite*

Dados em nível (*Level*) 1A, L1A, que consistem em medidas radométricas não calibradas e processadas, gerados pelo sensor satelital MODIS/Aqua, e dados auxiliares de concentração de ozônio e condições meteorológicas (velocidade do vento, concentração de oxigênio, vapor de água e pressão atmosférica), foram obtidos a partir do Centro de Distribuição de Dados da NASA (*Distributed NASA Active Archive Center*, *DAAC*). Imagens diárias, com cobertura de área local (*Local Area Coverage, LAC*), i.e., com resolução máxima (ou pixel) de 1,1 km e dos dias em que os cruzeiros PATEX 2 a PATEX 7 foram realizados, foram selecionadas para a avaliação de produtos derivados através de modelos bio-óticos empíricos e semi-analíticos. As imagens L1A foram transformadas em nível 2, L2, que consistem nos produtos da "cor do oceano" gerados pelos modelos. Para este estudo, foram considerados os seguintes produtos: i) Chl*a* estimada pelos modelos empíricos OC2v6, OC3v6, OC4v6 e semi-analítico GSM, ii) coeficientes de absorção da luz pelo fitoplâncton estimados pelos modelos semi-analíticos GSM e QAA. O processamento das imagens satelitais L1A para L2 foi realizado através do software *SeaDAS* (*SeaWiFS Data Analysis System,* http:// http://seadas.gsfc.nasa.gov/), versão 6.2.

Para a comparação entre os dados *in situ* e os produtos derivados por satélite, calculou-se a média do valor do produto para uma conjunto de 3 por 3 pixels, com a estação oceanográfica ocupando o centro do bloco de 3x3 pixels. Esse procedimento objetiva minimizar os erros no georeferenciamento das imagens de satélite. Além disso, calculou-se o coeficiente de variação (CV) dentro de cada conjunto de 9 pixels, excluindo-se das análises os grupos com CV maior que 0,2, evitando assim grupo de pixels não homogêneos espacialmente e, portanto, não representativos da estação correspondente. A diferença máxima de 3 horas entre a medida realizada pelo satélite

e a mesma realizada a bordo do navio foi considerada, seguindo o critério da NASA (Bailey *et al.,* 2000).

3. SÍNTESE DOS RESULTADOS

Os resultados gerados nesta tese estão detalhadamente descritos nos artigos que se encontram no Anexo, e aqui serão apresentados de forma sucinta.

3.1. Resultados referentes aos Objetivos Específicos 1, 2 e 3

Artigo 1: "*Bio-optical characteristics of the Patagonian Shelf-break waters: Implications for ocean color algorithms*", aceito para publicação.

Os valores de concentração de clorofila-*a* apresentados nessa seção correspondem a $[Chla]_F$ (concentração de clorofila-*a* determinada pelo método de fluorimetria), e nesta seção será indicada como Chl*a.* Os valores de Chl*a* em superfície variaram entre 0,10 e 18,87 mg m^{-3} durante os cruzeiros PATEX 2 a PATEX 7, com um valor médio de 2,85 mg de m^{-3}. Nas profundidades do pico de fluorescência da clorofila-*a* (*MCF*, *maximum chlorophyll fluorescence*) e profundidade da base deste pico (*bottom of the maximum chlorophyll fluorescence*, *BMCF*), a Chl*a* variou entre 0,08 e 24,05 mg m^{-3} e 0,08 e 12,03 mg m^{-3}, respectivamente. A grande variabilidade na Chl*a* refletiu diferenças nas áreas e períodos das florações do fitoplâncton amostrados em cada cruzeiro (de Souza, 2012). Essa variabilidade foi discutida no Artigo 2 em associação com a estrutura de tamanho do fitoplâncton em termos de Chl*a* fracionada para classes de tamanho do fitoplâncton.

3.1.1. Coeficientes de absorção e atenuação difusa da luz pelo material particulado

O coeficientes de absorção das partículas não-algais, $a_p(440)$ menos $a_{ph}(440)$, não covariou com a Chl*a* em nenhuma das profundidades amostradas e sua contribuição para $a_p(440)$ foi relativamente baixa durante todos cruzeiros (média de 13%), mesmo com a grande variabilidade em Chl*a* (Tabela 1 - Apêndice 1). Estes resultados sugerem que, ao menos na QPA e regiões adjacentes e durante as florações de primavera e verão, a absorção de luz pelas partículas é dominada por células vivas do fitoplâncton e a contribuição do material não-algal é baixa e pouco variável com o tempo. Os resultados de contribuição percentual do fitoplâncton para a absorção de luz do material particulado estão de acordo com o intervalo de 85 a 94% encontrado por Morel *et al.* (2006) para águas de Caso 1 com altas concentrações de clorofila-*a*.

Os valores de $a_p(440)$ variaram entre 0,026 e 0,492 m^{-1} e aumentaram regularmente (em escala log) com o aumento de Chl*a* (0,08 a 24,02 mg m^{-3}) (Figura 3a - Apêndice 1), e a regressão linear entre os dados logtransformados resultou em um R^2 de 0,77 (N=356). A equação de potência na forma de $a_p(440) = A \times \text{Chla}^{B}$ ajustada ao nossos dados, em que os parâmetros A e B são obtidos do ajuste, descreveu bem nossos dados, e foi comparada com as relações derivadas por outros autores para grandes bases de dados (e.g., Bricaud *et al.,* 1998; Morel *et al.,* 2006). Nossos valores de $a_p(440)$ são em média 75% acima do valores fornecidos pala equação de Bricaud *et al.* (1998), B98, a partir de Chl*a*, enquanto que 19% comparando-se com Morel *et al.* (2006), M06, que derivou sua equação especificamente para águas de Caso 1 com alta Chl*a*.

A tendência de nossos dados serem sistematicamente maiores que as tendências gerais para uma dada Chl*a* como observado para $a_p(440)$ também foi verificada para $K_{bio}(440)$ ($K_{bio}(440) = K_d(440) - K_w(440)$; Morel e Maritorena, 2001). Em média,

nossos valores de $K_{bio}(440)$ foram 26% maiores que o esperado pela equação de M07. Isto está de acordo com o fato de $K_d(\lambda)$ (atenuação difusa da luz ao longo da coluna d'água) ser essencialmente devido à absorção da luz pelo material presente (particulado e dissolvido) e, em muito menor grau, devido ao retro-espalhamento (Gordon, 1989), pelo menos quando o fitoplâncton é o componente dominante sobre o material particulado. Isso é o reflexo de que o coeficiente de retro-espalhamento de partículas orgânicas é muito menor em magnitude que o coeficientes de absorção.

Como mostrado na Seção 3.2. e Artigo 2, os coeficientes de absorção da luz pelo fitoplâncton, $a_{ph}(\lambda)$, também estiveram acima de tendências gerais para uma dada Chl*a* (Bricaud *et al*., 1995, Bricaud *et al*., 2004). Estudos anteriores atribuíram desvios sistemáticos com respeito às tendências gerais de $a_{ph}(\lambda)$ *vs.* Chl*a* principalmente como resultado de diferentes proporções entre partículas não-algais e o fitoplâncton (e.g., Morel *et al.*, 2007 e referências inclusas). Nossos resultados, no entanto, indicam que as partículas não-algais não são importantes em modificar as relações entre as propriedades ópticas inerentes e a Chl*a*, na qual geralmente as parametrizações incorporadas por tradicionais modelos bio-óticos se baseiam, nas águas da QPA. Na Seção 3.2, é demostrado que a maior parte da variação de $a_{ph}(\lambda)$ como função de Chl*a* é devido a variações no tamanho celular dominante do fitoplâncton.

Os resultados aqui apresentados contribuíram para a caracterização da variabilidade de propriedades ópticas para águas de Caso 1 com alta Chl*a*, como recomendado por Morel *et al.* (2006), através de dados das florações ao longo da quebra de plataforma Argentina. Os desvios sistemáticos em ambos $a_p(\lambda)$ e $K_d(\lambda)$ para uma dada Chl*a* em comparação com as tendências gerais observados aqui puderam ser atribuídos a variações no tamanho dominante do fitoplâncton. Isso foi melhor

discutido no Artigo 2.

3.1.2. Relação entre a concentração de clorofila-a e os coeficiente de atenuação da luz pelas partículas

Nesta seção investigou-se o potencial em parametrizar o coeficiente de atenuação da luz pelas partículas (soma do coeficiente de absorção e espalhamento), $c_p(660)$, como função da Chl*a*. A dependência encontrada nos nossos dados foi comparada com a relação derivada por Loisel e Morel (1998), LM98, para águas superficiais. Nossos menores valores de $c_p(660)$ para menores Chl*a* (PATEX 3, 6 e 7) estão de acordo geral com LM98 (Figura 4 - Apêndice 1), porém para maiores Chl*a* (PATEX 2 e 4), nossos valores de $c_p(660)$ são notadamente inferiores em relação à equação de LM98 para uma dada Chl*a*.

Similarmente para os coeficientes de absorção, um modelo não-linear geralmente descreve adequadamente a relação entre $c_p(660)$ e Chl*a* e uma função de potência, $c_p(660)=A \times \text{Chl}a^{B}$, ajustada aos nosso dados proveu um coeficiente A e um expoente B de 0,343 e 0,37 respectivamente, ou seja $c_p(660) = 0{,}343 \times \text{Chl}a^{0{,}37}$, considerando-se todo o conjunto de dados. Devido à grande dispersão dos dados, o coeficiente de determinação computado entre os dados logtransformados foi comparativamente baixo (R^2=0,60, p<0,0001 N=790). Note que parte da dispersão (expoente de 0,37) é devido às diferenças sistemáticas entre os cruzeiros (Figura 4 – Apêndice 1), que também foram notadas para $a_p(440)$, embora em menor grau (Figura 3a – Apêndice 1). De um modo geral, os coeficientes específicos de atenuação (ou espalhamento) em 660 nm (i.e., normalizados por Chl*a*), $c^*_p(660)$, foram relativamente maiores e menores para um dada Chl*a* para os cruzeiros PATEX 3, 6 e 7, e para o cruzeiros

PATEX 2 e 4, respectivamente. Altos valores de $c^*_p(660)$ que se distanciam da maioria dos dados e com maior dispersão foram verificados durante o cruzeiro PATEX 5, associados a uma floração de cocolitoforídeos (Garcia *et al.*, 2011).

Diferenças entre os cruzeiros para os coeficientes de espalhamento, $c_p(660)$, e absorção, $a_p(440)$, são semelhantes (Figura 3a e Figura 4 - Apêndice 1). Na verdade, como apresentado na Seção 3.2 e no Artigo 2, uma forte relação entre $b^*_p(660)$, e o coeficiente específico de absorção do fitoplâncton, $a_{ph}^*(440)$, foi verificada. De fato, os resultados da Seção 3.2 e Artigo 2 mostram relações estatísticas diferentes entre para $a_{ph}(440)$ e Chl*a*, de acordo com amostras dominadas por nano-fitoplâncton ou micro-fitoplâncton. Tais diferenças refletiram similarmente as diferenças aqui verificadas entre os cruzeiros para $c_p(660)$ e Chl*a*.

Assim, variações em $c_p(660)$ *vs.* Chl*a* para as águas da QPA não parecem refletir ajustamentos fisiológicos como proposto por Beherenfeld e Boss (2003), mas sim diferenças no tamanho dominante celular do fitoplâncton (ver Seção 3.2. e Artigo 2). Considerando que as relações existentes entre $c_p(660)$ e a biomassa de fitoplâncton podem ser conceitualmente estendida para os coeficientes de retroespalhamento das partículas, $b_{bp}(\lambda)$ (Westberry *et al*., 2010), a tendência de $c_p(660)$ *vs.* Chl*a*, à princípio, poderia estender-se a aplicações para os modelos semi-analíticos aplicados aos dados de reflectância, que depende de $b_b(\lambda)/a(\lambda)$. No entanto, a grande variabilidade na estrutura do tamanho das células, que depende do estágio da comunidade fitoplanctônica durante as florações, torna difícil estabelecer uma relação única de dependência entre Chl*a* e o coeficiente de espalhamento (ou retro-espalhamento) nessas águas.

3.1.3. Variabilidade nos espectros de reflectância do sensoriamento remoto

Os espectros da reflectância do sensoriamento remoto, $R_{rs}(\lambda)$, coletados durante os seis cruzeiros PATEX apresentaram grande variabilidade, tanto em magnitude quanto em comportamento (ou formato) espectral (Figura 5- Apêndice 1). Para classificar estes espectros, uma Análise Hierárquica de Cluster (HCA) foi aplicada sobre todos os espectros de $R_{rs}(\lambda)$. A aplicabilidade deste método em classificar espectros de $R_{rs}(\lambda)$ foi demonstrada por Lubac e Loisel (2007) para as águas costeiras da Europa. Por causa do ruído encontrado nas medidas na porção espectral do vermelho em vários espectros, apenas o intervalo entre 400 a 600 nm foi considerado neste trabalho. Antes da aplicação da *HCA*, cada espectro de $R_{rs}(\lambda)$ foi normalizado pelo seu próprio valor médio entre 400 e 600 nm, $nR_{rs}(\lambda)$, para minimizar o efeito da magnitude e realçar a variabilidade devido ao comportamento espectral.

O número de três classes foi pré-definido por meio de visualização de um dendrograma (não mostrado). As três classes de $nR_{rs}(\lambda)$ construídas pelo método de *HCA* estão ilustrados na Figura 6 - Apêndice 1. Os espectros absolutos de $R_{rs}(\lambda)$, i.e., sem normalização, referentes a cada classe também estão mostrados.

O agrupamento obtido pela *HCA* foi explicado principalmente pelos intervalos de variação de Chl*a*, com as menores concentrações correspondentes à Classe 1 (média de 0,86 ± 0,51 mg m^{-3}), seguido pela Classe 2 com concentrações intermediárias (média de 2,42 ± 1,62 mg m^{-3}) e a Classe 3 com as maiores Chl*a* (média de 8,40 ± 3,96 mg de m^{-3}). Quanto aos períodos de amostragem, a Classe 1 agrupou a maioria dos espectros de $R_{rs}(\lambda)$ medidos durante o PATEX 3, alguns durante os PATEX 2, 4 e 6 e todos os espectros medidos nos PATEX 5 e 7. A Classe 2 contém espectros de $R_{rs}(\lambda)$ associados às poucas estações com moderada Chl*a* durante o PATEX 2, e aquelas com mais altas concentrações medidas no PATEX 3, concentrações

intermediárias ocorridas durante o PATEX 4, e as concentrações elevadas durante o PATEX 6 e uma estação única do PATEX 5, que diferiu na comunidade fitoplanctônica das demais do mesmo cruzeiro por não ter o cocolitoforídeo como grupo dominante, mas diatomáceas (Garcia *et al.,* 2011). A Classe 3 agrupou apenas espectros medidos durante as massivas florações de primavera (PATEX 2 e 4).

Apesar de não termos dados de absorção de luz pela *modc*, sua contribuição sobre a variabilidade de $R_{rs}(\lambda)$ não parece considerável, já que não vemos diminuição notável em $R_{rs}(\lambda)$ nos menores comprimentos de onda incluindo a faixa UV (não mostrado), pois a absorção pela *modc* é importante ao redor de 440 nm e aumenta exponencialmente em direção ao UV espectral.

3.1.4. Avaliação do desempenho de algoritmos empíricos para estimar a concentração de clorofila-a

A análise anterior mostrou que os espectros de $R_{rs}(\lambda)$ medidos na QPA podem ser classificados de acordo com as características espectrais que resultam essencialmente devido à variabilidade em Chl*a*. Nesta seção, investigamos o desempenho de algoritmos (ou modelos) bio-ópticos empíricos, que se baseiam na relação entre razões de $R_{rs}(\lambda)$ nas faixas azul e verde espectrais, e que são aplicados rotineiramente sobre reflectância de imagens de satélites obtidas pelas agências espaciais (ex. NASA) para estimar Chl*a* nos oceanos do espaço. Os modelos empíricos utilizados neste trabalho foram os OC2v6, OC4v6 e OC3v6, onde 'v6' indica a versão mais atual. Os dois primeiros algoritmos foram desenvolvidos para os sensor SeaWiFS e o último para o sensor MODIS, onde os número 2, 3 e 4 indicam o número de bandas de $R_{rs}(\lambda)$ consideradas por cada modelo, como indicadas na Figura 7 - Apêndice 1. A

Chl*a* foi estimada a partir de nossas medições de $R_{rs}(\lambda)$ *in situ* durante todos os cruzeiros através dos três modelos, e então comparada com a Chl*a* superficial medida *in situ*. A Figura 7 - Apêndice 1, representa nossos valores de Chl*a* medidos como uma função das razões de $R_{rs}(\lambda)$ correspondentes a cada um dos três algoritmos empíricos, onde as curvas representam cada algoritmo. A Tabela 3 – Apêndice 1 apresenta os resultados estatísticos (ver descrição da Tabela 3 para definições) da comparação entre a Chla medid*a* e a estimada pelos modelos.

A fim de investigar se o desempenho dos modelos empíricos para estimar Chl*a* partir de razões de reflectância pode estar associado a variações no formato espectral de $R_{rs}(\lambda)$ e, consequentemente, aos intervalos de variação em Chl*a* (seção anterior), os mesmos modelos empíricos usados para estimar Chl*a* foram aplicados separadamente a cada classe previamente determinado pelo *HCA* (Figura 7 e Tabela 3 – Apêndice 1).

Em relação ao algoritmo OC4v6 (o mais amplamente utilizado devido aos melhores resultados por utilizar maior número de bandas de $R_{rs}(\lambda)$), erros maiores (*RPD*=31,80%; *APD*=51,57%) foram computados para a classe com moderada Chl*a* (Classe 2), mas os resultados para as classes com menor (Classe 1) e maior Chl*a* (Classe 3) revelam relativamente bom acordo entre os valores de Chl*a* medidos e estimados (*RPD*=-2,63%, *APD*=30,82%; *RPD*=6,30%, *APD*=50,21%, respectivamente, Tabela 3 – Apêndice 1). Note que o desempenho menos satisfatório do OC4v6 para a Classe 2 é parcialmente explicado pela faixa mais estreita de Chl*a* estimada (0,97 a 4,69 mg de m^{-3}), em comparação a uma grande variação na Chl*a* medida para esta classe (0,74-7,96 mg m^{-3}). Os desempenhos de ambos OC2v6 e OC3v6 foram sempre menos satisfatórios quando comparado com OC4v6 (Tabela 3 e Figura 7 – Apêndice 1).

3.1.5. Relação entre os erros dos algoritmos empíricos e as propriedades ópticas inerentes

Os algoritmos bio-ópticos empíricos utilizados para estimar Chl*a* se baseiam em relações estatísticas entre a Chl*a* e razões de bandas azuis e verdes de $R_{rs}(\lambda)$. Na verdade porém, as magnitudes e formas dos espectros de $R_{rs}(\lambda)$ dependem diretamente dos coeficientes de retro-espalhamento (de partículas) e inversamente dos coeficientes de absorção (de partículas e que, por sua vez, refletem as variações na concentração e composição dos componentes ópticos. Esta seção tem como objetivo investigar como variações nos coeficientes de absorção e espalhamento, em termos de normalização com Chl*a* (coeficientes específicos), podem influenciar o desempenho dos modelos empíricos para estimar Chl*a* nas águas da Patagônia. Para tanto, foram considerados os dados de $R_{rs}(\lambda)$ medidos *in situ*. Assim, esta análise não inclui qualquer incerteza atribuída a correção atmosférica ou acurácia na medida de $R_{rs}(\lambda)$ pelo satélite. Apenas o modelo OC4v6 foi considerado aqui, devido ao seu melhor desempenho quando aplicado ao nosso conjunto de dados (Seção 3.1.4).

A Figura 8 – Apêndice 1 mostra a dependência dos erros relativos nas estimativas de Chl*a* a partir do modelo OC4v6 como função da Chl*a* medida, de $a^*_{ph}(440)$, e de $b^*_p(660)$ (sendo os últimos $a_{ph}(440)$ e $b_p(660)$ normalizados por Chl*a*, em m^2 (mg *chla*)$^{-1}$). Observa-se os valores de *RE*, onde *RE*=100*(Chl*a* estimada–Chl*a* medida)/Chl*a* medida, apresentam grande dispersão ao longo do intervalo de Chl*a* (Figura 8a), mas relações significativas (α=95%) foram observadas quando consideramos cada classe de $R_{rs}(\lambda)$ separadamente (p<0,001 para Classe 1, Classe 2 e Classe 3), com um tendência geral de subestimativa de Chl*a* à medida que a Chl*a* aumenta. Da mesma forma para Chl*a*, foram encontradas correlações significativas entre *RE* e $a^*_{ph}(440)$ (p<0,001 para Classe 1, Classe 2 e Classe 3) e $b^*_p(660)$ (p=0,02

para a Classe 1 e p<0,0001 para Classe 2 e Classe 3) para as três classes de $R_{rs}(\lambda)$, com uma clara tendência de sobre-estimativa da Chl*a* estimada conforme o aumento de ambos $a^*_{ph}(440)$ e $b^*_{p}(660)$ (Figuras 8b e 8c – Apêndice 1).

3.1.6. Comparação com produtos estimados por satélite

Os modelos bio-ópticos semi-analíticos têm o potencial de melhorar a estimativa da Chl*a* e dos coeficientes absolutos de absorção e retroespalhamento para cada componente óptico, pois se baseiam na relação teórica entre esses coeficientes e a reflectância (Gordon *et al.,* 1988). Mesmo nesses casos porém, algumas aproximações devem ser assumidas. A parte empírica do modelo QAA extrapola o comportamento espectral de $b_b(\lambda)$ e assume razões entre bandas para $a(\lambda)$ (Lee *et al.*, 2002), enquanto o modelo GSM assume valores médios dos coeficientes específicos de absorção e de retroespalhamento do fitoplâncton, ou seja, coeficientes normalizados por Chl*a* e comportamentos espectrais exponenciais para os componentes não-algais (Maritorena *et al.*, 2002). Por exemplo, o valor médio do coeficiente específico de absorção do fitoplâncton, $a^*_{ph}(\lambda)$, incorporado atualmente pelo software *SeaDAS* (NASA) e considerado para nossas estimativas por satélite é 0,0558 m^2 (mg *chla*)$^{-1}$ em 443 nm (Maritorena *et al.*, 2002). Este coeficiente, no entanto, pode ser altamente variável devido a variações no tamanho de células do fitoplâncton e da composição dos pigmentos. Como mostrado neste estudo, o intervalo de variação de $a^*_{ph}(443)$ foi de 0,0180 a 0,2478, média de 0,0721 m^2 (mg *chla*)$^{-1}$, para o nosso conjunto de dados.

Nesta seção, avaliou-se o desempenho de modelos semi-analíticos em estimar os coeficientes de absorção da luz pelo fitoplâncton nas águas da QPA através de imagens de satélite, usando modelos embutidos no software *SeaDAS* e, portanto, com

comportamentos espectrais e razões entre bandas de entrada fixos.

Aqui são mostrados os resultados de comparação entre os coeficientes de absorção do fitoplâncton medidos *in situ* com os estimados pelos modelos semi-analíticos GSM e QAA através de satélite. Também são comparados os valores de Chl*a* medidos *in situ* com os estimados por satélite pelos três algoritmos empíricos (OC2v6, OC4v6, e OC3v6) e o modelo semi-analítico GSM. O número total de dados de Chl*a* e de $a_{ph}(\lambda)$ superficiais durante os seis cruzeiros foi de 176. Devido à cobertura de nuvens e após a aplicação dos critérios de seleção da NASA para diferença temporal (± 3 h) entre a medida *in situ* e a passagem do satélite, os pontos de comparação foram reduzidos a ± 30, dependendo da disponibilidade do dado satelital, do algoritmo aplicado e do comprimento de onda considerado no caso de $a_{ph}(\lambda)$. A avaliação do desempenho dos modelos aplicados aos dados de satélite considerou as mesmas estatísticas como na seção 3.1.4: R^2, inclinação da reta e intercepto computados entre os valores medidos e estimados logtransformados, *RPD* e *APD*. Os resultados estatísticos estão apresentados nas respectivas figuras (Figuras 9 a 11 – Apêndice 1).

A dispersão entre a Chl*a* medida e estimada pelos algoritmos empíricos (Figura 9a a 9c – Apêndice 1) é da mesma ordem daquela encontrada quando da aplicação dos modelos aos dados de $R_{rs}(\lambda)$ medidos *in situ* (R^2=0,66, 0,75 e 0,77 para OC2v6, OC3v6 e OC4v6, respectivamente). A tendência de sobre-estimativa da Chl*a* ao considerar ambos os conjuntos de dados, com *RPD* sempre positivo (Tabela 3 e Figura 9 – Apêndice 1 para dados de $R_{rs}(\lambda)$ *in situ* e de satélite, respectivamente) é verificada. Diferenças entre a Chl*a* medida e estimada foram semelhantes através do uso do modelo semi-analítico GSM (Figura 9d) e dos modelos empíricos OC4v6 e OC3v6, e a tendência de sobre-estimativa se verificou também para o modelo GSM .

As comparações entre os coeficientes $a_{ph}(\lambda)$ medidos *in situ* são mostrados nas

Figuras 10 e 11 para certos comprimentos de onda nas faixas espectrais azul e verde, para os modelos GSM e QAA, respectivamente.

Em geral, o algoritmo QAA mostrou melhor desempenho para estimar $a_{ph}(\lambda)$ a partir de dados de satélite, com os pontos mais próximos a linha 1:1 (ou inclinações próximas a 1), quando comparados com os dados derivados pelo GSM. O maior coeficiente de determinação (R^2=0,65) foi observado a 469 nm (Figura 1.11c). Os erros foram consideravelmente elevados em 555 nm (*RPD*=268% e *APD*=279%) e máxima divergência entre os dados *in situ* e de satélite foi observada a 645 nm (R^2 de 0,045), com uma grande sobre-estimativa (*RPD* e *APD* = 509%, não mostrado).

3.2. Resultados referentes ao Objetivo Específico 4

Artigo 2: *Variability in light absorption and scattering of phytoplankton in Patagonian waters: Role of community size structure and pigment composition*, publicado.

3.2.1. Concentração de clorofila-a e classes de tamanho do fitoplâncton

Os intervalos de variação da $[Chla]_F$ em superfície durante cada cruzeiro PATEX estão apresentados na Tabela 2 – Apêndice 2. Nas profundidades do pico de fluorescência da clorofila-*a*, a $[Chla]_F$ variou de 0.3 a 24 mg m^{-3} (não mostrado) e foram ligeiramente maiores que em superfície. A variabilidade em $[Chla]_F$ refletiu as diferenças no período e na localização das amostragens entre os cruzeiros.

Os resultados a seguir descritos podem ser visualizados na Figura 2 – Apêndice 2, que mostra a contribuição percentual das três classes de tamanho (pico-, nano- e

micro-fitoplâncton) para a $[Chla]_F$ total como função da $[Chla]_F$ total, para cada cruzeiro. A $[micro\ Chla]_F$ foi a fração dominante sobre a $[Chla]_F$ total apenas durante o PATEX 2 (Figura 2a – Apêndice 2). Entre a primavera de 2006 (PATEX 2) e início do outono 2007 (PATEX 3) uma mudança na dominância de tamanho algal foi observada, já que a $[pico + nano\ Chla]_F$ contribuiu, em média, com 90% sobre a $[Chla]_F$ total durante o PATEX 3.

Durante o cruzeiro seguinte de primavera em 2007 (PATEX 4), a fração $[nano\ Chla]_{F/HPLC}$ dominou a $[Chla]_F$ total (Figura 2c – Apêndice 2). A fração $[micro\ Chla]_F$ também contribuiu de forma importante, embora raramente dominante sobre a $[Chla]_F$ total (contribuição média de 26 ± 14%; Figura 2c – Apêndice 2). Durante a floração de cocolitoforídeos amostrada no PATEX 5 (janeiro de 2008), $[nano\ Chla]_{F/HPLC}$ foi a principal fração que controlou a $[Chla]_F$ total, com uma contribuição média de 72%, embora $[micro\ Chla]_F$ tenha contribuído substancialmente para a $[Chla]_F$ total em algumas amostras (Figura 2d – Apêndice 2). Situação similar ocorreu durante o PATEX 6, quando o $[nano\ Chla]_{F/HPLC}$ também foi a fração principal (contribuição média de 75%) ainda que com contribuição significativa de $[micro\ Chla]_F$ em várias amostras (Figura 2e). Para a maioria das amostras do PATEX 7, variações tanto em $[nano\ Chla]_{F/HPLC}$ e $[micro\ Chla]_F$ foram responsáveis pelas variações em $[Chla]_F$ total (Figura 2.2f). Embora $[pico\ Chla]_{HPLC}$ tenha sido geralmente pouco variável e com contribuição pequena sobre a $[Chla]_F$ total (Figura 2.2), a contribuição média de $[pico\ Chla]_{HPLC}$ para $[Chla]_F$ total foi de 28% em PATEX 7 (Tabela 2 – Apêndice 2). A contribuição de $[pico\ Chla]_{HPLC}$ sobre $[Chla]_F$ foi de cerca de 90% quando a $[Chla]_F$ total foi relativamente baixa (~ 1 mg m^{-3}; Figura 2f – Apêndice 2).

3.2.2. Coeficientes de absorção da luz pelo fitoplâncton

Para a análise apresentada nesta seção e na próxima, foram excluídos 37 espectros de absorção do fitoplâncton, $a_{ph}(\lambda)$, do total de 226 espectros. Os espectros excluídos apresentaram um pico de absorção atípico, em torno de 460 nm, e são discutidos separadamente na Seção 3.2.5. Estes espectros foram divididos em dois grupos de acordo com a dominância de tamanho algal: o grupo dominado pelo nano-fitoplâncton (N-grupo) com 151 amostras e pelo micro-fitoplâncton (M-grupo) com 38 amostras.

A máxima absorção de luz pelo fitoplâncton se dá por volta de 440 nm, e um segundo pico de menor magnitude ocorre ao redor de 676 nm, o que corresponde ao espectro de absorção do principal pigmento fitoplanctônico, a clorofila-*a*. A Figura 3 – Apêndice 2 revela ampla variação de $a_{ph}(440)$ e $a_{ph}(676)$, de 0,013 a 0,66 e de 0,008 a 0,42 m^{-1}, respectivamente, consequência da grande variabilidade observada em $[Chla]_F$ (Figura 3 – Apêndice 2). Os coeficientes específicos de absorção do fitoplâncton nesses comprimentos de onda (i.e., $a_{ph}(440)$ e $a_{ph}(676)$ normalizados por $[Chla]_F$ e indicados como $a^*_{ph}(440)$ e $a^*_{ph}(676)$) variaram entre 0,018 e 0,173 e entre 0,009 e 0,046 m^2 mg $chla^{-1}$, respectivamente (onde *chla* é a abreviação da palavra clorofila-*a*). Esses coeficientes normalizados indicam a eficiência da absorção de luz pelo fitoplâncton por unidade de clorofila-*a*. Um teste-t (α=99%) indicou que os coeficientes específicos foram significativamente maiores para o Grupo-N do que para o Grupo-M, em concordância que células menores apresentam uma maior eficiência de absorção de luz por unidade de clorofila-*a*, devido a um menor efeito "pacote". Assim, relações empíricas entre $a_{ph}(\lambda)$ e $[Chla]_F$ foram obtidas separadamente para cada grupo. A função de potência na forma $a_{ph}(\lambda)=A\,[Chla]_F^{B}$, em que os parâmetros *A* e *B* representam o melhor ajuste pela regressão de mínimos quadrados, descreveu bem a dependência de $a_{ph}(\lambda)$ pela $[Chla]_F$ nos nossos dados. Os

resultados desta análise de regressão são apresentados para 440 e 676 nm, na Tabela 3 e na Figura 3 Apêndice 2.

Para comparação com tendências já observadas, a Figura 3 – Apêndice 2 mostra também as relações entre $a_{ph}(\lambda)$ e Chl*a* obtidas por Bricaud *et al.* (1995), Bricaud *et al.* (2004), Devred *et al.* (2006), e Brewin *et al.* (2011b), com base em grandes conjuntos de dados coletados em diferentes regiões do oceano global. Estas relações são referidas como B95, B04, D06 e B11, respectivamente. Como exemplo, nossas tendências foram comparadas quantitativamente com os resultados dos dois estudos de Bricaud *et al*. As linhas que representam o melhor ajuste entre o $a_{ph}(\lambda)$ e $[Chla]_F$ tanto do N-grupo quanto do M-grupo apresentam valores consideravelmente mais elevados de $a_{ph}(440)$, para uma dada Chl*a* (em média, por um factor de 2), em comparação com a relação de B95 (Figura 3a – Apêndice 2). A relação de B04, que se baseia em um conjunto de dados diferente do que de B95, está mais próximo de nossos dados apesar das inclinações das retas serem consideravelmente diferentes. As curvas de D06 e B11 se encontram entre as B04 and B95. As diferenças entre as nossas relações e B95 são menores na faixa espectral vermelha, em 676 nm (Figura 2.3b). No entanto, a relação B95 ainda provê valores sistematicamente mais baixos de $a_{ph}(676)$ para uma dada Chl*a* do que nossos dados. A absorção de luz por outros pigmentos é muito baixa nesse comprimento de onda e portanto dominada pela Chl*a* (ver Figura 1 em Bricaud *et al.,* 2004).

As comparações acima sugerem que a magnitude de $a_{ph}(\lambda)$ a uma dada concentração de clorofila-*a* e, consequentemente, os valores de $a^*_{ph}(\lambda)$, são consideravelmente mais elevados para as águas da Patagonia em relação aos dados de obtidos em distintas regiões oceânicas do planeta. Este resultado sugere que o tamanho das células do fitoplâncton na região estudada é geralmente menor do que

em outras regiões oceânicas para uma mesma concentração de clorofila-*a*. A principal evidência para esta conclusão baseia-se nas nossas observações na faixa vermelha do espectro, em que as variações em um $a^*_{ph}(676)$ podem ser atribuídas principalmente a alterações no efeito do pacote e, portanto, no tamanho celular do fitoplâncton.

Esta suposição é reforçada pelas contribuições do micro-fitoplâncton (em termos de $[\text{micro Chla}]_{HPLC}$) terem sido superestimadas através da abordagem por pigmentos diagnósticos (Seção 2.4) quando comparadas às contribuições de $[\text{micro Chla}]_F$ obtidas pelo fracionamento físico da $[\text{Chla}]_F$. Isso é provavelmente explicado pelo fato de que a abordagem para estimar a composição taxonômica através de pigmentos diagnósticos estimados por HPLC baseia-se na premissa de que as diatomáceas pertencem a classe de tamanho do microplâncton e diatomáceas menores não pertencentes a esta classe de tamanho, e se presentes, serão incorretamente classificadas como micro-fitoplâncton. De fato, a análise por microscopia de amostras dos cruzeiros PATEX (de Souza, 2012) indicou que as florações do fitoplâncton nas águas da QPA são tipicamente dominadas por diatomáceas inclusas na classe de tamanho do nanoplâncton, embora ocasionalmente diatomáceas pertencentes ao microplâncton possam dominar em alguns casos (e.g., PATEX 2).

3.2.3. *Absorção de luz pelo fitoplâncton e o índice de tamanho celular*

Os espectros de absorção de luz fitoplâncton normalizados pelo valor médio de cada espectro, indicado como $a_{<ph>}(\lambda)$, são mostrados na Figura 2.4 – Apêndice 2 separadamente para os Grupo-N (dominado pelo nano-fitoplâncton) e Grupo-M (dominado pelo micro-fitoplâncton). Estes espectros médios foram calculados a partir dos valores compreendidos entre 400 e 700 nm. O efeito pacote é mais evidente para

os espectros do Grupo-M, que apresentam valores mais baixos da razão entre os picos de absorção azul (~ 440 nm) e vermelho (~ 676 nm) do que os espectros de Grupo-N (i.e., espectros mais achatados). Este resultado é consistente com observações anteriores da litaratura e especificamente com o estudo de Ciotti *et al*. (2002), no qual a variabilidade no formato (ou comportamento) espectral do coeficiente de absorção pelo fitoplâncton entre 400 e 700 nm pôde ser quantificada e explicada em grande parte pelo tamanho celular do grupo fitoplanctônico dominante.

No presente estudo, foi estimado o índice de tamanho celular do fitoplâncton, S_f, a partir de cada espectro de $a_{<ph>}(\lambda)$ (Ciotti *et al.*, 2002). Menores valores de S_f refletem menores razões entre os picos de absorção no azul (~440 nm) e no vermelho (~676 nm) e, portanto, espectros são mais achatados, ao passo que maiores valores de S_f indicam maiores razões entre esses picos. Os valores de S_f variaram entre 0,04 e 0,81 e os espectros de $a_{<ph>}(\lambda)$ foram geralmente bem reconstruídos quando comparado com os espectros de $a_{<ph>}(\lambda)$ originais, com R^2>0,92 para a maioria dos casos. A média (± desvio padrão) dos valores de S_f foram 0,52 (± 0,21) e 0,33 (± 0,14) para o N-Grupo e M-grupo, respectivamente. A maior variabilidade observada para o Grupo-N reflete a grande variação no tamanho das células que compreendem essa fração de tamanho do nanoplâncton (2-20 μm).

Uma tendência clara de diminuição nos coeficientes específicos de absorção do fitoplâncton, i.e., normalizado pela Chl*a*, $a^*_{ph}(\lambda)$, com o aumento da $[Chla]_F$ é observada na Figura 5 – Apêndice 2, o que é consistente com a literatura (e.g., Dmitriev *et al*., 2009 e referências inclusas). Esse padrão reflete a grande variação na biomassa do fitoplâncton, o efeito do pacote, e a composição de distintas espécies em nossas amostras. Como o índice de tamanho celular do fitoplâncton, S_f, varia dentro de um continuum de tamanho, i.e., de 0 (efeito pacote mais forte) a 1 (efeito pacote

mais fraco), na mesma figura estão mostrados também os valores de S_f a fim de investigar se houve variações em $a^*_{ph}(\lambda)$ ao longo do aumento em $[Chla]_F$ e para uma dada $[Chla]_F$.

Nossos resultados indicam a concordância entre os valores de S_f e a variabilidade em $a^*_{ph}(440)$ e $a^*_{ph}(676)$, como função da $[Chla]_F$. Em geral, valores baixos de $[Chla]_F$ e altos de $a^*_{ph}(440)$ e $a^*_{ph}(676)$, correspondem a altos valores de S_f (i.e., menor tamanho celular do fitoplâncton). Por outro lado, quanto maior a $[Chla]_F$, menores são os valores de $a^*_{ph}(440)$ e $a^*_{ph}(676)$ e de S_f (i.e., células maiores). Em particular, os valores mais baixos de S_f ($\leq 0,2$) correspondem a $[Chla]_F$ maior que 10 mg de m^{-3}. Apesar dessa tendência geral, uma grande variação em $a^*_{ph}(\lambda)$ é observada para uma dada $[Chla]_F$, e um dado valor de um $a^*_{ph}(\lambda)$ pode estar associado a uma grande variação em $[Chla]_F$.

Estes resultados indicam que variações em S_f ao longo do comportamento geral de decréscimo de $a^*_{ph}(\lambda)$ com o aumento em $[Chla]_F$ refletem variações no efeito pacote associados com variações no tamanho dominante do fitoplâncton, assim como também variações na concentração e composição de pigmentos acessórios. Nossos resultados apontam para a dificuldade em classificar as comunidades do fitoplâncton em intervalos discretos de tamanho (ex., pico-, nano-, e micro-fitoplâncton) para fins de modelagem bio-óptica. Tais dificuldades resultam do fato de que as comunidades fitoplanctônicas consistem de muitas espécies e de diferentes tamanhos, e que dentro dos intervalos discretos de tamanho, existe ainda a variabilidade de tamanho celular e composição de pigmentos.

3.2.4. Relação entre o coeficiente específico de absorção do fitoplâncton e a composição de pigmentos

Nesta seção, iremos considerar $[Chla]_{HPLC}$ e não $[Chla]_F$ e assim, o número de dados de Chl*a* foi reduzido de 236 para 132.

Nessa seção foram investigadas relações entre a variabilidade nos coeficientes específicos de absorção do fitoplâncton, $a^*_{ph}(\lambda)$, e razões de pigmentos. Aqui, $a^*_{ph}(\lambda)$ consiste nos coeficientes de absorção do fitoplâncton, $a_{ph}(\lambda)$, normalizados por $[Chla]_{HPLC}$, e não por $[Chla]_F$ como anteriormente. Apenas 12 amostras do M-grupo são incluídas nesta análise, porque os dados de HPLC se limitam aos cruzeiros PATEX 4 a 7, portanto indisponíveis para o PATEX 2, quando ocorreu a mais importante dominância do micro-fitoplâncton.

A Figura 2.6 – Apêndice 2 mostra que aumentos nas razões $[PSC]:[Chla]_{HPLC}$, $[PPC]:[Chla]_{HPLC}$, $[Hexa]:[Chla]_{HPLC}$ e $[Chlb]:[Chla]_{HPLC}$ foram acompanhados por aumentos em $a^*_{ph}(440)$, sendo isso bem pronunciado para $[Hexa]:[Chla]_{HPLC}$ (Figura 6c) e $[Chlb]:[Chla]_{HPLC}$ (Figura 6d). Padrões muito semelhantes foram observadas para $a^*_{ph}(676)$ (não mostrado), ainda que o efeito de pigmentos acessórios sobre a variabilidade em $a^*_{ph}(\lambda)$ seja muito pequena ou deprezível na faixa espectral do vermelho. Com efeito, uma relação robusta e direta foi encontrada entre os valores transformados em logaritmo de $a^*_{ph}(440)$ e $a^*_{ph}(676)$ (R^2=0,82, N=223, p<0,0001), embora a dispersão entre esses dados tenha aumentado com o aumento em $a^*_{ph}(\lambda)$ (não mostrado). Este resultado está de acordo com a expectativa de uma maior importância relativa dos pigmentos acessórios para menores concentrações de clorofila-*a* (e, portanto, maior $a^*_{ph}(\lambda)$) e/ou quando células menores são relativamente mais importantes do que maiores (ver revisão Bricaud *et al.*, 1995).

Os comportamentos semelhantes para ambos $a^*_{ph}(440)$ e $a^*_{ph}(676)$ como função das razões de pigmentos indica que a contribuição relativa dos carotenóides é inversamente correlacionada com o tamanho da célula e efeito pacote. Adicionalmente, os baixos valores de S_f (células maiores) foram relacionados com valores baixos de $a^*_{ph}(440)$ para as quatro razões de pigmentos (Figura 2.6). Estes resultados são consistentes com aqueles observados em análise anterior (Seção 3.2.3). Uma grande variação em $a^*_{ph}(440)$ esteve associada com uma estreita variação em [PSC]:$[Chla]_{HPLC}$.

Para $a^*_{ph}(440)$ *vs.* $[Hexa]:[Chla]_{HPLC}$, nota-se tanto uma menor variabilidade em torno da tendência central quanto menor sobreposição de pontos entre os intervalos de S_f (Figura 6c - Apêndice 2), em comparação com o observado para as demais razões de pigmentos apresentadas na Figura 6. O pigmento 19'-hexanoiloxifucoxantina é conhecido por ser típico do grupo fitoplanctônico *Phaeocystis* sp, e a concentração deste pigmento, [Hexa], em relação à Chl*a* foi sugerida como indicador da abundância deste grupo (Jeffrey e Wright, 1994). De fato, análises de microscopia e CHEMTAX (Mackey *et al.,* 1996) indicaram *Phaeocystis* sp como importante contribuinte para a biomassa total em todas as amostras dos cruzeiros PATEX (M.S. Souza e C.R. Mendes, comunicação pessoal, 2011). O tamanho destas células de fitoplâncton (2-6 μm) se encontra no limite inicial de tamanho do nanoplâncton (2-20 μm), sendo coerente que maiores valores de [Hexa] estejam tipicamente associados com maiores valores de S_f (Figura 6c – Apêndice 2). A relação positiva entre $a^*_{ph}(440)$ e a razão $[Chlb]:[Chla]_{HPLC}$ concorda com uma importância substancial de prasinofíceas encontrada durante todos os cruzeiros PATEX (de Souza, 2012), enquanto que a maior contribuição deste grupo fitoplanctônico foi encontrada durante

o PATEX 7. Neste, as amostras foram caracterizadas por maiores $a^*_{ph}(440)$, S_f ($0,4<S_f\leq0,6$) e razões [Chlb]:$[Chla]_{HPLC}$ (Figura 6d).

Os nossos resultados mostraram as co-variações entre o tamanho celular do fitoplâncton, a composição de pigmentos e os coeficientes específicos de absorção do fitoplâncton, $a^*_{ph}(\lambda)$, para as comunidades fitoplanctônicas da região Patagônica devido: 1) ao aumento de $a^*_{ph}(\lambda)$ com as razões entre pigmentos acessórios e Chl*a; e* 2) diminuição do tamanho celular do fitoplâncton com o aumento tanto de $a^*_{ph}(\lambda)$ quanto nas razões entre pigmentos acessórios e Chl*a*.

3.2.5. Relação entre o coeficiente de espalhamento da luz pelas partículas e tamanho celular do fitoplâncton

A dependência do coeficiente específico de espalhamento das partículas em 660 nm, $b^*_p(660)$ (i.e., $b_p(660)$ normalizado por $[Chla]_F$) da $[Chla]_F$ e sua relação com o tamanho celular do fitoplâncton foi investigada discriminando-se os intervalos do índice de tamanho celular, S_f, como o foi para os coeficientes específicos de absorção do fitoplâncton, $a^*_{ph}(\lambda)$. $b^*_p(660)$ variou amplamente entre 0,031-2,37 m^2 (mg *chla*)$^{-1}$ e mostrou uma clara dependência inversa com a $[Chla]_F$, qualitativamente muito semelhante ao que foi observado para $a^*_{ph}(\lambda)$ (Figura 5 – Apêndice 2).

A dispersão de $b^*_p(660)$ *vs.* $[Chla]_F$ e sua correspondência com a variabilidade em S_f (Figura 9 – Apêndice 2) é semelhante ao observado para $a^*_{ph}(\lambda)$. De fato, uma forte correlação positiva (R^2= 0,74, N=223, p<0,0001) entre $a_{ph}^*(\lambda)$ e $b^*_p(660)$ foi observada. Tanto $a_{ph}^*(\lambda)$ quanto $b^*_p(660)$ se mostraram inversamente proporcionais ao tamanho celular do fitoplâncton nas comunidades na QPA, de modo que um aumento do tamanho celular resulta em um decréscimo na eficiência tanto de

absorção quando de espalhamento de luz por unidade de pigmento, especificamente de Chl*a*, devido ao efeito pacote.

3.3. ***Resultados referentes aos objetivos específicos 5 e 6***

Artigo 3: "*Discrimination of phytoplankton assemblages in Patagonian waters from their absorption spectra*", em preparação.

A combinação de dados de concentração de pigmentos diagnósticos obtidas por HPLC (Seção 2.3.2), composição taxonômica por CHEMTAX (Seção 2.3.3) e espectros de absorção da luz pelo fitoplâncton, $a_{ph}(\lambda)$, resultou em 136 amostras disponíveis para discriminar o grupo taxonômico dominante do fitoplâncton a partir dos espectros de $a_{ph}(\lambda)$. Estas amostras correspondem aos cruzeiros de PATEX 4 a 7 e correspondem à superfície e *MCF*. A concentração de clorofila-*a* total (ver Seção 2.3.1), aqui indicada como TChl*a*, variou de 0,13 a 22,15 mg m^{-3}.

3.3.1. *Análise de agrupamento das razões de pigmentos diagnósticos do fitoplâncton*

A variabilidade nas razões de pigmentos diagnósticos (*DPR*, *diagnostic pigment ratios*), como organizada pela *HCA*, está ilustrada na Figura 2 – Apêndice 3. Através da visualização do dendograma criado a partir desses dados (não mostrado), 4 clusters foram assumidos, denominados a seguir como $C1_{diag}$ a $C4_{diag}$.

O cluster $C1_{diag}$ agrupou 38 amostras, onde 28 e 10 correspondem aos cruzeiros PATEX 4 e PATEX 6, respectivamente. As amostras deste cluster apresentaram a predominância de Fuco (Figura 2a – Apêndice 3), o que indica a dominância de

diatomáceas, confirmada por análise por microscopia (M. Souza, comunicação pessoal, 2011).

O cluster $C2_{diag}$ (Figura 2b – Apêndice 3) abrangeu 29 amostras (15 e 14 dos cruzeiros PATEX 5 e PATEX 6, respectivamente), sendo Hex o pigmento dominante (*DPR* média de 0,45), em associação com relativamente alta abundância de Chl*c3* (*DPR* média de 0,18) e Fuco (*DPR* média de 0,14). Neste cluster foram verificadas as maiores contribuições do pigmento Buta (*DPR* média de 0,08), um marcador inequívoco de haptofíceas. O pigmento Peri esteve presente em várias amostras, nas quais Hex ainda foi dominante (Figura 2b – Apêndice 3). Dados de *DPR* foram coerentes com os de microscopia, confirmando a dominância das haptofíceas, particularmente o cocolitoforídeo *Emiliania huxleyi,* presente em muitas amostras do PATEX 5 (Souza *et al.,* 2012), enquanto a haptofícea *Phaeocystis antarctica* foi abundante em várias amostras do PATEX 7 (M. Souza, comunicação pessoal, 2011).

A maioria das amostras (*N*=63) foram incluídas no $C3_{diag}$, com Fuco (*DPR* média de 0,31) e Hex (0,21) como os primeiro e segundo pigmentos diagnósticos mais importantes, respectivamente (Figura 2c – Apêndice 3). A contribuição acentuada de Chl*b* e Pras em todas as amostras do $C3_{diag}$ indica a presença das prasinofíceas. Assim, este cluster incluiu amostras com considerável abundância de diatomáceas, haptofíceas e prasinofíceas, mas sem grupo dominante (Figura 2c – Apêndice 3). Seis amostras tendo Peri como pigmento diagnóstico dominante (*DPR* média de 0,38) foram incluídas no cluster $C4_{diag}$, indicando inequivocamente a abundância de dinoflagelados com peridinina (Figura 2d – Apêndice 3).

3.3.2. *Análise de agrupamento sobre as contribuições dos grupos taxonômicos do fitoplâncton*

A técnica CHEMTAX aprimora a informação proveniente das razões de pigmentos diagnósticos, pois fornece a contribuição relativa dos grupos taxonômicos do fitoplâncton para a biomassa total em termos da concentração da clorofila-*a* total. Da mesma forma, 4 (quatro) clusters foram formados ao aplicar a análise HCA sobre os dados de contribuição relativa das classes taxonômicas fornecida pelo CHEMTAX ($C1_{CHEM}$ a $C4_{CHEM}$). Como esperado, os resultados da análise de cluster foram coerentes com a classificação anterior obtida com os dados de *DPR* (Figura 3 – Apêndice 3), com um índice cofenético computado de 0,69 entre os dendogramas de ambos os conjuntos de dados. Os dois primeiros clusters baseados nos dados do CHEMTAX agruparam 35 amostras dominadas por diatomáceas ($C1_{CHEM}$) e 39 por haptofíceas ($C2_{CHEM}$). O cluster $C3_{CHEM}$ separou amostras com contribuições importantes de diatomáceas, haptofíceas e prasinofíceas, sem dominância de algum grupo taxonômico ($C3_{CHEM}$, N=49).

3.3.3. Classificação das amostras com base no grupo taxonômico dominante

Nas seções anteriores, dados de pigmentos do fitoplâncton foram classificados através de análises de agrupamento utilizando pressupostos de similaridade em um conjunto de dados. Nesta seção, uma abordagem independente foi utilizada para classificar as amostras de acordo com o critério objetivo de dominância. O grupo taxonômico dominante do fitoplâncton foi definido com base na contribuição relativa de cada um dos grupos à biomassa total fornecida pela abordagem CHEMTAX. O

grupo foi considerado dominante quando sua contribuição à biomassa total foi maior que 50%.

Do total de 136 amostras, 38 amostras foram dominadas por diatomáceas, as quais 34 foram dominadas por diatomáceas-Chl*c1* e 3 por diatomáceas-Chl*c3* (ver Figura 3d – Apêndice 3). Uma única amostra foi classificada como dominada por diatomáceas através da soma das contribuições de diatomáceas-Chl*c1* (49,2%) e diatomáceas-Chl*c3* (33,3%). Haptofíceas foram predominantes em 40 amostras, incluindo todas as amostras agrupadas por $C2_{CHEM}$ e uma amostra por $C4_{CHEM}$ (Figura 3 – Apêndice 3). Três amostras indicaram a dominância de criptofíceas (1 amostra), dinoflagelados (1) e prasinofíceas (1) e todas as três incluíram $C3_{CHEM}$ (Figura 3c – Apêndice 3). Cincoenta e cinco (55) amostras não apresentaram dominância de algum grupo taxonômico. Assim, 58 amostras não foram dominadas por diatomáceas nem haptofíceas.

Esses resultados mostram que, apesar de sete grupos taxonômicos estarem presentes em nossas amostras (Figuras 2 e 3 – Apêndice 3), as florações do fitoplâncton na quebra de plataforma Argentina durante primavera e verão foram tipicamente dominadas por diatomáceas e haptofíceas. *Phaeocystis antarctica* é a espécie de haptofíceas dominante nessas águas, salvo quando condições ambientais específicas permitam a ocorrência de florações de cocolitoforídeos em dezembro (Balch *et al.,* 2011) e janeiro (e.g., PATEX 5) (*Garcia et al.,* 2011; *Souza et al.,* 2012).

Como o segundo item dessa seção e do Artigo 3 consiste na investigação do potencial em discriminar a dominância taxonômica do fitoplâncton com base nas características espectrais de $a_{ph}(\lambda)$, ou seja em termos de $\int a_{ph}(\lambda)$, cada amostra foi classificada como (1) dominada por diatomáceas, Dia-D (N=38) (2) dominada por haptofícea, Hap-D (N=40), ou (3) não dominada por qualquer um dos dois grupos

(*N*=58), Not-D. Not-D representa o grupo das poucas amostras não dominadas por diatomáceas nem haptofíceas, mas dominada por outro grupo taxonômico (ver Figura 3 – Apêndice 3). A inspecção visual dos espectros de $\int a_{ph}(\lambda)$ revelaram comportamentos espectrais muito semelhantes aos daqueles sem dominância de qualquer grupo. Este resulta mostra o potencial de discriminar amostras dominadas por diatomáceas e haptofíceas, porém não de outro grupo, através da metodologia que será proposta aqui.

3.3.4. *Análise de agrupamento sobre os espectros de absorção da luz pelo fitoplâncton*

A Figura 4a – Apêndice 3 ilustra os resultados do método de *HCA* aplicado sobre os coeficientes espectrais de absorção do fitoplâncton, $a_{ph}(\lambda)$, e que aqui estão mostrados na forma nomalizada $\int a_{ph}(\lambda)$. Diferentemente das análises de cluster anteriores aplicadas aos conjuntos de dados de razões de pigmentos diagnósticos e de contribuições dos grupos taxonômicos do fitoplâncton (Figuras 2 e 3 – Apêndice 3), um dendrograma (não mostrado) indicou a classificação dos espectros em 3 clusters, referidos como de $C1_{aph}$ a $C3_{aph}$.

O cluster $C1_{aph}$ agrupou os espectros com menores razões entre os picos de absorção nas faixas espectrais do azul e vermelho, i.e., mais 'achatados' (*N*=38). O cluster $C2_{aph}$ incluiu a maior parte dos espectros (*N*=71) que foram caracterizados por um 'ombro' entre 450-470 nm, com o principal pico de absorção ao redor de 440 nm, e menores razões entre os picos de absorção nas faixas espectrais do azul e vermelho (Figura 4a – Apêndice 3). Os espectros semelhantes aos do cluster $C2_{aph}$ na região espectral do azul, mas sem nenhum 'ombro' ao redor de 460 nm e valores

intermediários dos demais clusters nas regiões espectrais verde e vermelho foram agrupados em $C3_{aph}$ (Figura 4a – Apêndice 3).

As figuras 4b a 4d – Apêndice 3 mostram os espectros de $\int a_{ph}(\lambda)$ de acordo com as classificações resultantes do método de *HCA* aplicado às razões de pigmentos diagnósticos (Figura 4b – Apêndice 3), aos conjuntos de dados CHEMTAX (Figura 4c – Apêndice 3), e resultantes do critério de dominância taxonômica de 50% (Figura 4d – Apêndice 3). A semelhança entre as classificações baseadas nos espectros de $a_{ph}(\lambda)$ e as obtidas usando as razões de pigmentos diagnósticos e os dados de CHEMTAX é quantificada pelos índices cofenéticos de 0,67 e 0,66, respectivamente.

Resumidamente, o método de *HCA* aplicado aos dados de pigmento, que incluem as razões de pigmentos diagnósticos e a estrutura taxonômica formecida pelo CHEMTAX, e aos espectros de $a_{ph}(\lambda)$ essencialmente classificaram nossas amostras como dominadas por i) diatomáceas-Chl*c1* ($C1_{diag}$, $C1_{CHEM}$, $C1_{aph}$), ii) haptofíceas ($C2_{diag}$, $C2_{CHEM}$, $C2_{aph}$) e iii) sem dominância por qualquer um destes dois grupos ($C3_{diag}$, $C4_{diag}$, $C3_{CHEM}$, $C4_{CHEM}$, $C3_{aph}$).

Correspondência razoável entre os dados de pigmento e os espectros de absorção da luz pelo fitoplâncton ainda foi observada quando se aplicou a HCA sobre os dados multi-espectrais de absorção que correspondem às bandas de satélites da cor do oceano, 412, 443, 490, 510, 555 e 670 nm. Índices cofenéticos de 0,57 e 0,52 foram calculados ao comparar os dendrogramas gerados para os dados multi-espectrais e para DPR e dados do CHEMTAX, respectivamente. Isso indica um potencial para discriminar a comunidade fitoplanctônica dominante das florações da região da QPA através de coeficientes de absorção do fitoplâncton multi-espectrais estimados por satélite através de modelos semi-analíticos. Também, a discriminação do grupo dominante do fitoplâncton por sensoriamento remoto pode testada através da

investigação de coerência no agrupamento de espectros de reflectância e dados de pigmento medidos *in situ* (e.g., Alvain *et al,* 2004; Alvain *et al.,* 2008).

3.3.5. *Características do espectro de absorção do fitoplâncton de acordo com a dominância taxonômica*

Nesta secção, as características espectrais dos coeficientes de absorção do fitoplâncton foram investigadas para detectar a dominância taxonômica do fitoplâncton. Considerou-se como referência a classificação das amostras de acordo com o critério de dominância de 50%, ou seja, de acordo com os casos Dia-D, Hap-D e Not-D. Assim, procurou-se feições exclusivas nos espectros de $\int a_{ph}(\lambda)$ e o potencial para considerá-las para a discriminação entre aqueles três principais casos de estrutura taxonômica algal encontrados em nossas amostras.

A partir da inspeção visual dos espectros de $\int a_{ph}(\lambda)$, verifica-se que a grande maioria dos espectros Dia-D, que são comparativamente achatados, podem ser discriminados dos demais na faixa azul espectral pelo comprimento de onda de 443 nm (Figura 4d – Apêndice 3). A Figura 5 – Apêndice 3 ilustra bem essa constatação, pois revela uma dependência inversa de $\int a_{ph}(443)$ sobre a contribuição relativa de para a biomassa algal total, considerando-se todas as amostras. As amostras Dia-D, Hap-D, e Not-D são representadas como asteriscos, quadrados e as estrelas, respectivamente, na Figura 5 – Apêndice 3. Observa-se que 31 dos 38 (81,6%) espectros Dia-D mostraram $\int a_{ph}(443)$ inferiores a 0,0075 (Figura 5).

A Figura 5 – é dividida em quatro painéis (I, II, III, e IV) delimitados pelos valores de 0,0075 no eixo de $\int a_{ph}(443)$ e de 50% no eixo da contribuição relativa de diatomáceas. As amostras Dia-D com valores de $\int a_{ph}(443)$ menores que 0,0075 estão

representadas no painel de IV (31 de 38 amostras). Sete amostras Dia-D que apresentaram $\int a_{ph}(443)$ maior que 0,0075 e, portanto, que possuem espectros semehantes aos das amostras Not-D (rever Figura 4d – Apêndice 3) são indicados no painel I. A maior parte das amostras, que inclui os casos Hap-D e Not-D com $\int a_{ph}(443)$ maior que 0,0075, aparecem no Painel II. Uma única amostra Not-D, com contribuição das diatomáceas de 38%, é visualizada no Painel III.

A Figura 5 – Apêndice 3 também evidencia a concordância entre os valores de $\int a_{ph}(443)$ e o parâmetro do tamanho celular do fitoplâncton, S_f. Esse parâmetro varia de 0 a 1, como indicativo do efeito pacote que impacta o comportamento espectral da absorção da luz pelo fitoplâncton. Quanto menor o S_f, maior o efeito pacote (i.e., espectros mais achatados) (Ciotti *et al.,* 2002). Assim, S_f também apresenta o potencial de discriminar os espectros Dia-D. As amostras do painel IV possuem valores mais baixos de S_f (0,05 a 0,37, média de 0,18). Os casos Dia-D contidos pelo painel I foram associados aos valores de S_f entre 0,42 e 0,54 (média de 0,47). O parâmetro S_f variou entre 0,37 e 0,72 (média de 0,56) para os espectros de amostras Not-D e entre 0,42 e 0,82 (média de 0,68) em associação aos casos Hap-D, ou seja, com estreita faixa de sobreposição de valores para as amostras Dia-D (0,05 a 0,54). Este resultado é consistente com o maior efeito pacote para as maiores células das diatomáceas.

A Figura 5 evidencia que 31 de 32 espectros de absorção de fitoplâncton (ou seja, 97% destes espectros) com $\int a_{ph}(443)$ inferior a 0,0075 (ou seja, representados nos Painéis III e IV) estiveram associados à dominância de diatomáceas. Assumindo-se que nosso conjunto de dados é representativo da situação amostrada pelo nosso estudo, a probabilidade de que uma amostra com valor de $\int a_{ph}(443)$ menor que 0,0075 é dominada por diatomáceas é da ordem de 97%.

A distinção entre os espectros para as amostras classificadas como Hap-D ou Not-D não é tão evidente como o é para distinguir casos Dia-D dos demais, por causa da semelhança no comportamento espectral para Hap-D e Not-D praticamente em todo o espectro (rever Figura 4d – Apêndice 3). Um segundo pico de absorção na faixa azul do espectro (centrado em 463 nm) e que é atribuído à Hex, está presente na maior parte dos espectros de amostras Hap-D. No entanto, os espectros Not-D se mostraram muitos semelhantes em valores de $\int a_{ph}(\lambda)$ aos dos espectros Hap-D nesta região espectral (rever Figura 4d – Apêndice 3). A Figura 6 – Apêndice 3 está dividida em quatro painéis (I, II, III, e IV), assimo como a Figura 5), sendo delimitados agora através do valor de 0,0079 no eixo de $\int a_{ph}(463)$ e de 50% no eixo da contribuição relativa das haptofíceas. O valor de $\int a_{ph}(463)$ de 0,0082 está também indicado na figura.

Uma clara tendência de aumento em $\int a_{ph}(463)$ com o aumento da contribuição relativa de haptofíceas é observada na Figura 6 – Apêndice 3. A maioria dos espectros de Hap-D (30 a 40) mostraram $\int a_{ph}(463)$ maior que 0,0079 (Painel I). Quatro dos espectros de Hap-D divergem consideravelmente, mostrando valores de $\int a_{ph}(463)$ inferiores a 0,0079 (Painel IV). Espectros Not-D com valores de $\int a_{ph}(463)$ maiores que 0,0079 estão contidos no Painel II. O Panel III contém os casos restantes, que incluem todos as amostras Dia-D e a maioria Not-D. Inversamente ao que foi descrito para a contribuição relativa das diatomáceas, o aumento na contribuição relativa das haptofíceas é claramente acompanhado por aumento em S_f. Como já visto, este parâmetro variou entre 0,42 a 0,82 (média de 0,68) para amostras Hap-D e de 0,37 e 0,72 (média de 0,56) para as amostras Not-D. Valores mais elevados de S_f para os espectros associados com a dominância de haptofíceas são consistentes com o menor tamanho celular para este grupo. Apesar de alguma sobreposição de valores de S_f para

espectros Hap-D e Não-D existir, todos os valores de S_f maiores que 0,72 foram associados com dominância das haptofíceas.

A Figura 6 – Apêndice 3 mostra que 30 de 37 espectros (ou 81%) com $\int a_{ph}(463)$ maior que 0,0079 (i.e., contidos nos Painéis I e II) estiveram em associação à dominância de haptofíceas. Quando esse valor foi maior que 0,0082, todas as amostras estiveram associadas a tal dominância. Portanto, pode-se assumir que a probabilidade de que a comunidade do fitoplâncton de uma amostra com valor de $\int a_{ph}(463)$ maior que 0,0079 é dominada por haptoficeas é de cerca de 81%. Esta probabilidade atinge 100% no caso de $\int a_{ph}(463)$, para nossas amostras, é maior do que 0,0082.

A aplicação da nossa abordagem de detecção e dominância taxonômica do fitoplâncton através de técnicas de clusters ou a baseada em um comprimento de onda para espectros de absorção pelo fitoplâncton, como mostrada aqui, estaria sujeita a interferências através de dados de satélite. Erros na correção atmosférica (*International Ocean Colour Coordinating Group*, 2010) e os pressupostos dos modelos bio-óticos semi-analíticos (*International Ocean Colour Coordinating Group*, 2006) ainda tem sido fontes de incertezas nas estimativas dos coeficientes de absorção da luz pelo fitoplâncton através de satélite. Uma vez que as diferenças que foram observadas nas feições dos espectros em coerência com a dominância taxonômica são espectralmente dependentes (os espectros de absorção foram normalizados pela soma de todos os valores de cada espectro), é indicada a utilização de um modelo semi-analítico que não assuma a forma espectral de $a_{ph}(\lambda)$ para estimar esses coeficientes por satélite (e.g., Lee *et al.,* 2002) e então testar a coerência dos dados satelitais com dados de pigmentos e composição taxonômica *in situ*.

No que diz respeito às técnicas operacionais atuais para sensoriamento remoto e os nossos resultados, um aspecto positivo é o potencial de discriminar a dominância de diatomáceas e/ou haptofíceas nas águas da QPA a partir da estimativa do índice de tamanho celular S_f através de satélite (Ciotti e Bricaud, 2006). As maiores contribuições à biomassa do fitoplâncton de diatomáceas e haptofíceas estiveram associadas com os extremos desse índice (0,05 a 0,35 para diatomáceas e valores maior que 0,72 para haptofíceas). Isto é devido a um efeito muito maior de efeito pacote (baixo S_f) para as diatomáceas do que para as células menores de haptofíceas (maior S_f). Ao menos os valores extremos do intervalo de variação de S_f podem então ser adequadamente atribuídos à dominância taxonômica de diatomáceas e haptofíceas durantes as florações da região da quebra de plataforma Argentina.

4. *CONCLUSÕES*

1) Os coeficientes de absorção, espalhamento e atenuação difusa da luz obtidos para uma dada concentração de clorofila-*a* durante as florações do fitoplâncton na quebra de plataforma Argentina variaram devido ao tamanho celular do fitoplâncton e, portanto, ao efeito "pacote". Este resultado indica a limitação de modelos tradicionais bio-óticos nos quais o fitoplâncton é parametrizado somente em termos de concentração da clorofila-*a*.

2) A caracterização da variabilidade nos espectros de reflectância do sensoriamento remoto (propriedade óptica aparente) medidos *in situ* revelou o fitoplâncton como componente dominante das propriedades ópticas durante as florações na região da quebra de plataforma Argentina. Ainda assim, a variabilidade nos coeficientes de absorção e espalhamento (propriedades ópticas inerentes), devido a variações no tamanho celular do fitoplâncton, influencia o desempenho de modelos bio-óticos que se baseiam em razões de banda de reflectância do sensoriamento remoto para estimar concentração de clorofila-*a* por satélite. Erros nessas estimativas mostraram relações significativas com a própria concentração de clorofila-*a* e com os coeficientes de absorção do fitoplâncton e de espalhamento pelas partículas, ambos normalizados pela concentração de clorofila-*a*. Embora tenha sido encontrada boa concordância entre a concentração de clorofila-*a* e coeficientes de absorção do fitoplâncton medidos *in situ* e os estimados por satélite a partir de algoritmos aplicados globalmente, ajustes regionais destes modelos que levem em conta as variações nesses coeficientes para dada concentração de clorofila-*a* devem ser adotados para melhorar tais estimativas por satélite;

3) Três principais situações de composição taxonômica do fitoplâncton ocorrem durantes as florações na quebra de plataforma Argentina: (1) águas dominadas por diatomáceas, (2) haptofíceas, e (3) com contribuições destes e de outros grupos, sem dominância de algum. Essas três situações foram refletidas de forma coerente nos comportamentos espectrais de absorção da luz pelo fitoplâncton, indicando o potencial em discriminar as assembleias das florações na região através de dados ópticos. Especificamente, análises de cluster podem ser utilizadas para esta finalidade. A dominância de diatomáceas, haptofíceas ou assembleias não dominadas por algum grupo taxonômico também podem ser identificadas através dos espectros de absorção do fitoplâncton a partir de um comprimento de onda. Quanto maior a dominância de diatomáceas ou haptofíceas, maior a certeza dessa identificação. Esses resultados sugerem a aplicação dessa abordagem por sensoriamento remoto para a região. A dominância de diatomáceas e haptofíceas pode ser também identificada através de um fator de tamanho celular do fitoplâncton, atualmente estimado por satélite.

5. REFERÊNCIAS BILBIOGRÁFICAS

Acha, E. M., H. Mianzan , R. Guerrero, M. Favero, e J. Bava (2004), Marine fronts at the continental shelves of austral South America: physical and ecological processes, *J. Mar. Sys., 44,* 83–105.

Aiken, J., J. R. Fishwick, S. Lavender, R. Barlow, G. F. Moore, H. Sessions, S. Bernard, J. Ras, e N. J. Hardman-Mountford (2006), Validation of MERIS reflectance and chlorophyll during the BENCAL cruise October, 2002: preliminary validation of new demonstration products for phytoplankton functional types and photosynthetic parameters, *Int. J. Remote Sens., 28,* 497-516, doi:10.1080/01431160600821036.

Alvain, S., C. Moulin, Y. Dandonneau, e F. M. Bréon (2005), Remote sensing of phytoplankton groups in case 1 waters from global SeaWiFS imagery, *Deep Sea Res. Part I, 52,* 1989-2004.

Alvain, S., C. Moulin, Y. Dandonneau, e H. Loisel (2008), Seasonal distribution and succession of dominant phytoplankton groups in the global ocean: a satellite view, *Global Biogeochem. Cy., 22,* GB3001, doi:10.1029/2007GB003154.

Atlas, T., e T. T. Bannister (1980), Dependence of mean spectral extinction coefficient of phytoplankton on depth, water colour, and species, *Limnol. Oceanogr., 19,* 1-12.

Austin, R. W. (1974), Inherent spectral radiance signatures of the ocean surface In Ocean Color Analysis (La Jolla, CA: Scripps Inst. Oceanogr.) p. 195.

Babin, M. e D. Stramski (2004), Variations in the mass-specific absorption coefficient of mineral particles suspended in water, *Limnol. Oceanogr., 49,* 756–767.

Bailey, S. W., C. R. McClain, P. J. Werdell, e B. D. Schieber (2000), Normalized water-leaving radiance and chlorophyll a match-up analyses. NASA Tech. Memo. 206892, National Aeronautics and Space Administration, Goddard. Space Flight Center, Greenbelt, MD.

Balch, W. M., D. T. Drapeau, B. C. Bowler, E. Lyczskowski, E. S. Booth, e D. Alley (2011), The contribution of coccolithophores to the optical and inorganic carbon budgets during

the Southern Ocean Gas Exchange Experiment: New evidence in support of the "Great Calcite Belt" hypothesis, *J. Geophys. Res.*, *116,* C00F06, doi:10.1029/2011JC006941.

Behrenfeld, M. J., e E. Boss (2003), The beam attenuation to chlorophyll ratio: an optical index of phytoplankton photoacclimation in the surface ocean?, *Deep Sea Res. Part I, 50,* 1537-1549, doi:10.1016/j.dsr.2003.09.002.

Behrenfeld, M. J., e E. Boss (2006), Beam attenuation and chlorophyll concentrations as alternative optical indices of phytoplankton biomass, *J. Mar. Res., 64,* 431–451.

Bertolotti, M. I., N. E. Brunetti, et al. (1996), Influence of Shelf-Break Fronts on Shellfish and Fish Stocks off Argentina, INIDEP, International Council for the Exploration of the Sea, CM 1996/S, 41, 23.

Bianchi, A. A., D. R. Pino, H. G. I. Perlender, A. P. Osiroff, V. Segura, V. Lutz, M. L. Clara, C. F. Balestrini, e A. R. Piola (2009), Annual balance and seasonal variability of sea-air CO_2 fluxes in the Patagonia Sea: Their relationship with fronts and chlorophyll distribution, *J. Geophys. Res., 114,* C03018, doi:10.1029/2008JC004854.

Bouman, H. A., T. Platt, S. Sathyendranath, W. K. W. Li, V. Stuart, C. Fuentes-Yaco, H. Maass, E. P. W. Horne, O. Ulloa, V. Lutz, e M. Kyewalyanga (2003), Temperature as indicator of optical properties and community structure of marine phytoplankton: implications for remote sensing, *Mar. Ecol. Prog. Ser., 258,* 19-30, doi:10.3354/meps258019.

Bracher, A., M. Vountas, T. Dinter, J. P. Burrows, R. Röttgers, e I. Peeken (2009), Quantitative observation of cyanobacteria and diatoms from space using PhytoDOAS on SCIAMACHY data, *Biogeosciences*, *6,* 751-764.

Brewin, R. J. W., S. J. Lavender, N. J. Hardman-Mountford, e T. Hirata (2010), A spectral response approach for detecting dominant phytoplankton size class from satellite remote sensing, *Acta Oceanol. Sin., 29*, 14-32.

Brewin, R. J. W., N. J. Hartman-Mountford, S. J. Lavender, D. E. Raitsos, T. Hirata, J. Uitz, E. Devred, A. Bricaud, A. M. Ciotti, e B. Gentili (2011a), An intercomparison of bio-optical techniques for detecting dominant phytoplankton size class from satellite remote

sensing, *Remote Sens. Environ., 115,* 325–339, doi:10.1016/j.rse.2010.09.004.

Brewin, R. J. W., E. Devred, S. Sathyendranath, S. J. Lavender, e N. J. Hartman-Mountford (2011b), Model of phytoplankton absorption based on three size classes, *Appl. Opt., 22,* 4535-4549, doi:\10.1364/AO.50.004535.

Bricaud, A., M. Babin, A. Morel, e H. Claustre (1995), Variability in the chlorophyll-specific absorption coefficient of natural phytoplankton: analysis and parameterization, *J. Geophys. Res., 100*(C7), 13321-13332, doi:10.1029/95JC00463.

Bricaud, A., A. Morel, M. Babin, K. Allali, e H. Claustre (1998), Variations of light absorption by suspended particles with the chlorophyll a concentration in oceanic (Case 1) waters: analysis and implications for bio-optical models, *J. Geophys. Res., 103*(13), 31,033-31,044, doi:10.1029/98JC02712.

Bricaud, A., H. Claustre, J. Ras, e K. Oubelkheir (2004), Natural variability of phytoplankton absorption in oceanic waters: influence of the size structure of algal populations, *J. Geophys. Res., 109,* C11010, doi:10.1029/2004JC002419.

Bricaud, A., C. Mejia, D. Blondeau-Patissier, H. Claustre, M. Crepon, e S. Thiria (2007), Retrieval of pigment concentrations and size structure of algal populations from their absorption spectra using multilayered perceptrons, *Appl. Opt.,* 46, 1251-1260.

Brown, C. W., e J. A. Yoder (1994), Coccolithophorid blooms in the global ocean, *J. Geophys. Res., 99,* 7467–7482, doi:10.1029/93JC02156.

Brown, C. W., e G. P. Podestá (1997), Remote sensing of coccolithophore blooms in the western South Atlantic Ocean, *Remote Sens. Environ., 60,* 83–91, doi:10.1016/S0034-4257(96)00140-X.

Brown, C. A., Y. Huot, P. J. Werdell, B. Gentili, e H. Claustre (2008), The origin and global distribution of second order variability in satellite ocean color and its potential applications to algorithm development, *Remote Sens. Environ., 112*, 4186-4203, doi:10.1016/j.rse.2008.06.008.

Carreto, J. I., R. M. Negri, H. R. Benavides, and R. Akselman (1985), Toxic dinoflagellates blooms in the Argentine Sea, in *Toxic Dinoflagellates*, edited by D. M. Anderson et al., pp.

147-152, Elsevier, New York.

Carreto, J. I., V. A. Lutz, M. O. Carignan, A. D. Cucchi Coleoni, e S. G. De Marco (1995), Hydrography and chlorophyll a in a transect from the coast to the shelf break in the Argentinian Sea, *Cont. Shelf Res., 15*(2-3)*,* 315–336, doi:10.1016/0278-4343(94)E0001-3.

Carreto, J. I., N. G. Montoya, H. R. Benavides, R. Guerrero, e M. O. Carignan (2003), Characterization of spring phytoplankton communities in the Río de La Plata maritime front using pigment signatures and cell microscopy, *Mar. Biol., 143,* 1013–1027.

Carreto, J. I., N. Montoya, R. Akselman, M. O. Carignan, R. I. Silva, e A. D. Cucchi Colleoni (2008), Algal pigment patterns and phytoplankton assemblages in different water masses of the Río de la Plata maritime front, *Cont. Shelf Res., 28,* 1589-1606, doi:10.1016/j.csr.2007.02.012.

Carreto, J. I., and M. O. Carignan (2011), Mycosporine-Like Amino Acids: Relevant Secondary Metabolites. Chemical and Ecological Aspects, *Mar. Drugs, 9*, 387-446, doi:10.3390/md9030387.

Chazottes, A., A. Bricaud, M. Crepon, e S. Thiria (2006), Statistical analysis of a data base of absorption spectra of phytoplankton and pigment concentrations using Self-Organizing Maps, *Appl. Opt., 45,* 8102-8115.

Chazottes, A., M. Crepon, A. Bricaud, J. Ras, e S. Thiria (2007), Statistical analysis of absorption spectra of phytoplankton and of pigment concentrations observed during three POMME cruises using a neural network clustering method*, Appl. Opt., 46*, 3790-3799, doi:10.1364/AO.46.003790.

Chisholm, S. W. 1992. Phytoplankton size, p. 213–238. In P. G. Falkowski and A. Woodhead [eds.], Primary productivity and biogeochemical cycles in the sea. Plenum Press.

Ciotti, A. M., J. J. Cullen, e M. R. Lewis, (1999), A semi-analytical model of the influence of phytoplankton community structure on the relationship between light attenuation and ocean color, *J. Geophys. Res., 104,* 1559-1578.

Ciotti, A. M., M. R. Lewis, e J. J. Cullen (2002), Assessment of the relationships between

dominant cell size in natural phytoplankton communities and the spectral shape of the absorption coefficient, *Limnol. Oceanogr., 47,* 404-417.

Ciotti, A.M., e A. Bricaud (2006), Retrievals of a size parameter for phytoplankton and spectral light absorption by Colored Detrital Matter from water-leaving radiances at SeaWiFS channels in a continental shelf region off Brazil, *Limnol. Oceanogr. Methods*, *4,* 237–253.

Comin, R. (2009), Composição e biomassa do fitoplâncton no talude da Patagônia, na primavera de 2006 e verão de 2007, Monografia de Graduação, FURG, Rio Grande, 41p.

Copello, S., A. I. Dogliotti, D. A. Gagliardini, e Q. Flavio (2011), Oceanographic and biological landscapes used by the Southern Giant Petrel during the breeding season at the Patagonian Shelf, *Mar. Biol.,* 1-11, doi:10.1007/s00227-011-1645-3.

Cousseau, M. B. e R. G. Perrota (2000), Peces marinos de Argentina. Biología, distribución y pesca. INIDEP, Mar del Plata, 167 pp.

Craig, S. E., S. E. Lohrenz, Z. Lee, K. L. Mahoney, G. J. Kirkpatrick, O. M. Schofield, e R. G. Steward (2006), Use of hyperspectral remote sensing reflectance for detection and assessment of the harmful alga, Karenia brevis, *Appl. Opt., 45,* 5414– 5425.

de Souza, M. S., C. R. B, Mendes, V. M. T. Garcia, R. Pollery, e V. Brotas (2012), Phytoplankton community during a coccolithophorid bloom in the Patagonian Shelf: microscopic and HPLC pigment analyzes, *J. Mar. Biol. Assoc. UK, 92*, 13-27, doi:10.1017/S0025315411000439.

de Souza, M. S. (2012), Comunidades fitoplanctônicas da Península Antártica e Patagônica, na primavera e verão: distribuição especial e relação com parâmetros oceanográficos, Tese de doutorado, FURG, Rio Grande, 305 p.

Devred E., S. Sathyendranath, V. Stuart, H. Maass, O. Ulloa, e T. Platt (2006), Bio-Optics of the Ocean: a Two-component Model of Absorption by Phytoplankton, *J. Geophys. Res., 111*, C03011, doi:10.1029/2005jc002880.

Devred, E., S. Sathyendranath, V. Stuart, e T. Platt (2011), Absorption-derived phytoplankton cell size: application to satellite ocean-colour data in the Northwest Atlantic, *Remote Sens. Environ.,115,* 2255-2266.

Dmitriev, E. V., G. Khomenko, M. Chami, A. A. Sokolov, T. Y. Churilova, e G. K. Korotaev (2009), Parameterization of light absorption by components of seawater in optically complex coastal waters of the Crimea Peninsula (Black Sea), *Appl. Opt., 48,* 1249–1261.

Duysens, L. M. N. (1956), The flattening of absorption spectrum of suspensions, as compared to that of solutions, *Biochim. Biophys. Acta, 19,* 1-12.

Feldman, G. C. (1989), Ocean Colors Imaged from Space Track the Distribution of Marine Phytoplankton, Earth in Space Vol.2 No. 2, 5-7.

Ferreira, A., V. M. T. Garcia, e C. A. E. Garcia (2009), Light absorption by phytoplankton, non-algal particles and dissolved organic matter at the Patagonia shelf-break in spring and summer, *Deep Sea Res. Part I, 56,* 2162-2174, doi:10.1016/ j.dsr.2009.08.002.

Fishwick, J. R., J. Aiken, R. G. Barlow, H. Sessions, S. Bernard, e J. Ras (2006), Functional relationships and bio-optical properties derived from phytoplankton pigments, optical and photosynthetic parameters; a case study of the Benguela ecosystem, *J. Mar. Biol. Assoc. UK, 86,* 1267−1280, doi:10.1017/S0025315406014287.

Garcia, C. A. E., Y. V. B., Sarma, M. M. Mata, e V. M. T. Garcia (2004), Chlorophyll variability and eddies in the Brazil-Malvinas Confluence region, *Deep Sea Res. Part II, 51*, 159-172, doi:10.1016/j.dsr2.2003.07.016.

Garcia, V. M. T., C. A. E. Garcia, M. M. Mata, R. C. Pollery, A. R. Piola, S. R. Signorini, C. R. McClain, e M. D. Iglesias-Rodriguez (2008), Environmental factors controlling the phytoplankton blooms at the Patagonia shelf-break in spring, *Deep Sea Res. Part I, 55*, 1150-1166, doi:10.1016/j.dsr.2008.04.011.

Garcia, C. A. E., V. M. T. Garcia, A. I. Dogliotti, A. Ferreira, S. I. Romero, A. Mannino, M. S. de Souza, e M. M. Mata (2011), Environmental conditions and bio-optical signature of a coccolithophorid bloom in the Patagonian shelf, *J. Geophys. Res.*, *116,* C03025, doi:10.1029/2010JC006595.

Gernez, P., D. Antoine, e Y. Huot (2011), Diel cycles of the particulate beam attenuation coefficient under varying trophic conditions in the northwestern Mediterranean Sea: observations and modeling, *Liminol. Oceanogr., 56,* 17-36, doi:10.4319/lo.2011.56.1.0017.

Gieskes, W. W. C., G. W. Kraay, A. Nontji, D. Sstiapermana, e D. Sutomo (1988), Monsoonal alternation of a mixed and a layered structure in the phytoplankton of the euphotic zone of the Banda Sea (Indonesia): A mathematical analysis of algal pigment fingerprints, *Neth. J. Sea Res., 22,* 123-137.

Gordon, H., e A. Morel (1983), Remote Assessment of Ocean Color for Interpretation of Satellite Visible Imagery: A Review. Lecture Notes on Coastal and Estuarine Studies, Vol. 4, Springer Verlag, New York, 114 pp.

Gordon, H. R., O. B. Brown, R. H. Evans, J. W. Brown, R. C. Smith, K. S. Baker, e D. K. Clark (1988), A semianalytic radiance model of ocean color, *J. Geophys. Res., 93,* 10,909–10,924, doi:10.1029/JD093iD09p10909.

Gordon, H. R., G. C. Boynton, W. M. Balch, S. B. Groom, D. S. Harbour, e T. J. Smyth (2001), Retrieval of coccolithophore calcite concentration from SeaWiFS imagery, *Geophys. Res. Lett., 28,* 1587–1590, doi:10.1029/2000GL012025.

Gregg, W. W., N. W. Casey, e C. R. McClain (2005), Recent trends in global ocean chlorophyll, *Geophys. Res. Lett.*, *32,* L03606, doi:10.1029/2004GL021808.

Guerrero, R.A., A. Baldoni, e H. R. Benavides (1999), Oceanographic conditions at the southern end of the Argentine continental slope. INIDEP Doc. Cient. 5, 7 – 22.

Hair, J.F., W. Black, B. Babin, R. E. Anderson e R. L. Tatham (2009), Análise multivariada de dados. Bookman, Porto Alegre.

Hirata, J. A., J. Aiken, N. J. Hardman-Mountford, T. J. Smyth, e R. Barlow (2008), An absorption model to derive phytoplankton size classes from satellite ocean color, *Remote Sens. Environ., 112*, 3153– 3159, doi:10.1016/j.rse.2008.03.011.

Hoepffner, N. e S. Sathyendranath (1993), Determination of the major groups of phytoplankton pigments from the absorption spectra of total particulate matter, *J.*

Geophys. Res., 98, 22789–22803.

Holligan, P. M., et al. (1993), A biogeochemical study of the coccolithophore, Emiliania huxleyi, in the north Atlantic, *Global Biogeochem. Cycles, 7,* 879–900, doi:10.1029/93GB01731.

Huot, Y., A. Morel, M. S. Twardowski, D. Stramski, e R. A. Reynolds (2008), Particle optical backscattering along a chlorophyll gradient in the upper layer of the eastern south pacific ocean, *Biogeosciences, 5*, 495-507.

IOCCG, "Remote Sensing of Inherent Optical Properties: Fundamentals, Tests of Algorithms, and Applications," in Reports of the International Ocean-Colour Coordinating Group, No. 5, Z. P. Lee, ed. (IOCCG, Dartmouth, 2006).

Jeffrey, S. W., e S. W. Wright (1994), Photosynthetic pigments in the Haptophyta, in *The Haptophyte Algae*, edited by J. C. Green, and B. S. C. Leadbeater, pp. 111–132, Clarendon Press, Oxford.

Jeffrey, S.W., R. F. C. Mantoura, e T. Bjørnland (1997), Data for the identification of 47 key phytoplankton pigments. In: Jeffrey, S.W., Mantoura, R.F.C., Wright, R.W. (Eds.), Phytoplankton Pigments in Oceanography, vol. IV, pp. 449–559.

Kirk, J.T.O. (1994), Light and Photosynthesis in Aquatic Ecosystems, Cambridge University Press, Cambrigde, United Kingdom.

Kishino M, N. Takahashi, N. Okami, e S. Ichimura (1985), Estimation of the spectral absorption coefficients of phytoplankton in the sea, *Bull. Mar. Sci., 37*, 634–642.

Kostadinov, T. S., D. A. Siegel, e S. Maritorena (2009), Retrieval of the particle size distribution from satellite ocean color observations, *J. Geophys. Res., 114,* C09015, doi:10.1029/2009JC005303.

Le Quéré, C., et al. (2005), Ecosystem dynamics based on plankton functional types for global ocean biogeochemistry models, *Global Change Biol.,* 11, 2016–2040.

Lee, Z. P., K. L. Carder, R. A. Arnone (2002), Deriving inherent optical properties from water color: a multiband quasi-analytical algorithm for optically deep waters, *Appl. Opt*., *41,* 5755-5772.

Lee, Z. P., R. Arnone, C. M. Hu, P. J. Werdell, e B. Lubac (2010), Uncertainties of optical parameters and their propagations in an analytical ocean color inversion algorithm. *Appl. Opt., 49,* 369−381.

Lewis, M. R., J. J. Cullen, e T. Platt (1983), Phytoplankton and Thermal Structure in the Upper Ocean: Consequences of Nonuniformity in Chlorophyll Profile, *J. Geophys. Res*., *88*, 2565–2570, doi:10.1029/JC088iC04p02565.

Lohrenz, S, E., A. D. Weidemann, e M. Tuel (2003), Phytoplankton spectral absorption as influenced by community size structure and pigment composition, *J. Plankton Res., 25*, 35-61, doi:10.1093/plankt/25.1.35.

Loisel, H., e A. Morel (1998), Light scattering and chlorophyll concentration in Case 1 waters: a reexamination*, Limnol. Oceanogr., 43,* 847–858, doi:10.4319/lo.1998.43.5.0847.

Loisel, H., J.-M. Nicolas, A. Sciandra, D. Stramski, e A. Poteau (2006), Spectral dependency of optical backscattering by marine particles from satellite remote sensing of the global ocean, *J. Geophys. Res., 111*, C09024, doi:10.1029/2005JC003367.

Loisel, H., B. Lubac, D. Dessailly, L. Duforer-Gaurier, e V. Vantrepotte (2010), Effect of inherent optical properties variability on the chlorophyll retrieval from ocean color remote sensing: An in situ approach, *Opt. Express, 18,* 20,949 20,959.

Lubac, B., e H. Loisel (2007), Variability and classification of remote sensing reflectance spectra in the eastern English Channel and southern North Sea, *Rem. Sens. of Environ., 110*(1), 45-58, doi:10.1016/j.rse.2007.02.012.

Lubac, B., H. Loisel, N. Guiselin, R. Astoreca, L. Felipe Artigas, e X. Mériaux (2008), Hyperspectral and multispectral ocean color inversions to detect Phaeocystis globosa blooms in coastal waters. *J. Geophys. Res., 113,* C06026, doi:10.1029/2007JC004451.

Lutz, V. A., V. Segura, A. I. Dogliotti, D. A. Gagliardini, A. A. Bianchi, e C. F. Balestrini (2010), Primary Production in the Argentine Sea during Spring Estimated by Field and Satellite Models, *J. Plankton Res., 32,* 181-195, doi:10.1093/plankt/ fbp117.

Mackey, M. D., D. J. Mackey, H. W. Higgins, e S. W. Wright (1996), CHEMTAX – a program for estimating class abundances from chemical markers: application to HPLC measurements of phytoplankton, *Mar. Ecol. Prog. Ser., 144,* 265–283, doi:10.3354/meps144265.

Malone, T. C. (1980), Algal size, p. 433–463. In I. Morris [ed.], The physiological ecology of phytoplankton. Univ. of California Press.

Mao, Z., V. Stuart, D. Pan, J. Chen, F. Gong, H. Huang, e Q. Zhu (2010), Effects of phytoplankton species composition on absorption spectra and modeled hyperspectral reflectance, *Ecol. Inform., 5,* 359-366.

Maritorena, S., D. A. Siegel, e A. R. Peterson (2002), Optimization of a semianalytical ocean color model for global-scale applications. *Appl. Opt., 41,* 2705−2714.

Marra, J., C. C. Trees, e J. E. O'Reilly (2007), Phytoplankton pigment absorption: A strong predictor of primary productivity in the surface ocean, *Deep Sea Res. Part I*, *54*, 155–163, doi:10.1016/j.dsr.2006.12.001.

Matano, R. P. e E. D. Palma (2008), On the Upwelling of Downwelling Currents, *J. Phys. Oceanogr., 38,* 2482–2500, doi:10.1175/2008JPO3783.1.

Matano, R. P., E. D. Palma, e A. R. Piola (2010), The influence of the Brazil and Malvinas Currents on the Southwestern Atlantic Shelf circulation. *Ocean Sci., 6,* 983–995.

Matsuoka, A., V. Hill, Y. Huot, M. Babin, e A. Bricaud (2011), Seasonal variability in the light absorption coefficient of phytoplankton, non-algal particles, and colored dissolved organic matter in western Arctic waters: parameterization of the individual components of absorption for ocean color applications, *J. Geophys. Res., 116,* C02007, doi:10.1029/2009JC005594.

Mendes, C. R., P. Cataxana, e V. Brotas (2007), HPLC determination of phytoplankton and microphytobenthos pigments: Comparing resolution and sensitivity of a C18 and a C8 method, *Limnol. Oceanogr. Methods, 5,* 362–370.

Mitchell, G., et al. (2000), Determination of spectral absorption coefficients of particles, dissolved material and phytoplankton for discrete water samples, in Ocean Optics

Protocols for Satellite Ocean Color Sensor Validation, Revision 2, edited by G. S. Fargion, J. L. Mueller, and C. R. McClain, pp. 125–153, NASA, Goddard Space Flight Cent., Greenbelt, Md.

Moisan, J. R., T. A. H. Moisan, e M. A. Linkswiler (2011), An inverse modeling approach to estimating phytoplankton pigment concentrations from phytoplankton absorption spectra, *J. Geophys. Res., 116,* C09018, doi:10.1029/2010JC006786.

Morel, A., e L. Prieur (1977), Analysis of variation in ocean color. *Liminol. Oceanogr., 22,* 709−722.

Morel, A., e A. Bricaud (1981), Theoretical results concerning light absorption in a discrete medium, and application to specific absorption of phytoplankton, *Deep Sea Res., 28,* 1375-1393, doi:10.1016/0198-0149(81)90039-X.

Morel, A. (1988), Optical modeling of the upper ocean in relation to its biogenous matter content (case 1 water), *J. Geophys. Res., 93*, 10,749-10,768.

Morel, A. (1991), Light and marine photosynthesis: a spectral model with geochemical and climatological implications, *Prog. Oceanogr., 26*, 263-306, doi:10.1016/0079-6611(91)90004-6.

Morel, A., e Y.-H. Ahn (1991), Optics of heterotrophic nanoflagellates and ciliates: A tentative assessment of their scattering role in oceanic waters compared to those of bacterial and algal cells, *J. Mar. Res., 49*, 177-202, doi:10.1357/002224091784968639.

Morel, A., e S. Maritorena, (2001), Bio-optical properties of oceanic waters: A reappraisal, *J. Geophys. Res., 106*, 7763-7780.

Morel, A., B. Gentili, M. Chami, e D. J. Ras (2006), Bio-optical properties of high chlorophyll Case 1 waters and of yellow-substance-dominated Case 2 waters, *Deep Sea Res. Part I, 53*, 1439−1459.

Morel, A., H. Claustre, D. Antoine, e B. Gentili (2007), Natural variability of bio-optical properties in Case 1 waters: attenuation and reflectance within the visible and near-UV spectral domains, as observed in South Pacific and Mediterranean waters, *Biogeosciences, 4*, 913-925.

Mouw, C.B., e J. A. Yoder (2010), Optical determination of phytoplankton size composition from global SeaWiFS imagery, *J. Geophys. Res., 115,* C12018. doi:10.1029/2010JC006337.

Nair, N., S. Sathyendranath, T. Platt, J. Morales, V. Stuart, M.-H. Forget, E. Devred, e H. Bouman (2008), Remote sensing of phytoplankton functional types, *Remote Sens. Environ.*, 112, 3366–3375.

Negri, R. M., J. I. Carreto, H. R. Benavides, R. Akselman, e V. A. Lutz (1992), An unusual bloom of Gyrodinium cf. aureolum in the Argentine Sea: community structure and conditioning factors, *J. Plankton Res., 14*(2), 261–269, doi:10.1093/plankt/14.2.261.

O'Reilly, J. E., S. Maritorena, B. G. Mitchell, D. S. Seigel, K. L. Carder, S. A. Garver, M. Kahru, e C. McClain (1998), Ocean color chlorophyll algorithms for SeaWiFS, *J. Geophys. Res., 103,* 24937−24953.

O'Reilly, J. E., et al., Ocean color chlorophyll a algorithms for SeaWiFS, OC2, and OC4: Version 4," In S. B. Hooker & E.R. Firestone (Eds.), SeaWiFS Postlaunch Calibration and Validation Analyses, Part 3, vol. 11. (pp. 9−23) Greenbelt, Maryland: NASA, Goddard Space Flight Center (2000).

Piola, A. R., N. Martínez-Avellaneda, R. A. Guerrero, F. P. Jardón, E. D. Palma, e S. I. Romero (2010), Malvinas-slope water intrusions on the northern Patagonia continental shelf, *Ocean Sci., 6,* 345–359.

Platt, T., S. Sathyendranath, e V. Stuart (2006), Why study biological oceanography? *Aquabiology, 28,* 542−557.

Pope, R. M., e E. S. Fry (2007), Absorption spectrum (380-700 nm) of pure water; II, Integrating cavity measurements, *Appl. Opt., 36,* 8710- 8723.

Preisendorfer, R. W. (1961), Application of radiative transfer theory to light measurement in the sea, Int. Union Geod. Geophys. Monogr., 10, 11 – 30.

Prézelin, B. B., E. E. Hofmann, C. Mengelt, e J. M. Klinck (2000), The linkage between Upper Circumpolar Deep Water (UCDW) and phytoplankton assemblages on the west Antarctic Peninsula continental shelf, *J. Mar. Res., 58*, 165-202.

Raitsos, D. E., S. J. Lavender, C. D. Maravelias, J. Haralambous, A. J. Richardson, e P. C. Reid (2008), Identifying four phytoplankton functional types from space: An ecological approach, *Limnol. Oceanogr., 53,* 605–613.

Ras, J., H. Claustre, e J. Uitz (2008), Spatial variability of phytoplankton pigment distributions in the subtropical South Pacific Ocean: Comparison between in situ and modeled data, *Biogeosciences*, *5*, 353–369, doi:10.5194/bg-5-353-2008.

Reynolds, R. A., D. Stramski, e B. G. Mitchell (2001), A chlorophyll-dependent semianalytical reflectance model derived from field measurement of absorption and backscattering coefficients within the Southern Ocean, *J. Geophys. Res., 106*, 7125–7138, doi:10.1029/1999JC000311.

Rivas, A. L., A. I. Dogliotti, e A. Gagliardini (2006), Seasonal variability in satellite-measured surface chlorophyll in the Patagonian Shelf, *Cont. Shelf Res., 26,* 703-720.

Roesler, C. S. e M. J. Perry (1995), In situ phytoplankton absorption, fluorescence emission, and particulate backscattering spectra determined from reflectance, *J. Geophys. Res., 100,* 13279–13294.

Romero, S. I., A. R. Piola, M. Charo, e C. A. E. Garcia (2006), Chlorophyll-a variability off Patagonia based on SeaWiFS data, *J. Geophys. Res., 111,* C05021, doi:10.1029/2005JC003244.

Rudorff, N. M., e M. Kampel (2011), Orbital remote sensing of phytoplankton functional types: a new review, *Int. J. Remote Sens., 33,* 1967-1990, doi:10.1080/01431161.2011.601343.

Saraceno, M., C. Provost, e A. R. Piola (2005), On the relationship between satellite-retrieved surface temperature fronts and chlorophyll a in the western South Atlantic, *J. Geophys. Res., 110,* C11016, doi:10.1029/2004JC002736.

Sathyendranath, S., L. Lazzara, e L. Prieur (1987), Variations in the spectral values of specific absorption of phytoplankton, *Limnol. Oceanogr., 32,* 403–415.

Sathyendranath, S., e T. Platt (1988), The spectral irradiance field at the surface and in the interior of the ocean: A model for applications in oceanography and remote sensing, *J.*

Geophys. Res., 93, 9270-9280, doi:10.1029/JC093iC08p09270.

Sathyendranath, S., G. Cota, V. Stuart, H. Maas, e T. Platt (2001), Remote sensing of phytoplankton pigments: a comparison of empirical and theoretical approaches, *Int. J. Remote Sens., 22,* 249–273, doi:10.1080/014311601449925.

Sathyendranath, S., L. Watts, E. Devred, T. Platt, C. Caverhill, e H. Maass (2004), Discrimination of diatoms from other phytoplankton using ocean colour data, *Mar. Ecol. Prog. Ser.,* 272, 59–68.

Schloss, I. R., G. A. Ferreyra, M. E. Ferrario, G. O. Almandoz, R. Codina, A. A. Bianchi, C. F. Balestrini, H. A. Ochoa, D. Ruiz-Pino, e A. Poisson (2007), Role of plankton communities in sea-air variations in pCO2 in the SW Atlantic Ocean, *Mar. Ecol. Prog. Ser., 332*, 93-106, doi:10.3354/meps332093.

Siegel, H., T. Ohde, M. Gerth, G. Lavik, e T. Leipe (2007), Identification of coccolithophore blooms in the SE Atlantic Ocean off Namibia by satellites and in situ methods, *Cont. Shelf Res., 27,* 258–274.

Signorini, S., V. M. T. Garcia, A. R. Piola, C. A. E. Garcia, M. M. Mata, e C. R. McClain (2006), Seasonal and interannual variability of calcite in the vicinity of the Patagonian Shelf Break (38°S–52°S), *Geophys. Res. Lett., 33,* L1, 6610, doi:10.1029/2006GL026592.

Sokal, R. R., e F. J. Rohlf (1962), The comparison of dendrograms by objective methods, *Taxonomy, 11*, 33–40.

Stæhr, P. A. e J. J. Cullen (2003), Detection of *Karenia mikimotoi* by spectral absorption signatures, *J. Plankton Res., 25,* 1237-1249.

Stauber, J. L., e S. W. Jeffrey (1988), Photosynthetic pigments in fifty-one species of marine diatoms, *J. Phycol., 24,* 158–172.

Stramska, M., e T. Dickey (1993), Phytoplankton bloom and the vertical thermal structure of the upper ocean, *J. Mar. Res*., *51*, 819-842, doi:10.1357/0022240933223918.

Stramska, M., D. Stramski, S. Kaczmarek, D. B. Allison, e J. Schwarz (2006), Seasonal and regional differentiation of bio-optical properties within the north polar Atlantic, *J.*

Geophys. Res., 111, C08003, doi:10.1029/2005JC003293.

Stramski, D., e D. A. Kiefer (1991), Light scattering by microorganisms in the open ocean, *Prog. Oceanogr., 28*, 343-383, doi:10.1016/0079-6611(91)90032-H.

Stramski, D., e R. A. Reynolds (1993), Diel variations in the optical properties of a marine diatom, *Limnol. Oceanogr., 38*, 1347-1364.

Stramski, D., A. Bricaud, e A. Morel (2001), Modeling the inherent optical properties of the ocean based on the detailed composition of the planktonic community, *Appl. Opt., 40,* 2929-2945, doi:10.1364/AO.40.002929.

Stuart, V., S. Sathyendranath, T. Platt, H. Maass e B. D. Irwin (1998), Pigments and species composition of natural phytoplankton populations: effect on the absorption spectra, *J. Plankton Res., 20,* 187-217.

Subramaniam, A., E. J. Carpenter, e P. G. Falkowski (1999), Optical properties of the marine diazotrophic cyanobacteria Trichodesmium spp.; II - a reflectance model for remote-sensing, *Limnol. Oceanogr., 44,* 618–627.

Subramaniam, A., Brown, C. W., Hood, R. R., E. J. Carpenter, e D. G. Capone (2002), Detecting Trichodesmium blooms in SeaWiFS imagery, *Deep Sea Res. Part II, 49,* 107–121.

Szeto, M., P. J. Werdell, T. S. Moore, e J. W. Campbell (2011), Are the world's oceans optically different?, *J. Geophys. Res., 116,* C00H04, doi:10.1029/2011JC007230.

Takahashi, T., S. Sutherland, C. Sweeney, A. Poisson, N. Metzl, B. Tilbrook, N. Bates, R. Wanninkhof, R. Feely, e C. Sabine (2002), Global sea-air CO2 flux based on climatological surface ocean pCO2 and seasonal biological and temperature effects, *Deep Sea Res. Part II, 49,* 1601–1622, doi:10.1016/S0967- 0645(02)00003-6.

Tassan, S., e G. M. Ferrari (1995), An alternative approach to absorption measurements of aquatic particles retained on filters, *Limnol. Oceanogr., 40,* 1358–1368.

Taylor, B. B., E. Torrecilla, A. Bernhardt, M. H. Taylor, I. Peeken, R. Röttgers, J. Piera, e A. Bracher (2011), Bio-optical provinces in the eastern Atlantic Ocean and their biogeographical relevance, *Biogeosciences, 8,* 3609-3629.

Toepel, J., U. Langner, e C. Wilhelm (2005), Combination of flow cytometry and single cell absorption spectroscopy to study the phytoplankton structure and to calculate the chl *a* specific absorption coefficients at the taxon level, *J. Phycol. 41*, 1099-1109, doi:10.1111/j.1529-8817.2005.00137.x.

Torrecilla, E., D. Stramski, R. A. Reynolds, E. Millán-Núñez, e J. Piera (2011), Cluster analysis of hyperspectral optical data for discriminating phytoplankton pigment assemblages in the open ocean, *Remote Sens. Environ.*, *115,* 2578-2593.

Trees, C. C., D. K. Clark, R. R. Bidigare, M. E. Ondrusek, e J. L. Mueller (2000), Accessory pigments versus chlorophyll a concentrations within the euphotic zone: A ubiquitous relationship, *Limnol. Oceanogr., 45*(5), 1130–1143.

Uitz, J., H. Claustre, A. Morel, e S. B. Hooker (2006), Vertical distribution of phytoplankton communities in open ocean: An assessment based on surface chlorophyll, *J. Geophys. Res., 111,* C08005, doi:10.1029/2005JC003207.

Uitz, J., Y. Huot, F. Bruyant, M. Babin, e H. Claustre (2008), Relating phytoplankton photophysiological properties to community structure on large scale, *Limnol. Oceanogr.*, *53*, 614-630, doi:10.4319/lo.2008.53.2.0614.

Vidussi, F., H. Claustre, B. B. Manca, A. Luchetta, e J. C. Marty (2001), Phytoplankton pigment distribution in relation to upper thermocline circulation in the eastern Mediterranean Sea during winter, *J. Geophys. Res. 106,* 19939–19956, doi:10.1029/1999JC000308.

Voss, K. J. (1992), A spectral model of the beam attenuation coefficient in the ocean and coastal areas, *Limnol. Oceanogr., 37,* 501-509.

Wang, G., W. Cao, D. Xu, e Y. Yang (2007), Variability of phytoplankton absorption in the northern South China Sea: influence of the size structure and pigment composition of algal populations, *Acta Oceanol. Sin., 26*, 12-25.

Welschmeyer, N. A. (1994), Fluorometric analysis of chlorophyll-a in the presence of chlorophyll-b and pheopigments, *Limnol. Oceanogr., 39*, 1985–1992.

Werdell, P. J. e S. W. Bailey (2005), An improved in situ bio-optical data set for ocean color

algorithm development and satellite data product validation, *Remote Sens. Environ., 98*, 122–140.

Westberry, T. K., D. A. Siegel, e A. Subramaniam (2005), An improved bio-optical model for the remote sensing of Trichodesmium spp. blooms *J. Geophys. Res.*, *110,* C06012, doi:10.1029/02004JC002517.

Westberry, T. K, G. Dall'Olmo, E. Boss, M. J. Behrenfeld, e T. Moutin (2010), Coherence of particulate beam attenuation and backscattering coefficients in diverse open ocean environments, *Opt. Express, 18*, 15419-15425, doi:10.1364/OE.18.015419.

Wright, W., D. P. Thomas, J. Marchant, H. W. Higgins, M. D. Mackey, e D. J. Mackey (1996), Analysis of phytoplankton of the Australian sector of the Southern Ocean: comparisons of microscopy and size frequency data with interpretations of pigment HPLC data using the 'CHEMTAX' matrix factorization program, *Mar. Ecol. Progress Ser., 144,* 285–298.

Yentsch, C. S., e D. A. Phinney, (1989), A bridge between ocean optics and microbial ecology., *Limnol. Oceanogr. 34,* 1694-1705.

Zapata, M., S. W. Jeffrey, S. W. Wright, F. Rodríguez, J. L. Garrido, e L. Clementson (2004), Photosynthetic pigments in 37 species (65 strains) of Haptophyta: implications for oceanography and chemotaxonomy, *Mar. Ecol. Progress Ser., 270,* 83–102.

Apêndice 1

November 27, 2012

Dr. M. Bauer
Editor in Chief
Remote Sensing of Environment

Dear Dr. Bauer,

We are pleased to submit our manuscript entitled "Bio-optical characteristics of the Patagonian shelf break waters: Implications for ocean color algorithms" for consideration for publication in *Remote Sensing of Environment*.

This work is part of the PATEX project (PATagonia EXperiment) conducted in the Brazilian Antarctic Program. The PATEX project aims to study bio-optical properties and biogeochemical processes at the Patagonia shelf break and vicinities (Southwestern Atlantic), where conspicuous phytoplankton blooms are consistently observed with satellite ocean color data during austral spring and summer.

Four papers on the PATEX project outcomes have been recently published: i) Environmental factors controlling the phytoplankton blooms at the Patagonia shelf-break in spring [*Garcia et al.,* 2008, *Deep Sea Res. Part I*, *55*(9), 1150-1166]; ii) Light absorption by phytoplankton, non-algal particles, and dissolved organic matter at the Patagonia shelf-break in spring and summer [*Ferreira et al.,* 2009, *Deep Sea Res. Part I, 56*(12)*,* 2162-2174]; iii) Environmental conditions and bio-optical signature of a coccolithophorid bloom in the Patagonian Shelf [*Garcia et al.,* 2011, *J. Geophys. Res.*, *116,* C03025]; iv) Phytoplankton community during a coccolithophorid bloom in the Patagonian Shelf: microscopic and HPLC pigment analyzes [*Souza et al.,* 2012, *J. Mar. Biol. Assoc. UK, 92*(1), 13-27].

A paper entitled "Variability in light absorption and scattering of phytoplankton in Patagonian waters: Role of community size structure and pigment composition" is currently under second review for publication in Journal of Geophysical Research-Oceans. This work investigated the variability of the absorption coefficients of phytoplankton and scattering coefficients of particles as a function of chlorophyll-*a* in terms of the phytoplankton cell size and pigment composition for part of the data presented in our submitted manuscript. We believe that we have made appropriate revisions in the above paper following the reviewers' comments and the consequent changes will lead to publication soon. At present this work is cited in our manuscript as *Ferreira et al.* (under review).

We expect that our work will be an important contribution for application of remote sensing of ocean color in the Patagonia shelf break waters.
Sincerely,

Amabile Ferreira, MSc.
Institute of Oceanography
Federal University of Rio Grande, Brazil

Manuscript submitted to Remote Sensing of Environment

Bio-optical characteristics of the Patagonia shelf break waters: Implications for ocean color algorithms

Amabile Ferreira*[1], Carlos Alberto Eiras Garcia[1], Ana Inês Dogliotti[2], Virginia Maria Tavano[1]

[1] *Instituto de Oceanografia, Universidade Federal do Rio Grande – FURG, Av. Itália, Km 8, 96201-900, Rio Grande, Brazil*

[2] *Instituto de Astronomía y Física del Espacio (IAFE-CONICET), Ciudad Universitaria, Casilla de Correo 67 - Suc. 28 (C1428ZAA), Ciudad Autónoma de Buenos Aires – Argentina*

*Corresponding author: amabilefr@gmail.com

Index terms:

Keywords: phytoplankton; absorption; scattering; remote sensing reflectance; Patagonia

Running title: Bio-optical characteristics of the Patagonia shelf break waters

Abstract

Bio-optical data for spring and summer phytoplankton blooms at 176 stations along the Patagonia shelf break and adjacent areas were collected from October 2006 to January 2009 during six cruises. Data included chlorophyll-*a* concentration (Chl*a*), coefficients of particulate absorption, $a_p(\lambda)$, phytoplankton absorption, $a_{ph}(\lambda)$, beam attenuation, $c_p(660)$, diffuse attenuation, $K_d(\lambda)$, and hyperspectral remote sensing reflectance, $R_{rs}(\lambda)$. Surface Chl*a* varied within a wide range from 0.10 to 18.87 mg m^{-3} (mean of 2.82 ± 3.35), reflecting differences in both the timing of the blooms and the geographical sampling area. Considerable dispersion was verified for $a_p(\lambda)$, $c_p(660)$, and $K_{bio}(440)$ ($K_d(440)$ minus diffuse attenuation for pure water) as a function of Chl*a*, which was attributed to variations in phytoplankton cell size within the study area. A hierarchical cluster analysis (HCA) applied to the $R_{rs}(\lambda)$ spectra (N=116) resulted in three classes ordered by spectral features that varied according to Chl*a*. Class 1 (N=22), Class 2 (N=52), and Class 3 (N=42) were grouped according to the $R_{rs}(\lambda)$ associated with Chl*a* average of 0.86 (± 0.51), 2.42 (± 1.62), and 8.40 mg m^{-3} (± 3.96), respectively. The estimation of Chl*a* and $a_{ph}(\lambda)$ by empirical and semi-analytical algorithms was evaluated using satellite data. Errors in the Chl*a* estimates from the empirical algorithm OC4v6 using *in situ* $R_{rs}(\lambda)$ showed significant statistical relationships with Chl*a*, $a_{ph}(440)$/Chl*a*, and $b_p(660)$/Chl*a* (where $b_p(660) = c_p(660) - a_p(660)$). Although reasonable agreements were found between the measured and satellite-estimated values, the dependence of the OC4v6 errors on the Chl*a*-specific phytoplankton absorption and particulate scattering coefficients reinforces the need to regionally refine both empirical and semi-analytical algorithms to improve satellite estimates of the bio-optical variables for the Patagonia region.

1. Introduction

At present, several bio-optical studies seek to reduce the oversimplification associated with models of optical properties that use chlorophyll-*a* concentration as a proxy for phytoplankton and related water constituents (Arnone et al., 2004; Mobley et al., 2004); however, the classical bio-optical classification of waters as Case 1 or 2 is still useful for modeling purposes. In Case 1 waters, phytoplankton and their accompanying retinue of dissolved and particulate biological material govern the water's bio-optical properties. The opposite is true of Case 2 waters, which are significantly influenced by non-algal constituents, including mineral particles, Colored Dissolved Organic Matter (CDOM), microbubbles, the concentrations of which do not vary with the phytoplankton concentration (Morel & Prieur, 1977).

Apparent and inherent optical properties, AOP and IOP, respectively (*sensu* Preisendorfer, 1961), have been widely analyzed for Case 1 waters and are empirically correlated with chlorophyll-*a* concentration (Chl*a*). Indeed, the relationship between IOP and Chl*a* shows robust general trends over orders of magnitudes (e.g., Morel, 1988, Morel & Maritorena, 2001; Morel et al., 2007). For a given Chl*a*, variations in the AOP and IOP is expected because of possible fluctuations in (1) the pigment composition and packaging effects within the phytoplankton assemblages, (2) the proportion of algal and non-algal particles, and (3) the proportion of particulate matter (algal plus non-algal) and CDOM. In high-Chl*a* Case 1 waters, bio-optical properties could be even influenced by the age and nutrient status of the algal population (Morel et al., 2006). Furthermore, due to lack of data for eutrophic waters, the empirical relationships between Chl*a* and AOP or IOP seem to be less robust and noisier then in oligotrophic regions (O'Reilly et al., 1998). In order to address the question of whether there is a greater bio-optical variability in high-Chl*a* (Case 1) waters, the analysis of a more diversified dataset is required including data from upwelling zones (Morel et al., 2006).

In general, phytoplankton absorption properties have been well characterized through laboratory and field measurements. The relationship between the phytoplankton absorption and Chl*a* has shown high variability (e.g., Bricaud et al., 1995; Dmitriev et al., 2009). Based on a large dataset, Bricaud et al. (2004) examined the causes of phytoplankton absorption variability by explicitly separating the impact of changes in pigment composition from changes in pigment packaging, which are due to intracellular pigment concentrations and variations in cell size (Kirk, 1975). The variation around the mean was systematic rather than random and primarily resulted from variability in the packaging effect associated with variations in the size structure of the algal community, even within a given geographical area. This could be attributed to both regional and seasonal changes in the phytoplankton communities. Several approaches involving both *in situ* and satellite remote sensing of phytoplankton absorption coefficients have been used to derive size structure of algal communities (e.g., Ciotti et al., 2002; Aiken et al., 2006; Ciotti & Bricaud, 2006; Hirata et al., 2008; Brewin et al., 2010).

Empirical relationships using field data have related Chl*a* to the beam attenuation coefficient (e.g., Voss, 1992; Loisel & Morel, 1998), the scattering coefficient (Loisel & Morel, 1998), and the backscattering coefficient (Stramska et al., 2006; Huot et al., 2008; Martinez-Vicente et al., 2010). Irrespective of the variability found in those relationships among different studies, Behrenfeld & Boss (2006) noted that the beam attenuation at 660 nm, $c_p(660)$, may be used as a viable index of phytoplankton carbon biomass in ecosystems where phytoplankton biomass and $c_p(660)$ are temporally stable and also as a phytoplankton physiological index in

changing growth conditions (Behrenfeld & Boss, 2003). Recently, Westberry et al. (2010) argued that both phytoplankton biomass and physiological indices can be conceptually assessed by analyzing the relationships between either $c_p(\lambda)$ or Chl*a*:$c_p(\lambda)$ and the particulate backscattering coefficient, $b_{bp}(\lambda)$.

Satellite estimates of Chl*a* have been extensively based on empirical algorithms derived from statistical relationships between Chl*a* and the normalized water leaving radiance, $L_{wn}(\lambda)$, or remote sensing reflectance, $R_{rs}(\lambda)$ (the ratio of water leaving radiance to downwelled irradiance), such as the OC4v6 model currently used to estimate Chl*a* from the Sea-viewing Wide Field-of-view Sensor (SeaWiFS) data (O'Reilly et al., 1998, updated in http://oceancolor.gsfc.nasa.gov/REPROCESSING/R2009/ocv6/). However, a new empirical approach that reduces the bias of ocean chlorophyll estimates has been recently developed (*Gregg et al*., 2009).

$R_{rs}(\lambda)$ is not solely dependent on phytoplankton biomass (indexed as Chl*a*) but is directly proportional to the ratio of backscattering and absorption coefficients for all components in the water, $b_b(\lambda)/a(\lambda)$, including the scattering and absorption of the water itself. Understanding the processes that cause changes in the spectral behavior of the optical components and quantifying the variability of their IOP should improve the retrieval accuracy of individual parameters using remote-sensing techniques (IOCCG, 2006; *Lee et al*., 2010). For instance, although IOP-based algorithms are comparable in performance to the standard empirical chlorophyll algorithms, the semi-analytical models also allow studies of chlorophyll biomass variability as a function of phytoplankton and CDOM absorption (Szeto et al., 2011 and references therein). Brown et al. (2008) have quantified the impact of optical anomalies on the ocean color signal based on their optical sources (absorption and backscattering coefficients). The authors have identified two sources of secondary variability: 1) the amount of non-algal absorption, especially due to CDOM and 2) the amplitude of the particle backscattering coefficient.

During the austral spring and summer, satellite ocean color images have revealed that high levels of phytoplankton biomass persistently occur in the Patagonia inner shelf and shelf break region, which is considered one of the most globally productive ocean zones. The seasonal cycle of phytoplankton biomass in the vicinity of the Patagonia shelf break front has been well described by remote sensing in recent years (Garcia et al., 2004; Rivas et al., 2006; Romero et al., 2006; Signorini et al., 2006).

The development and maintenance of these phytoplankton blooms are associated with nutrient supply from Malvinas Current and the water column stability along the shelf-break front (Garcia et al., 2008). In fact, upwelling process at that front (Matano & Palma, 2008) also contributes with deep nutrient supply for phytoplankton growth. The Argentinean continental shelf has been recognized as a relevant region in terms of standing stocks of primary producers and contribution to the global primary production (e.g., Gregg et al., 2005). High primary productivity rates (1.9 to 7.8 mg C m^{-2} d^{-1}) were measured in the area during spring (Garcia et al., 2008) and the variability in photosynthetic parameters was shown to be associated with the light absorption properties of the phytoplankton composition (Lutz et al., 2010). Specifically, Ferreira et al. (2009) described an important difference in phytoplankton absorption coefficients between spring and late summer periods that was attributed to differences in the phytoplankton size structure.

The observed seasonality of phytoplankton properties (composition, light absorption, and photosynthetic parameters) has an important implication for the

regional ecology and carbon cycle, because the efficiency of energy transfer throughout the trophic levels is related to the phytoplankton cell size (Kiørboe, 1993; Guidi et al., 2010), and the CO_2 uptake by seawater is influenced by the phytoplankton composition (Bopp et al., 2005; see revision by Le Quéré et al., 2005). For instance, studies in the Argentinean continental shelf have shown that when phytoplankton assemblages were dominated by large diatoms, both phytoplankton biomass (Chl*a*) and net community production were inversely proportional to ΔpCO_2 and directly related to % O_2 saturation (Schloss et al., 2007). This was not the case when small ($\leq$5 μm) flagellates dominated. The region makes an important contribution to the global oceanic CO_2 uptake from the atmosphere (Bianchi et al., 2009).

Despite the ecological and biogeochemical relevance of the Patagonia shelf, *in situ* bio-optical measurements (IOP and AOP properties) are scarce in the region and the lack of a comprehensive bio-optical study is a major obstacle for better estimates of ocean color products such as Chl*a*. Regional particularities in the optical properties of the Patagonia waters might impact the performance of bio-optical algorithms. Moreover, there is a lack of specific analyses of the performance of existing algorithms for the region's satellite data. *Dogliotti et al*. (2009) reported that NASA's operational algorithms generally overestimates at low Chl*a* (<1 mg m^{-3}) and underestimates at high Chl*a* (>1 mg m^{-3}). This was attributed to the lack of bio-optical measurements at high pigment concentrations when the algorithm was generated in the late 1990s (O'Reilly et al., 1998, 2000).

The Patagonia experiment (PATEX) is a research project conducted under the Brazilian Antarctic Program umbrella. Within the project objectives are the characterization of the phytoplankton assemblages, bio-optical properties, and primary production rates of the waters along the Argentinean shelf break and the environmental constraints associated with the blooms during spring and summer. Seven cruises were conducted between 2004 and 2009 in the Argentinean Patagonia shelf break and adjacent areas. In this study, we present results of the bio-optical data from six cruises carried out in the region during spring and summer phytoplankton blooms.

The present work aims to investigate the relationships between Chl*a* and IOP (particulate absorption and attenuation coefficients) and AOP (diffuse attenuation coefficient) within the phytoplankton blooms in the Patagonia waters, contributing with data on bio-optical properties of high-Chl*a* waters (Morel et al., 2006). We also describe the variability in the spectra of hyperspectral remote sensing reflectance and evaluate the retrieval of Chl*a* and phytoplankton absorption coefficients through current empirical and semi-analytical algorithms using both *in situ* and satellite reflectance data. In addition, we investigate the relationship between the variations in absorption and scattering coefficients normalized by Chl*a* and the errors associated with Chl*a* estimates from empirical algorithms.

2. Material and Methods

2.1. Oceanographic cruises and sections

The Patagonia shelf break and a portion of the inner shelf were extensively sampled (176 stations) by performing cross- and along-shelf transects during the PATEX cruises in the austral spring (October 2006, 2007, and 2008 and PATEX 2, 4 and 6, respectively) and summer (March 2007, January 2008 and 2009 and PATEX 3, 5 and 7, respectively). The geographical positions of the sampling stations (Figure 1) spanned from the northern portion of the Argentinean Shelf (PATEX 6) through the

highly productive waters along both the Patagonia shelf break (PATEX 2 to 4) and the southern inner shelf (PATEX 5) to the southern end of the Malvinas Islands (PATEX 7).

The following measurements used in this study were performed at all stations (N=176): (i) total Chl*a*, (ii) particulate (phytoplankton and detritus) absorption, and (iii) beam attenuation coefficient at 660 nm. The (iv) diffuse attenuation coefficient and (v) hyperspectral remote sensing reflectance were measured at stations during daylight hours (N=116) and are indicated in Figure 1 as filled markers.

2.2. Chlorophyll-a concentration

Discrete samples for Chl*a* were collected at the surface and selected depths based on the chlorophyll fluorescence profile and filtered onto 25-mm glass fiber filters (Whatman® GF/F). After filtration, the filters were wrapped in aluminum foil and transferred to liquid nitrogen for later analysis. At the laboratory, the pigment was extracted in 90% acetone and the fluorescence was determined with a Turner Designs TD-700 fluorometer (previously calibrated with Sigma® chlorophyll-*a* standard) following the non-acidification method from Welschemeyer (1994). In the present study, we considered Chl*a* (i) from the surface, the depths of maximum chlorophyll fluorescence (MCF), and bottom of the peak of chlorophyll fluorescence (BMCF) for analysis of particulate absorption (N=356) (ii) from along the water column to relate to the beam attenuation coefficient at 660 nm (N=790) (iii) and from the surface for analysis of the diffuse attenuation coefficient and (iv) hyperspectral remote sensing reflectance (N=176). For the last two cases, the number of surface Chl*a* measurements was reduced to 116, matching the availability of both *in situ* diffuse attenuation and remote sensing reflectance.

2.3. Particulate absorption coefficient

The spectra of the particulate absorption coefficient, $a_p(\lambda)$ in m^{-1}, were obtained with the quantitative filter pad technique (Kishino et al., 1985) using water samples (0.5-2 L) collected at the surface, MCF, and BMCF that were filtered onto 25-mm Whatman GF/F filters. Immediately after filtration, the GF/F filters were wrapped in aluminum foil and placed in liquid nitrogen for storage. The $a_p(\lambda)$ measurements were made in the 300–750 nm spectral range at 1-nm intervals with a dual beam spectrophotometer (Cary Model 1E). Immediately after the $a_p(\lambda)$ measurements, the sample filters were subjected to methanol extraction (for the PATEX 2 and 3 cruises) and bleaching with sodium hypochlorite (PATEX 4, 5, 6 and 7 cruises) and then re-scanned to obtain estimates of the non-algal particle (detritus) absorption coefficient, $a_d(\lambda)$ (Kishino et al., 1985; Tassan & Ferrari, 1995; Mitchell et al., 2000). For the calculations of the $a_p(\lambda)$ and $a_d(\lambda)$ coefficients, the amplification factor β given by Ferreira et al. (2009) was used. The spectral absorption coefficient of phytoplankton, $a_{ph}(\lambda)$, was calculated as the difference between $a_p(\lambda)$ and $a_d(\lambda)$.

2.4. Particulate attenuation coefficient

The beam attenuation coefficient of suspended particles at 660 nm, $c_p(660)$ in m^{-1}, was measured with a C-star beam transmissometer (WETLabs, Inc.) along a 25-cm pathlength through the water column. Details of the protocol for determining $c_p(660)$ are provided by the manufacturer of the C-star beam transmissometer (http://www.wetlabs.com/cstar). We assumed that measurements taken in deep waters (~1,000 m) but still far away from the sea bottom provided the best estimate of particle-free attenuation of the seawater (Loisel & Morel, 1998). These deep-water

measurements were subtracted from all beam attenuation measurements taken at the surface ocean layer on a cruise-by-cruise basis to remove the contribution of pure seawater. The resulting values represent the beam attenuation by particles, assuming that the contribution of dissolved matter to the attenuation of light at 660 nm is negligible. We also note that the measurements taken at 5 m depth were assumed to represent the near-surface beam attenuation, which is reasonable given that it avoids or minimizes the potential intermittent contributions of air bubbles injected by breaking waves.

2.5. Hyperspectral Diffuse Attenuation Coefficient and Remote Sensing Reflectance

Underwater radiometric measurements were obtained with a hyperspectral profiling radiometer (HyperOCR, Satlantic, Inc.), which measures the upwelling radiance, $L_u(\lambda,z)$, and the downward irradiance, $E_d(\lambda,z)$, over the 350–800 nm spectral range with a resolution of 3.3 nm (137 spectral bands). The spectral remote sensing reflectance, $R_{rs}(\lambda)$ in sr^{-1}, is defined as the ratio of nadir water-leaving radiance, $L_w(\lambda)$, to the downwelling plane irradiance, $E_d(\lambda)$, just above the sea surface (0^+). The measured $L_u(\lambda,z)$ and $E_d(\lambda,z)$ in the water column are used to estimate their values just beneath the surface, $L_u(\lambda, 0^-)$ and $E_d(\lambda, 0^-)$, and then are propagated through to the sea-air interface to obtain $L_w(\lambda)$ and $E_d(\lambda,0^+)$.

The initial data processing was performed using ProSoft ver. 7.7.11 processing software, developed and distributed by Satlantic Inc. Dark offsets and the manufacturer's radiometric calibrations were applied to the raw data, and the spectral radiometric data were binned every 0.1 m. Because of surface waves, it was rarely possible to measure $E_d(\lambda,z)$ and $L_u(\lambda,z)$ closer to the sea surface. The shallowest reliable readings typically occurred at depths ranging from 0.5-2 m. The data from this zone usually exhibited strong fluctuations associated with surface waves, and thus it was necessary to extrapolate the data upward to the sea surface. Matlab® routines were developed to analyze each radiometric profile and process the radiometric data. Visualization of $E_d(\lambda,z)$, $L_u(\lambda,z)$, *PAR* (Photosynthetic Available Radiance) percentage, and tilt angle were used to analyze the quality of each profile and the depth interval to be used to extrapolate the values to just below the water surface.

The diffuse attenuation coefficients of downwelling irradiance, $K_d(\lambda)$, and upwelling radiance, $K_u(\lambda)$, were calculated as the slope of a least-squares linear regression of the log-transformed $E_d(\lambda,z)$ and $L_u(\lambda,z)$, respectively, within the selected depth interval, which generally ranged between 2 to 7 m. Using these coefficients, $L_u(\lambda,z)$ and $E_d(\lambda,z)$ were propagated to just below the water surface by fitting an exponential function to the profile data. The remote sensing reflectance was then calculated using the following equation: $R_{rs}(\lambda) = 0.54\, L_u(\lambda,0^-) / (1.04\, E_d(\lambda,0^-))$, where 0.54 and 1.04 are the transfer coefficients of the air-sea interface for $L_u(\lambda)$ and $E_d(\lambda)$, respectively (Austin, 1974). The fraction of $K_d(\lambda)$ associated with the presence of particulate and dissolved materials was computed as $K_{bio} = K_d - K_w$ for 440 nm, where K_w is the coefficient for pure water equal to 0.00885 m^{-1} at 440 nm (Morel & Maritorena, 2001).

A hierarchical cluster analysis (HCA) was applied in order to classify the $R_{rs}(\lambda)$ spectra into coherent groups. The applicability of this method in the classification of hyperspectral $R_{rs}(\lambda)$ dataset for coastal waters was demonstrated by Lubac & Loisel (2007). Because the preliminary classification from HCA was greatly degraded by noise in the red range of several $R_{rs}(\lambda)$ spectra, only the range between 400 to 600 nm was considered. Prior to running the HCA, each $R_{rs}(\lambda)$ spectrum was normalized to its mean value computed on the basis of all spectral values between 400

and 600 nm. The normalized spectrum is denoted $nR_{rs}(\lambda)$.

2.6. Bio-optical Algorithms Evaluation

A comparison was carried out between the measured Chl*a* with values retrieved from three bio-optical empirical algorithms, OC2v6 and OC4v6 derived for SeaWiFS data and OC3v6 for MODIS/Aqua (*http://oceancolor.gsfc.nasa.gov/REPROCESSING/R2009/ocv6),* using *in situ* measurements of $R_{rs}(\lambda)$. Furthermore, a matchup analysis was performed comparing *in situ* and remote-sensed Chl*a* retrieved from the Garver-Siegel-Maritorena semi-analytical algorithm (GSM) and *in situ* and remote-sensed phytoplankton absorption coefficients estimated from the GSM (*Maritorena et al*., 2002) and QAA (*Lee et al*., 2002) semi-analytical algorithms. The statistical parameters used for these evaluations were the mean relative percentage difference, *RPD*, and the mean absolute percentage difference, *APD*. The definitions of *RPD* and *APD* are presented in Table 3. The coefficient of determination, R^2, slope, and intercept obtained from the regression analysis of the log-transformed *in situ* measured data and algorithm-derived were also considered for evaluation of the performance of the empirical and semi-analytical algorithms.

2.7. Matchup analysis

MODIS satellite/Aqua level 1A and ancillary data of ozone concentration and meteorological conditions (wind speed, oxygen concentration, water vapor and atmospheric pressure) were obtained from NASA's Distributed Active Archive Center (DAAC). Full resolution imagery of the local area coverage (LAC) for the PATEX 2 to PATEX 7 cruises was used to evaluate products derived from empirical and semi-analytical algorithms. The selected images were processed to level 2 (L2), and the following data products were obtained: the Chl*a* retrieved from empirical (OC2v6, OC3v6, OC4v6) and semi-analytical (GSM) algorithms, the phytoplankton absorption coefficient retrieved from GSM and QAA algorithms, and the ancillary information, such as the solar and sensor zenith angles and the L2 processing flags. The SeaWiFS Data Analysis System (SeaDAS) software version 6.4 was used to process data from level 1 and the product retrievals.

For comparison between the *in situ* data and satellite products and to minimize georeference errors, median values were computed for all products in a 3-by-3 pixel window centered on the locations of the oceanographic stations. Furthermore, the coefficient of variation (CV) was computed for the Chl*a* within each 3 by 3 window, and the retrieved value was excluded if CV>0.2. This process was carried out to avoid strong variation from non-homogeneous regions within each window. For the temporal threshold coincidence between the satellite and *in situ* measurements, we considered a ± 3 hours window around the satellite overpass, which follows the NASA's criterion (*Bailey et al.* 2000).

3. Results and Discussion

The surface Chl*a* for all six PATEX cruises varied in a wide range from 0.10 to 18.87 mg m^{-3} with a mean value of 2.85 mg m^{-3}. The Chl*a* for MCF and BMCF varied from 0.08 to 24.05 mg m^{-3} and 0.08 to 12.03 mg m^{-3}, respectively. The frequency distribution of Chl*a* at the surface, MCF, and BMCF are shown in Figure 2 (N=176, 159 and 85, respectively). The variability in Chl*a* reflected differences in both the timing of the blooms and the geographical distribution of the sampling sites (discussed by Ferreira et al., under review) and the phytoplankton size structure based

on fractionated Chl*a* for size classes.

3.1. Phytoplankton and Particulate Absorption and Diffuse Attenuation Coefficients

Table 1 shows the absorption coefficients at 440 nm of particulate material, $a_p(440)$, and phytoplankton, $a_{ph}(440)$, and the percent contribution of phytoplankton to the particulate absorption, $a_{ph}(440)/a_p(440)$, for each cruise. The data include surface, MCF, and BMCF measurements. Non-algal absorption, $a_p(440)$ - $a_{ph}(440)$, did not co-vary with Chl*a,* regardless of the sampled depth (not shown), and its contribution was relatively low during all cruises (average of 13%), even with the high variability in Chl*a*.

Phytoplankton was the dominant component of the particulate absorption (Table 1), with the lowest and highest average contributions during PATEX 3 (81%) and PATEX 4 (96%). These results suggest that for the shelf break and adjacent areas during the blooms in spring and summer, the particulate absorption is largely dominated by living cells and the relative proportions of detrital particulates shows little seasonal and interannual change. Our results on the percent contribution by phytoplankton are in agreement with the range of 85 to 94% found by Morel et al. (2006) for Case 1 waters with high chlorophyll concentrations.

$a_p(440)$ ranged from 0.026 to 0.492 m^{-1} and increased (on a log scale) with increasing Chl*a* (0.08 to 24.02 mg m^{-3}) (Figure 3a). Linear fitting between log-transformed data provided a R^2 of 0.77 (N=356). Inferred from the general nonlinear character of this dependence (Bricaud et al., 1998) and the broad range of Chl*a* covered by our dataset, the chlorophyll-specific particle absorption, $a_p^*(440)$ ($a_p(440)$:Chl*a*) decreased with increasing Chl*a* and ranged widely from 0.023 to 0.237 m^2 mg^{-1}. The power function $a_p(440) = A\ \mathrm{Chl}a^{B}$, where the A and B parameters are derived from regression analysis, provided a reasonably good fit to our data and was comparable to previously derived average relationships (Bricaud et al., 1998; Morel et al., 2006). Our $a_p(440)$ values average 75% above the mean relationship of Bricaud et al. (1998), B98, whereas the positive departure from Morel et al. (2006) equation, M06, derived for Case 1 waters with high chlorophyll content averages only 19%.

The dependence of $K_{bio}(440)$ on Chl*a* is displayed in Figure 3b, and a power law described this dependence in the same way as for $a_p(440)$. The lower R^2 (0.65) computed between Chl*a* and log-transformed $K_{bio}(440)$ was comparable to that for $a_p(440)$ and may be partially attributed to the lower number of $K_{bio}(\lambda)$ data, which comprises only surface samples (N=116). We also compared our fitting relationship for Chl*a* and $K_{bio}(440)$ to the general prediction model recently re-analyzed by Morel et al. (2007), M07. The same systematically higher trend of our $a_p(440)$ compared to the general fittings (B98 and M06) was also verified for $K_{bio}(440)$ (Figure 3b). On average, our $K_{bio}(440)$ was higher by approximately 26% to what was expected from M07. This finding is in agreement with $K_d(\lambda)$ being a rough proxy of the absorption coefficient, merging the dominant effect of absorption and to a lesser extent backscattering (Gordon, 1989), mainly when the phytoplankton is the dominant particulate component. Indeed, $K_{bio}(440)$ and $a_p(440)$ were linearly correlated (Figure 3c) with a R^2 of 0.67. As expected, $K_{bio}(440)$ was higher than $a_p(440)$, as seen by the points above the 1:1 line, on average by 1.67-fold. It is important to note that the CDOM absorption increases exponentially towards blue and UV wavelengths, so its absorption contributes with an important amount to the diffuse attenuation at 440 nm. Although we could not quantify the effect of CDOM absorption on $K_{bio}(440)$, part of the variability in $K_{bio}(440)$ not explained by $a_p(440)$ may be attributed to CDOM absorption. The importance of CDOM in explaining part of the $K_{bio}(\lambda)$ variability

towards lower wavelengths is emphasized by the lower R^2 (0.42) obtained between $K_{bio}(360)$ ($K_w(360)$ equal to 0.0216 m^{-1}, as provided by Morel & Maritorena, 2001) and $a_p(360)$. However, part of the dispersion for this dependence may be attributed to the correction procedure adopted for the β amplification factor, which is not optimized for computation of $a_p(\lambda)$ in the UV range.

Our previous work characterized the variability in the coefficients of phytoplankton absorption, $a_{ph}(\lambda)$, instead of $a_p(\lambda)$, as a function of Chl*a* for part of the data shown here (Ferreira et al., under review). As inferred from the dominance of phytoplankton on particulate absorption showed in the present work, our $a_{ph}(\lambda)$ values were generally above the general relationships (Bricaud et al., 1995; Bricaud et al., 2004) for a given Chl*a*. Previous studies concluded that differing non-algal detrital material content for a given Chl*a* caused the systematic deviations from the average of particulate absorption vs. Chl*a* (e.g., Morel et al., 2007 and references therein). Our results for $a_p(\lambda)$ however, suggest that non-algal particles may not modify the relationship between the bulk optical properties and Chl*a*, which is generally used as a single index by traditional bio-optical models, but actually show that the dispersion between Chl*a* and $a_p(440)$ (R^2=0.77) is practically the same as for $a_{ph}(440)$ (R^2=0.78, Ferreira et al., under review). Ferreira et al. also demonstrated that most of the variability in $a_{ph}(\lambda)$ as a function of Chl*a* was caused by variations in the dominant cell size of phytoplankton. The systematic deviations in both $a_p(\lambda)$ and $K_{bio}(\lambda)$ for the Patagonia waters found in this study compared to general trends can be therefore attributed to variations in the phytoplankton size.

3.2. Relationship Between Chlorophyll-a and Particulate Attenuation Coefficient

At 660 nm (after deducting the attenuation by pure seawater), the particle attenuation coefficient is primarily (~ 97%, Loisel & Morel, 1998) caused by particle scattering. Figure 4 shows $c_p(660)$ as a function of Chl*a* for the six PATEX cruises. Because the measurements of $c_p(660)$ were taken along the water column and Chl*a* concentrations data are from several discrete depths, a higher number of Chl*a* vs. $c_p(660)$ pairs were available (N=790) than for $a_p(440)$ (N=356). We compared our data to the relationship derived by Loisel & Morel (1998), LM98, for near-surface waters (their Equation 5). We note that the LM98 relationship was established for a narrower Chl*a* range (0.2 to 3.0 mg m^{-3}), unlike the range of our dataset (0.08 to 24.05 mg m^{-3}). Our $c_p(660)$ data correspond to lower Chl*a* (PATEX 3, 6 and 7) and are in agreement with LM98 (Figure 4). Conversely, Chl*a* and $c_p(660)$ pairs were considerably lower than LM98 for higher Chl*a* (PATEX 2 and 4).

Regarding the particulate absorption coefficients, a non-linear model described the dependence of $c_p(660)$ on Chl*a,* and a power function fit provided the relationship $c_p(660)=0.343\ Chla^{0.37}$ for the entire dataset. Owing to the large dispersion of the data, the coefficient of determination obtained between the log-transformed data was relatively low (R^2=0.60, N=790). The low exponent (0.37) indicates a deviation from linearity and relatively weak dependence. The high dispersion was partially associated with systematic differences between the cruises (Figure 4), which was also observed for $a_p(440)$, although to a lesser extent (Figure 3a). In general, higher and lower values of $c_p(660)$:Chl*a* for a given Chl*a* was observed for PATEX 3, 6 and 7 and PATEX 2 and 4, respectively. Relatively high $c_p(660)$:Chl*a* ratios for PATEX 5 associated with a coccolithophorid bloom (Garcia et al., 2011) stand out from most of the data and were also more scattered. Therefore, a distinct fitting was applied to represent (i) PATEX 2 and 4 and (ii) PATEX 3, 6, and 7; (iii) PATEX 5 was considered separately.

Table 2 shows the power law equations resulting from the combination of all PATEX data and the data derived separately according to similar trends between cruises. The lowest coefficient A of the relationship obtained for PATEX 2 and 4 (0.254) indicates a lower relative magnitude of attenuation for a given Chl*a*, which indicates that the strong non-linearity (exponent=0.471) may be explained by higher Chl*a* and large phytoplankton cells (Ferreira et al., under review). The PATEX 3, 6, and 7 cruises, which showed relatively low Chl*a* in association with smaller-sized cells (Ferreira et al., under review), revealed higher relative attenuation coefficients (A=0.333) and a clear dependence on Chl*a* (exponent B=0.818) tending to linearity ($c_p(660)$:Chl*a* nearly constant for all Chl*a* ranges). The highest coefficient A (0.610) and lowest exponent B (0.40) derived for PATEX 5 indicates relatively high attenuation values and a weak dependence on Chl*a* (R^2=0.56). This highlights the limitation of parameterizations for scattering (or backscattering) coefficients according to chlorophyll-*a* during coccolithophorid blooms because of the high scattering properties of the coccoliths ($CaCO_3$ platelets around cells) independent of Chl*a* (see Garcia et al., 2011). As expected, the generally weak dependence of $c_p(660)$ on Chl*a* for PATEX 5 is not verified for particulate absorption coefficients (Figure 3a), which are specifically resultant from pigments.

Despite the variability around the mean in $c_p(660)$ as a function of Chl*a* (Loisel & Morel, 1998; this work) that was greater than the variability in $a_p(440)$, there was a general similarity in the variability of both coefficients (Figure 3a and Figure 4) caused by variations among the cruises. Our previous work (Ferreira et al., under review) showed a strong relationship between the chlorophyll-specific particulate scattering coefficient at 660 nm, $b^*_p(660)$ ($b_p(660)$ normalized by Chl*a*) and the chlorophyll-specific phytoplankton absorption coefficient, $a^*_{ph}(440)$ ($a_{ph}(440)$ normalized by Chl*a*). Also, variations in chlorophyll-specific coefficients as a function of Chl*a* were mostly explained by differences in the phytoplankton cell size. In fact, Ferreira et al. (under review) derived two distinct power law relationships for $a_{ph}(440)$ as a function of Chl*a* by analyzing samples dominated by either nanophytoplankton or microphytoplankton.

Variations in $c_p(660)$ as a function of Chl*a* for Patagonia waters does not appear to reflect the physiological adjustments proposed by Behrenfeld & Boss (2003). Since the existing relationships between $c_p(\lambda)$ and phytoplankton biomass can be conceptually extended to use of particulate backscattering coefficients (Westberry et al., 2010), the variability in $c_p(660)$:Chl*a* presented here could be extended to applications of existing ocean color reflectance retrievals that depend on $b_b(\lambda)/a(\lambda)$. However, pronounced differences in scattering caused by a great variability in cell size structure associated with different stages of the bloom makes it difficult to establish a unique relationship between Chl*a* and scattering (or backscattering) for Patagonia waters.

3.3. Variability in Hyperspectral Remote Sensing Reflectance Spectra

The hyperspectral remote sensing reflectance spectra, $R_{rs}(\lambda)$, derived from the six PATEX cruises showed a great variability in both the magnitude and spectral shape (Figure 5). The exclusion of the 600 to 700 nm range for the HCA (section 2.5) eliminated the chlorophyll-*a* fluorescence peak centered at 683 nm, which was a conspicuous feature of several $R_{rs}(\lambda)$ spectra (Figure 5). As expected, this peak was associated with $R_{rs}(\lambda)$ spectra in high Chl*a* samples. Three distinct classes were identified through a dendrogram and are illustrated in Figure 6. The ordinary spectra, $R_{rs}(\lambda)$, for the three classes are also shown.

Class 1 covered the largest number of spectra ($N = 52$) and showed the highest $R_{rs}(\lambda)$ magnitudes among the three classes (Figure 6a) and the greatest variability at lower wavelengths. The maximum reflectance was found at approximately 490 nm, and the magnitudes decreased towards higher wavelengths. Class 1 peaks corresponding to chlorophyll-*a* fluorescence at approximately 683 nm were not evident (not shown). Spectra with $R_{rs}(\lambda)$ higher than 0.01 sr^{-1} in the blue to the green wavelengths were found during the PATEX 5 cruise (Figure 5d, Figure 6a) and were associated with a great abundance of coccolithophorids (Garcia et al., 2011).

The $R_{rs}(\lambda)$ spectra of Class 2 and Class 3 were similar at the blue range and showed a concave shape between the main chlorophyll-*a* absorption band and the lowest reflectance at approximately 450 nm. The major differences between both the classes were found in the green range, where Class 2 $R_{rs}(\lambda)$ spectra presented a wide peak between 490 and 560 nm, and Class 3 $R_{rs}(\lambda)$ spectra showed a distinct peak at 570 nm. Class 2 $R_{rs}(\lambda)$ spectra also showed a double peak in the green range of the spectrum with variable shapes ($N = 42$). Class 3 comprised the lowest number of spectra ($N = 22$), and except for two spectra with approximately 0.005 sr^{-1} close to 570 nm (Figure 6e), the maximum absolute reflectance was always lower than 0.004 sr^{-1}. For both Class 2 and Class 3, the Chl*a* fluorescence emission peak near 683 nm can be seen (see Figure 5).

The wide range of Chl*a* in the study region primarily explained the clustering identified through the HCA, with the lowest concentrations corresponding to Class 1 (mean 0.86 ± 0.51 mg m^{-3}) followed by intermediate concentrations in Class 2 (mean 2.42 ± 1.62 mg m^{-3}), and the highest concentrations in Class 3 (mean 8.40 ± 3.96 mg m^{-3}). Class 1 contained few $R_{rs}(\lambda)$ spectra from PATEX 2, PATEX 4 and PATEX 6, most $R_{rs}(\lambda)$ spectra from PATEX 3, and all spectra from PATEX 5 and PATEX 7. Class 2 comprised $R_{rs}(\lambda)$ spectra associated with moderate Chl*a* concentrations found in PATEX 2, the highest concentrations found in PATEX 3, the intermediate concentrations found in PATEX 4, the relatively high concentrations found in PATEX 6 and one sample of PATEX 5. This was different from the other samples because, unlike other sites, diatoms were dominant (Garcia et al., 2011). Class 3 only included spectra from PATEX 2 and 4 (spring cruises).

Although no data for CDOM absorption is available, its contribution to the $R_{rs}(\lambda)$ spectra was probably minor because a noticeable decrease in $R_{rs}(\lambda)$ at the blue portion of the spectra and towards shorter wavelengths was not observed.

3.4. Evaluation of Chlorophyll-a Empirical Algorithms

The analysis above showed that the $R_{rs}(\lambda)$ spectra from the Patagonia region may be separated according to spectral features that vary according to Chl*a*. In this section, we investigate the performance of operational empirical models that rely on the relationship between $R_{rs}(\lambda)$ band ratios and Chl*a*. Chl*a* was estimated from *in situ* $R_{rs}(\lambda)$ measurements from all cruises using the OC2v6, OC3v6 and OC4v6 empirical algorithms and compared to the *in situ* measured Chl*a*. Figure 7 depicts the measured Chl*a* as a function of the $R_{rs}(\lambda)$ band ratios, relative to each of the three Chl*a* empirical algorithms, and their respective representational curves. The NOMAD dataset is also plotted as background for comparison.

Both the SeaWiFS 2-band (OC2v6) and MODIS 3-band (OC3v6) algorithms showed some deviation towards overestimating Chl*a* when considering the whole PATEX dataset (Figure 7), with R^2=0.67 and 0.62, respectively, and a positive *RPD* (Table 3). The SeaWiFS 4-band (OC4v6) algorithm performed better ($R^2 = 0.78$) and

had the lowest bias (*RPD* = 11.54%), and a mean absolute percentage difference (*APD* = 42.05%, Table 3). The results shown here are in agreement with previous analyses based on satellite data for the region (Garcia et al., 2006; Dogliotti et al., 2009).

In order to investigate whether the performance of chlorophyll empirical models are associated with variations in the spectral shape of $R_{rs}(\lambda)$ and variations in Chl*a*, the same empirical models used to retrieve Chl*a* were applied separately to each $R_{rs}(\lambda)$ class previously determined by HCA (Figure 7). Linear fitting adjusted to measured and estimated log-transformed Chl*a* pairs were not statistically significant for most cases, which was probably due to the narrower Chl*a* range and the smaller dataset within each class. Thus, the performance of the models for each class was evaluated separately using R^2, slope, and intercept (Table 3). Regarding the OC4v6 algorithm, large errors (*RPD* = 31.80%; *APD* = 51.57%) were found for the class relative to moderate Chl*a* (Class 2), but there was a good agreement of the tested algorithm for the classes associated with the lowest (Class 1) and highest (Class 3) Chl*a* (*RPD* = -2.63% and *APD* = 30.82%; *RPD* = 6.30% and *APD* = 50.21%, respectively) (Table 3). Note that the poorer performance of the model for Class 2 was primarily explained by a narrower range of the estimated Chl*a* (0.97 to 4.69 mg m^{-3}), unlike the larger range found in the measured Chl*a* (0.74 to 7.96 mg m^{-3}). The performances of both the OC2v6 and OC3v6 algorithms were always poorer compared with the OC4v6 (Table 3 and Figure 7).

Based on remote sensing reflectance, Moore et al. (2009) classified eight optical water types representative of the global ocean as determined from the NOMAD dataset. Although they verified a general pattern of increasing Chl*a* across the water types, the Chl*a* ranges overlapped between the types. The overlapping occurs in waters with the same chlorophyll-*a* content but distinct optical properties, such as suspended sediments and organic matter, pigment composition and cell size structure of phytoplankton. In our work, as the phytoplankton was shown to be the dominant particulate component and CDOM did not seem to play a noticeable role in determining the $R_{rs}(\lambda)$ spectra (Figures 5 and 6), the overlap observed between the three classes in our data (Figure 7) most likely reflects differences in phytoplankton optical properties for a given Chl*a*.

High relative errors are expected in the performance of empirical bio-optical models in high Chl*a* waters because of the increasing optical complexity from additional material besides phytoplankton in the eutrophic waters (Morel et al., 2006). Interestingly, the errors associated with Class 3 (high Chl*a*) were relatively low (Table 3). Thus, very high Chl*a* associated with phytoplankton blooms along the Patagonia shelf break waters does not appear to result in large errors from empirical model performances. However, large errors were associated with intermediate to high Chl*a* (Class 2, Table 3). Although the CDOM contribution to the reflectance spectra appears to be low, its contribution to absorption should be properly assessed to determine how it might impact the empirical model's performance (e.g., Szeto et al., 2011).

3.5. Relations Between Empirical Algorithm Errors and Inherent Optical Properties

Most of the empirical bio-optical algorithms used to derive Chl*a* rely upon relationships between the Chl*a* and the blue-to-green spectral ratios of $R_{rs}(\lambda)$. However, the shape and magnitude of the $R_{rs}(\lambda)$ spectra actually depend on backscattering and absorption coefficients (IOP), which reflect variations in the optical components of seawater. In this section, we investigate how the variations in

the IOP in terms of normalization to Chl*a* might influence the performance of the chlorophyll-*a* empirical models applied to Patagonia *in situ* $R_{rs}(\lambda)$ data. As it is based solely on *in situ* radiometric and Chl*a* measurements, this analysis does not include any uncertainty attributed to atmospheric correction or satellite radiance accuracy. Only the OC4v6 model was considered in this analysis, because it performed best when applied to our dataset (section 3.4). The relative error (*RE*) was defined as *RE* = 100* (retrieved Chl*a* – measured Chl*a*) / measured Chl*a*.

Figure 8 shows the dependence of relative errors of the OC4v6 algorithm-retrieved Chl*a* on the measured Chl*a* (Figure 8a), $a_{ph}(440)$ (Figure 8b), and $b_p(660)$ (Figure 8c), both coefficients normalized by Chl*a* (a_{ph}*(440) and b_p*(660), respectively, in m^2 mg^{-1}). $b_p(660)$ was computed as $c_p(660)$ subtracted $a_p(660)$.

The *RE* is scattered over the entire Chl*a* range (Figure 8a), but significant relationships (α = 95%) were observed when each class was considered separately (p<0.001 for Class 1, Class 2, and Class 3), and a general trend of underestimation emerged as Chl*a* increased. Likewise for Chl*a*, significant correlations were found between *RE* and a_{ph}*(440) (p < 0.001 for Class 1, Class 2, and Class 3) and b_p*(660) (p=0.02 for Class 1 and p< 0.0001 for Class 2, and Class 3) and a clear tendency towards overestimation emerged for the retrieved Chl*a* according to increases in both a_{ph}*(440) and b_p*(660) (Figure 8b and 8c).

Variations in a_{ph}*(λ) are associated with phytoplankton pigment packaging, which may be affected by variations in both the accessory pigments and cell size. Relatively lower Chl*a* and higher a_{ph}*(λ) are indicative of phytoplankton with small and lesser-packaged cells, whereas high Chl*a* and lower a_{ph}*(λ) are associated with large, highly packaged cells (Bricaud et al., 1995 and references therein). Our previous work (Ferreira et al., under review) confirmed that variations in a_{ph}*(440) were related to cell size for the data presented here, indicating that most of the variability in phytoplankton absorption and scattering coefficients in Patagonia waters is explained by changes in the dominant cell size. Interestingly, the same trend was verified for b_p*(660), whereas a linear relationship held between a_{ph}*(440) and b_p*(660) (Ferreira et al., under review). The direct dependence of *RE* on both a_{ph}*(440) and b_p*(660) shown here indicates that the empirical algorithm's uncertainties vary systematically with phytoplankton size structure.

The empirical algorithms assume that the sources of variability in $R_{rs}(\lambda)$ originate from Chl*a* and the covariation between the detrital (dissolved and particulate) component and Chl*a* (O'Reilly et al., 2000). Thus, variations in pigment packaging, species composition, and the abundance of colored detrital matter (CDM) relative to phytoplankton biomass lead to errors in the performance of empirical algorithms. The trend of increasing errors with increasing Chl*a*-specific phytoplankton absorption coefficients observed here was verified by Loisel et al. (2010) and Szeto et al. (2011) using the NOMAD global dataset, which covered a large, dynamic range that had systematic differences among the oceans with respect to a_{ph}*(λ) and CDM contribution (Szeto et al., 2011). It is interesting to note that regional and temporal differences associated with the phytoplankton blooms in Patagonia waters resulted in a Chl*a* range (0.10 to 18.87 mg m^{-3} at surface) wide enough to produce differences in Chl*a*-specific IOP and impact the Chl*a* retrieval from empirical models. The b_p*(660) was also shown to explain the OC4v6 algorithm errors. Although $R_{rs}(\lambda)$ depends on backscattering instead of scattering coefficients, the dependence of *RE* on b_p*(660) found here agrees with *Westberry et al*. (2010), who argued that variations in $b_p(\lambda)$ could be conceptually extended to particulate

backscattering coefficients.

Our results clearly address the need to account for the influence of Chl*a*-specific IOP variability in Chl*a* retrieval algorithms for Patagonia waters. Regional parameterizations of semi-analytical ocean color algorithms with chlorophyll-specific IOP derived from the cluster analysis have the potential to improve product retrievals, as shown by Tilstone et al. (2012). Classification of the $R_{rs}(\lambda)$ spectra prior to application of specific bio-optical algorithms may also represent a valuable method of improving remote sensing retrievals (Lubac & Loisel, 2007; Moore et al., 2009).

3.6. Matchup Analyses

Although semi-analytical ocean color models, which are based on the relationship between oceanic constituents and the IOP (Gordon et al., 1988), have the potential to improve the retrieval estimates from remote sensing reflectance, some approximations have to be assumed. An empirical step of the QAA model (Lee et al., 2002) assumes spectral ratios of $R_{rs}(\lambda)$, whereas the GSM model (Maritorena et al., 2002) requires the assumption of mean spectral shapes for absorption and backscattering coefficients. For instance, the mean assumed value of the chlorophyll-specific phytoplankton absorption, $a^*_{ph}(\lambda)$, is 0.0558 m^2 mg^{-1} at 443 nm (Seadas software). This parameter, however, can be highly variable because of differences in algal cell size and pigment composition. In our work, the variation range of $a^*_{ph}(443)$ was 0.0180 to 0.2478 and averaged 0.0721 m^2 mg^{-1}. In this section, we evaluated the performance of semi-analytical algorithms in retrieving phytoplankton absorption coefficients for Patagonia waters using models embedded in the SeaDAS software, that have fixed input parameters for the semi-analytical models.

Matchup analyses were performed to compare *in situ* measured phytoplankton absorption coefficients with those estimated by the GSM and QAA semi-analytical models. We also compared *in situ*-measured Chl*a* with satellite-derived Chl*a* from the three empirical algorithms (OC2v6, OC4v6, and OC3v6) and the GSM semi-analytical model. The total number of *in situ* surface Chl*a* and $a_{ph}(\lambda)$ samples collected during the six cruises was 176 (see Figure 2 for Chl*a*). Because of cloud cover and the application of NASA's selection criteria of the temporal window (± 3 h), the matchup points were reduced to about 30 depending on the availability of satellite data required by the applied algorithm and the wavelength.

The matchup results are sorted by cruise instead of by $R_{rs}(\lambda)$ classes that was done for the retrievals using *in situ* $R_{rs}(\lambda)$ (section 3.4), because the reduced satellite data. Evaluation of the satellite model performance was made using the same statistics as in section 3.4: R^2, slope, and the intercept between the log-transformed measured Chl*a* and satellite-estimated. The statistical evaluation of the algorithms is provided in each respective panel (Figures 9 to 11).

Figure 9 presents a comparison between the measured Chl*a* and algorithm-derived estimates. The dispersion between measured Chl*a* and satellite-estimated Chl*a* from empirical algorithms (Figure 9a to 9c) was very similar to the dispersions using the *in situ* $R_{rs}(\lambda)$ dataset (R^2=0.66, 0.75 and 0.77 for OC2v6, OC3v6, and OC4v6, respectively). The major difference is that the estimates based on *in situ* $R_{rs}(\lambda)$ data tended to overestimate lower Chl*a* concentrations and underestimate higher Chl*a* concentrations, while the opposite was true for the satellite data (Figure 9). This difference could be attributed to the discrepancy in the amount of data ($N \sim$ 33 for matchup analysis against N = 116 for *in situ* dataset). Even so, there is a general trend of Chl*a* overestimation for both *in situ* and satellite $R_{rs}(\lambda)$ data, with

RPD always positive (Table 3 and Figure 9). The performance and overestimation of the GSM model is comparable to that of the empirical models (Figure 9).

Scatter plots for satellite vs. measured $a_{ph}(\lambda)$ for blue and green wavelengths are shown in Figures 10 and 11 as estimated by the GSM and QAA algorithms, respectively. The GSM model generally underestimated the $a_{ph}(412)$ values (*RPD* = -59%) (Figure 10a), and a similar result was found for the QAA model (*RPD* = -11%), although to a lesser degree because of two high satellite-derived $a_{ph}(412)$ values for PATEX 2 (Figure 11a). This underestimation at 412 nm is likely attributed to errors in atmospheric correction. The GSM $a_{ph}(\lambda)$ at 443, 469 and 488 nm corresponded relatively well to *in situ* data despite the general trend of underestimating lower $a_{ph}(\lambda)$ and overestimating higher $a_{ph}(\lambda)$ (Figure 10b to d). The errors for the green range of the spectrum, $a_{ph}(555)$, were larger (R^2 = 0.47, Figure 10f), and the lowest dispersion was achieved at 645 nm (R^2 = 0.80), although with the highest absolute and relative errors because of an considerable overestimation (*RPD* = 90% and *APD* = 94%, not shown).

In general, the QAA algorithm showed a better performance in retrieving $a_{ph}(\lambda)$ and showed points closer to the 1:1 line (with slopes close to 1) when compared with the GSM-derived data. The highest determination coefficient (R^2 = 0.65) was observed at 469 nm (Figure 11c). The errors were considerably higher at 555 nm (*RPD* = 268% and *APD* = 279%), and the maximum disagreement between *in situ* and satellite data was observed at 645 nm (R^2 of 0.045) with a pronounced overestimation (*RPD* and *APD* = 509%, not shown).

4. Conclusions

In this study, a considerable variability was observed in the coefficients of particulate absorption, attenuation, and diffuse attenuation as a function of chlorophyll-*a* concentration, Chl*a*, in Patagonia waters during spring and summer phytoplankton blooms, which was attributed to variations in the phytoplankton cell size. This variability was shown to influence the performance of empirical models that derive Chl*a* from ratios of remote sensing reflectance. The errors in Chl*a* estimates from the empirical algorithm OC4v6 using *in situ* $R_{rs}(\lambda)$ showed significant statistical relationships with Chl*a*, $a_{ph}(440)$/Chl*a*, and $b_p(660)$/Chl*a*.

A hierarchical cluster analysis classified the hyperspectral $R_{rs}(\lambda)$ into three classes according to spectral features that corresponded to the variability in Chl*a*. This result indicates the dominant role of phytoplankton in controlling the optical properties of the spring and summer blooms along the Patagonia shelf break region.

Although reasonable agreements were found between the measured and satellite-estimated Chl*a* and phytoplankton absorption coefficients, regional refinements of both empirical and semi-analytical algorithms that take into account the variability in Chl*a*-specific IOP should improve the satellite estimates of the bio-optical properties for the Patagonia region. Our work contributed to the documentation of the bio-optical properties for high-Chl*a* waters, as recommended by Morel et al. (2006).

5. References

Aiken, J., Fishwick, J. R., Lavender, S., Barlow, R., Moore, G. F., Sessions, H., et al. (2006). Validation of MERIS reflectance and chlorophyll during the BENCAL cruise October, 2002: preliminary validation of new demonstration products for phytoplankton functional types and photosynthetic parameters. *International Journal of Remote Sensing, 28,* 497-516.

744 Arnone, R. A., Wood, A. M., & Gould Jr., R. W. (2004). Water mass classification.
745 *Oceanography, 17*, 14-15.
746 Austin, R.W. (1974). The remote sensing of spectral radiance from below the ocean
747 Surface. In N. G. Jerlov, & E. S. Nielsen (Eds.), *Optical Aspects of*
748 *Oceanography* (pp. 317−344). La Jolla: Academic Press.
749 Bailey, S. W., McClain, C. R., Werdell, P. J., & Schieber, B. D. (2000). Normalized
750 water-leaving radiance and chlorophyll a match-up analyses. NASA Tech.
751 Memo. 206892, National Aeronautics and Space Administration, Goddard.
752 Space Flight Center, Greenbelt, MD.
753 Behrenfeld, M. J., & Boss, E. (2003). The beam attenuation to chlorophyll ratio: an
754 optical index of phytoplankton photoacclimation in the surface ocean?. *Deep*
755 *Sea Research Part I, 50,* 1537-1549. doi:10.1016/j.dsr.2003.09.002.
756 Behrenfeld, M. J., & Boss, E. (2006). Beam attenuation and chlorophyll
757 concentrations as alternative optical indices of phytoplankton biomass. *Journal*
758 *of Marine Research, 64,* 431–451. doi:10.1357/002224006778189563.
759 Bianchi, A. A., Pino, D. R., Perlender, H. G. I., Osiroff, A. P., Segura, V., Lutz, V.,
760 Clara, M. L., Balestrini, C. F., & Piola, A. R. (2009). Annual balance and
761 seasonal variability of sea-air CO_2 fluxes in the Patagonia Sea: Their
762 relationship with fronts and chlorophyll distribution. *Journal of Geophysical*
763 *Research, 114,* C03018. doi:10.1029/2008JC004854.
764 Bopp, L., Aumont, O., Cadule, P., Alvain, S., & Gehlen, M. (2005). Response of
765 diatoms distribution to global warming and potential implications: A global
766 model study. *Geophysical Research Letters, 32,* L19606.
767 doi:10.1029/2005GL023653.
768 Brewin, R. J. W., Lavender, S. J., Hardman-Mountford, N. J., & Hirata, T. (2010). A
769 spectral response approach for detecting dominant phytoplankton size class
770 from satellite remote sensing. *Acta Oceanologica Sinica, 29*(2), 14-32.
771 doi:10.1007/s13131-010-0018-y.
772 Bricaud, A., Babin, M., Morel, A., & Claustre, H. (1995). Variability in the
773 chlorophyll-specific absorption coefficient of natural phytoplankton: analysis
774 and parameterization. *Journal of Geophysical Research, 100,* C7, 13321-13332.
775 Bricaud, A., Claustre, H., Ras, J., & Oubelkheir, K. (2004). Natural variability of
776 phytoplankton absorption in oceanic waters: influence of the size structure of
777 algal populations. *Journal of Geophysical Research, 109*(C11), C11010.
778 doi:10.1029/2004JC002419.
779 Bricaud, A., Morel, A., Babin, M., Allali, K., & Claustre, H. (1998). Variations of
780 light absorption by suspended particles with the chlorophyll a concentration in
781 oceanic (Case 1) waters: analysis and implications for bio-optical models.
782 *Journal of Geophysical Research, 103*(13), 31,033-31,044.
783 doi:10.1029/98JC02712.
784 Brown, C. A., Huot, Y., Werdell, P. J., Gentili, B., & Claustre, H. (2008). The origin
785 and global distribution of second order variability in satellite ocean color and its
786 potential applications to algorithm development. *Remote Sensing of*
787 *Environment, 112*, 4186–4203. doi:10.1016/j.rse.2008.06.008.
788 Ciotti, A.M., & Bricaud. A. (2006). Retrievals of a size parameter for phytoplankton
789 and spectral light absorption by Colored Detrital Matter from water-leaving
790 radiances at SeaWiFS channels in a continental shelf region off Brazil.
791 *Limnology and Oceanography Methods*, ***4***, 237–253.
792 Ciotti, A. M., Lewis, M. R., & Cullen, J. J. (2002). Assessment of the relationships
793 between dominant cell size in natural phytoplankton communities and the

794 spectral shape of the absorption coefficient. *Limnology and Oceanography,*
795 *47*(2)*,* 404-417.
796 Dmitriev, E. V., Khomenko, G., Chami, M., Sokolov, A. A., Churilova, T. Y., &
797 Korotaev, G. K. (2009). Parameterization of light absorption by components of
798 seawater in optically complex coastal waters of the Crimea Peninsula (Black Sea).
799 *Applied Optics, 48,* 1249–1261.
800 Dogliotti, A. I., Schloss, I. R., Almanedoz, G. O., & Gagliardini, D. A. (2009).
801 Evaluation of SeaWiFS and MODIS chlorophyll-a products in the Argentinean
802 Patagonia Continental Shelf (38°S-55°S). *International Journal of Remote*
803 *Sensing, 30,* 251-273. doi:10.1080/01431160802311133.
804 Ferreira, A., Garcia, V. M. T., & Garcia, C. A. E. (2009). Light absorption by
805 phytoplankton non-algal particles and dissolved organic matter at the Patagonia
806 shelf-break in spring and summer. *Deep Sea Research Part I, 56,* 2162-2174.
807 doi:10.1016/j.dsr.2009.08.002.
808 Ferreira, A., Stramski, D., Garcia, C. A. E., Ciotti, A. M., Tavano, V. M., & Mendes, C.
809 R. B. (under second review). Variability in light absorption and scattering of
810 phytoplankton in Patagonia waters: Role of community size structure and
811 pigment composition. *Journal of Geophysical Research.*
812 Garcia, C. A. E., Garcia, V. M. T., Dogliotti, A. I., Ferreira, A., Romero, S. I.,
813 Mannino, A., Souza, M. S., & Mata, M. M. (2011). Environmental conditions
814 and bio-optical signature of a coccolithophorid bloom in the Patagonia shelf.
815 *Journal of Geophysical Research*, *116,* C03025. doi:10.1029/2010JC006595.
816 Garcia, V. M. T., Garcia, C. A. E., Mata, M. M., Pollery, R. C., Piola, A. R.,
817 Signorini, S. R., McClain, C. R., & Iglesias-Rodriguez, M. D. (2008).
818 Environmental factors controlling the phytoplankton blooms at the Patagonia
819 shelf-break in spring. *Deep Sea Research Part I, 55*(9), 1150-1166.
820 doi:10.1016/j.dsr.2008.04.011.
821 Garcia, C. A. E., Sarma Y. V. B., Mata, M. M., & Garcia, V. M. T. (2004).
822 Chlorophyll variability and eddies in the Brazil-Malvinas Confluence region.
823 *Deep Sea Research Part II, 51*(1–3), 159– 172. doi:10.1016/j.dsr2.2003.07.016.
824 **Garcia, V. M. T**, Signorini, S., **Garcia, C. A. E.** & McClain, C. R. (2006). Empirical
825 and semi-analytical chlorophyll algorithms in the Southwestern Atlantic coastal
826 region (250 -400 S and 600-450 W). *International Journal of Remote Sensing*,
827 *27*(8), 1539–1562. doi:10.1080/01431160500382857.
828 Gordon, H. R. (1989). Can the Lambert-Beer law be applied to the diffuse attenuation
829 coefficient of ocean water?. *Limnology and Oceanography, 34,* 1389–1409.
830 Gregg, W. W., Casey, N. W., & McClain, C. R. (2005). Recent trends in global ocean
831 chlorophyll. *Geophysical Research Letters*, *32*(3)*,* L03606.
832 doi:10.1029/2004GL021808.
833 Gregg, W. W, Casey, N. W., O'Reilly, J. E., & Esaias, W. E. (2009). An empirical
834 approach to ocean color data: reducing bias and the need for post launch
835 radiometric re-calibration. *Remote Sensing of Environment, 113,* 1598–1612.
836 doi:10.1016/j.rse.2009.03.005.
837 Guidi, L., Stemmann, L., Jackson, G. A., Ibanez, F., Claustre, H., Legendre, L.,
838 Picheral, M., & Gorsky, G. (2010). Effects of phytoplankton community on
839 production, size, and export of large aggregates: A World-Ocean analysis.
840 *Limnology and Oceanography, 54*(6), 1951–1963.
841 Hirata, J. A., Aiken, J., Hardman-Mountford, N. J., Smyth, T. J., & Barlow, R.
842 (2008). An absorption model to derive phytoplankton size classes from satellite
843 ocean color. *Remote Sensing of Environment, 112*, 3153– 3159,

844 doi:10.1016/j.rse.2008.03.011.
845 http://oceancolor.gsfc.nasa.gov/REPROCESSING/R2009/ocv6/
846 http://www.wetlabs.com/cstar/
847 Huot, Y., Morel, A., Twardowski, M. S., Stramski, D., & Reynolds, R. A. (2008).
848 Particle optical scattering along a chlorophyll gradient in the upper layer of the
849 eastern South Pacific Ocean. *Biogeosciences, 5*(2), 495–507.
850 International Ocean Colour Coordinating Group (IOCCG) (2006). Remote sensing of
851 inherent optical properties: Fundamentals, tests of algorithms, and applications,
852 edited by Z. P. Lee, *IOCCG Rep. 5*, Dartmouth, N. S., Canada.
853 Kiørboe, T. (1993). Turbulence, phytoplankton cell size, and the structure of pelagic
854 food webs. *Advances in Marine Biology, 29*, 1-72.
855 Kirk, J. T. O. (1975). A theoretical analysis of the contribution of algal cells to the
856 attenuation of light within natural waters. I. General treatment of suspensions of
857 pigmented cells, *New Phytologist,* 75, 11–20.
858 Kishino M, Takahashi, N., Okami, N., & Ichimura, S. (1985). Estimation of the
859 spectral absorption coefficients of phytoplankton in the sea. *Bulletin of Marine*
860 *Science, 37*(2), 634–642.
861 Le Quéré, C., Harrison, S. P., Prentice, C. I., Buitenhuis, E. T., Aumont, O., Bopp, L.,
862 et al. (2005). Ecosystem dynamics based on plankton functional types for global
863 ocean biogeochemistry models. *Global Change Biology, 11*, 2016−2040.
864 doi:10.1111/j.1365-2468.2005.01004.x.
865 Lee, Z. P., Arnone, R., Hu, C. M., Werdell, P. J., & Lubac, B. (2010). Uncertainties of
866 optical parameters and their propagations in an analytical ocean color inversion
867 algorithm. *Applied Optics, 49,* 369−381.
868 Lee, Z. P., Carder, K. L., & Arnone, R. (2002). Deriving inherent optical properties
869 from water color: A multi-band quasi-analytical algorithm for optically deep
870 waters. *Applied Optics, 41*, 5755−5772.
871 Loisel, H., Lubac, B., Dessailly, D., Duforer-Gaurier, L., & Vantrepotte, V. (2010).
872 Effect of inherent optical properties variability on the chlorophyll retrieval from
873 ocean color remote sensing: An in situ approach. *Optical Express, 18*(20)*,*
874 20,949 20,959. doi:10.1364/OE.18.020949.
875 Loisel, H., & Morel, A. (1998). Light scattering and chlorophyll concentration in
876 Case 1 waters: a reexamination*. Limnology and Oceanography, 43,* 847–858,
877 doi:10.4319/lo.1998.43.5.0847.
878 Lubac, B., & Loisel, H. (2007). Variability and classification of remote sensing
879 reflectance spectra in the eastern English Channel and southern North Sea.
880 *Remote Sensing of Environment, 110*, 45-58. doi:10.1016/j.rse.2007.02.012.
881 Lutz, V. A., Segura, V., Dogliotti, A. I., Gagliardini, D. A., Bianchi, A. A., &
882 Balestrini, C. F. (2010). Primary Production in the Argentine Sea during Spring
883 Estimated by Field and Satellite Models. *Journal of Plankton Research, 32,* 181-
884 195. doi:10.1093/plankt/ fbp117.
885 Maritorena, S., Siegel, D. A., & Peterson, A. R. (2002). Optimization of a
886 semianalytical ocean color model for global-scale applications. *Applied Optics,*
887 *41,* 2705−2714.
888 Martinez-Vicente, V., Land, P. E., **Tilstone, G. H.**, Widdicombe, C., & Fishwick, J.
889 R. (2010). Particulate scattering and backscattering related to water constituents
890 and seasonal changes in the Western English Channel. *Journal of Plankton*
891 *Research*, *32,* 603-619. doi:10.1093/plankt/fbq013.
892 Matano, R. P. & Palma, E. D. (2008). On the Upwelling of Downwelling Currents.
893 *Journal of Physical Oceanography, 38,* 2482–2500.

doi:10.1175/2008JPO3783.1.
Mitchell, B. G., *et al.* (2000). Determination of spectral absorption coefficients of particles, dissolved material and phytoplankton for discrete water samples, in *Ocean Optics Protocols For Satellite Ocean Color Sensor Validation, Tech. Memo. 2000-209966*, pp. 125-153, NASA, Greenbelt, Md.
Mobley, C. D., Stramski, D., Bissett, W.P., & Boss, E. (2004). Optical Modeling of Ocean Waters: Is the Case 1 - Case 2 Classification Still Useful?. *Oceanography, 17*, 60-67.
Moore, T. S., Campbell, J. W., & Dowell, M. D. (2009). A class-based approach to characterizing and mapping the uncertainty of the MODIS ocean chlorophyll product. *Remote Sensing of Environment*, *113,* 2424-2430. doi:10.1016/j.rse.2009.07.016.
Morel, A. (1988). Optical modeling of the upper ocean in relation to its biogenous matter content (case 1 water). *Journal of Geophysical Research, 93*, 10,749-10,768.
Morel, A., Claustre, H., Antoine, D. & Gentili, B. (2007). Natural variability of bio-optical properties in Case 1 waters: attenuation and reflectance within the visible and near-UV spectral domains, as observed in South Pacific and Mediterranean waters. *Biogeosciences, 4*, 913-925.
Morel, A., Gentili, B., Chami, M., & Ras, D. J. (2006). Bio-optical properties of high chlorophyll Case 1 waters and of yellow-substance-dominated Case 2 waters. *Deep-Sea Research Part I, 53*, 1439−1459. doi:10.1016/j.dsr.2006.07.007.
Morel, A., & Maritorena, S. (2001). Bio-optical properties of oceanic waters: A reappraisal. *Journal of Geophysical research*, *106*, 7763-7780. doi:10.1029/2000JC000319.
Morel, A., & Prieur, L. (1977). Analysis of variation in ocean color. *Limnology and Oceanography, 22,* 709−722.
O'Reilly, J. E., Maritorena, S., Mitchell, B. G., Seigel, D. S., Carder, K. L., Garver, S. A., Kahru, M., & McClain, C. (1998). Ocean color chlorophyll algorithms for SeaWiFS. *Journal of Geophysical Research, 103,* 24937−24953.
O'Reilly, J. E., Maritorena, S., Siegel, D. A., O'Brien, M. C., Toole, D., Mitchell, B. G., et al. (2000). Ocean color chlorophyll a algorithms for SeaWiFS, OC2, and OC4: Version 4. In S. B. Hooker & E.R. Firestone (Eds.), SeaWiFS Postlaunch Calibration and Validation Analyses, Part 3, vol. 11. (pp. 9−23) Greenbelt, Maryland: NASA, Goddard Space Flight Center.
Preisendorfer, R. W. (1961). Application of radiative transfer theory to light measurement in the sea. *International Union of Geodesy and Geophysics Monograph, 10,* 11–30.
Rivas, A. L., Dogliotti, A. I., & Gagliardini, D. A. (2006), Seasonal variability in satellite measured surface chlorophyll in the Patagonia Shelf. *Continental Shelf Research, 26*(6)*,* 703-720. doi:10.1016/j.csr.2006.01.013.
Romero, S. I., Piola, A. R., Charo, M., & Garcia, C. A. E. (2006). Chlorophyll-a variability off Patagonia based on SeaWiFS data. *Journal of Geophysical Research, 111,* C05021. doi:10.1029/ 2005JC003244.
Schloss, I. R., Ferreyra, G. A., Ferrario, M. E., Almandoz, G. O., Codina, R., Bianchi, A. et al. (2007). Role of plankton communities in sea-air variations in pCO2 in the SW Atlantic Ocean. *Marine Ecology Progress Series, 332*, 93-106. doi:10.3354/meps332093.
Signorini, S., Garcia, V. M. T., Piola, A. R., Garcia, C. A. E., Mata, M. M., & McClain, C. R. (2006). Seasonal and interannual variability of calcite in the

vicinity of the Patagonia Shelf Break (38°S–52°S). *Geophysical Research Letters, 33*(16)*,* L1, 6610. doi:10.1029/2006GL026592.
Stramska, M., Stramski, D., Kaczmarek, S., Allison, D. B., & Schwarz, J. (2006). Seasonal and regional differentiation of bio-optical properties within the north polar Atlantic. *Journal of Geophysical Research, 111*(C8), C08003. doi:10.1029/2005JC003293.
Szeto, M., Werdell, P. J., Moore, T. S., & Campbell, J. W. (2011). Are the world's oceans optically different?. *Journal of Geophysical Research*, *116,* C00H04. doi:10.1029/2011JC007230.
Tassan, S., & Ferrari, G. M. (1995). An alternative approach to absorption measurements of aquatic particles retained on filters. *Limnology and Oceanography, 40*(8)*,* 1358–1368.
Tilstone, G. H., Peters, S. W. M., van der Woerd, H. J., Eleveld, M. A., Ruddick, K., Schönfeld, W., et al. (2012). Variability in specific-absorption properties and their use in a semi-analytical Ocean Colour algorithm for MERIS in North Sea and Western English Channel coastal waters. *Remote Sensing of Environment 118*, 320-338. doi:10.1016/j.rse.2011.11.019.
Voss, K. J. (1992). A spectral model of the beam attenuation coefficient in the ocean and coastal areas. *Limnology and Oceanography, 37*, 501–509, 1992.
Westberry, T. K, Dall'Olmo, G., Boss, E., Behrenfeld, M. J., & Moutin, T. (2010). Coherence of particulate beam attenuation and backscattering coefficients in diverse open ocean environments. *Optical Express, 18*(15), 15419-15425. doi:10.1364/OE.18.015419.
Welschmeyer, N.A. (1994). Fluorometric analysis of chlorophyll-a in the presence of chlorophyll-b and pheopigments. *Limnology and Oceanography, 39*(8), 1985–1992.
Werdell, P. J., & Bailey, S. W. (2005). An improved in situ bio-optical data set for ocean color algorithm development and satellite data product validation. *Remote Sensing Environment, 98*(1), 122–140. doi:10.1016/j.rse.2005.07.001.

Figure captions

Figure 1. Locations of the 176 oceanographic stations where measurements and sample collections were taken during the PATEX cruises along the Patagonian shelf break and adjacent areas. Filled symbols indicate the stations where data collection was carried out during the daylight hours and $K_d(\lambda)$ and $R_{rs}(\lambda)$ data are available.

Figure 2. Frequency histogram of the chlorophyll-*a* concentration, Chl*a*, measured at the near-surface (N=176), the depths of maximum chlorophyll fluorescence, MCF

(*N*=159), and the base of maximum chlorophyll fluorescence, BMCF (*N*=85), during the PATEX 2 to PATEX 7 cruises.

Figure 3. (a) The particulate absorption coefficient at 440 nm, $a_p(440)$, as a function of chlorophyll-*a* concentration, Chl*a*, for near-surface depths, depths of maximum chlorophyll fluorescence and the base of the maximum depths during PATEX 2 to PATEX 7 cruises (N=356, R^2 for log-transformed data = 0.77). As indicated, the lines represent the best fit regression between $a_p(\lambda)$ and Chl*a* ($a_p(440) = 0.096\ \text{Chl}a^{0.539}$) and lines B98 and M06 represent the previously derived relationships (Bricaud et al., 1998; Morel et al., 2006). (b) The diffuse attenuation coefficient at 440 nm, $K_d(440)$, as a function of Chl*a* for near-surface depths during PATEX 2 to PATEX 7 cruises (N=116, R^2 for log-transformed data = 0.65). As indicated, the lines represent the best fit regression between $K_d(\lambda)$ and Chl*a* ($K_d(440) = 0.121\ \text{Chl}a^{0.644}$), and line M07 represents a previously derived relationship (*Morel et al*., 2007). (c) The diffuse attenuation coefficient at 440 nm, $K_d(440)$, as a function of $a_p(440)$ for near-surface depths during PATEX 2 to PATEX 7 cruises (N=116, R^2 = 0.67). The dashed line represents a 1:1 ratio.

Figure 4. (a) The particulate attenuation coefficient at 660 nm, $c_p(660)$, as a function of chlorophyll-*a* concentration, Chl*a*, for samples collected along the water column during the PATEX 2 through the PATEX 7 cruises (N=790, R^2 for log-transformed data = 0.60). The line represents the best fit regression between $c_p(\lambda)$ and Chl*a* for the whole dataset. (b) The best fit regressions between $c_p(\lambda)$ and Chl*a* obtained separately according to cruises, as indicated (see Table 2). The previously derived relationship by Loisel and Morel (1998), LM98, derived for the Chl*a* range of 0.2 to 3.0 mg m^{-3} is shown in (a) and (b) for comparison.

Figure 5. Spectra of remote sensing reflectance, $R_{rs}(\lambda)$ in sr^{-1}, shown separately for (a) the PATEX 2 through the (b) PATEX 7 cruises. Note the different scales.

Figure 6. Results of the hierarchical cluster analysis applied to the normalized remote sensing reflectance spectra, $nR_{rs}(\lambda)$. Both the absolute remote sensing reflectance, $R_{rs}(\lambda)$ in sr^{-1} (a, c, and e) and the $nR_{rs}(\lambda)$ with no unit (b, d, and f) are shown.

Figure 7. Chlorophyll-*a* concentration, Chl*a*, as a function of the $R_{rs}(\lambda)$ band ratios used for the three Chl*a* empirical algorithms: (a) OC2v6, (b) OC3v6, and (c) OC4v6. The OC3v6 and OC4v6 algorithms use any of the two and three maximum (max) band ratios, respectively, as indicated on the *x* axes. The data are shown separately for the three $R_{rs}(\lambda)$ classes ordered by a hierarchical cluster analysis. The grey circles and solid curves represent NASA's Bio-optical Marine Algorithm Data Set (NOMAD) (Werdell & Bailey, 2005) and the indicated algorithms, respectively. Note that the axes have logarithmic scales.

Figure 8. Relative errors (*RE*) of the OC4v6 algorithm (see text for definition) as a function of (a) chlorophyll-*a* concentration, Chl*a*, (b) chlorophyll-specific absorption coefficient of phytoplankton at 440 nm, $a^*_{ph}(440)$, and (c) chlorophyll-specific scattering coefficient of particles at 660 nm, $b^*_p(660)$. The data are shown separately for the three $R_{rs}(\lambda)$ classes ordered by a hierarchical cluster analysis.

Figure 9. Comparison between *in situ*-measured and satellite-retrieved chlorophyll-*a* concentration, Chl*a*, from the (a) OC2v6, (b) OC3v6, and (c) OC4v6 empirical algorithms, and the (d) GSM semi-analytical algorithm. Coefficient of determination, R^2, slope, and intercept obtained from regression analysis on log-transformed algorithm-derived and *in situ* measured data, the mean relative percentage difference, *RPD*, and mean absolute percentage difference, *APD,* are shown. The data are sorted by cruise, as indicated.

Table 1 – The mean, standard deviation (Std), and range of the absorption coefficient at 440 nm for particulates, $a_p(\lambda)$, and phytoplankton, $a_{ph}(\lambda)$, and the percent contribution of $a_{ph}(440)$ to $a_p(440)$ for each PATEX cruise. The data are means of pooled data from the near-surface, depths of maximum chlorophyll fluorescence, and the base of maximum chlorophyll fluorescence.

		PATEX 2 *N*=44	PATEX 3 *N*=54	PATEX 4 *N*=66	PATEX 5 *N*=51	PATEX 6 *N*=79	PATEX 7 *N*=62
$a_p(440)$	Mean	0.22	0.14	0.21	0.08	0.14	0.04
	Std	0.08	0.05	0.16	0.04	0.08	0.02
	Range	0.07-0.36	0.02-0.27	0.02-0.68	0.02-0.20	0.03-0.37	0.01-0.09
$a_{ph}(440)$	Mean	0.19	0.11	0.20	0.07	0.12	0.04
	Std	0.06	0.04	0.15	0.03	0.08	0.02
	Range	0.07-0.32	0.01-0.26	0.02-0.67	0.02-0.17	0.02-0.36	0.008-0.09
$a_{ph}(440)/a_p(440)$	Mean	0.83	0.81	0.96	0.84	0.92	0.91
	Std	0.07	0.15	0.07	0.13	0.08	0.12
	Range	0.51-0.92	0.25-0.97	0.71-1.00	0.48-1.00	0.49-0.98	0.25-1.00

1055 Table 2 – Results from regression analysis between the beam attenuation at 660 nm,
1056 $c_p(660)$, and the chlorophyll-*a* concentration, Chl*a*, for PATEX 2 to 7 cruises. The
1057 regression formula is $c_p(660) = A\ \mathrm{Chl}a^{\,B}$ where *A* and *B* are the best-fit parameters.
1058 The determination coefficient, R^2, and the number of data, *N*, are also shown. The
1059 results are presented for surface and selected depths based on the chlorophyll
1060 fluorescence profile. All regression analyses are significant for $p<0.001$.

Cruise	Equation derived	R^2	*N*
All PATEX	$c_p(660) = 0.343\ \mathrm{Chl}a^{\,0.370}$	0.60	790
PATEX 2 and 4	$c_p(660) = 0.254\ \mathrm{Chl}a^{\,0.471}$	0.70	299
PATEX 3, 6 and 7	$c_p(660) = 0.333\ \mathrm{Chl}a^{\,0.818}$	0.70	397
PATEX 5	$c_p(660) = 0.610\ \mathrm{Chl}a^{\,0.400}$	0.56	94

1061

1062

Table 3 - Statistical results for the performance of the three empirical algorithms, OC2v6, OC3v6, and OC4v6, to estimate the surface chlorophyll-*a* concentration, Chl*a*, from *in situ* $R_{rs}(\lambda)$ data collected during the PATEX 2 to PATEX 7 cruises. The algorithms were applied to all $R_{rs}(\lambda)$ data and separately to each of the three $R_{rs}(\lambda)$ classes obtained with a hierarchical cluster analysis. The mean relative percentage difference, *RPD* [a], and mean absolute percentage difference, *APD* [b], were computed between the measured Chl*a* and Chl*a* estimated from the algorithm. The R^2, slope and intercept derived from linear regression analysis on log-transformed measured and retrieved data were computed only when all $R_{rs}(\lambda)$ data were considered. The mean and standard deviation (Std) of surface Chl*a* corresponding to all $R_{rs}(\lambda)$ and to each $R_{rs}(\lambda)$ class are also shown (column 1).

Dataset Mean (Std)	Algorithm	*RPD*	*APD*	R^2	*Slope*	*Intercept*	*N*
All data 2.45 (3.42)	OC2v6	27.53	59.30	0.67	0.82	0.06	116
	OC3v6	39.31	70.78	0.62	0.77	0.09	
	OC4v6	11.54	42.05	0.78	0.86	0.03	
Class 1 0.86 (0.51)	OC2v6	-2.93	29.95	--	--	--	22
	OC3v6	1.82	31.84	--	--	--	
	OC4v6	-2.63	30.82	--	--	--	
Class 2 2.42 (1.62)	OC2v6	77.34	94.98	--	--	--	42
	OC3v6	103.91	122.12	--	--	--	
	OC4v6	31.80	51.57	--	--	--	
Class 3 8.40 (3.96)	OC2v6	4.46	60.55	--	--	--	52
	OC3v6	3.44	64.84	--	--	---	
	OC4v6	6.30	50.21	--	--	--	

[a] $RPD = \sum_{n=1}^{N} \frac{Xalg - Xmeas}{Xmeas} \frac{1}{N} \times 100$

[b] $APD = \sum_{n=1}^{N} \left| \frac{Xalg - Xmeas}{Xmeas} \right| \frac{1}{N} \times 100$

where *Xalg* and *Xmeas* represent the measured and algorithm-retrieved values, respectively.

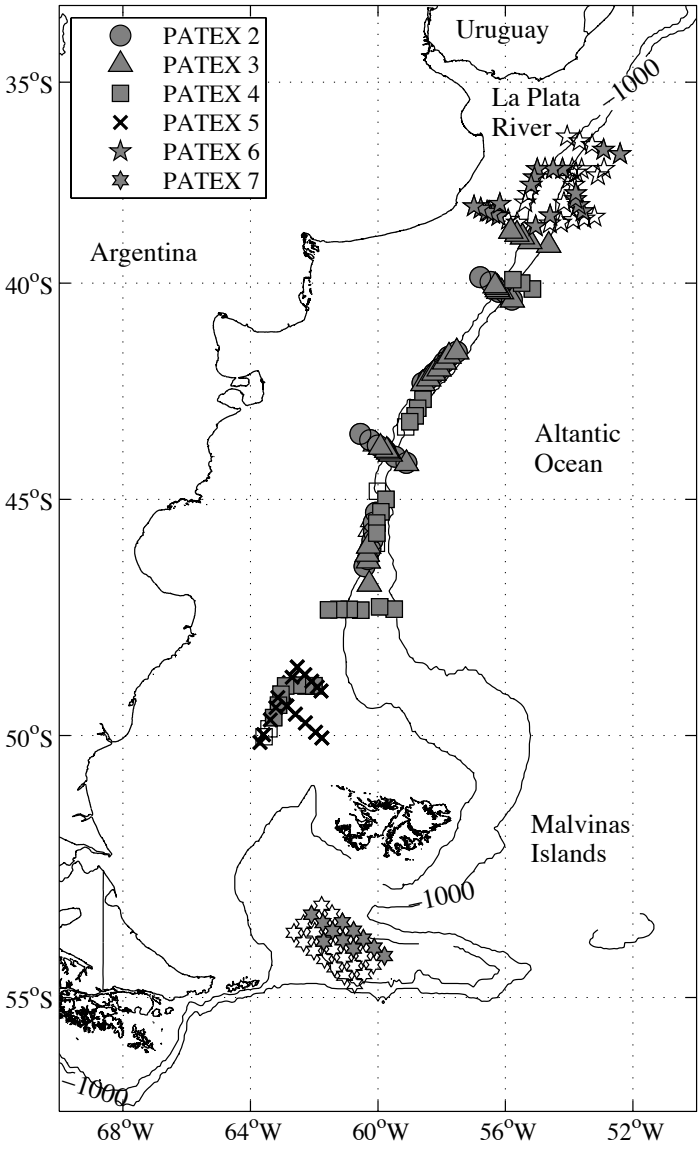

1078

1079 Figure 1. Locations of the 176 oceanographic stations where measurements and
1080 sample collections were taken during the PATEX cruises along the Patagonian shelf
1081 break and adjacent areas. Filled symbols indicate the stations where data collection
1082 was carried out during the daylight hours and $K_d(\lambda)$ and $R_{rs}(\lambda)$ data are available.

1083

1084

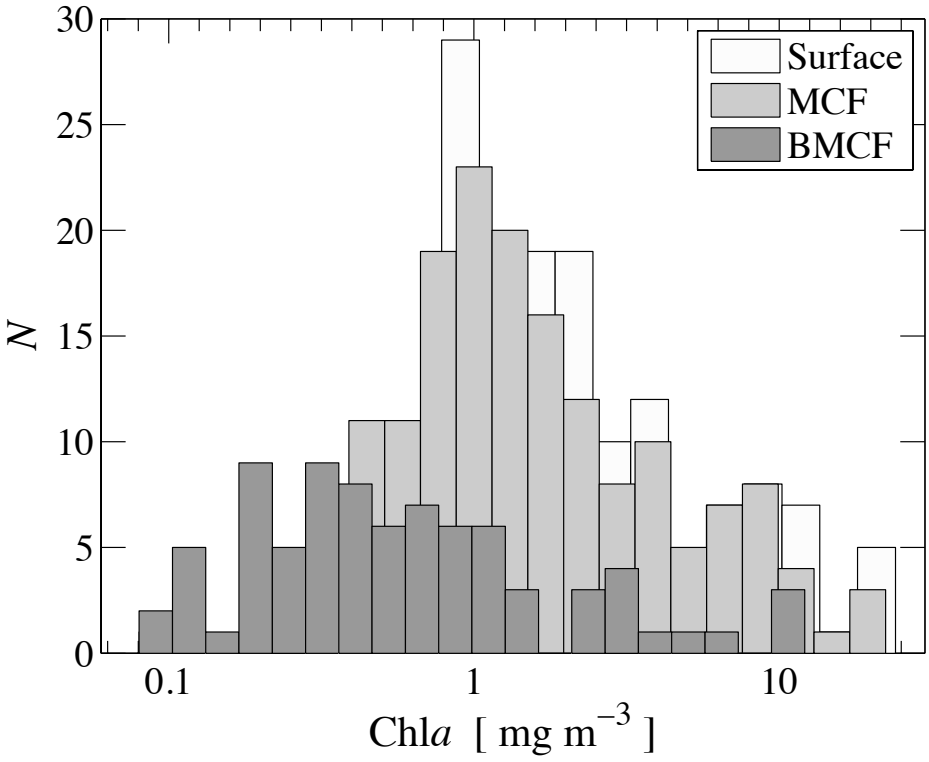

Figure 2. Frequency histogram of the chlorophyll-*a* concentration, Chl*a*, measured at the near-surface (*N*=176), the depths of maximum chlorophyll fluorescence, MCF (*N*=159), and the base of maximum chlorophyll fluorescence, BMCF (*N*=85), during the PATEX 2 to PATEX 7 cruises.

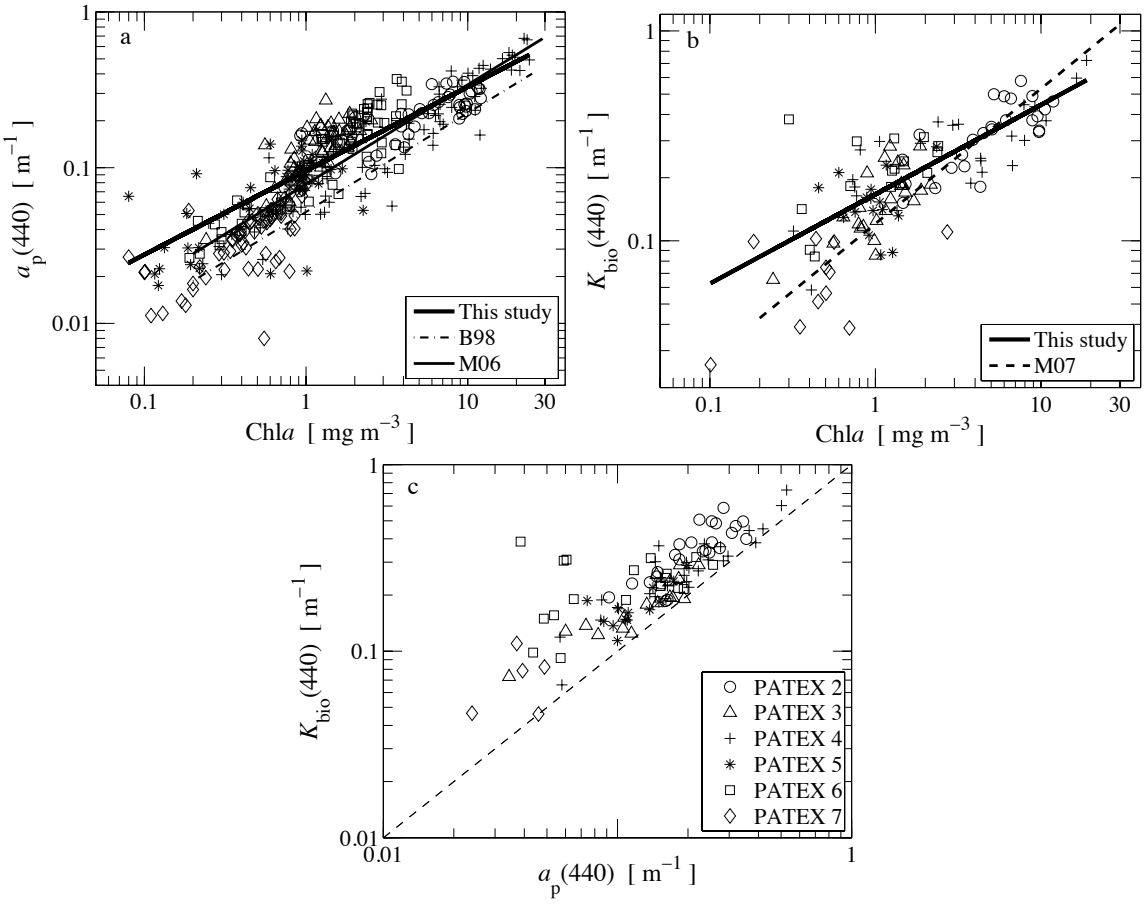

Figure 3. (a) The particulate absorption coefficient at 440 nm, $a_p(440)$, as a function of chlorophyll-*a* concentration, Chl*a*, for near-surface depths, depths of maximum chlorophyll fluorescence and the base of the maximum depths during PATEX 2 to PATEX 7 cruises (N=356, R^2 for log-transformed data = 0.77). As indicated, the lines represent the best fit regression between $a_p(\lambda)$ and Chl*a* ($a_p(440) = 0.096\ \text{Chl}a^{0.539}$) and lines B98 and M06 represent the previously derived relationships (Bricaud et al., 1998; Morel et al., 2006). (b) The diffuse attenuation coefficient at 440 nm, $K_d(440)$, as a function of Chl*a* for near-surface depths during PATEX 2 to PATEX 7 cruises (N=116, R^2 for log-transformed data = 0.65). As indicated, the lines represent the best fit regression between $K_d(\lambda)$ and Chl*a* ($K_d(440) = 0.121\ \text{Chl}a^{0.644}$), and line M07 represents a previously derived relationship (Morel et al., 2007). (c) The diffuse attenuation coefficient at 440 nm, $K_d(440)$, as a function of $a_p(440)$ for near-surface depths during PATEX 2 to PATEX 7 cruises (N=116, R^2 = 0.67). The dashed line represents a 1:1 ratio.

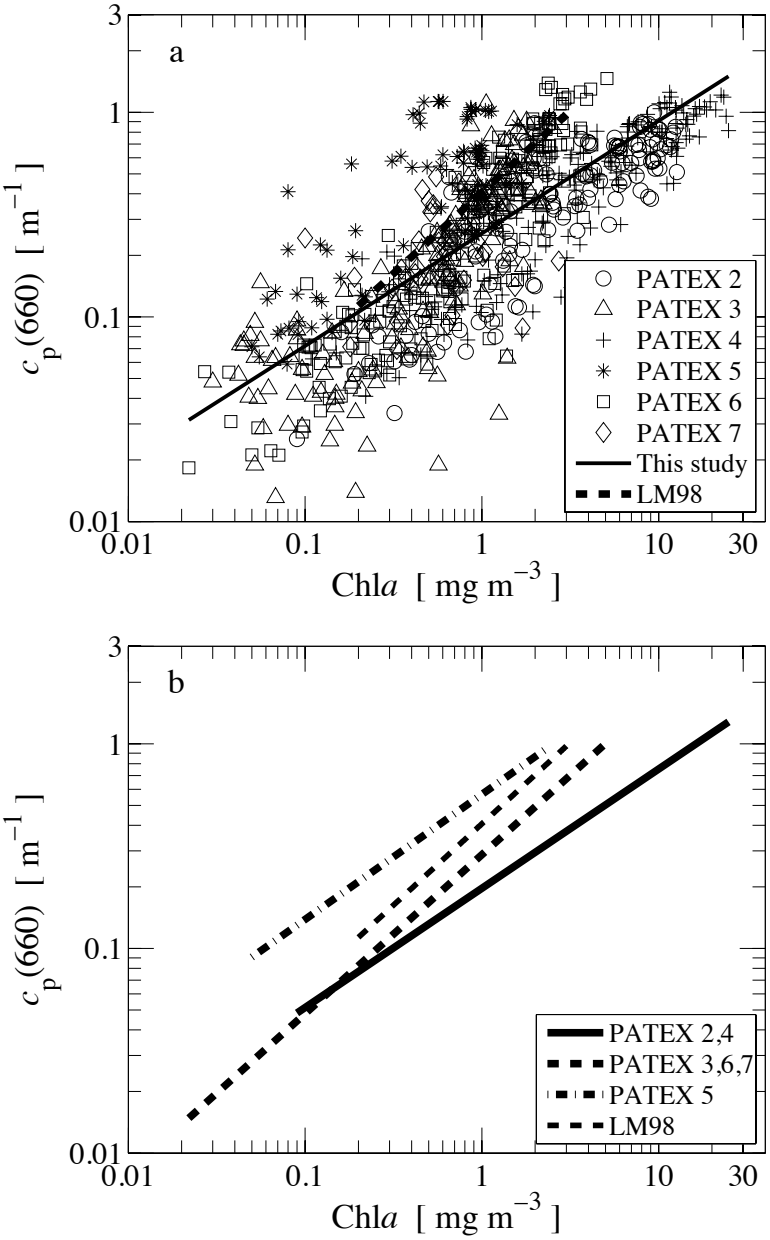

Figure 4. (a) The particulate attenuation coefficient at 660 nm, $c_p(660)$, as a function of chlorophyll-*a* concentration, Chl*a*, for samples collected along the water column during the PATEX 2 through the PATEX 7 cruises (N=790, R^2 for log-transformed data = 0.60). The line represents the best fit regression between $c_p(\lambda)$ and Chl*a* for the whole dataset. (b) The best fit regressions between $c_p(\lambda)$ and Chl*a* obtained separately according to cruises, as indicated (see Table 2). The previously derived relationship by Loisel and Morel (1998), LM98, derived for the Chl*a* range of 0.2 to 3.0 mg m^{-3} is shown in (a) and (b) for comparison.

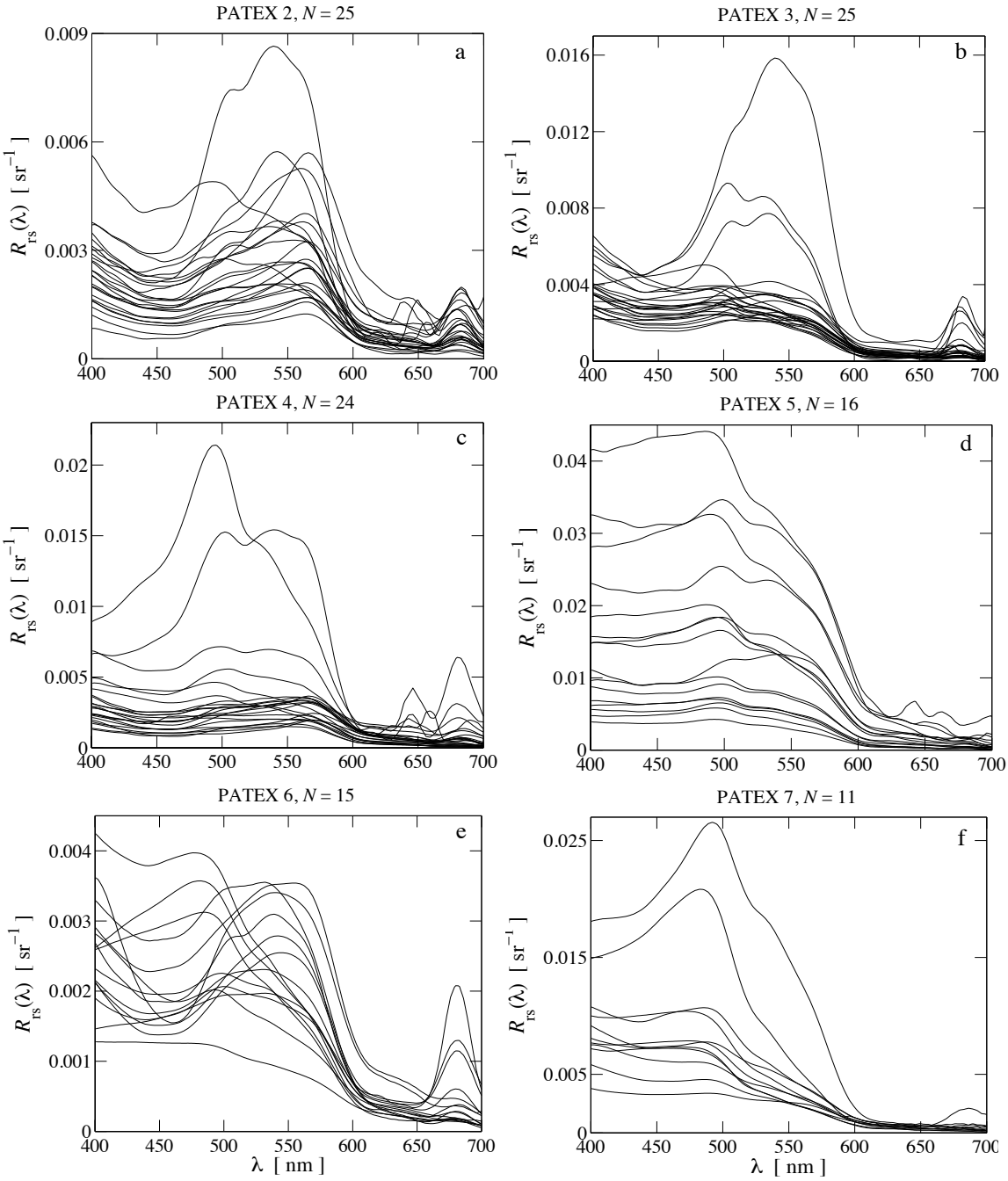

Figure 5. Spectra of remote sensing reflectance, $R_{rs}(\lambda)$ in sr^{-1}, shown separately for (a) the PATEX 2 through the (b) PATEX 7 cruises. Note the different scales.

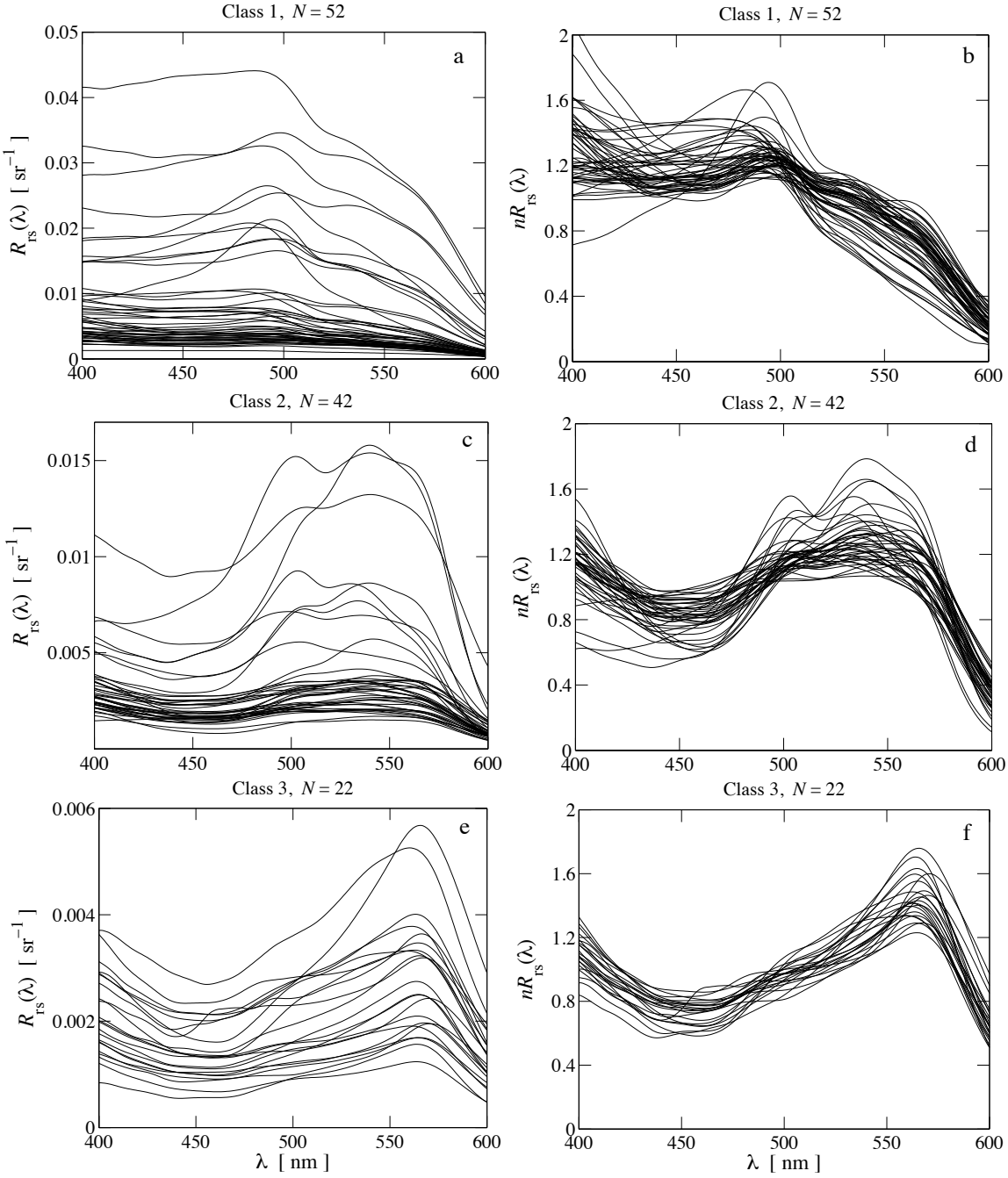

Figure 6. Results of the hierarchical cluster analysis applied to the normalized remote sensing reflectance spectra, $nR_{rs}(\lambda)$. Both the absolute remote sensing reflectance, $R_{rs}(\lambda)$ in sr^{-1} (a, c, and e) and the $nR_{rs}(\lambda)$ with no unit (b, d, and f) are shown.

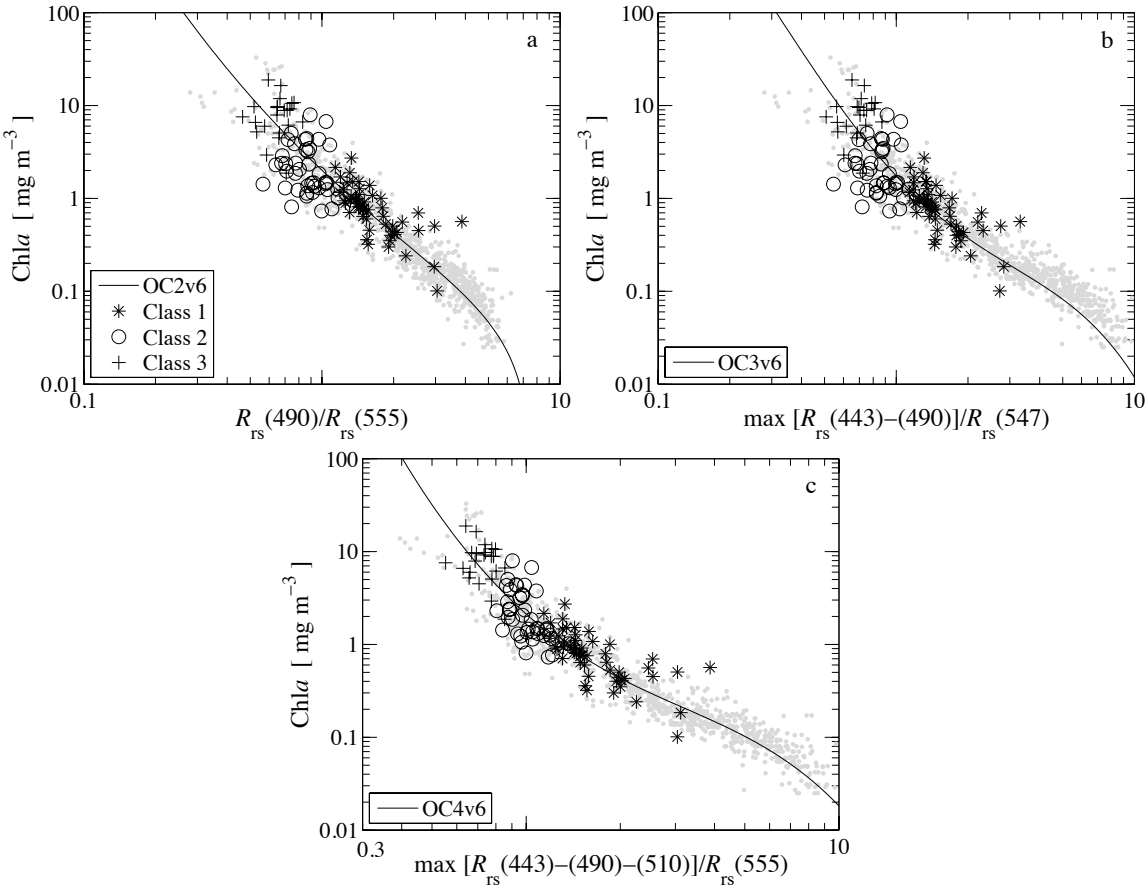

Figure 7. Chlorophyll-*a* concentration, Chl*a*, as a function of the $R_{rs}(\lambda)$ band ratios used for the three Chl*a* empirical algorithms: (a) OC2v6, (b) OC3v6, and (c) OC4v6. The OC3v6 and OC4v6 algorithms use any of the two and three maximum (max) band ratios, respectively, as indicated on the *x* axes. The data are shown separately for the three $R_{rs}(\lambda)$ classes ordered by a hierarchical cluster analysis. The grey circles and solid curves represent NASA's Bio-optical Marine Algorithm Data Set (NOMAD) (Werdell & Bailey, 2005) and the indicated algorithms, respectively. Note that the axes have logarithmic scales.

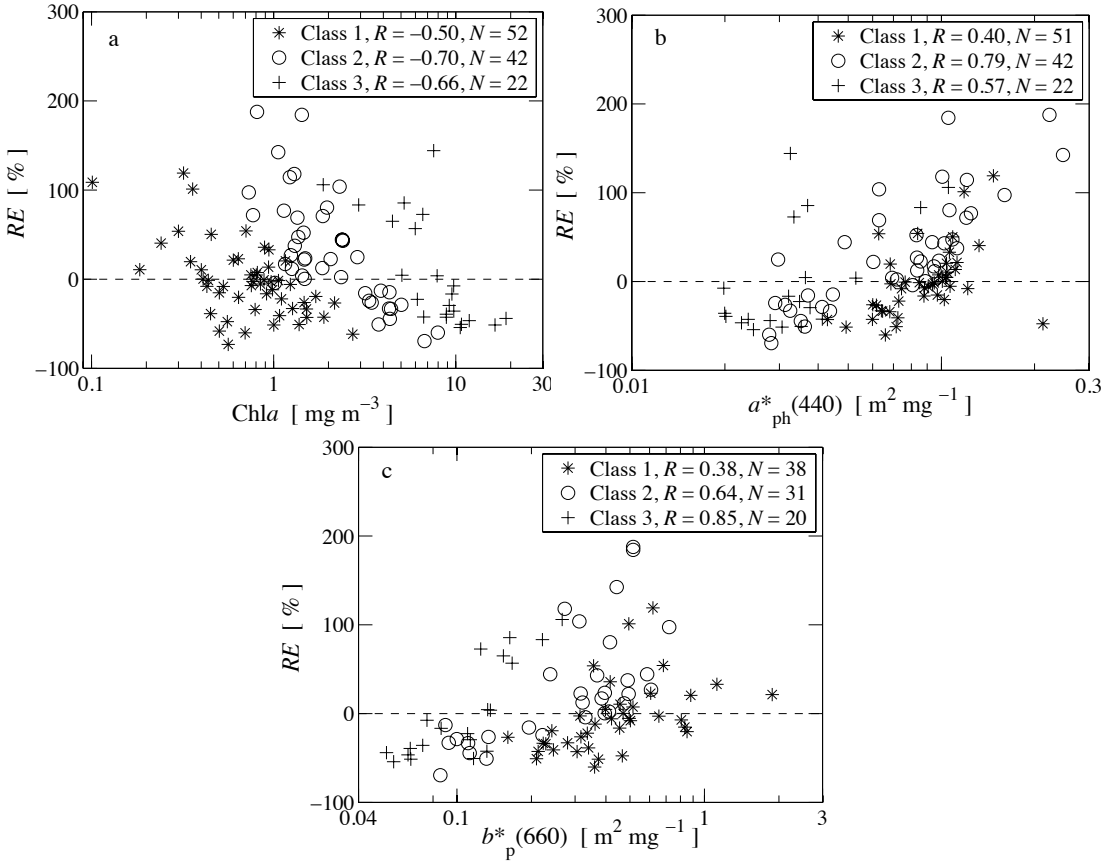

Figure 8. Relative errors (*RE*) of the OC4v6 algorithm (see text for definition) as a function of (a) chlorophyll-*a* concentration, Chl*a*, (b) chlorophyll-specific absorption coefficient of phytoplankton at 440 nm, $a^*_{ph}(440)$, and (c) chlorophyll-specific scattering coefficient of particles at 660 nm, $b^*_p(660)$. The data are shown separately for the three $R_{rs}(\lambda)$ classes ordered by a hierarchical cluster analysis.

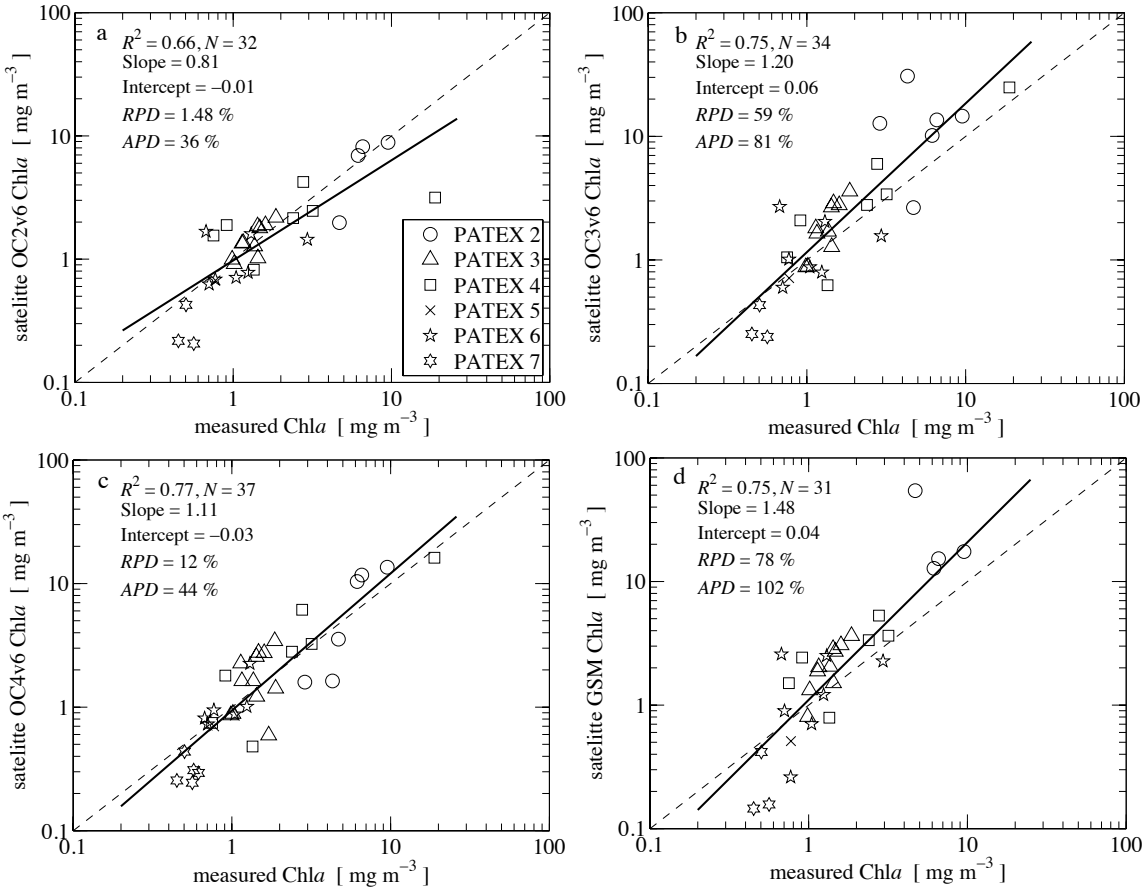

Figure 9. Comparison between *in situ*-measured and satellite-retrieved chlorophyll-*a* concentration, Chl*a*, from the (a) OC2v6, (b) OC3v6, and (c) OC4v6 empirical algorithms, and the (d) GSM semi-analytical algorithm. Coefficient of determination, R^2, slope, and intercept obtained from regression analysis on log-transformed algorithm-derived and *in situ* measured data, the mean relative percentage difference, *RPD*, and mean absolute percentage difference, *APD,* are shown. The data are sorted by cruise, as indicated.

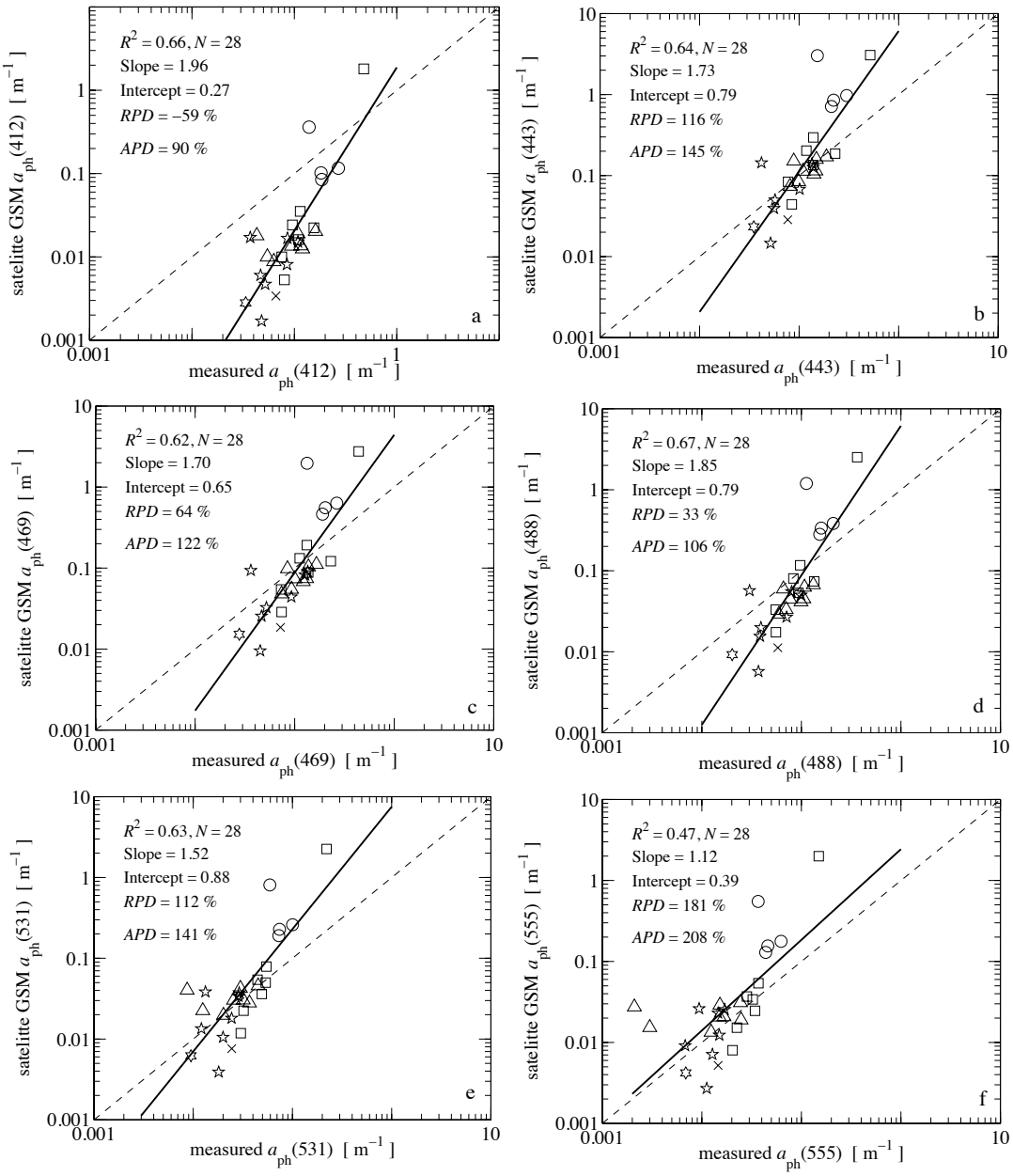

Figure 10. Comparison between the *in situ*-measured and satellite-retrieved phytoplankton absorption coefficient, $a_{ph}(\lambda)$, from the GSM semi-analytical algorithm for blue and green wavelengths. The coefficient of determination, R^2, slope, and intercept obtained from regression analysis on log-transformed, algorithm-derived and *in situ* measured data, the mean relative percentage difference, *RPD*, and mean absolute percentage difference, *APD,* are shown. The data are sorted by cruise, with symbols as indicated in Figure 9.

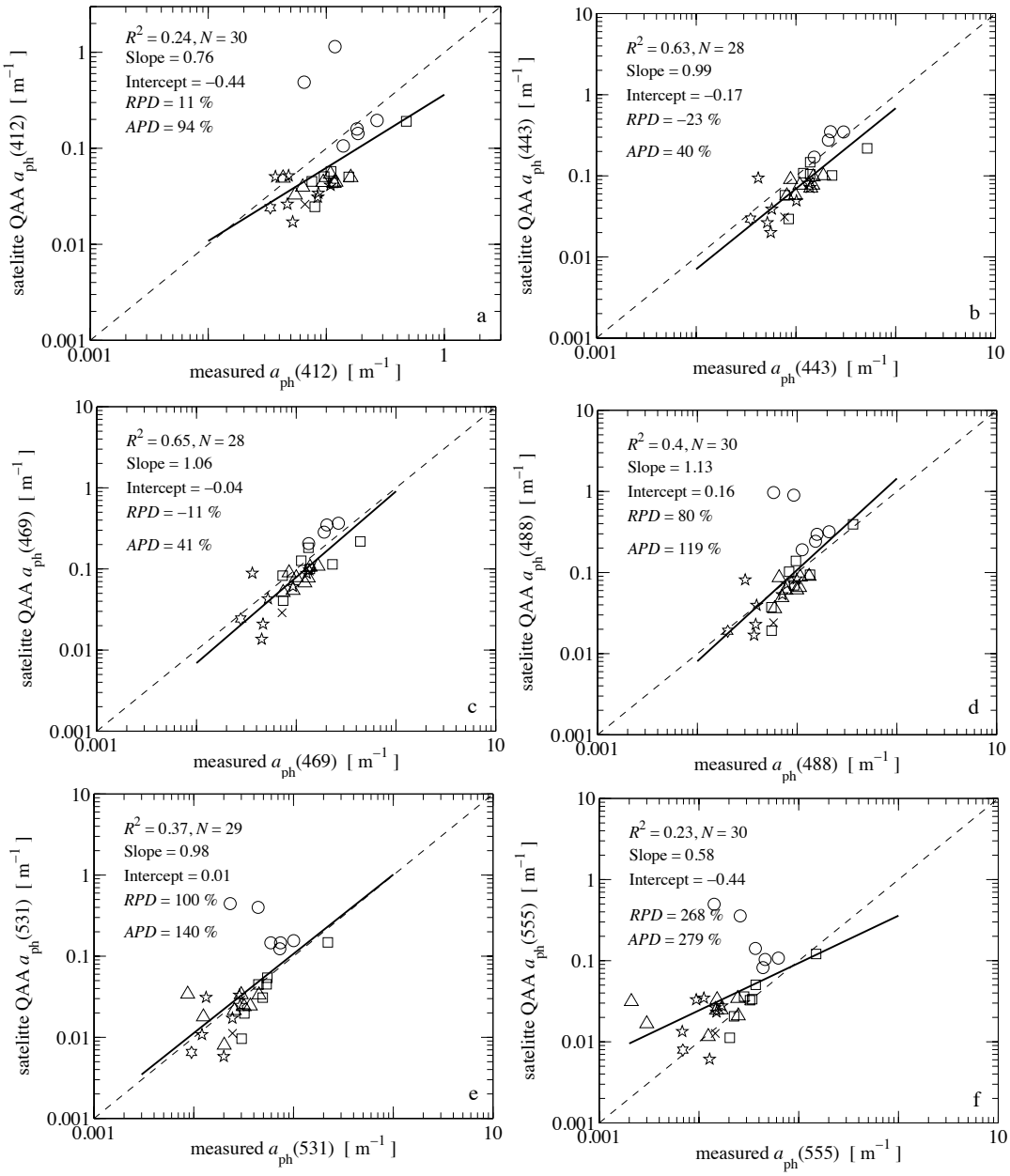

Figure 11. Comparison between the *in situ*-measured and satellite-retrieved phytoplankton absorption coefficient, $a_{ph}(\lambda)$, from the QAA semi-analytical algorithm for blue and green wavelengths. The coefficient of determination, R^2, slope, and intercept obtained from regression analysis on log-transformed, algorithm-derived and *in situ* measured data, the mean relative percentage difference, *RPD*, and mean absolute percentage difference, *APD,* are shown. The data are sorted by cruise, with symbols as indicated in Figure 9.

Variability in light absorption and scattering of phytoplankton in Patagonian waters: Role of community size structure and pigment composition

Amabile Ferreira,[1] Dariusz Stramski,[2] Carlos A. E. Garcia,[1] Virginia M. T. Garcia,[1] Áurea M. Ciotti,[3] and Carlos R. B. Mendes[1,4]

Received 6 June 2012; revised 9 January 2013; accepted 10 January 2013.

[1] Intense phytoplankton blooms were observed along the Patagonian shelf-break with satellite ocean color data, but few in situ optical observations were made in that region. We examine the variability of phytoplankton absorption and particulate scattering coefficients during such blooms on the basis of field data. The chlorophyll-*a* concentration, [Chla], ranged from 0.1 to 22.3 mg m^{-3} in surface waters. The size fractionation of [Chla] showed that 80% of samples were dominated by nanophytoplankton (N-group) and 20% by microphytoplankton (M-group). Chlorophyll-specific phytoplankton absorption coefficients at 440 and 676 nm, $a^*_{ph}(440)$ and $a^*_{ph}(676)$, and particulate scattering coefficient at 660 nm, $b^*_p(660)$, ranged from 0.018 to 0.173, 0.009 to 0.046, and 0.031 to 2.37 m^2 (mg Chl*a*)$^{-1}$, respectively. Both $a^*_{ph}(440)$ and $a^*_{ph}(676)$ were statistically higher for the N-group than M-group and also considerably higher than expected from global trends as a function of [Chla]. This result suggests that size of phytoplankton cells in Patagonian waters tends to be smaller than in other regions at similar [Chla]. The phytoplankton cell size parameter, S_f, derived from phytoplankton absorption spectra, proved to be useful for interpreting the variability in the data around the general inverse dependence of $a^*_{ph}(440)$, $a^*_{ph}(676)$, and $b^*_p(660)$ on [Chla]. S_f also showed a pattern along the increasing trend of $a^*_{ph}(440)$ and $a^*_{ph}(676)$ as a function of the ratios of some accessory pigments to [Chla]. Our results suggest that the variability in phytoplankton absorption and scattering coefficients in Patagonian waters is caused primarily by changes in the dominant phytoplankton cell size accompanied by covariation in the concentrations of accessory pigments.

Citation: Ferreira, A., D. Stramski, C. A. E. Garcia, V. M. T. Garcia, Á. M. Ciotti, and C. R. B. Mendes (2013), Variability in light absorption and scattering of phytoplankton in Patagonian waters: Role of community size structure and pigment composition, *J. Geophys. Res. Oceans*, *118*, doi:10.1002/jgrc.20082.

1. Introduction

[2] The absorption coefficient of phytoplankton, $a_{ph}(\lambda)$, plays an important role for a variety of oceanographic science questions and applications, including the propagation of light [e.g., *Atlas and Bannister*, 1980; *Sathyendranath and Platt*, 1988], primary production [e.g., *Morel*, 1991; *Marra et al*., 2007], algal physiology [e.g., *Stramski and Reynolds*, 1993; *Bouman et al*., 2003], and thermal structure [e.g., *Lewis et al*., 1983; *Stramska and Dickey*, 1993] within the upper water column. Because $a_{ph}(\lambda)$ is one of principal inherent optical properties of seawater affecting the spectral reflectance of the ocean, this absorption coefficient is also important to science and applications associated with the use of satellite and airborne observations of ocean color [e.g., *Morel and Bricaud*, 1981; *Roesler and Perry*, 1995; *Sathyendranath et al*., 2001].

[3] Variations in $a_{ph}(\lambda)$ may result from changes in phytoplankton concentration, optical properties of individual cells, or both [e.g., *Morel and Bricaud*, 1981; *Stramski et al*., 2001]. In particular, the variability observed around the general trends of statistical relationships between the concentration of chlorophyll-*a*, [Chla], and $a_{ph}(\lambda)$ is related to pigment packaging (or package effect) and pigment composition in phytoplankton cells. Pigment packaging is a well-documented source of variability in $a_{ph}(\lambda)$, which depends on cell size and intracellular concentration of pigments [*Morel and Bricaud*, 1981; *Bricaud and Morel*, 1986; *Sathyendranath et al*., 1987; *Ciotti et al*., 1999]. The chlorophyll-specific absorption coefficient of phytoplankton,

[1]Instituto de Oceanografia, Universidade Federal do Rio Grande, Rio Grande, Brazil.
[2]Marine Physical Laboratory, Scripps Institution of Oceanography, University of California San Diego, La Jolla, California, USA.
[3]Centro de Biologia Marinha, Universidade de São Paulo, São Sebastião, Brazil.
[4]Centro de Oceanografia, Faculdade de Ciências, Universidade de Lisboa, Lisbon, Portugal.

Corresponding author: Amabile Ferreira, Instituto de Oceanografia, Universidade Federal do Rio Grande, Rio Grande, RS 96201-900, Brazil. (amabilefr@gmail.com)

2169-9275/13/10.1002/jgrc.20082

$a^*_{ph}(\lambda)$ (i.e., $a_{ph}(\lambda)$ per unit of [Chla]), is generally found to decrease with an increase in both [Chla] and the average cell size within phytoplankton populations, and is also related to the proportions of accessory pigments relative to [Chla] [e.g., *Bricaud et al*., 2004].

[4] Following the work of *Sathyendranath et al*. [1987], a number of recent studies have attempted to separate the effect of pigment composition from that of pigment packaging upon the $a_{ph}(\lambda)$ spectra [*Lohrenz et al*., 2003; *Toepel et al*., 2005; *Fishwick et al*., 2006; *Chazottes et al*., 2007; *Wang et al*., 2007; *Matsuoka et al*., 2011]. In general, the effects caused by variations in pigment composition are smaller than those produced by cell size [e.g., *Bricaud et al*., 2004]. However, seasonal variability in the relative importance of both factors was observed in specific regions of the oceans [e.g., *Toepel et al*., 2005].

[5] Significant efforts have been devoted to the development of models and approaches, including those involving satellite remote sensing of ocean color, for deriving information about cell size from phytoplankton absorption spectra [see *Brewin et al*., 2011b for a review]. *Ciotti et al*. [2002] introduced a phytoplankton cell size parameter, S_f, and showed that combined effects of the dominant cell size and covarying pigments can explain about 80% of the variability in phytoplankton absorption spectra in surface oceanic waters. It was postulated that the shape of phytoplankton absorption spectra can be reproduced with the parameter S_f, which describes the complementary contributions of two basis vectors representing the extreme cases of spectral shapes corresponding to the smallest (picophytoplankton) and largest (microphytoplankton) dominant cell sizes of phytoplankton community. *Ciotti et al*. [2002] emphasized that S_f is not dependent solely on the cell size, and that the pigment packaging also plays a role implying the effect of intracellular concentrations of various pigments. For example, for the same dominant cell size, the S_f values will tend to decrease if phytoplankton community shows an increase in the concentrations of intracellular pigments caused, for instance, by photoacclimation [see also *Ciotti et al*., 1999].

[6] Phytoplankton is also an important light-scattering agent in seawater [*Morel and Ahn*, 1991; *Stramski and Kiefer*, 1991]. Empirical relationships based on in situ measurements have been proposed between [Chla] and the beam attenuation (scattering plus absorption) coefficient [e.g., *Voss*, 1992; *Loisel and Morel*, 1998; *Behrenfeld and Boss*, 2006], scattering coefficient [e.g., *Gordon and Morel*, 1983; *Loisel and Morel*, 1998; *Huot et al*., 2008], and backscattering coefficient [e.g., *Reynolds et al*., 2001; *Stramska et al*., 2006; *Huot et al*., 2008]. Changes in chlorophyll-specific particulate scattering coefficient, $b^*_p(\lambda)$ (i.e., particulate scattering coefficient per unit of [Chla]), observed in the field have been related to phytoplankton physiological status [*Behrenfeld and Boss*, 2003], but the role of cell size in scattering properties of natural phytoplankton communities has been addressed only in few recent studies [*Gernez et al*., 2011; *Brewin et al*., 2012; *Martinez-Vicente et al*., 2012]. The potentially high correlation between scattering and backscattering coefficients may support the use of satellite-derived [Chla] and particulate backscattering for investigation of phytoplankton biomass and physiology [*Westberry et al*., 2010] as well as size structure [*Loisel et al*., 2006]. The quantification and understanding of the causes of variability in both absorption and scattering properties of natural phytoplankton communities are thus essential for improving our ability to retrieve biologically relevant information from in situ and remote-sensing optical data. This study aims to provide a contribution to such understanding of phytoplankton-related optical variability in Patagonian waters.

[7] During austral spring and summer, high levels of phytoplankton biomass persistently occur in the Patagonian inner shelf and shelf-break region, making it one of the most productive zones in the global ocean [*Takahashi et al*., 2002; *Gregg et al*., 2005]. The seasonal cycle of phytoplankton biomass in the vicinities of the Patagonian shelf-break was recently examined using remote-sensing data [*Garcia et al*., 2004; *Rivas et al*., 2006; *Romero et al*., 2006; *Signorini et al*., 2006]. Fieldwork in this region suggests that the development and sustainability of phytoplankton blooms are associated with both nutrient supply from the Malvinas Current and water column stability along the shelf-break front [*Carreto et al*., 1995; *Garcia et al*., 2008]. The Patagonian shelf waters have been also recognized to play an important role in the global oceanic uptake of CO_2 from the atmosphere [*Takahashi et al*., 2002; *Bianchi et al*., 2009]. Specifically, *Schloss et al*. [2007] demonstrated an inverse relationship between the air-sea differences of CO_2 partial pressure with surface [Chla] under the dominance of diatoms in the Argentinean continental shelf. Such scenario was not observed when small ($\leq 5\ \mu$m) flagellates dominated the phytoplankton assemblages.

[8] Optical measurements have been rarely conducted in the Patagonian waters [*Ferreira et al*., 2009; *Lutz et al*., 2010; *Garcia et al*., 2011]. The objective of this study is to characterize the variability of phytoplankton absorption and particulate scattering coefficients in the Patagonian shelf-break waters and vicinities on the basis of large data set collected during six cruises in austral spring and summer from 2006 to 2009. Our data analysis also aims at providing insights on influences of the dominant cell size and pigment composition on variability in phytoplankton absorption and scattering coefficients as a function of bulk chlorophyll-*a* concentration.

2. Data and Methods

2.1. Oceanographic Cruises and Data Collection

[9] Data analyzed in this study were collected on six research cruises in the Patagonian inner-shelf and shelf-break region. Three cruises referred to as PATEX 2, PATEX 4, and PATEX 6 took place during the austral spring season, specifically 28–31 October 2006, 16–21 October 2007, and 14–18 October 2008, respectively. Two cruises, PATEX 5 and PATEX 7, were conducted in austral summer during the periods of 4–7 January 2008 and 5–8 January 2009, respectively. Finally, PATEX 3 took place during transition between summer and fall from 25 to 29 March 2007. The locations of stations (Figure 1) extend from the northern portion of the Argentinean shelf (PATEX 6) through the highly productive waters along the Patagonian shelf-break (PATEX 2, 3, and 4) and the southern inner shelf (PATEX 5), to the area south of Malvinas (Falkland) Islands (PATEX 7). Overall 176 stations were visited by performing cross-shelf

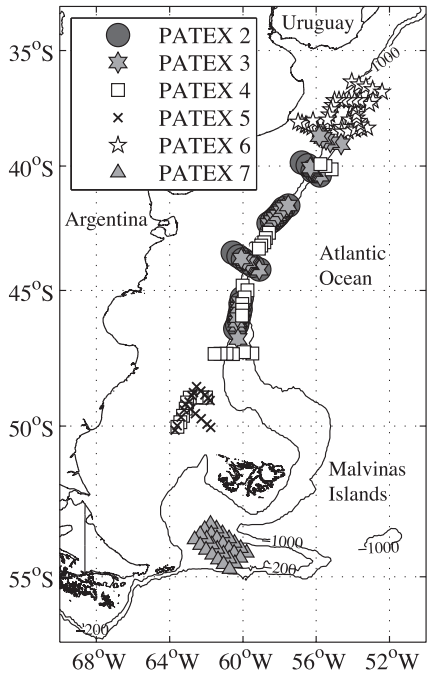

Figure 1. Locations of 176 oceanographic stations where measurements and sample collections were made during the PATEX cruises within the Patagonian shelf-break and adjacent areas.

and along-shelf transects during the six cruises. At all stations, vertical profiles of temperature, salinity, dissolved oxygen, chlorophyll fluorescence, and beam attenuation coefficient at 660 nm were taken with a CTD/Rosette system (SeaBird® 911+) which included 5 L Niskin bottles for water sampling. Seawater was collected at several depths for further laboratory analysis. We also note that research conducted on an earlier cruise PATEX 1 (October 2004) was described by *Garcia et al*. [2008] and these data are not analyzed in this study.

[10] Measurements of the following bio-optical parameters are used in this study: the concentration of total chlorophyll-*a*, size-fractionated chlorophyll-*a*, concentrations of phytoplankton accessory pigments, spectral absorption coefficients of particulate matter including the partitioning into phytoplankton and non-phytoplankton components, and the beam attenuation coefficient at a single light wavelength of 660 nm. The chlorophyll-*a* concentration was determined with the fluorometric (F) and High Performance Liquid Chromatography (HPLC) methods. We use data only from near-surface depths and depths of maximum chlorophyll fluorescence. For all PATEX cruises, the depths of maximum fluorescence varied between about 15 and 30 m and were typically located just below the mixed layer. Microscopy and HPLC analyses showed very similar phytoplankton community composition near the surface and at depths of maximum fluorescence [*Souza et al*., 2012; *Gonçalves-Araujo et al*., 2012; M. S. Souza, personal communication, 2011]. In addition, no clear difference was observed in phytoplankton absorption and particulate scattering properties between the near-surface and maximum fluorescence depths. Therefore, our analysis was applied to a single data set with no discrimination between these depths. This data set includes 236 measurements of absorption spectra and chlorophyll-*a* concentration with fluorometric method, 223 measurements of beam attenuation coefficient, and 132 HPLC determinations of pigments.

2.2. Determinations of Phytoplankton Pigments and Size Fractions

Fluorometric Determinations of Chlorophyll-a

[11] Discrete water samples (0.5–1 L) were filtered onto 25-mm glass fiber filters (Whatman GF/F) for post-cruise determinations of the concentration of total chlorophyll-*a* by fluorometric method, which is denoted by $[\mathrm{Chla}]_F$. In addition, samples were filtered through a 20 μm mesh and the collected filtrate was subsequently filtered on the GF/F filter for the determination of the fraction of chlorophyll-*a* associated with phytoplankton cells less than 20 μm in size. This fraction of chlorophyll-*a* concentration represents the combined contributions of picophytoplankton and nanophytoplankton, which is denoted by $[\mathrm{pico+nano\ Chla}]_F$. The difference between $[\mathrm{Chla}]_F$ and $[\mathrm{pico+nano\ Chla}]_F$ yields a contribution of microphytoplankton (>20 μm in size), which is denoted by $[\mathrm{micro\ Chla}]_F$.

[12] Immediately after filtration, the GF/F filters were wrapped in aluminum foil and placed in liquid nitrogen for storage until post-cruise analysis. After the cruises, pigments were extracted in 90% acetone and chlorophyll-*a* determinations were made with a calibrated Turner Designs TD-700 Fluorometer [*Welschmeyer*, 1994]. These fluorometric determinations were made for both total and fractionated chlorophyll-*a* in all samples collected on the six cruises.

HPLC Determinations of Pigments

[13] The concentrations of phytoplankton pigments were obtained by HPLC technique for samples collected during four cruises, PATEX 4, 5, 6, and 7. The protocol for collection and storage of HPLC samples was the same as that for the fluorometric determinations. *Mendes et al*. [2007] and *Souza et al*. [2012] described in detail the HPLC procedure used in this work. A specific set of pigments detected with the HPLC method is used in our study, which includes (1) total chlorophyll-*a*, $[\mathrm{Chla}]_{\mathrm{HPLC}}$, which is the sum of monovinyl chlorophyll-*a*, chlorophyllide-*a*, and the chlorophyll-*a* epimers and allomers (note that divinyl chlorophyll-*a* was undetectable); (2) chlorophyll-*b*, [Chlb]; (3) 19′-hexanoyloxyfucoxanthin, [Hexa]; (4) photosynthetic carotenoids, [PSC], which include [Hexa], fucoxanthin, 19′-butanoyloxyfucoxanthin, and peridinin; and (5) photoprotective carotenoids, [PPC], which include diadinoxanthin, alloxanthin, and zeaxanthin. Other pigments, whose concentrations are typically very low, are considered to be less important and are not included in our analysis.

[14] An unknown carotenoid with absorption peak centered at about 460 nm was detected in 37 samples collected on four cruises, PATEX 2, 3, 4, and 6. The presence of this carotenoid consistently shifted the primary blue peak of phytoplankton absorption from about 440 nm towards 460 nm (see section 3.5). This pigment is hereafter referred to as P460.

Estimation of Phytoplankton Size Fractions From HPLC Data

[15] The fluorometric determinations made on unfractionated samples and 20 μm filtrates provided the estimates of

$[\text{pico} + \text{nano Chla}]_F$ and $[\text{micro Chla}]_F$. It is also useful to obtain additional information on separate contributions of picophytoplankton and nanophytoplankton to total chlorophyll-*a* concentration from HPLC pigment data. This information can be obtained from a method proposed by *Vidussi et al*. [2001] with refinements by *Uitz et al*. [2006]. In this method several diagnostic accessory pigments serve as biomarkers of specific phytoplankton taxonomic groups and these taxa are assigned to one of the three size classes: pico-, nano-, or microphytoplankton. This assignment is based on observations that microphytoplankton include primarily diatoms, nanophytoplankton prymnesiophytes, and picophytoplankton prokaryotic species. It must be recognized that this approach has limitations because various phytoplankton groups can share certain diagnostic pigments and some taxa include cells covering a wide range of size. Despite these limitations, this method has proven to provide useful information about pigment-based composition and size structure of phytoplankton communities [*Bricaud et al*., 2004; *Uitz et al*., 2006, 2008; *Ras et al*., 2008].

[16] We used our HPLC data of diagnostic pigments from four cruises (PATEX 4, 5, 6, and 7) to obtain estimates of chlorophyll-*a* concentrations associated with the three size classes, $[\text{pico Chla}]_{HPLC}$, $[\text{nano Chla}]_{HPLC}$, and $[\text{micro Chla}]_{HPLC}$. We found poor agreement between the relative contributions of size fractions to total chlorophyll-*a* obtained from HPLC-derived diagnostic pigments and from fluorometric measurements of samples fractionated by filtration. These differences are quantified through slopes of the following linear relationships: (i) $[\text{pico} + \text{nano Chla}]_F$ versus $[\text{Chla}]_F$, (ii) $[\text{micro Chla}]_F$ versus $[\text{Chla}]_F$, (iii) $[\text{pico} + \text{nano Chla}]_{HPLC}$ (i.e., the sum of $[\text{pico Chla}]_{HPLC}$ and $[\text{nano Chla}]_{HPLC}$) versus $[\text{Chla}]_F$, and (iv) $[\text{micro Chla}]_{HPLC}$ versus $[\text{Chla}]_F$ (see Table 1). Specifically, the contribution of $[\text{micro Chla}]_{HPLC}$ estimated from HPLC-derived diagnostic pigments is significantly higher than the contribution of $[\text{micro Chla}]_F$ obtained from the sample fractionation with fluorometric measurements. The opposite result is observed for the sum of picophytoplankton and nanophytoplankton contributions, for which the method based on diagnostic pigments yields lower values compared with the fractionation/fluorometric data.

[17] The observed discrepancies are, at least partly, related to limitations of the method based on diagnostic pigments as briefly mentioned above. For example, the relatively high estimates of $[\text{micro Chla}]_{HPLC}$ may result from the fact that fucoxanthin is assumed to be diagnostic of large-sized diatoms that belong to microphytoplankton although this pigment can be also present in smaller diatoms and prymnesiophytes within the nanoplankton size class. Therefore, we decided to base our analysis on the use of data of $[\text{pico} + \text{nano Chla}]_F$ and $[\text{micro Chla}]_F$, which are available for all six PATEX cruises. In addition, for the four cruises for which HPLC data are available, we also partitioned $[\text{pico} + \text{nano Chla}]_F$ into two components $[\text{pico Chla}]_{HPLC}$ and $[\text{nano Chla}]_{F/HPLC}$. The $[\text{pico Chla}]_{HPLC}$ component is estimated from the method based on HPLC-derived diagnostic pigments, and the $[\text{nano Chla}]_{F/HPLC}$ component is estimated as a difference between $[\text{Chla}]_F$ and $[\text{micro Chla}]_F$ plus $[\text{pico Chla}]_{HPLC}$. We assume that the estimates of $[\text{pico Chla}]_{HPLC}$ are reasonable because the diagnostic pigments of picophytoplankton are present exclusively in this cell size range.

2.3. Classification of Samples Based on the Dominant Size Fraction of Phytoplankton

[18] The dominant size fraction of phytoplankton was defined on the basis of relative contribution of each size class-specific concentration of chlorophyll-*a* to total $[\text{Chla}]_F$. Specifically, we assumed that a contribution greater than 50% defines the dominance. The picophytoplankton and nanophytoplankton contributions were not distinguished from one another for the PATEX 2 and PATEX 3 samples, but we can assume that the nanophytoplankton was dominating in cases when $[\text{pico} + \text{nano Chla}]_F$ was dominant. This assumption is supported by generally very small contributions of picophytoplankton estimated from HPLC pigment analysis performed on samples from PATEX 4, 5, 6, and 7 (Table 1). For these cruises, only two samples were dominated by picophytoplankton and eight samples did not satisfy our 50% criterion for the size fraction dominance. We ignore these 10 samples in further analysis, so the total number of samples in our analysis is reduced from 236 to 226. The majority of samples (181 out of 226) were classified as nanophytoplankton dominated. The remaining 45 samples were dominated by microphytoplankton. The absorption and scattering coefficients are discussed below within the context of these two groups, which are referred to as N-group (nanophytoplankton-dominated group) and M-group (microphytoplankton-dominated group).

2.4. Determinations of Particulate and Phytoplankton Absorption Coefficients

[19] Spectra of particulate absorption coefficient, $a_p(\lambda)$ in m^{-1}, were measured with a quantitative filter pad technique

Table 1. The Values for the Slope Parameter of the Linear Function Derived From Regression Analysis of the Chlorophyll-*a* Concentration Associated With Phytoplankton Size Classes Versus the Total Chlorophyll-*a* Concentration, $[\text{Chla}]_F$ or $[\text{Chla}]_{HPLC}$[a]

	Slopes			
Cruise	$[\text{pico} + \text{nano Chla}]_F$ versus $[\text{Chla}]_F$	$[\text{micro Chla}]_F$ versus $[\text{Chla}]_F$	$[\text{pico} + \text{nano Chla}]_{HPLC}$ versus $[\text{Chla}]_{HPLC}$	$[\text{micro Chla}]_{HPLC}$ versus $[\text{Chla}]_{HPLC}$
PATEX 4	0.65	0.35	0.02	0.99
PATEX 5	0.89	0.11	0.27	0.73
PATEX 6	0.99	0.02	0.44	0.56
PATEX 7	0.41	0.59	0.19	0.81

[a]The information on the class-specific chlorophyll-*a* concentration was derived from the size fractionation method followed by fluorometric determinations of chlorophyll-*a* in fractionated samples (subscript F) or from HPLC analysis of pigments (HPLC subscript). See text in section 2.2 for details.

[*Mitchell et al*., 2000]. Water samples (0.5–2 L) for these measurements were filtered onto 25 mm Whatman GF/F filters. The $a_p(\lambda)$ measurements were made in the 300–750 nm spectral range at 1 nm intervals with a dual beam spectrophotometer (Cary Model 1E). Immediately upon the $a_p(\lambda)$ measurements, the sample filters were subject to methanol extraction (PATEX 2 and 3) and bleaching with sodium hypochlorite (PATEX 4, 5, 6 and 7), and then rescanned in a spectrophotometer to obtain the estimates of non-algal (also referred to as detrital) absorption coefficient, $a_d(\lambda)$ [*Kishino et al*., 1985; *Tassan and Ferrari*, 1995; *Mitchell et al*., 2000]. For the calculations of $a_p(\lambda)$ and $a_d(\lambda)$ coefficients, we used the amplification factor β given by *Ferreira et al*. [2009]. The spectral absorption coefficient of phytoplankton, $a_{ph}(\lambda)$, was calculated as a difference between $a_p(\lambda)$ and $a_d(\lambda)$.

2.5. Estimation of Phytoplankton Cell Size Parameter

[20] To examine differences in the shape of phytoplankton absorption spectra and to estimate a cell size parameter for phytoplankton, each phytoplankton absorption spectrum was normalized to its mean value computed on the basis of all spectral values between 400 and 700 nm [*Ciotti et al*., 2002]. The normalized spectrum is denoted as $a_{<ph>}(\lambda)$. Assuming that variations in the spectral shape of phytoplankton absorption are mainly driven by the dominant cell size, *Ciotti et al*. [2002] developed a model that reconstructs the shape of $a_{<ph>}(\lambda)$ with a linear combination of two spectra representing complementary contributions of the smallest (picophytoplankton) and largest (microphytoplankton) cell sizes. We used a least squares Levenberg-Marquardt algorithm to fit the observed $a_{<ph>}(\lambda)$ to a linear model by adjusting the values of the derived cell size parameter, S_f [see equation 3 in *Ciotti et al*., 2002]. This procedure yields an estimate of the size parameter S_f that is consistent with a given observed spectrum of $a_{<ph>}(\lambda)$ and the model-reconstructed spectrum of $a_{<ph>}(\lambda)$. The values of S_f are constrained to vary from 0 to 1. S_f tends to 0 when large cells of phytoplankton (>20 μm) are dominant, and 1 when small cells (<2 μm) dominate. The intermediate values represent all possible situations between these two extremes. The goodness of the model fit was evaluated for each phytoplankton-normalized spectrum by computing the coefficient of determination, R^2, between all spectral values of the observed spectrum and all spectral values of the spectrum reconstructed by the model.

2.6. Determinations of Particulate Scattering Coefficient

[21] The beam attenuation coefficient of suspended particles, $c_p(660)$ in m^{-1}, was measured at a light wavelength of 660 nm with a C-star beam transmissometer (WETLabs, Inc.) along a 25 cm pathlength throughout the water column. Details of the protocol for determining $c_p(660)$ are provided by WETLabs., Inc. (http://www.wetlabs.com/products/). We assumed that measurements taken in deep waters (~1000 m) but far away from the sea bottom provide the best estimate of particle-free attenuation of seawater [*Loisel and Morel*, 1998]. These deep-water measurements were subtracted from all beam attenuation measurements taken in surface ocean layer on a cruise-by-cruise basis to remove the contribution of pure seawater. The resulting values are considered to represent the beam attenuation by particles under the assumption that the contribution of dissolved matter to the attenuation of light at 660 nm is negligible. The measurements taken at 5 m depth were assumed to represent the near-surface beam attenuation, which is reasonable from the standpoint of avoiding or minimizing the potential intermittent contributions of air bubbles injected by breaking waves. For the purposes of analysis in this study, we use the particulate scattering coefficient at 660 nm, $b_p(660)$, for the near-surface and fluorescence maximum depths. This coefficient was calculated as $b_p(660) = c_p(660) - a_p(660)$.

3. Results and Discussion

3.1. Total and Fractionated Chlorophyll-*a*

[22] The range of variation in surface $[Chla]_F$ is shown in Table 2. At the depth of maximum chlorophyll fluorescence, $[Chla]_F$ ranged from about 0.3 to 24 mg m^{-3} (not shown) and was slightly higher than surface concentrations. The variability in $[Chla]_F$ was mainly associated with differences in both the time and geographical location of sampling among the different cruises.

[23] Very high surface pigment concentrations with the mean values of about 6.2 and 6.0 mg m^{-3} were measured along the Patagonian shelf-break during the austral spring cruises, PATEX 2 and PATEX 4 (Table 2 and Figure 2).

Table 2. The Minimum (Min), Maximum (Max), and Mean Values (Mean ± Std Where Std Is Standard Deviation) of Near-Surface Concentrations of Total Chlorophyll-*a*, $[Chla]_F$, for Each PATEX Cruise[a]

Cruise	Min $[Chla]_F$ mg m^{-3}	Max $[Chla]_F$ mg m^{-3}	Mean ± Std $[Chla]_F$ mg m^{-3}	Mean ± Std pico + nano %	Mean ± Std pico %	Mean ± Std nano %	Mean ± Std micro %	*N*
PATEX 2	1.46	11.85	6.24 ± 2.96	38 ± 25	–	–	62 ± 25	26
PATEX 3	0.24	2.16	1.35 ± 0.42	89 ± 8	–	–	11 ± 8	30
PATEX 4	0.32	22.30	5.99 ± 6.05	74 ± 14	1 ± 1	74 ± 14	26 ± 14	33
PATEX 5	0.45	2.35	1.01 ± 0.40	79 ± 20	6 ± 5	72 ± 22	21 ± 21	18
PATEX 6	0.21	3.13	1.29 ± 0.77	87 ± 18	13 ± 12	75 ± 21	13 ± 16	41
PATEX 7	0.10	2.72	0.67 ± 0.52	78 ± 26	28 ± 28	50 ± 31	22 ± 28	28

[a]The mean (±Std) for the percent contributions of picophytoplankton (pico), nanophytoplankton (nano), and microphytoplankton (micro) to total $[Chla]_F$, and the number of data (*N*) are also shown. Note that the sum of separate contributions of pico- and nanophytoplankton based on the combination of fractionation with fluorometric determinations of chlorophyll-*a* and HPLC pigment analysis (columns 6 and 7) is slightly different than the combined pico + nano contribution based on the sample fractionation (column 5). See text in section 2.2 for details.

Satellite-based ocean color observations during austral spring usually show conspicuous phytoplankton blooms along the shelf-break zone, which is in contrast with the surrounding areas [*Rivas et al*., 2006; *Romero et al*., 2006]. *Garcia et al*. [2008] suggested that the supply of macronutrients by upwelling, and possibly also iron by upwelling and transport over the continental shelf, contribute to the maintenance of the spring blooms. The maximum surface values of $[Chla]_F$ on PATEX 2 and 4 (11.85 and 22.30 mg m^{-3}, respectively) were observed at the shelf-break zone between 42°S and 45°S, likely due to intense shelf-break upwelling processes. These observations are consistent with the study of *Carreto et al*. [2008].

[24] The northernmost transect around 40°S occupied during PATEX 2 (Figure 1) showed relatively low $[Chla]_F$ in the range of 1.46–3.45 mg m^{-3}. This observation likely reflects a late phase of the bloom compared with higher latitudes of the continental shelf-break, as the blooms tend

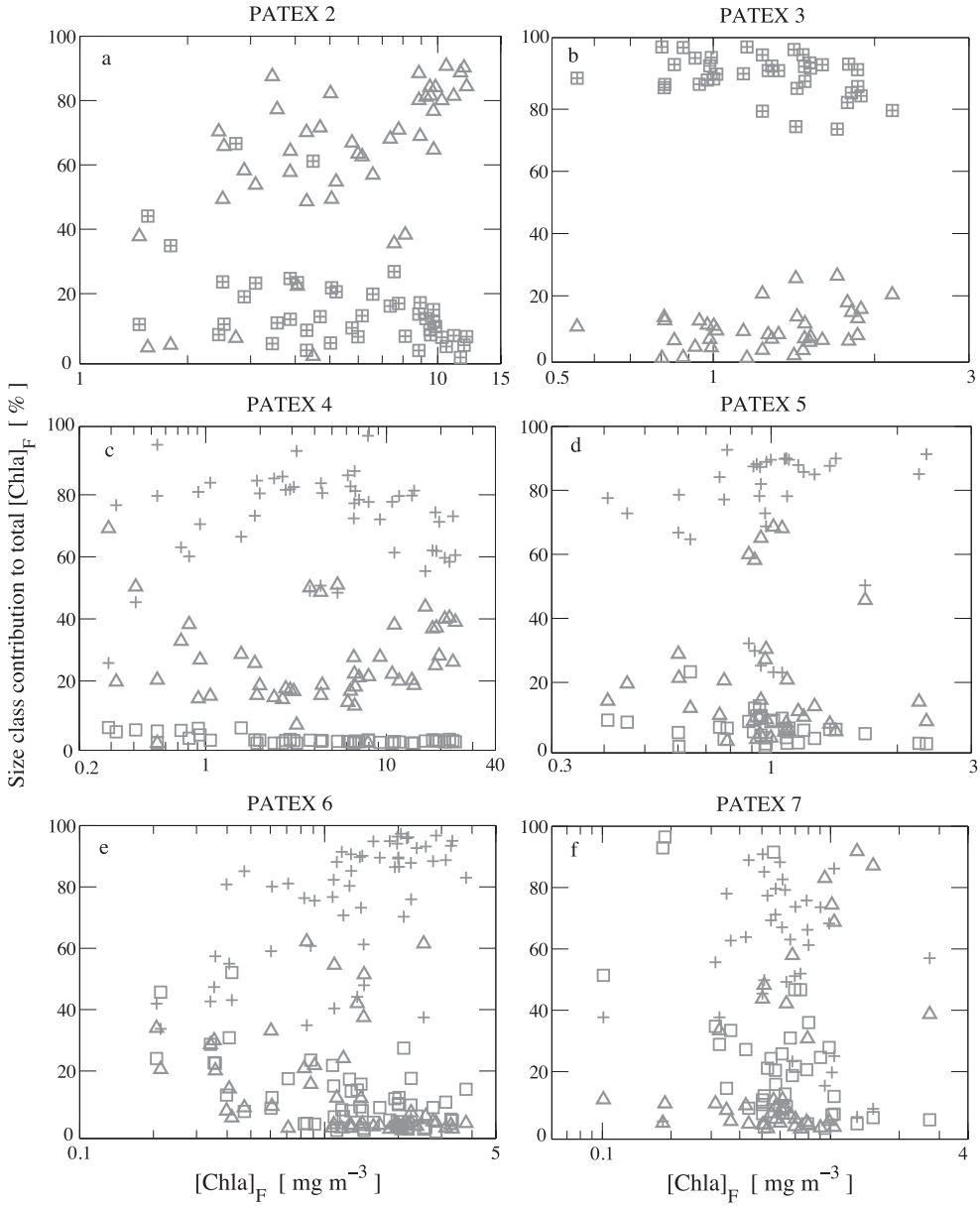

Figure 2. The percent contributions of chlorophyll-*a* concentration associated with the three phytoplankton size-classes to total chlorophyll-*a* concentration, $[Chla]_F$, as a function of $[Chla]_F$, for each PATEX cruise: (a) PATEX 2, (b) PATEX 3, (c) PATEX 4, (d) PATEX 5, (e) PATEX 6, and (f) PATEX 7. The data points shown as squares are for contribution of picophytoplankton (i.e., 100× [pico $Chla]_{HPLC}$/$[Chla]_F$); crosses for nanophytoplankton (i.e., 100× [nano $Chla]_{F/HPLC}$ / $[Chla]_F$); and triangles for microphytoplankton (i.e., 100 x [micro $Chla]_F$ / $[Chla]_F$). In Figures 2a and 2b, squares and crosses combined correspond to data for picophytoplankton and nanophytoplankton combined (i.e., 100× [pico + nano $Chla]_F$ / $[Chla]_F$) for PATEX 2 and 3 (see text in section 2.2 for details).

to start in the north and develop progressively in the southward direction following typical pattern associated with increasing light and temperature [*Rivas et al*., 2006].

[25] During another spring cruise, PATEX 6, the observations were made at latitudes lower than 40°S within the northernmost part of the region investigated in our study (Figure 1). These observations showed relatively low values of surface $[Chla]_F$ with the mean of about 1 mg m^{-3}, when compared to generally higher values that were observed also in spring but at higher latitudes during PATEX 2 and PATEX 4. This difference can be attributed to specific conditions that occur within the region of PATEX 6. Specifically, this is the Brazil-Malvinas Confluence Zone, which is a highly energetic region of waters just off the coast of Argentina and Uruguay where the warm poleward-flowing Brazil Current encounters the cold equatorward-flowing Malvinas Current. The environmental conditions and their effect on phytoplankton biomass and community during PATEX 6 are described elsewhere [*Gonçalves-Araujo et al*., 2012].

[26] In late summer (March 2007), relatively low to moderate values of surface $[Chla]_F$ from 0.24 to 2.16 mg m^{-3} were measured during PATEX 3. A region characterized by high ocean reflectance and surface values of $[Chla]_F$ ranging from 0.45 to 2.35 mg m^{-3} was investigated during the PATEX 5 cruise (January 2008). Microscopic and pigment analyses confirmed the significant abundance of coccolithophorides [*Souza et al*., 2012] and the optical properties associated with the coccolithophorid bloom are described by *Garcia et al*. [2011]. Another summer cruise (PATEX 7) was carried out in the southernmost part of the investigated region (January 2009). This cruise was also an attempt to sample waters with high reflectance detected by satellite ocean color sensors south of the Malvinas Islands. However, the expected coccolithophorid bloom was not found at the visited stations. Fairly low surface values of $[Chla]_F$ with the mean of 0.67 mg m^{-3} were typically observed during PATEX 7.

[27] Figure 2 shows the percent contribution of the three phytoplankton size classes (pico-, nano-, and microphytoplankton) to total $[Chla]_F$ as a function of total $[Chla]_F$ for each cruise. The percent contribution of picophytoplankton could not be estimated for PATEX 2 and PATEX 3 because HPLC analysis was not performed for these two cruises (see section 2.2). Thus, in addition to [micro $Chla]_F$, [pico + nano $Chla]_F$ was estimated for PATEX 2 and PATEX 3 cruises. Considering the biomass ranges on both cruises and the generally small picophytoplankton contributions estimated from HPLC pigment analysis for other cruises (Table 2), significant role of picophytoplankton in waters sampled during PATEX 2 and PATEX 3 is highly unlikely. Therefore, we can assume that nanophytoplankton is the dominant size fraction for PATEX 2 and PATEX 3 in cases when [pico + nano $Chla]_F$ dominates the total $[Chla]_F$. For PATEX 2, 75% of samples were dominated by microphytoplankton and the remainder by nanophytoplankton. For PATEX 3, all samples showed dominance by nanophytoplankton (Figure 2).

[28] The [micro $Chla]_F$ component made a main contribution to total $[Chla]_F$ only during PATEX 2 (Figure 2a), with the exception of the northernmost transect visited during this cruise where the lowest $[Chla]_F$ values were measured (1.46–4.05 mg m^{-3}). If the six stations of this transect are excluded, the mean contribution of [micro $Chla]_F$ to total $[Chla]_F$ is 69% for PATEX 2. Between the spring 2006 (PATEX 2) and summer 2007 (PATEX 3), a shift from the dominance of [micro $Chla]_F$ to [pico + nano $Chla]_F$ was observed (Figure 2b). The [pico + nano $Chla]_F$ component contributed, on average, 90% to total $[Chla]_F$ on the PATEX 3 cruise.

[29] During the following spring cruise in 2007 (PATEX 4), $[nano\ Chla]_{F/HPLC}$ was mostly responsible for the generally increased values of total $[Chla]_F$ (Figure 2c). We recall that the highest $[Chla]_F$ values were found on this cruise. The [micro $Chla]_F$ component generally made a significant, albeit not dominant contribution to total $[Chla]_F$ on the PATEX 4 cruise (on average 26%; Figure 2c and Table 2). However, for four samples [micro $Chla]_F$ contributed 50, 50, 59, and 51% to total $[Chla]_F$ which was 3.77, 0.41, 0.29, and 5.36 mg m^{-3}, respectively. Microscopy analysis revealed a general dominance of diatoms from nanoplankton size range (mainly *Thalassiosira ssp*.) in the PATEX 4 samples (M. S. Souza, personal communication, 2011). These results are consistent with earlier findings from the PATEX 1 cruise [*Garcia et al*., 2008].

[30] During the coccolithophoride bloom on PATEX 5 (January 2008), $[nano\ Chla]_{F/HPLC}$ was the primary component that controlled the total $[Chla]_F$ with an average contribution of 72%. For some samples, [micro $Chla]_F$ contributed substantially to total $[Chla]_F$ (Figure 2d). On PATEX 6, $[nano\ Chla]_{F/HPLC}$ was also the major component of total $[Chla]_F$ (an average contribution of 75%) and [micro $Chla]_F$ made a significant contribution in several samples (Figure 2e). For most samples collected on PATEX 7, changes in both $[nano\ Chla]_{F/HPLC}$ and [micro $Chla]_F$ were responsible for variations in total $[Chla]_F$ (Figure 2f). We note, however, that whereas $[pico\ Chla]_{HPLC}$ remained generally weakly variable with very small contribution to total $[Chla]_F$ (Figure 2), the average contribution of $[pico\ Chla]_{HPLC}$ to total $[Chla]_F$ reached 28% on PATEX 7 (Table 2). For many PATEX 7 samples, the total $[Chla]_F$ increased slightly as a result of increases in $[pico\ Chla]_{HPLC}$ as shown in Figure 2f. For two samples, the $[pico\ Chla]_{HPLC}$ contribution to total $[Chla]_F$ reached about 90% when $[Chla]_F$ was relatively low (~1 mg m^{-3}; Figure 2f).

3.2. Phytoplankton Absorption as a Function of Chlorophyll-*a*

[31] For the analysis presented in this and next section, we excluded 37 phytoplankton absorption spectra from the total of 226 spectra. The excluded spectra show atypical absorption peak around 460 nm and are discussed separately in section 3.5. As a result of such data selection, we obtained 189 phytoplankton absorption spectra, $a_{ph}(\lambda)$, combined with the data of size-fractionated chlorophyll-*a*. These spectra are divided into two groups; the nanophytoplankton-dominated group (N-group) with 151 samples and microphytoplankton-dominated group (M-group) with 38 samples.

[32] The absorption coefficients of phytoplankton at 440 and 676 nm, $a_{ph}(440)$ and $a_{ph}(676)$, varied broadly from about 0.013 to 0.66 and 0.008 to 0.42 m^{-1}, respectively, and this variation is accompanied by large variability in $[Chla]_F$ (Figure 3). The chlorophyll-specific absorption coefficients of phytoplankton at 440 and 676 nm, i.e., the phytoplankton absorption coefficients normalized by $[Chla]_F$,

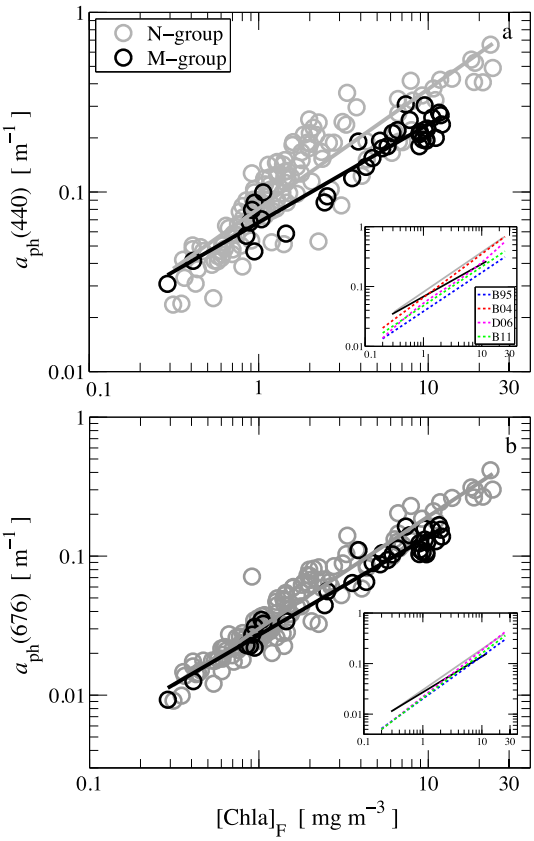

Figure 3. The phytoplankton absorption coefficient $a_{ph}(\lambda)$ at two light wavelengths, (a) 440 nm and (b) 676 nm, as a function of total chlorophyll-*a* concentration, $[Chla]_F$, for PATEX 2 to PATEX 7 cruises. The data points are shown for samples dominated by nanophytoplankton (N-group) and microphytoplankton (M-group), where the dominance is determined in terms of contributions of these size classes to total chlorophyll-*a* concentration $[Chla]_F$. The lines represent the best fit regression between $a_{ph}(\lambda)$ and $[Chla]_F$ (see Table 3). The inset graphs compare our regression lines (N-group in grey and M-group in black) with relationships from literature, which include B95 [*Bricaud et al*., 1995], B04 [*Bricaud et al*., 2004], D06 [*Devred et al*., 2006], and B11 [*Brewin et al*., 2011a]. The equation for $a_{ph}(676)$ versus chlorophyll-*a* concentration was not provided by *Bricaud et al*. [2004]. The relationships of *Devred et al*. [2006] and *Brewin et al*. [2011a] are for 443 nm and 670 nm rather than 440 nm and 676 nm.

denoted hereafter as $a^*_{ph}(440)$ and $a^*_{ph}(676)$, ranged from 0.018 to 0.173 and from 0.009 to 0.046 m^2 (mg Chl*a*)$^{-1}$, respectively (note that Chl*a* is here used as an abbreviation for the word chlorophyll-*a*). Also, the T-student analysis ($\alpha = 99\%$) showed that these coefficients were significantly higher for the N-group than M-group.

[33] Empirical relationships between $a_{ph}(\lambda)$ and $[Chla]_F$ were determined separately for each group. A power function in the form $a_{ph}(\lambda) = A\ [Chla]_F{}^B$, where the A and B parameters are derived from regression analysis, provided reasonably good fits to our data. The results of this regression analysis are shown for two example wavelengths, 440 and 676 nm, in Table 3 and Figure 3. It is generally known that variations in the size structure of phytoplankton population and the intracellular concentrations of various pigments are responsible for the variability of $a_{ph}(\lambda)$ at a given chlorophyll-*a* concentration in water [e.g., *Bricaud et al*., 2004]. Our data support the notion that the contributions of accessory pigments and package effect to this variability seem to be greater at shorter wavelengths because the data points at 440 nm are scattered more around the best-fit lines compared with 676 nm.

[34] For comparison, Figure 3 also shows the relationships obtained by *Bricaud et al*. [1995], *Bricaud et al*. [2004], *Devred et al*. [2006], and *Brewin et al*. [2011a], on the basis of large data sets collected in different regions of the world's ocean. These relationships are referred to as B95, B04, D06, and B11, respectively. Our best fit lines for both the N-group and M-group show considerably higher values of $a_{ph}(440)$ at any given chlorophyll-*a* concentration (on average by a factor of 2) compared with the B95 relationship (Figure 3a). The B04 relationship, which is based on a different data set than B95, is closer to our relationships although the slopes are considerably different. The D06 and B11 curves are between B04 and B95. Compared with the blue spectral band at 440 nm, the differences between our relationships and B95 are smaller in the red band at 676 nm (Figure 3b). However, the B95 relationship still yields systematically lower values of $a_{ph}(676)$ than the PATEX relationships. Because the contribution by pigments other than chlorophyll-*a* to absorption in this spectral band is very small or negligible, this result may suggest that cell size of phytoplankton in the Patagonian region is generally smaller than in other oceanic regions at similar chlorophyll-*a* concentrations.

[35] One possible cause of the differences between our results and those of Bricaud and co-workers can be attributed to the choice of the correction algorithm for the β amplification factor in the calculations of particulate absorption. We verified that the β correction from *Bricaud and Stramski* [1990], which was used in subsequent studies of Bricaud and co-workers, would increase the $a_{ph}(\lambda)$ values for the PATEX data set by a factor of approximately 1.2 to 1.3 in the blue spectral band. Therefore, this would explain

Table 3. Results From the Regression Analysis Between The Phytoplankton Absorption Coefficients at 440 and 676 nm, $a_{ph}(440)$ and $a_{ph}(676)$, and the Total Chlorophyll-*a* Concentration, $[Chla]_F$[a]

		$a_{ph}(440)$	$a_{ph}(676)$
N-Group	A	0.09	0.03
	B	0.56	0.74
	R^2	0.82	0.92
	N	151	151
M-Group	A	0.07	0.03
	B	0.51	0.62
	R^2	0.91	0.95
	N	38	38

[a]The regression formula is $a_{ph}(\lambda) = A\ [Chla]_F{}^B$ where A and B are the best fit parameters. The determination coefficient, R^2, and the number of data, N, are also shown. The results are presented for the samples dominated by nanophytoplankton (N-group) and microphytoplankton (M-group) during the PATEX 2 to 7 cruises. All regression analyses are significant for $p < 0.0001$.

only a fraction of the differences between our relationships and the B95 relationship, but could possibly explain the differences with the B04 relationship.

[36] Another factor that may contribute to these differences is that the HPLC-derived chlorophyll-*a* is used in B95 and B04, which can differ markedly from the fluorescence-derived chlorophyll-*a* in our study, especially for diatom-dominated waters. A linear fit applied to our data of $[\text{Chla}]_{\text{HPLC}}$ versus $[\text{Chla}]_{\text{F}}$ provided the equation $[\text{Chla}]_{\text{F}} = 1.19\ [\text{Chla}]_{\text{HPLC}} + 0.42$ ($R^2 = 0.95$; $N = 175$; $p < 0.0001$, where N is the number of observations), which indicates significantly higher values of $[\text{Chla}]_{\text{F}}$ compared with $[\text{Chla}]_{\text{HPLC}}$. However, we also note that the total chlorophyll-*a* in the studies of *Bricaud et al.* [1995, 2004] includes phaeopigments, which may reduce the differences between the HPLC and fluorometric determinations of chlorophyll-*a* concentrations. To address the potential issue of phaeopigments in our comparisons, we also determined the linear relationships between the absorption coefficients, $a_{\text{ph}}(440)$ and $a_{\text{ph}}(676)$, and the sum of $[\text{Chla}]_{\text{HPLC}}$ and phaeopigments, [Phaeo], without considering the dominant size class. Our $a_{\text{ph}}(440)$ values are higher than both the B95 (on average 2.9-fold) and B04 (on average 1.7-fold) values, and our $a_{\text{ph}}(676)$ values are higher on average 2.2-fold than the values derived from the B95 relationship.

[37] The above comparisons suggest that the magnitude of $a_{\text{ph}}(\lambda)$ at a given chlorophyll-*a* concentration, and hence the values of $a^*_{\text{ph}}(\lambda)$, are considerably higher for Patagonian waters compared with the average trends based on data from many other regions within the world's ocean. The main supporting evidence for this finding is based on our observations in the red spectral band, where variations in $a^*_{\text{ph}}(676)$ can be attributed primarily to changes in the package effect. It therefore appears that cells forming the blooms in Patagonian waters are relatively small compared with cells present in many other oceanic regions with similar chlorophyll-*a* biomass. This observation is also supported by our Patagonian data set which shows relatively high estimates of [micro $\text{Chla}]_{\text{HPLC}}$ from HPLC-derived diagnostic pigments (see section 2.2) when compared to [micro $\text{Chla}]_{\text{F}}$ obtained from fractionated $[\text{Chla}]_{\text{F}}$. This is because the approach for taxonomic composition that uses the HPLC-derived diagnostic pigments makes a general assumption that diatoms belong to microplankton-size class, so smaller diatom cells, if present, can be misclassified as microphytoplankton. Microscopy analysis of PATEX samples indicated that blooms in Patagonian waters are typically dominated by diatoms from the nanoplankton size range, although occasionally diatoms from the microplankton size range may dominate (e.g., PATEX 2).

3.3. Phytoplankton Absorption and Cell Size Parameter

[38] The phytoplankton absorption spectra normalized to their mean value computed on the basis of all spectral values between 400 and 700 nm, denoted as $a_{<\text{ph}>}(\lambda)$, are shown in Figure 4 for the N-group and M-group. A stronger package effect is evident for the M-group spectra, which show lower values for the ratio of the blue-to-red absorption peak than the N-group spectra. This result is generally consistent with the study of *Ciotti et al*. [2002], who found that most of the variability in the spectral shape of phytoplankton absorption

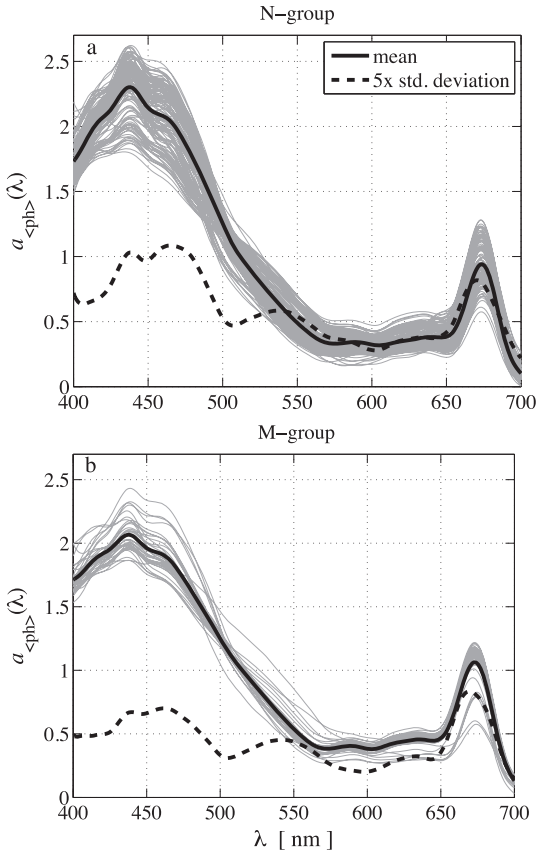

Figure 4. Spectra of phytoplankton absorption coefficient normalized by the average value of absorption between 400 and 700 nm (thin grey lines), for PATEX 2 to PATEX 7 cruises. The data are shown separately for (a) nanophytoplankton-dominated samples (N-group) and (b) microphytoplankton-dominated samples (M-group). For each group of data, the mean normalized spectrum (thick solid line) and the standard deviation spectrum multiplied by 5 to facilitate visualization (dashed line) are also shown.

coefficient between 400 and 700 nm can be explained by specifying the cell size of dominant phytoplankton. Note also that the standard deviation of $a_{<\text{ph}>}(\lambda)$ for N-group is generally higher than for M-group in the 420–490 nm spectral range, which likely reflects a larger contribution of accessory pigments associated with smaller cells [*Bricaud et al*., 1995].

[39] In the present study, S_{f} was estimated from each $a_{<\text{ph}>}(\lambda)$ spectrum for the six PATEX cruises. The values of S_{f} varied from 0.04 to 0.81 and the model of *Ciotti et al*. [2002] provided generally good agreement between the observed and model-reconstructed spectra of $a_{<\text{ph}>}(\lambda)$, with $R^2 > 0.92$ for most cases. The average ($\pm$standard deviation) values of S_{f} are 0.52 ($\pm$0.21) and 0.33 ($\pm$0.14) for the N-group and M-group, respectively.

[40] A clear trend of decrease in the chlorophyll-specific absorption coefficient of phytoplankton, $a^*_{\text{ph}}(\lambda)$, with an increase in $[\text{Chla}]_{\text{F}}$ is shown in Figure 5, which is consistent with similar data presented previously [*Dmitriev et al*., 2009 and references therein]. Such pattern reflects large variability in phytoplankton biomass, package effect, and species composition in our samples. Because the parameter S_{f} varies

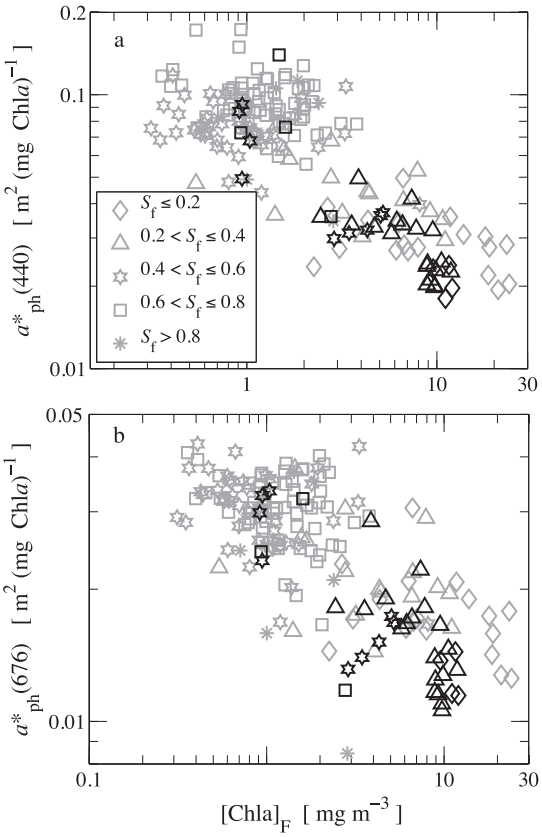

Figure 5. (a) Chlorophyll-specific absorption coefficient of phytoplankton at 440 nm, $a^*_{ph}(440)$, as a function of total concentration of chlorophyll-*a*, $[Chla]_F$, for PATEX 2 to PATEX 7 cruises. (b) Same as Figure 5a but for the chlorophyll-specific absorption coefficient of phytoplankton at 676 nm, $a^*_{ph}(676)$. The data are shown for samples dominated by nanophytoplankton (grey symbols) and microphytoplankton (black symbols) for different ranges of cell size parameter, S_f, as indicated. The statistics for the linear regression on log-transformed data for the N-group are $R^2 = 0.51$, $p < 0.0001$, $N = 151$ for $a^*_{ph}(440)$ versus $[Chla]_F$ and $R^2 = 0.40$, $p < 0.0001$, $N = 151$ for $a^*_{ph}(676)$ versus $[Chla]_F$. For the M-group the statistics are $R^2 = 0.84$, $p < 0.0001$, $N = 38$ for $a^*_{ph}(440)$ versus $[Chla]_F$ and $R^2 = 0.71$, $p < 0.0001$, $N = 38$ for $a^*_{ph}(676)$ versus $[Chla]_F$.

within a continuum of cell sizes, i.e., from 0 (the strongest package effect) to 1 (the weakest package effect), it is useful to examine whether S_f can explain the large variability observed in $a^*_{ph}(\lambda)$ at any given $[Chla]_F$. A closer inspection of results presented in Figure 5 indicates that S_f agrees with the variability in $a^*_{ph}(440)$ and $a^*_{ph}(676)$ as a function of $[Chla]_F$. In general, the lower $[Chla]_F$ and higher $a^*_{ph}(440)$ and $a^*_{ph}(676)$ correspond to higher values of S_f (i.e., smaller phytoplankton cells). The higher $[Chla]_F$ and lower values of $a^*_{ph}(440)$ and $a^*_{ph}(676)$ are related to lower S_f (larger cells). In particular, the lowest values of S_f (≤ 0.2) corresponded to $[Chla]_F$ higher than 10 mg m^{-3}. In addition to this overall pattern, a wide range of $a^*_{ph}(\lambda)$ was observed at any given $[Chla]_F$, and any given value of $a^*_{ph}(\lambda)$ was associated with large variation in $[Chla]_F$.

[41] The determinations of S_f aid to some extent in clarifying the seemingly random variability in $a^*_{ph}(\lambda)$ as a function of $[Chla]_F$. For instance, over similar ranges of $a^*_{ph}(\lambda)$ two distinct groups of S_f were observed: (i) $0.4 < S_f \le 0.6$ when $[Chla]_F$ was less than 1 mg m^{-3}, and (ii) $S_f > 0.6$ for $[Chla]_F$ from 1 to 2 mg m^{-3} (Figure 5). These results do not seem surprising even though they are not fully consistent with the general expectation of increasing cell size with increasing chlorophyll-*a* concentration [*Bricaud et al*., 1995 and references therein]. During the PATEX cruises, the variability in timing, location, and environmental factors controlling phytoplankton blooms resulted in relatively low S_f values (i.e., relatively large cells) in waters with relatively low chlorophyll-*a* concentrations.

[42] It is noteworthy that similar S_f values are observed within relatively wide ranges of variation in both $[Chla]_F$ and $a^*_{ph}(\lambda)$ (Figure 5). Another observation is that samples with the smallest values of $S_f \le 0.2$ belong to the N-group and not M-group. This result, which is observed at high concentrations $[Chla]_F$, appears inconsistent with the general expectation that the smallest values of S_f correspond to the largest cells. Such inconsistencies can occur because the parameter S_f does not depend solely on cell size, but instead reflects a combined effect of several factors affecting the spectral shape of phytoplankton absorption [*Ciotti et al*., 2002]. These factors include the pigment composition and the package effect that depends not only on the cell size but also the intracellular pigment concentration [*Morel and Bricaud*, 1981]. The generally good agreement between the cell size parameter S_f and $a^*_{ph}(\lambda)$ relies largely on the degree of covariation between the cell size and other factors controlling the phytoplankton absorption spectrum, as proposed in the original model of *Ciotti et al*. [2002]. Therefore, the parameter S_f cannot be simply interpreted to represent solely a dominant cell size because the intracellular concentration of various pigments will also influence this parameter at a given cell size. This is well illustrated by our observation that some of the S_f values smaller than 0.2 belong to the N-group. This observation suggests that the package effect caused by high intracellular pigment concentration was particularly important for the nanophytoplankton size range, which resulted in flattening of absorption spectra, and hence relatively small values of S_f.

[43] Summarizing the results in Figure 5, we note that variations in the cell size parameter S_f along the general pattern of decrease in $a^*_{ph}(\lambda)$ with increasing $[Chla]_F$ reflect variations in the package effect associated with changes in the dominant cell size and also variations in intracellular pigment concentrations and pigment composition. These different sources of variability are generally difficult to separate. In addition, our results point to challenges of classification of phytoplankton populations into discrete size classes, pico-, nano-, and microphytoplankton. These challenges result from the fact that phytoplankton communities consist of very many species of different sizes and there is some variability due to changes in cell size and taxonomic composition within the predefined size ranges.

3.4. Phytoplankton Absorption and Pigment Composition

[44] For the analysis involving pigment composition we consider 132 HPLC determinations of concentrations of total chlorophyll-*a*, $[Chla]_{HPLC}$, and accessory pigments along with the corresponding absorption measurements. We found

a high correlation between the log-transformed $[Chla]_{HPLC}$ and [PSC + PPC] ($R^2 = 0.89$; $N = 132$; $p < 0.0001$), which is consistent with earlier observations [*Trees et al.*, 2000]. The [PSC]:$[Chla]_{HPLC}$ ratio was weakly correlated with the $a_{ph}(490):a_{ph}(676)$ ratio ($R^2 = 0.35$; $N = 132$; $p < 0.0001$). A much stronger correlation ($R^2 = 0.71$; $N = 132$; $p < 0.0001$) was found between [PPC]:$[Chla]_{HPLC}$ and $a_{ph}(490):a_{ph}(676)$. Note that the $a_{ph}(490):a_{ph}(676)$ ratio is indicative mainly of variability in accessory pigments rather than the package effect, which is supported by weak although significant correlation with $[Chla]_{HPLC}$ ($R^2 = 0.19$; $N = 132$; $p < 0.001$). This ratio showed a strong correlation with [Hexa]:$[Chla]_{HPLC}$ ($R^2 = 0.60$; $N = 132$; $p < 0.0001$). Other pigment ratios did not provide significant correlation with $a_{ph}(490):a_{ph}(676)$. These results indicate that the pigment ratios [PPC]:$[Chla]_{HPLC}$ and [Hexa]:$[Chla]_{HPLC}$, and to a lesser extent also [PSC]:$[Chla]_{HPLC}$, contribute to the variability of $a_{ph}(490):a_{ph}(676)$.

[45] We next examine the variability of $a^*_{ph}(\lambda)$ as a function of pigment ratios. In this analysis, we consider both the N-group and M-group data separately. The $a_{ph}(\lambda)$ coefficient is here normalized by $[Chla]_{HPLC}$ and not by $[Chla]_F$ as previously. Only 12 samples for the M-group are included because the HPLC data are not available for PATEX 2 and 3.

[46] Figure 6 shows that an increase in the [PSC]:$[Chla]_{HPLC}$, [PPC]:$[Chla]_{HPLC}$, [Hexa]:$[Chla]_{HPLC}$, and [Chlb]:$[Chla]_{HPLC}$ ratios is accompanied by an increase in $a^*_{ph}(440)$. This is especially well pronounced for the relationships between $a^*_{ph}(440)$ and [Hexa]:$[Chla]_{HPLC}$ (Figure 6c) and [Chlb]:$[Chla]_{HPLC}$ (Figure 6d). These results are consistent with the expectation of greater relative importance of accessory pigments at relatively low chlorophyll-*a* concentrations and/or when small cells are more important than larger cells [see *Bricaud et al.*, 1995]. We also note that similar patterns to those presented in Figure 6 were observed for $a^*_{ph}(676)$ despite the fact that the effect of accessory

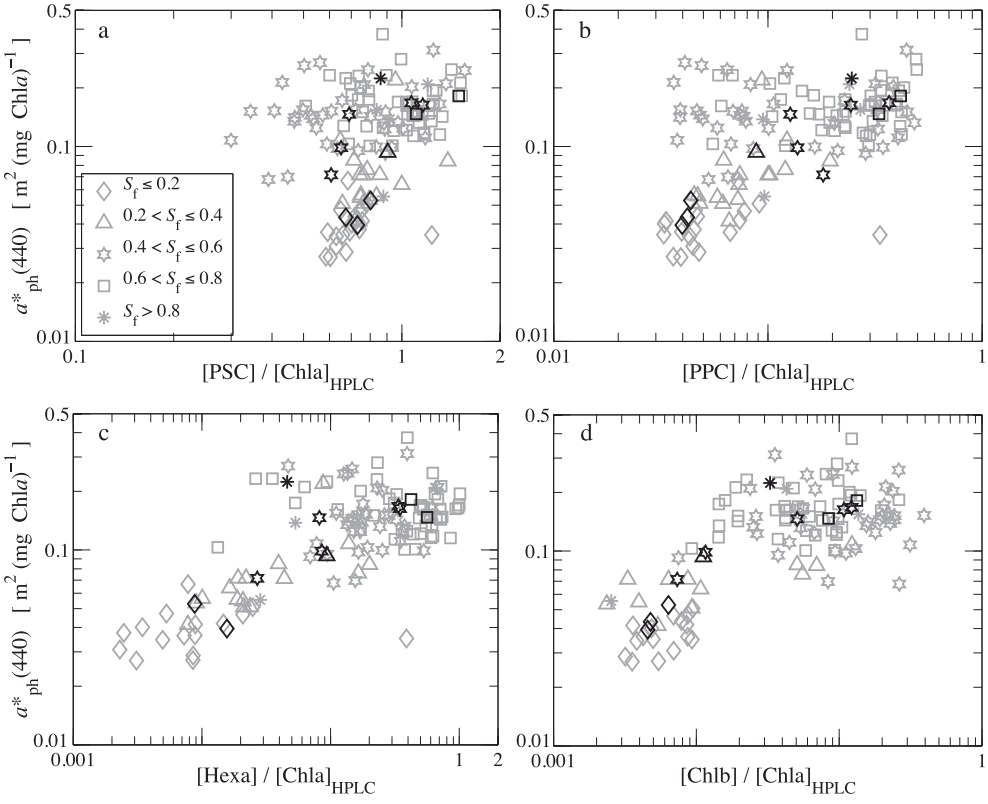

Figure 6. Chlorophyll-specific absorption coefficient of phytoplankton at 440 nm, $a^*_{ph}(440)$, plotted as a function of the ratio of the concentration of various pigments to the concentration of total chlorophyll-*a*, $[Chla]_{HPLC}$: (a) the ratio of photosynthetic carotenoids [PSC] to $[Chla]_{HPLC}$, (b) the ratio of photoprotective carotenoids [PPC] to $[Chla]_{HPLC}$, (c) the ratio of 19′-hexanoyloxyfucoxanthin [Hexa] to $[Chla]_{HPLC}$, and (d) the ratio of chlorophyll-*b* [Chlb] to $[Chla]_{HPLC}$. The data are shown for samples dominated by nanophytoplankton (grey symbols) and microphytoplankton (black symbols) for different ranges of cell size parameter, S_f, as indicated, for PATEX 4 to PATEX 7 cruises. The statistics for the linear regression on log-transformed data for the N-group are $R^2 = 0.07$, $p = 0.002$, $N = 129$ for $a^*_{ph}(440)$ versus [PSC]/$[Chla]_F$; $R^2 = 0.23$, $p < 0.0001$, $N = 129$ for $a^*_{ph}(440)$ versus [PPC]/$[Chla]_F$; $R^2 = 0.47$, $p < 0.0001$, $N = 124$ for $a^*_{ph}(440)$ versus [Hexa]/$[Chla]_F$; $R^2 = 0.40$, $p < 0.0001$, $N = 115$ for $a^*_{ph}(440)$ versus [Chlb]/$[Chla]_F$. For the M-group the statistics are $R^2 = 0.25$, $p = 0.07$, $N = 12$ for $a^*_{ph}(440)$ versus [PSC]/$[Chla]_F$; $R^2 = 0.61$, $p = 0.001$, $N = 12$ for $a^*_{ph}(440)$ versus [PPC]/$[Chla]_F$; $R^2 = 0.53$, $p = 0.004$, $N = 12$ for $a^*_{ph}(440)$ versus [Hexa]/$[Chla]_F$; $R^2 = 0.74$, $p < 0.0001$, $N = 12$ for $a^*_{ph}(440)$ versus [Chlb]/$[Chla]_F$.

pigments is very small or negligible in the red spectral band (not shown). The coefficients $a^*_{ph}(440)$ and $a^*_{ph}(676)$ were found to be significantly correlated ($R^2 = 0.82$; $N = 226$; $p < 0.0001$ for the log-transformed data).

[47] Similar trends observed for both $a^*_{ph}(440)$ and $a^*_{ph}(676)$ as a function of pigment ratios indicate that the relative contribution of carotenoids is correlated with cell size and package effect. Also, lower values of S_f (larger phytoplankton cells) are related to lower values of $a^*_{ph}(440)$ for all four pigment ratios (Figure 6). These results are consistent with those observed in previous analysis (section 3.3). For instance, a broad range of variation in $a^*_{ph}(440)$ is associated with a narrower variability in [PSC]:[Chla]$_{HPLC}$, although several data points in the range $0.4 < S_f \leq 0.6$ clearly depart from the average trend (Figure 6a). Interestingly, these samples were taken in the southernmost region of the Patagonia shelf-break during PATEX 7 (Figure 1). For this cruise, the biomass levels were among the lowest observed (Figure 2 and Table 2) and were associated with the presence of prasinophytes (M. S. Souza, personal communication, 2011) that contain chlorophyll-*b*. The samples from PATEX 7 showed variations in $a^*_{ph}(440)$ as a function of [PPC]:[Chla]$_{HPLC}$ ratios, which also departed from the mean trend observed when considering the whole data set (Figure 6b).

[48] The plot of $a^*_{ph}(440)$ versus [Hexa]:[Chla]$_{HPLC}$ ratio shows smaller variability around the mean trend and less overlapping of the data points between the S_f ranges (Figure 6c) than the other pigment ratios presented in Figure 6. The 19′-hexanoyloxyfucoxanthin pigment is known to be typical for *Phaeocystis* microorganisms and the concentration of this pigment, [Hexa], relative to chlorophyll-*a* concentration was suggested as a proxy for the abundance of this phytoplankton group [*Jeffrey and Wright*, 1994]. On the basis of microscopy and CHEMTAX technique [*Mackey et al*., 1996], we observed that *Phaeocystis* was an important contributor to total biomass in all samples from the PATEX cruises (M. S. Souza, personal communication, 2011). The size of these phytoplankton cells (2–6 μm) falls within the lower range of nanoplankton class, thus the increase in [Hexa] is typically associated with high S_f values (Figure 6c). The lowest [Hexa]:[Chla]$_{HPLC}$ ratio (<0.04; Figure 6c) and $a^*_{ph}(440)$ were observed on PATEX 4 during an intense bloom of diatoms with very high biomass levels (see Figure 2c).

[49] The general dependence of $a^*_{ph}(440)$ on [Chlb]:[Chla]$_{HPLC}$ agrees with a substantial importance of prasinophytes during all PATEX cruises (M. S. Souza, personal communication, 2011). The most important contribution of this phytoplankton group was found for the PATEX 7 samples. During that cruise, the surface waters were characterized by relatively high $a^*_{ph}(440)$, intermediate S_f ($0.4 < S_f \leq 0.6$), and the highest [Chlb]:[Chla]$_{HPLC}$ ratios (Figure 6d).

[50] In summary, our results indicate significant degree of covariation between the dominant cell size of phytoplankton, pigment composition, and chlorophyll-specific absorption coefficient of phytoplankton. The trend of increasing cell size is accompanied by a decreasing trend in both the ratios of accessory pigments to chlorophyll-*a* and the chlorophyll-specific absorption coefficient. The increase in the ratios of accessory pigments to chlorophyll-*a* is accompanied by an increasing trend in the chlorophyll-specific absorption coefficient.

3.5. Special Features in Phytoplankton Absorption Spectra

[51] We now turn our discussion to special or unusual features within the UV and visible spectral regions, which were observed in the spectra of phytoplankton absorption in the Patagonian waters. For the discussion of the features within the UV region, we present the total particulate absorption spectra, $a_p(\lambda)$, rather than phytoplankton spectra, $a_{ph}(\lambda)$. This is because the method of determining $a_{ph}(\lambda)$, which involves the measurement of detrital absorption, $a_d(\lambda)$, on samples bleached with sodium hypochlorite did not provide reliable results in the UV region. Each $a_p(\lambda)$ spectrum was normalized by its average value based on all spectral absorption values between 300 and 700 nm. This normalized spectrum is denoted as $a_{<p>}(\lambda)$. The mean normalized spectrum for each PATEX cruise shows the $a_p(\lambda)$ maximum around 330 nm (Figure 7a), which indicates the presence of Mycosporine-like amino acids, MAAs

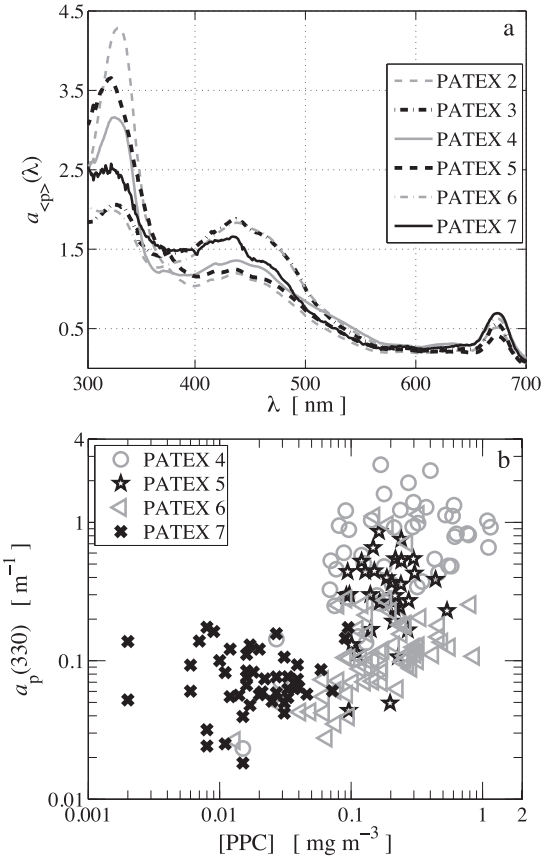

Figure 7. (a) The mean spectra of particulate absorption coefficient for each PATEX cruise as indicated. The spectra are normalized to the average value of particulate absorption between 300 and 700 nm. (b) The particulate absorption coefficient at 330 nm, $a_p(330)$, as a function of the concentration of photoprotective carotenoids, [PPC], for PATEX 4 to PATEX 7 cruises. The statistics for the linear regression on log-transformed data of $a_p(330)$ versus [PPC] are $R^2 = 0.35$, $p < 0.0001$, $N = 132$.

[*Whitehead and Vernet*, 2000]. The MAAs are considered to act as potential blockers for the UV damaging radiation. The absorption peak centered at about 330 nm was observed in the majority of spectra at both near-surface depths and the depths of maximum chlorophyll fluorescence. The presence of MAAs has already been reported in the Argentine Sea [*Negri et al*., 1992; *Carreto and Carignan*, 2011]. *Negri et al*. [1992] observed the occurrence of MAAs in association with a dinoflagellates bloom over the Argentine Shelf. These compounds were interpreted as a genetic adaptation that provides these microorganisms with a competitive advantage under high radiation intensities at the UV wavelengths. Negri and co-workers suggested that the above mentioned physiological property can provide dinoflagellates with a competitive advantage over diatoms in nutrient-rich, well-illuminated, and low-turbulent environments. Our results show, however, the presence of MAAs during all PATEX cruises (Figure 7), even during massive diatom blooms (PATEX 2 and PATEX 4) along the Patagonian shelf-break waters. The PATEX cruises covered a relatively wide range of seasonal conditions (October to late March), which suggests that light conditions during spring and summer periods support elevated MAAs concentrations regardless of the dominant phytoplankton groups.

[52] Significant variations in the shape and position of the UV absorption maximum observed in the data collected in the eastern South Pacific were suggested to reflect the presence of different types of MAAs [*Bricaud et al*., 2010]. In contrast, on all PATEX cruises this maximum was relatively stable and always centered at about 330 nm, which suggests a dominance of a specific type of MAAs (Figure 7a). By analyzing the dependence of $a_p(330)$ on [PPC] we tested whether the magnitude of the UV peak can reflect an intracellular photoprotective process. We note, however, that the quantitative results regarding the magnitude of the MAAs peak in the $a_p(\lambda)$ spectra must be interpreted with special caution because (i) the correction procedure for the β amplification factor has not been optimized for the UV spectral region, (ii) $a_p(\lambda)$ includes not only phytoplankton absorption but also the detrital absorption, and (iii) MAAs are soluble in water, so they can be released through the intact cell membranes during freezing process of the samples. Moreover, MAAs can be released during or very shortly after filtration [*Laurion et al*., 2003]. Despite these reservations a general pattern can be observed, with relatively low $a_p(330)$ associated with low [PPC] during PATEX 7 and an increase of $a_p(330)$ with [PPC] for other cruises (Figure 7b). Further research is needed to examine how MAAs might be associated with photoprotection within the visible and UV spectral regions in phytoplankton communities in the Patagonian shelf-break and surrounding waters.

[53] Another spectral feature that deserves special attention in our study is the blue absorption maximum of phytoplankton absorption. For 37 samples from the PATEX cruises, i.e., five samples from PATEX 2, four from PATEX 3, 21 from PATEX 4, and seven from PATEX 6, we observed that the blue maximum peaked at about 460 nm rather than at typical wavelengths around 440 nm (Figure 8a). Closer inspection of HPLC chromatograms for these samples showed a pronounced absorbance at 460 nm caused by an unknown carotenoid, which is here referred

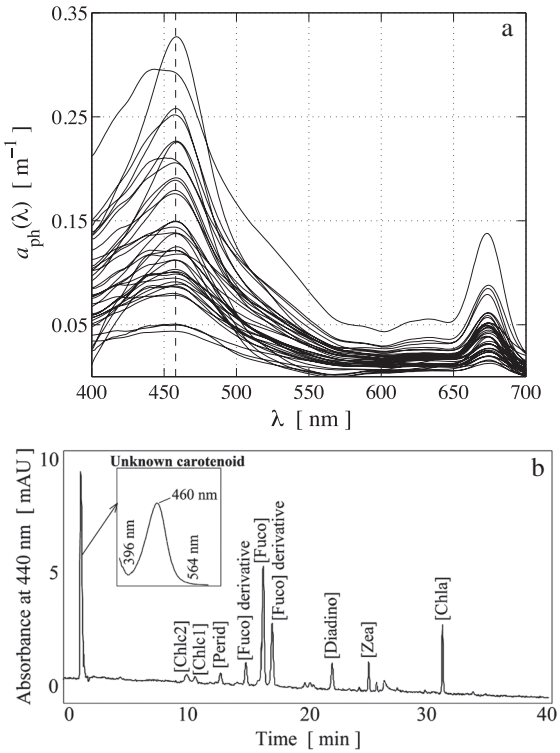

Figure 8. (a) Spectra of phytoplankton absorption coefficient of 37 samples for PATEX 2 to PATEX 7 cruises, which show an unusual absorption maximum around 460 nm. (b) The HPLC chromatogram of absorbance at 440 nm in mAU (mass Absorbance Unit) obtained for an example near-surface sample. The inset graph shows the peak of absorbance centered at 460 nm of an unknown carotenoid referred hereto as P460.

to as P460 (Figure 8b). Other investigations detected a fucoxanthin derivative with maximum absorbance at 460 nm in the Patagonian waters in association with other degraded pigments such as pheophytin-*a* and pyropheophytin-*a* (J. Carreto, personal communication, 2009). These observations suggest that the fucoxanthin derivative could be derived from grazing by mixotrophic dinoflagellates [*Carreto et al*., 1985]. Grazing by zooplankton might be the main regulating factor of spring phytoplankton blooms in the neritic region of the Argentinean shelf-break (J. Carreto, personal communication, 2009).

[54] In order to investigate if the presence of the P460 pigment could be related to the anomalous maximum in the phytoplankton absorption spectra, we applied a principal component analysis to the unusual $a_{ph}(\lambda)$ spectra to extract information on the $a_{ph}(\lambda)$ variance structure [e.g., *Lubac and Loisel*, 2007]. A moderately strong correlation ($R^2 = 0.66$; $N = 28$; $p < 0.001$) was found between the scores of the first mode of variability in $a_{ph}(\lambda)$ (which explained 93% of the variance) and the P460 pigment. No significant correlation between P460 and other pigments was found, although the correlation with [Fuco] is not very small ($R = -0.40$; $N = 28$; $p = 0.06$). This may support the notion that P460 is derived from fucoxanthin. These results indicate that the P460 pigment is the main factor responsible for the anomalous blue peak in the phytoplankton absorption spectra

observed in some samples collected in the Patagonian shelf-break waters.

[55] We also note that an enhancement of phytoplankton absorption in the 460–470 nm range was observed in the study of coastal waters in the western North Atlantic, which was attributed to an increase in chlorophyll-*b* concentration relative to chlorophyll-*a* [*Hoepffner and Sathyendranath*, 1992]. This feature did not, however, produce a distinct primary maximum in the blue spectral region because maximum or nearly maximum values of absorption were still observed at usual spectral location close to 440 nm. In addition, *Hoepffner and Sathyendranath* [1992] observed an enhancement of absorption near 650 nm, which corresponds to the maximum absorption of chlorophyll-*b* in the red part of the spectrum. In contrast, in our study the uncommon phytoplankton spectra show a distinct peak of absorption at about 460 nm and no additional feature in the red (Figure 8a).

3.6. Particulate Scattering Coefficient and Phytoplankton Cell Size

[56] The relationship between the chlorophyll-specific particulate scattering coefficient at 660 nm, $b^*_p(660)$ (i.e., $b_p(660)$ normalized by $[\mathrm{Chla}]_F$) and $[\mathrm{Chla}]_F$ was examined with the data partitioned into different ranges of size parameter S_f in a similar fashion as was done for chlorophyll-specific absorption coefficients. The $b^*_p(660)$ coefficient varied from 0.031 to 2.37 m^2 (mg Chl*a*)$^{-1}$ and showed a clear inverse dependence on $[\mathrm{Chla}]_F$, which is qualitatively similar to what has been observed for chlorophyll-specific absorption coefficients. The patterns and scatter in the data points of $b^*_p(660)$ versus $[\mathrm{Chla}]_F$ associated with the variability in S_f (Figure 9) are also similar to those observed for the absorption data. We note that a strong relationship ($R^2 = 0.74$; $N = 223$; $p < 0.0001$) between $a^*_{ph}(440)$ and $b^*_p(660)$ was found. Both the chlorophyll-specific phytoplankton absorption and chlorophyll-specific particulate scattering tend to be inversely related to cell size parameter S_f, so that the dominance of relatively larger cells results in lower chlorophyll-specific optical coefficients.

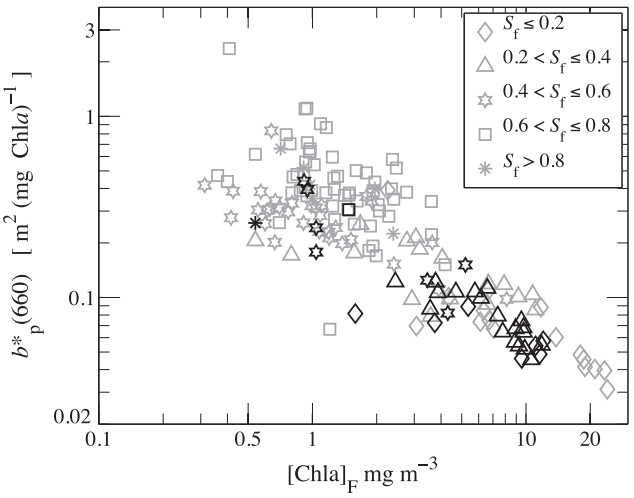

Figure 9. Chlorophyll-specific scattering coefficient of particles at 660 nm, $b^*_p(660)$, as a function of total concentration of chlorophyll-*a*, $[\mathrm{Chla}]_F$, for PATEX 2 to PATEX 7 cruises. The data are shown for samples dominated by nanophytoplankton (grey symbols) and microphytoplankton (black symbols) for different ranges of cell size parameter, S_f, as indicated. The statistics for the linear regression on log-transformed data of $b^*_p(660)$ versus $[\mathrm{Chla}]_F$ are $R^2 = 0.63$, $p < 0.0001$, $N = 151$ for N-group and $R^2 = 0.86$, $p < 0.0001$, $N = 38$ for M-group.

4. Conclusions

[57] We have demonstrated that nanophytoplankton is mostly responsible for elevated levels of phytoplankton biomass in the Patagonian shelf-break and adjacent waters. The microscopic analysis of samples indicates that diatoms from nanoplankton size range typically dominate the blooms in these waters. These results point to limitations of approaches based on HPLC-derived diagnostic pigments for estimating relative proportions of phytoplankton size classes, because these approaches generally assume that diatoms are associated primarily with the microplankton size range. Our data also point to differences between the cell size structure of phytoplankton assemblages in Patagonian waters and other oceanic regions at similar chlorophyll-*a* biomass. The magnitude of absorption coefficients of phytoplankton at a given chlorophyll-*a* concentration and also the chlorophyll-specific absorption coefficients of phytoplankton are typically considerably higher in Patagonian waters compared with the average trends based on data collected in various regions of the world's ocean. Also, we observed that the chlorophyll-specific absorption coefficients in Patagonian waters are significantly different for assemblages dominated by nanophytoplankton and microphytoplankton.

[58] A cell size parameter derived from the phytoplankton absorption spectra varied in a consistent fashion with chlorophyll-*a* concentration for both the chlorophyll-specific phytoplankton absorption and chlorophyll-specific particulate scattering coefficients. Smaller cells are typically associated with lower chlorophyll-*a* concentrations and higher chlorophyll-specific optical coefficients. The cell size parameter also showed a rather well-behaved pattern along the increasing trend of the chlorophyll-specific phytoplankton absorption as function of the ratios of photosynthetic and photoprotective pigments to chlorophyll-*a* concentration. These results suggest that most of the variability in phytoplankton absorption and scattering coefficients in Patagonian waters is explained by changes in the dominant cell size accompanied by covariation in the concentrations of accessory pigments. Hence, the considerable variability in both chlorophyll-specific phytoplankton absorption and chlorophyll-specific particulate scattering that we observed at any given chlorophyll-*a* concentration highlights the limitation of traditional bio-optical models in which the phytoplankton component is parameterized in terms of total chlorophyll-*a* concentration alone.

[59] All absorption spectra of phytoplankton measured in this study showed consistent features in the UV spectral regions around 330 nm, which are caused by the presence of Mycosporine-like amino acids. Also, in some samples we observed the occurrence of anomalous maximum of phytoplankton absorption in the blue spectral region around

460 nm, which is associated with an unknown carotenoid likely related to grazing processes. Further studies are required to examine the extent to which the photoprotective processes and the presence of unusual pigments in phytoplankton of Patagonian waters might produce special features in the optical properties which differ from those normally observed in most other regions of the world's ocean. The findings of our study have implications to bio-optical modeling of Patagonian waters and emphasize the need for increased efforts aiming at detailed characterization of regional optical properties in order to improve the usefulness of optical measurements, including ocean color remote sensing, for the study of these marine ecosystems.

[60] **Acknowledgments.** The PATagonian EXperiment (PATEX) is a multidisciplinary project conducted by the Group of High Latitude Oceanography (GOAL) in the Brazilian Antarctic Program. We are grateful to the crew of the Brazilian Navy R/V *Ary Rongel* for their assistance during field experiments. We also acknowledge Servicio de Hidrografia Naval (Argentina) for their cooperation in obtaining clearance for carrying out the fieldwork within the Argentinean EEZ. The PATEX 5, 6, and 7 cruises were conducted as part of the Southern Ocean Studies for Understanding Climate Changes Issues (SOS-CLIMATE) project, a Brazilian contribution to the International Polar Year. The SOS-Climate project was funded by the Ministry of Science and Technology (MCT) and Brazilian National Council on Research and Development (CNPq, grant 520189/2006-0). This work was also partly supported by GSFC/NASA through the project OCEANS/04123400362 and by the NASA Biodiversity Program (Grant NNX09AK17G awarded to D.S.). A. Ferreira was funded by CNPq with a graduate scholarship (Proc. 143234/2008-0) and the Brazilian agency CAPES (Coordenação de Aperfeiçoamento de Pessoal de Ensino Superior) with a doctoral student grant (Proc. 6999/10-7). Part of the work was done during a 1 year research visit of A. Ferreira to the Marine Physical Laboratory, Scripps Institution of Oceanography in San Diego, California. The Center of Oceanography of FCUL (Lisbon, Portugal) provided the facilities for the HPLC analysis. We also thank three anonymous reviewers for their comments on the manuscript.

References

Atlas, T., and T. T. Bannister (1980), Dependence of mean spectral extinction coefficient of phytoplankton on depth, water colour, and species, *Limnol. Oceanogr.*, *19*, 1–12.

Behrenfeld, M. J., and E. Boss (2003), The beam attenuation to chlorophyll ratio: An optical index of phytoplankton photoacclimation in the surface ocean?, *Deep Sea Res. Part I*, *50*, 1537–1549, doi:10.1016/j.dsr.2003.09.002.

Behrenfeld, M. J., and E. Boss (2006), Beam attenuation and chlorophyll concentrations as alternative optical indices of phytoplankton biomass, *J. Mar. Res.*, *64*, 431–451, doi:10.1357/002224006778189563.

Bianchi, A. A., D. R. Pino, H. G. I. Perlender, A. P. Osiroff, V. Segura, V. Lutz, M. L. Clara, C. F. Balestrini, and A. R. Piola (2009), Annual balance and seasonal variability of sea-air CO_2 fluxes in the Patagonia Sea: Their relationship with fronts and chlorophyll distribution, *J. Geophys. Res.*, *114*, C03018, doi:10.1029/2008JC004854.

Bouman, H. A., et al. (2003), Temperature as indicator of optical properties and community structure of marine phytoplankton: Implications for remote sensing, *Mar. Ecol. Prog. Ser.*, *258*, 19–30, doi:10.3354/meps258019.

Brewin, R. J. W., E. Devred, S. Sathyendranath, S. J. Lavender, and N. J. Hartman-Mountford (2011a), Model of phytoplankton absorption based on three size classes, *Appl. Opt.*, *22*, 4535–4549, doi:10.1364/AO.50.004535.

Brewin, R. J. W., N. J. Hartman-Mountford, S. J. Lavender, D. E. Raitsos, T. Hirata, J. Uitz, E. Devred, A. Bricaud, A. M. Ciotti, and B. Gentili (2011b), An intercomparison of bio-optical techniques for detecting dominant phytoplankton size class from satellite remote sensing, *Remote Sens. Environ.*, *115*, 325–339, doi:10.1016/j.rse.2010.09.004.

Brewin, R. J. W., G. Dall'Olmo, S. Sathyendranath, and N. J. Hardman-Mountford (2012), Particle backscattering as a function of chlorophyll and phytoplankton size structure in the open-ocean, *Opt. Express*, *20*, 17,632–17,652, doi:10.1364/OE.20.017632.

Bricaud, A., and A. Morel (1986), Light attenuation and scattering by phytoplanktonic cells: A theoretical modeling, *Appl. Opt.*, *25*, 571–580.

Bricaud, A., and D. Stramski (1990), Spectral absorption coefficients of living phytoplankton and nonalgal biogenous matter: A comparison between the Peru upwelling area and the Sargasso Sea, *Limnol. Oceanogr.*, *35*, 562–582.

Bricaud, A., M. Babin, A. Morel, and H. Claustre (1995), Variability in the chlorophyll-specific absorption coefficient of natural phytoplankton: Analysis and parameterization, *J. Geophys. Res.*, *100*, 13,321–13,332, doi:10.1029/95JC00463.

Bricaud, A., H. Claustre, J. Ras, and K. Oubelkheir (2004), Natural variability of phytoplankton absorption in oceanic waters: Influence of the size structure of algal populations, *J. Geophys. Res.*, *109*, C11010, doi:10.1029/2004JC002419.

Bricaud, A., M. Babin, H. Claustre, J. Ras, and F. Tièche (2010), Light absorption properties and absorption budget of Southeast Pacific waters, *J. Geophys. Res.*, *115*, C08009, doi:10.1029/2009JC005517.

Carreto, J. I., R. M. Negri, H. R. Benavides, and R. Akselman (1985), Toxic dinoflagellates blooms in the Argentine Sea, in Toxic Dinoflagellates, edited by D. M. Anderson, et al., pp. 147–152, Elsevier, New York.

Carreto, J. I., V. A. Lutz, M. O. Carignan, A. D. Cucchi Coleoni, and S. G. De Marco (1995), Hydrography and chlorophyll a in a transect from the coast to the shelf break in the Argentinian Sea, *Cont. Shelf Res.*, *15*, 315–336, doi:10.1016/0278-4343(94)E0001-3.

Carreto, J. I., N. Montoya, R. Akselman, M. O. Carignan, R. I. Silva, and A. D. Cucchi Colleoni (2008), Algal pigment patterns and phytoplankton assemblages in different water masses of the Río de la Plata maritime front, *Cont. Shelf Res.*, *28*, 1589–1606, doi:10.1016/j.csr.2007.02.012.

Carreto, J. I., and M. O. Carignan (2011), Mycosporine-like amino acids: Relevant secondary metabolites. chemical and ecological aspects, *Mar. Drugs*, *9*, 387–446, doi:10.3390/md9030387.

Chazottes, A., M. Crepon, A. Bricaud, J. Ras, and S. Thiria (2007), Statistical analysis of absorption spectra of phytoplankton and of pigment concentrations observed during three POMME cruises using a neural network clustering method, *Appl. Opt.*, *46*, 3790–3799, doi:10.1364/AO.46.003790.

Ciotti, A. M., J. J. Cullen, and M. R. Lewis (1999), A semi-analytical model of the influence of phytoplankton community structure on the relationship between light attenuation and ocean color, *J. Geophys. Res.*, *104*, 1559–1578, doi:10.1029/1998JC900021.

Ciotti, A. M., M. R. Lewis, and J. J. Cullen (2002), Assessment of the relationships between dominant cell size in natural phytoplankton communities and the spectral shape of the absorption coefficient, *Limnol. Oceanogr.*, *47*, 404–417.

Devred E., S. Sathyendranath, V. Stuart, H. Maass, O. Ulloa, and T. Platt (2006), Bio-optics of the ocean: A two-component model of absorption by phytoplankton, *J. Geophys. Res.*, *111*, C03011, doi:10.1029/2005jc002880.

Dmitriev, E. V., G. Khomenko, M. Chami, A. A. Sokolov, T. Y. Churilova, and G. K. Korotaev (2009), Parameterization of light absorption by components of seawater in optically complex coastal waters of the Crimea Peninsula (Black Sea), *Appl. Opt.*, *48*, 1249–1261.

Ferreira, A., V. M. T. Garcia, and C. A. E. Garcia (2009), Light absorption by phytoplankton, non-algal particles and dissolved organic matter at the Patagonia shelf-break in spring and summer, *Deep Sea Res. Part I*, *56*, 2162–2174, doi:10.1016/ j.dsr.2009.08.002.

Fishwick, J. R., J. Aiken, R. G. Barlow, H. Sessions, S. Bernard, and J. Ras (2006), Functional relationships and bio-optical properties derived from phytoplankton pigments, optical and photosynthetic parameters: A case study of the Benguela ecosystem, *J. Mar. Biol. Assoc. UK*, *86*, 1267–1280, doi:10.1017/S0025315406014287.

Garcia, C. A. E., Y. V. B. Sarma, M. M. Mata, and V. M. T. Garcia (2004), Chlorophyll variability and eddies in the Brazil-Malvinas Confluence region, *Deep Sea Res. Part II*, *51*, 159–172, doi:10.1016/j.dsr2.2003.07.016.

Garcia, V. M. T., C. A. E. Garcia, M. M. Mata, R. C. Pollery, A. R. Piola, S. R. Signorini, C. R. McClain, and M. D. Iglesias-Rodriguez (2008), Environmental factors controlling the phytoplankton blooms at the Patagonia shelf-break in spring, *Deep Sea Res. Part I*, *55*, 1150–1166, doi:10.1016/j.dsr.2008.04.011.

Garcia, C. A. E., V. M. T. Garcia, A. I. Dogliotti, A. Ferreira, S. I. Romero, A. Mannino, M. S. Souza, and M. M. Mata (2011), Environmental conditions and bio-optical signature of a coccolithophorid bloom in the Patagonian shelf, *J. Geophys. Res.*, *116*, C03025, doi:10.1029/2010JC006595.

Gernez, P., D. Antoine, and Y. Huot (2011), Diel cycles of the particulate beam attenuation coefficient under varying trophic conditions in the northwestern Mediterranean Sea: Observations and modeling, *Liminol. Oceanogr.*, *56*, 17–36, doi:10.4319/lo.2011.56.1.0017.

Gonçalves-Araujo, R., M. S. Souza, C. R. B. Mendes, V. M. Tavano, R. C. Pollery, and C. A. E. Garcia (2012), Brazil-Malvinas confluence: Effects

of environmental variability on phytoplankton community structure, *J. Plankton Res.*, *34*, 399–416, doi:10.1093/plankt/fbs013.

Gordon, H. R., and A. Morel (1983), Remote assessment of ocean color for interpretation of satellite visible imagery, a review, *Lect. Notes Coast. Estuarine Stud.*, *4*, 1–114, Springer-Verlag, New York.

Gregg, W. W., N. W. Casey, and C. R. McClain (2005), Recent trends in global ocean chlorophyll, *Geophys. Res. Lett.*, *32*, L03606, doi:10.1029/2004GL021808.

Hoepffner, N., and S. Sathyendranath (1992), Bio-optical characteristics of coastal waters: Absorption spectra of phytoplankton and pigment distribution in the western North Atlantic, *Limnol. Oceanogr.*, *37*, 1660–1679.

Huot, Y., A. Morel, M. S. Twardowski, D. Stramski, and R. A. Reynolds (2008), Particle optical backscattering along a chlorophyll gradient in the upper layer of the eastern South Pacific Ocean, *Biogeosciences*, *5*, 495–507.

Jeffrey, S. W., and S. W. Wright (1994), Photosynthetic pigments in the Haptophyta, in The Haptophyte Algae, edited by J. C. Green, and B. S. C. Leadbeater, pp. 111–132, Clarendon Press, Oxford.

Kishino, M, N Takahashi, N. Okami, and S. Ichimura (1985), Estimation of the spectral absorption coefficients of phytoplankton in the sea, *Bull. Mar. Sci.*, *37*, 634–642.

Laurion, I., F. Blouin, and S. Roy (2003), The quantitative filter technique for measuring phytoplankton absorption: Interference by MAAs in the UV waveband, *Limnol. Oceanogr. Meth.*, *1*, 1–9.

Lewis, M. R., J. J. Cullen, and T. Platt (1983), Phytoplankton and thermal structure in the upper ocean: Consequences of nonuniformity in chlorophyll profile, *J. Geophys. Res.*, *88*, 2565–2570, doi:10.1029/JC088iC04p02565.

Lohrenz, S. E., A. D. Weidemann, and M. Tuel (2003), Phytoplankton spectral absorption as influenced by community size structure and pigment composition, *J. Plankton Res.*, *25*, 35–61, doi:10.1093/plankt/25.1.35.

Loisel, H., and A. Morel (1998), Light scattering and chlorophyll concentration in Case 1 waters: A reexamination, *Limnol. Oceanogr.*, *43*, 847–858, doi:10.4319/lo.1998.43.5.0847.

Loisel, H., J.-M. Nicolas, A. Sciandra, D. Stramski, and A. Poteau (2006), Spectral dependency of optical backscattering by marine particles from satellite remote sensing of the global ocean, *J. Geophys. Res.*, *111*, C09024, doi:10.1029/2005JC003367.

Lubac, B., and H. Loisel (2007), Variability and classification of remote sensing reflectance spectra in the eastern English Channel and southern North Sea, *Rem. Sens. Environ.*, *110*, 45–58, doi:10.1016/j.rse.2007.02.012.

Lutz, V. A., V. Segura, A. I. Dogliotti, D. A. Gagliardini, A. A. Bianchi, and C. F. Balestrini (2010), Primary production in the Argentine Sea during spring estimated by field and satellite models, *J. Plankton Res.*, *32*, 181–195, doi:10.1093/plankt/ fbp117.

Mackey, M. D., D. J. Mackey, H. W. Higgins, and S. W. Wright (1996), CHEMTAX—A program for estimating class abundances from chemical markers: application to HPLC measurements of phytoplankton, *Mar. Ecol. Prog. Ser.*, *144*, 265–283, doi:10.3354/meps144265.

Marra, J., C. C. Trees, and J. E. O'Reilly (2007), Phytoplankton pigment absorption: A strong predictor of primary productivity in the surface ocean, *Deep Sea Res. Part I*, *54*, 155–163, doi:10.1016/j.dsr.2006.12.001.

Martinez-Vicente, V., G. H. Tilstone, S. Sathyendranath, P. Miller, and S. B. Groom (2012), Contributions of phytoplankton and bacteria to the optical backscattering coefficient over the Mid-Atlantic Ridge, *Mar. Ecol. Prog. Ser.*, *445*, 37–51, doi:10.3354/meps09388.

Matsuoka, A., V. Hill, Y. Huot, M. Babin, and A. Bricaud (2011), Seasonal variability in the light absorption coefficient of phytoplankton, non-algal particles, and colored dissolved organic matter in western Arctic waters: Parameterization of the individual components of absorption for ocean color applications, *J. Geophys. Res.*, *116*, C02007, doi:10.1029/2009JC005594.

Mendes, C. R., P. Cataxana, and V. Brotas (2007), HPLC determination of phytoplankton and microphytobenthos pigments: Comparing resolution and sensitivity of a C-18 and a C-8 method, *Limnol. Oceanogr. Meth.*, *5*, 362–370, doi:10.4319/lom.2007.5.363.

Mitchell, B. G., et al. (2000), Determination of spectral absorption coefficients of particles, dissolved material and phytoplankton for discrete water samples, in Ocean Optics Protocols for Satellite Ocean Color Sensor Validation, Tech. Memo. 2000-209966, pp. 125–153, NASA, Greenbelt, Md.

Morel, A., and A. Bricaud (1981), Theoretical results concerning light absorption in a discrete medium, and application to specific absorption of phytoplankton, *Deep Sea Res.*, *28*, 1375–1393, doi:10.1016/0198-0149(81)90039-X.

Morel, A. (1991), Light and marine photosynthesis: A spectral model with geochemical and climatological implications, *Prog. Oceanogr.*, *26*, 263–306, doi:10.1016/0079-6611(91)90004-6.

Morel, A., and Y.-H. Ahn (1991), Optics of heterotrophic nanoflagellates and ciliates: A tentative assessment of their scattering role in oceanic waters compared to those of bacterial and algal cells, *J. Mar. Res.*, *49*, 177–202, doi:10.1357/002224091784968639.

Negri, R. M., J. I. Carreto, H. R. Benavides, R. Akselman, and V. A. Lutz (1992), An unusual bloom of *Gyrodinium cf. aureolum* in the Argentine Sea: Community structure and conditioning factors, *J. Plankton Res.*, *14*, 261–269, doi:10.1093/plankt/14.2.261.

Ras, J., H. Claustre, and J. Uitz (2008), Spatial variability of phytoplankton pigment distributions in the subtropical South Pacific Ocean: Comparison between in situ and modeled data, *Biogeosciences*, *5*, 353–369, doi:10.5194/bg-5-353-2008.

Reynolds, R. A., D. Stramski, and B. G. Mitchell (2001), A chlorophyll-dependent semianalytical reflectance model derived from field measurement of absorption and backscattering coefficients within the Southern Ocean, *J. Geophys. Res.*, *106*, 7125–7138, doi:10.1029/1999JC000311.

Rivas, A. L., A. I. Dogliotti, and D. A. Gagliardini (2006), Seasonal variability in satellite measured surface chlorophyll in the Patagonian Shelf, *Cont. Shelf Res.*, *26*, 703–720, doi:10.1016/j.csr.2006.01.013.

Roesler, C. S., and M. J. Perry (1995), In situ phytoplankton absorption, fluorescence emission, and particulate backscattering spectra determined from reflectance, *J. Geophys. Res.*, *100*, 13,279–13,294, doi:10.1029/95JC00455.

Romero, S. I., A. R. Piola, M. Charo, and C. A. E. Garcia (2006), Chlorophyll-a variability off Patagonia based on SeaWiFS data, *J. Geophys. Res.*, *111*, C05021, doi:10.1029/ 2005JC003244.

Sathyendranath, S., L. Lazzara, and L. Prieur (1987), Variations in the spectral values of specific absorption of phytoplankton, *Limnol. Oceanogr.*, *32*, 403–415.

Sathyendranath, S., and T. Platt (1988), The spectral irradiance field at the surface and in the interior of the ocean: A model for applications in oceanography and remote sensing, *J. Geophys. Res.*, *93*, 9270–9280, doi:10.1029/JC093iC08p09270.

Sathyendranath, S., G. Cota, V. Stuart, H. Maas, and T. Platt (2001), Remote sensing of phytoplankton pigments: A comparison of empirical and theoretical approaches, *Int. J. Remote Sens.*, *22*, 249–273, doi:10.1080/014311601449925.

Schloss, I. R., G. A. Ferreyra, M. E. Ferrario, G. O. Almandoz, R. Codina, A. A. Bianchi, C. F. Balestrini, H. A. Ochoa, D. Ruiz-Pino, and A. Poisson (2007), Role of plankton communities in sea-air variations in pCO2 in the SW Atlantic Ocean, *Mar. Ecol. Prog. Ser.*, *332*, 93–106, doi:10.3354/meps332093.

Signorini, S., V. M. T. Garcia, A. R. Piola, C. A. E. Garcia, M. M. Mata, and C. R. McClain (2006), Seasonal and interannual variability of calcite in the vicinity of the Patagonian Shelf Break (38°S–52°S), *Geophys. Res. Lett.*, *33*(L1), 6610, doi:10.1029/2006GL026592.

Souza, M. S., C. R. B. Mendes, V. M. T. Garcia, R. Pollery, and V. Brotas (2012), Phytoplankton community during a coccolithophorid bloom in the Patagonian Shelf: Microscopic and HPLC pigment analyzes, *J. Mar. Biol. Assoc. UK*, *92*, 13–27, doi:10.1017/S0025315411000439.

Stramska, M., and T. Dickey (1993), Phytoplankton bloom and the vertical thermal structure of the upper ocean, *J. Mar. Res.*, *51*, 819–842, doi:10.1357/0022240933223918.

Stramska, M., D. Stramski, S. Kaczmarek, D. B. Allison, and J. Schwarz (2006), Seasonal and regional differentiation of bio-optical properties within the north polar Atlantic, *J. Geophys. Res.*, *111*, C08003, doi:10.1029/2005JC003293.

Stramski, D., and D. A. Kiefer (1991), Light scattering by microorganisms in the open ocean, *Prog. Oceanogr.*, *28*, 343–383, doi:10.1016/0079-6611(91)90032-H.

Stramski, D., and R. A. Reynolds (1993), Diel variations in the optical properties of a marine diatom, *Limnol. Oceanogr.*, *38*, 1347–1364.

Stramski, D., A. Bricaud, and A. Morel (2001), Modeling the inherent optical properties of the ocean based on the detailed composition of the planktonic community, *Appl. Opt.*, *40*, 2929–2945, doi:10.1364/AO.40.002929.

Takahashi, T., S. Sutherland, C. Sweeney, A. Poisson, N. Metzl, B. Tilbrook, N. Bates, R. Wanninkhof, R. Feely, and C. Sabine (2002), Global sea-air CO2 flux based on climatological surface ocean pCO2 and seasonal biological and temperature effects, *Deep Sea Res. Part II*, *49*, 1601–1622, doi:10.1016/S0967- 0645(02)00003-6.

Tassan, S., and G. M. Ferrari (1995), An alternative approach to absorption measurements of aquatic particles retained on filters, *Limnol. Oceanogr.*, *40*, 1358–1368.

Toepel, J., U. Langner, and C. Wilhelm (2005), Combination of flow cytometry and single cell absorption spectroscopy to study the

phytoplankton structure and to calculate the chl *a* specific absorption coefficients at the taxon level, *J. Phycol.*, *41*, 1099–1109, doi:10.1111/j.1529-8817.2005.00137.x.

Trees, C. C., D. K. Clark, R. R. Bidigare, M. E. Ondrusek, and J. L. Mueller (2000), Accessory pigments versus chlorophyll a concentrations within the euphotic zone: A ubiquitous relationship, *Limnol. Oceanogr.*, *45*, 1130–1143.

Uitz, J., H. Claustre, A. Morel, and S. B. Hooker (2006), Vertical distribution of phytoplankton communities in open ocean: An assessment based on surface chlorophyll, *J. Geophys. Res.*, *111*, C08005, doi:10.1029/2005JC003207.

Uitz, J., Y. Huot, F. Bruyant, M. Babin, and H. Claustre (2008), Relating phytoplankton photophysiological properties to community structure on large scale, *Limnol. Oceanogr.*, *53*, 614–630, doi:10.4319/lo.2008.53.2.0614.

Vidussi, F., H. Claustre, B. B. Manca, A. Luchetta, and J. C. Marty (2001), Phytoplankton pigment distribution in relation to upper thermocline circulation in the eastern Mediterranean Sea during winter, *J. Geophys. Res.*, *106*, 19,939–19,956, doi:10.1029/1999JC000308.

Voss, K. J. (1992), A spectral model of the beam attenuation coefficient in the ocean and coastal areas, *Limnol. Oceanogr.*, *37*, 501–509.

Wang, G., W. Cao, D. Xu, and Y. Yang (2007), Variability of phytoplankton absorption in the northern South China Sea: Influence of the size structure and pigment composition of algal populations, *Acta Oceanol. Sin.*, *26*, 12–25.

Welschmeyer, N. A. (1994), Fluorometric analysis of chlorophyll-a in the presence of chlorophyll-b and pheopigments, *Limnol. Oceanogr.*, *39*, 1985–1992.

Westberry, T. K., G. Dall'Olmo, E. Boss, M. J. Behrenfeld, and T. Moutin (2010), Coherence of particulate beam attenuation and backscattering coefficients in diverse open ocean environments, *Opt. Express*, *18*, 15,419–15,425, doi:10.1364/OE.18.015419.

Whitehead, K., and M. Vernet (2000), Influence of Mycosporine-like amino acids (MAAs) on UV absorption by particulate and dissolved organic matter in La Jolla Bay, *Limnol. Oceanogr.*, *45*, 1788–1796, doi:10.4319/lo.2000.45.8.1788.

Apêndice 3

Manuscript in preparation for submission to Journal of Geophysical Research

Discrimination of phytoplankton assemblages in Patagonian waters from their light absorption spectra

Amabile Ferreira[1*], Dariusz Stramski[2], Carlos Alberto Eiras Garcia[1], Carlos Rafael Borges Mendes[1], and Virginia Maria Tavano[1]

[1] *Instituto de Oceanografia, Universidade Federal do Rio Grande, Rio Grande, RS 96201-900, Brazil*

[2] *Marine Physical Laboratory, Scripps Institution of Oceanography, University of California San Diego, La Jolla, CA 92093-0238, USA*

*Corresponding author: amabilefr@gmail.com

Index terms: 0422 Bio-optics; 4855 Phytoplankton

Keywords: phytoplankton, pigments, CHEMTAX, light absorption spectra, Patagonia

Running title: Phytoplankton assemblages and their light absorption spectra

Abstract
In situ and satellite optical observations of ocean waters provide a potential tool for the identification of phytoplankton groups, which have characteristic roles in the biogeochemical cycles of the ocean. Spatial and temporal taxonomic changes are associated with intense phytoplankton blooms that occur along the Patagonian shelf break (PSB) throughout spring and summer. Through application of a hierarchical cluster analysis, we examined the consistency between algal pigment information, including diagnostic pigment ratios and taxonomic structure data provided by the CHEMTAX approach, and field hyperspectral absorption spectra of phytoplankton for 136 samples from the PSB blooms. Each dataset was coherently separated into three broad clusters comprising samples dominated by diatoms, haptophytes, or without dominance of any of these groups. Our analyses showed that these three main cases of taxonomic dominance can be also reasonably identified on the basis of absorption spectra of phytoplankton at one single wavelength. The greater the relative contribution of diatoms or haptophytes, the higher is the chance to detect correctly the dominant group. Application of the clustering methodology for other regions may require the use of regional reference subsets. The one wavelength-based approach for a given region demand local investigation of the dominant phytoplankton groups and a wavelength that can be useful to define an absorption value as a threshold to identify dominance. Our results indicate that a cell size parameter retrieved from the phytoplankton absorption spectra, which can be currently estimated from satellite remote sensing, has also potential to assign cases of strong dominance of diatoms or haptophytes in PSB waters.

1. Introduction

Phytoplankton governs the primary production and biogeochemical cycles in the open oceans and an accurate quantification of these processes requires knowledge of the spatial and temporal evolutions of algal biomass at global and regional scales. Since the launch of the first satellite ocean color sensor Coastal Zone Color Scanner (CZCS) in 1978 [*Feldman et al*., 1989], the remote sensing of ocean color has achieved a quasi-permanent monitoring of the phytoplankton biomass indexed as chlorophyll-*a* concentration, Chl*a*.

However, Chl*a* is not sufficient to properly assess the contribution of the phytoplankton photosynthesis to the oceanic biogeochemical cycles because algal groups differ greatly in their biogeochemical functions [see *Le Quéré et al*., 2005 and *Nair et al*., 2008 for a review]. In this context, a phytoplankton functional type represents a group of species that, regardless the phylogeny, share similar traits [*Nair et al.,* 2008]. For instance, silica, calcium, and nitrogen are mainly utilized by diatoms, coccolithophores, and some cyanobacteria (e.g. *Trichodesmium*), respectively. Dinoflagellates and haptophytes appear responsible for an enhanced dimethylsulfide (DMS) production in the oceans, contributing to an exchange of sulphur between the ocean and atmosphere. The algal cell size has also an obvious ecological importance, as it can provide information on the phytoplankton community structure and insights on energy transference through the trophic web. Picophytoplankton cells can absorb nutrients with high efficiency under nutrient-limited conditions, and therefore dominate oligotrophic waters. However, as they sink more slowly than larger cells, the picophytoplankton role in carrying carbon to deeper waters is limited. Microphytoplankton is the principal agent for efficient food webs, particle sinking, and carbon export.

In the last decade, remote detection studies have evolved towards the identification of phytoplankton groups [see *Rudorff et al*., 2011 for a review], potentially to enhance our understanding of biogeochemical processes in the global ocean. Algorithms based on optical measurements including satellite remote sensing have been developed either to map the distribution of phytoplankton types [*Subramaniam et al*., 1999; *Sathyendranath et al*., 2004; *Alvain et al*., 2005; *Bracher et al*., 2009] or phytoplankton size classes [*Aiken et al*., 2006; *Ciotti and Bricaud*, 2006; *Uitz et al.,* 2006; *Hirata et al.*, 2008; *Kostadinov et al*., 2009; *Brewin et al*., 2010; *Mouw and Yoder,* 2010; *Devred et al.,* 2011].

The feasibility of accessing phytoplankton information from space relies on the fact that the spectral reflectance in open ocean waters is largely determined by light absorption properties of the phytoplankton present in the upper layers [*Morel and Prieur*, 1977; *Sathyendranath and Platt*, 1989]. The variability in the light absorption spectra of algal populations is strongly dependent on (1) cellular pigment composition [*Sathyendranath et al*., 1997; *Ciotti et al*., 1999; *Lohrenz et al*., 2003; *Lutz et al*., 2003] and (2) pigment package effect. This effect, as predicted by theory, depends on cell size and intracellular pigment concentrations [*Kirk*, 1975; *Morel and Bricaud*, 1981; *Bricaud et al*., 2004 and references therein]. Hence, a covariation between the effects of pigment composition and cell size is expected in natural environments, as cell size is in general positively correlated to the availability of nutrients [e.g., *Yentsch and Phinney*, 1989], while pigment composition can also be related to eutrophic state due to the competition among different taxa and physiological responses [*Claustre*, 1994; *Kostadinov et al*., 2003; *Lutz et al*., 2003].

Some studies have attempted to extract pigment information from phytoplankton absorption spectra [*Hoepffner and Sathyendranath*, 1993; *Stuart et al*., 1998; *Moisan et al*., 2011], but these methods remain a difficult inverse problem. This is because a separation of the effect of concentration of accessory pigments from that of package effect on the absorption spectra of phytoplankton is difficult. Improvements in retrieving pigment concentrations from spectral absorption characteristics have been achieved with advanced statistics [*Chazottes et al.*, 2006, 2007; *Bricaud et al*., 2007] that might not be feasible in a routine fashion.

The possibility of identifying algal dominant groups directly from absorption spectral patterns or after inversion from remote sensing reflectance has been more extensively exploited [e.g., *Millie et al.,* 1997; *Stæhr and Cullen*, 2003; *Craig et al*., 2006; *Lubac et al*., 2008; *Mao et al*., 2010]. Specifically, cluster methodologies applied to spectral absorption properties in conjunction to reference datasets of phytoplankton assemblage compositions have been tested as automated approaches for identification of groups dominance [*Taylor et al*., 2011; *Torrecilla et al*., 2011]. These studies have confirmed the advantage of hyperspectral over multispectral inversion and derivative techniques for species identification and enumeration from satellite observations of ocean color [see also *Lubac et al.,* 2008]. Nevertheless, the applicability of these techniques to detect different phytoplankton communities from satellite is still a major challenge, mainly because of regional specific characteristics [*Alvain et al.*, 2008] and the sparseness of *in situ* data required to validate these techniques [*Platt et al.,* 2006]. The successful of these approaches is particular motivating for remote sensing applications in regions with recognized importance on the global ecology and carbon cycle.

During austral spring and summer, high levels of phytoplankton biomass persistently occur in the Patagonian inner shelf and shelf break region, making it one of the most productive zones in the global ocean [*Takahashi et al*., 2002; *Gregg et al*., 2005]. The seasonal cycle of phytoplankton biomass in the vicinities of Patagonian shelf break was recently examined using remote sensing data [*Garcia et al*., 2004; *Rivas et al*., 2006; *Romero et al*., 2006; *Signorini et al*., 2006]. Fieldwork in this region suggests that the development and sustainability of phytoplankton blooms are associated with nutrient supply from the Malvinas Current and water column stability along the shelf break front [*Carreto et al*., 1995; *Garcia et al*., 2008]. Spatial and temporal taxonomic changes in the phytoplankton structure have been reported in association with those blooms [*Carreto et al.,* 2008; *Garcia et al.,* 2008; de *Souza et al.,* 2012; *de Souza et al.,* unpublished data]. The Patagonian waters have been recognized to play an important role in the global oceanic uptake of CO_2 from the atmosphere, with an important contribution from biological production [*Takahashi et al*., 2002; *Bianchi et al*., 2009].

In a previous work, we showed that a cell size parameter that describes the shape of phytoplankton absorption spectra [*Ciotti et al*., 2002] varied in a consistent fashion with chlorophyll-*a* concentration for both the chlorophyll-specific phytoplankton absorption and chlorophyll-specific particulate scattering coefficients in Patagonian shelf break waters [*Ferreira et al.,* in press]. A dominance of smaller cells was typically associated with lower chlorophyll-*a* concentrations and higher chlorophyll-specific optical coefficients. Because of the relationship between algal cell size and taxonomy, it is worthy to investigate whether differences in the spectral shapes of absorption coefficients of phytoplankton also reflect taxonomic dominance.

In this study, we analyze the algal composition in conjunction with absorption coefficients of phytoplankton measured during austral spring and summer along the Patagonian inner-shelf and shelf break region. Our first objective is to examine the feasibility of classifying the phytoplankton absorption spectra according to their assemblage composition. In order to address this question, a cluster analysis is applied separately to datasets of pigment composition, relative contributions of algal taxonomic classes, and phytoplankton absorption spectra. Secondly, we examine the absorption spectral signatures of phytoplankton and their potential as a short cut to identify the dominant algal group.

2. Measurements and data analysis

The approach of this study consists of two components: (1) investigation of the coherence between algal composition and light absorption properties of phytoplankton by performing cluster analysis based on (i) diagnostic pigment ratios of phytoplankton, (ii) relative contributions of algal taxonomic classes, and (iii) light absorption spectra of phytoplankton; (2) investigation of specific features in phytoplankton absorption spectra in association with the dominance of a algal taxonomic class.

Data analyzed in this study were collected on four campaigns in the Patagonian inner-shelf and shelf break region. Two cruises referred to as PATEX 4, and PATEX 6 took place during the austral spring season, specifically 16 - 21 October 2007, and 14 - 18 October 2008 respectively. PATEX 5 and PATEX 7 were conducted in summer during the periods of 4 - 7 January 2008 and 5 - 8 January 2009 respectively. Geographical locations of the sampling stations (Figure 1) extended from the northern portion of the Argentinean shelf (PATEX 6) through the highly productive waters along both the Patagonian shelf break (PATEX 4) and the southern inner shelf (PATEX 5), to the area south of Malvinas Islands (PATEX 7). Overall, 120 stations were visited by performing cross-shelf and along-shelf transects during the four cruises.

HPLC Pigment Analysis - Concentrations of chlorophyll-*a* and accessory pigments of phytoplankton were measured using the High Performance Liquid Chromatography (HPLC) technique. At each station discrete water samples (0.5-1 L) were collected at near-surface and depths at which the maximum fluorescence by chlorophyll-*a* was observed. The samples were filtered onto 25-mm glass fiber filters (Whatman GF/F) for post-cruise analyses. The HPLC procedure used in this work is described in detail by *Mendes et al*. [2007] and *de Souza et al*. [2012].

The concentrations of the following pigments were determined by HPLC: (1) total chlorophyll-*a*, TChl*a*, which is the sum of monovinyl chlorophyll-*a*, chlorophyllide-*a*, and the chlorophyll-*a* epimers and allomers (divinyl chlorophyll-*a* was not detectable in any sample) (2) chlorophyll-*b*; (3) the sum of chlorophylls-c_1, c_2, and c_3; (4) prasinoxanthin, (5) 19'-butanoyloxyfucoxanthin, (6) fucoxanthin, (7) 19'-hexanoyloxyfucoxanthin, (8) peridinin, (9) diadinoxanthin, (10) diatoxanthin, (11) alloxanthin, (12) zeaxanthin, (13) neoxanthin, and (14) pheophytin-*a* and pheophorbide-*a*.
Determination of diagnostic pigments of phytoplankton - Although 13 pigments besides chlorophyll-*a* were detected in our samples, some of them occurred generally in very small concentrations while others co-varied with the major pigments or are normally redundant [*Vidussi et al*., 2001]. We thus considered convenient to use diagnostic

pigment ratios as a dataset to perform cluster analysis instead of all pigments to determine subsets that characterizes phytoplankton composition [*Torrecilla et al*., 2011]. Eight biomarkers of phytoplankton taxonomic groups [see *Vidussi et al*., 2001] were detected in our samples: chlorophyll-*b* (Chl*b*), prasinoxanthin (Pras), 19'-butanoyloxyfucoxanthin (But), fucoxanthin (Fuco), 19'-hexanoyloxyfucoxanthin (Hex), peridinin (Peri), alloxanthin (Allo), and zeaxanthin (Zea).

Although generally not considered as marker pigments, we included chlrophyll-*c1* (Chl*c1*) and chlrophyll-*c3* (Chl*c3*) in our analysis, which resulted in a dataset with 10 diagnostic pigments, because Chl*c1* and Chl*c3* occasionally distinguish two types of diatoms [*Stauber and Jeffrey*, 1988]. *Stauber and Jeffrey* [1988] verified that, while chlorophyll-*c2* (Chl*c2*) was present in all diatoms tested in their study, 12% of them contained Chl*c3* instead of Chl*c1*. Besides the Chl*c1*-containing diatoms, microscopy analysis revealed the occurrence of the Chl*c3*-containing diatoms in our samples. Specifically, the species *Thalassiothrix antarctica* e *Rhizosolenia crassa* occurred exclusively during the PATEX 4 and PATEX 7 cruises, respectively. It is noteworthy that Chl*c3* can be a marker of *Phaeocystis* species [*Claustre et al.*, 1990; *Antajan et al.,* 2004], but a very good relationship was observed between Chl*c3* and the abundance of these diatom species (M. Souza, personal communication, 2011). These two categories of diatoms will be further referred to as Chl*c1*-diatoms and Chl*c3*-diatoms. For each sample, the 10 ratios of diagnostic pigments were computed by normalizing the concentration of each diagnostic pigment to the sum of the 10 diagnostic pigment concentrations [*Uitz et al*., 2006].

Determination of relative contributions of taxonomic groups of phytoplankton - The relative abundance of phytoplankton taxonomic groups to TChl*a* biomass was calculated from pigment concentration data using the chemical taxonomy software CHEMTAX v1.95 [*Mackey et al.,* 1996]. CHEMTAX uses a factor analysis and steepest-descent algorithm to best fit the pigment data of a given sample to an initial pigment ratio matrix, which contains diagnostic pigments of phytoplankton to TChl*a* ratios that are representative of the region of interest [*Mackey et al.*, 1996]. Initial ratios for the major algal classes were obtained from a previous study at the Patagonian shelf waters [*Carreto et al*., 2003]. The output data for a sample contains absolute amounts (mg m^{-3}) of TChl*a* attributed to each phytoplankton group. The basis for calculations and procedures are fully described in *Mackey et al.* [1996].

Based on the diagnostic pigments detected and microscopy analysis, 6 algal groups were loaded into the CHEMTAX running: (1) diatoms (2) haptophytes, (3) dinoflagellates, (4) cryptophytes, (5) prasinophytes, and (6) cyanobacteria. The identification of Chl*c3*-diatoms on microcopy justifies the discrimination of this group besides Chl*c1*-diatoms, thus their respective ratios of pigments to TChl*a* were separately loaded in the CHEMTAX running for the PATEX 4 and 7 cruises, when both types of diatoms were identified. Therefore, 7 algal groups were loaded to the CHEMTAX procedure for these cruises instead of 6. The CHEMTAX results will be shown according to the occurrence of the 7 taxonomic groups, i.e., with discrimination among Chl*c1*-diatoms and Chl*c3*-diatoms. The CHEMTAX procedure used in this work is described in detail by *Gonçalves-Araújo et al.* [2012] and *de Souza et al*. [2012]. For each sample, relative contributions of the 6 (or 7 for PATEX 4 and 7 cruises) taxonomic classes were then computed by dividing the chlorophyll-*a* concentration attributed to a given

taxonomic group to TChl*a*.

Determination of light absorption coefficients of phytoplankton – The spectra of the particulate absorption coefficient, $a_p(\lambda)$ in m^{-1}, were obtained with the quantitative filter pad technique (*Kishino et al.,* 1985) using water samples (0.5-2 L) were collected at the same depths as the samples for pigment determinations, and were filtered onto 25-mm Whatman GF/F filters. The $a_p(\lambda)$ measurements were made in the 300–750 nm spectral range at 1-nm intervals with a dual beam spectrophotometer (Cary Model 1E). Immediately after the $a_p(\lambda)$ measurements, the sample filters were subjected to bleaching with sodium hypochlorite and then re-scanned to obtain estimates of the non-algal particle (detritus) absorption coefficient, $a_d(\lambda)$ in m^{-1} [*Kishino et al*., 1985*; Tassan and Ferrari*, 1995; *Mitchell et al*., 2000]. For the computation of the $a_p(\lambda)$ and $a_d(\lambda)$ coefficients we used the amplification factor *beta* given by *Ferreira et al*. [2009]. The spectral absorption coefficients of phytoplankton, $a_{ph}(\lambda)$ in m^{-1}, were computed as the difference between $a_p(\lambda)$ and $a_d(\lambda)$. In order to emphasize differences in spectral shapes, each phytoplankton absorption spectrum was normalized to its sum of all spectral values between 400 and 700 nm. The normalized spectrum is referred to as $\int a_{ph}(\lambda)$. In this study, all absorption spectra of phytoplankton will be presented in the form of $\int a_{ph}(\lambda)$.

Computation of a cell size parameter of phytoplankton - To estimate a cell size parameter for phytoplankton, each phytoplankton absorption spectrum was normalized to its mean value computed on the basis of all spectral values between 400 and 700 nm [*Ciotti et al*., 2002]. The normalized spectrum is denoted as $a_{<ph>}(\lambda)$. Assuming that variations in the spectral shape of phytoplankton absorption are mainly driven by the dominant cell size, *Ciotti et al*. [2002] developed a model that reconstructs the shape of $a_{<ph>}(\lambda)$ with a linear combination of two spectra representing complementary contributions of the smallest (picophytoplankton) and largest cell sizes (microphytoplankton) [see Equation 3 in *Ciotti et al.* 2002]. This procedure yields an estimate of the size parameter S_f that is consistent with a given observed spectrum of $a_{<ph>}(\lambda)$ and the model-reconstructed spectrum of $a_{<ph>}(\lambda)$. The values of S_f are constrained to vary from 0 to 1. S_f tends to 0 when large cells of phytoplankton (> 20 μm) are dominant, and 1 when small cells (< 2 μm) dominate. The usefulness of the size parameter S_f for interpreting the variability in the phytoplankton absorption spectra showed in the present study was assessed elsewhere [*Ferreira et al*., in press].

Hierarchical cluster analysis - An unsupervised Hierarchical Cluster Analysis (HCA) was applied to classify our samples into different groups on the basis of three datasets, which included i) diagnostic pigment ratios, ii) relative contribution of algal groups derived from CHEMTAX, and iii) light absorption coefficients of phytoplankton. The HCA has been applied in other studies with similar purposes of our analysis using small selected sets of data with significant contrasts in pigment composition [*Torrecilla et al*., 2011] or broader datasets [*Taylor et al*., 2011]. HCA is a cluster method that builds a hierarchical cluster tree (or a dendrogram), where clusters at one level are joined with clusters at the next higher level. The level of clustering most appropriate is defined by inspection of this dendrogram.

The construction of a dendrogram involves a measure of the proximity (distance)

between par of observations and a linkage criterion that specifies the dissimilarity of sets as a function of the pairwise distances of observations in the sets [e.g., *Hair et al.,* 2009]. In this study, the Euclidean distance and a linkage algorithm referred to as the furthest neighbor, which uses the largest distance between objects of two clusters, were utilized for the diagnostic pigment ratios and CHEMTAX datasets. The cosine distance was chosen to be most appropriate upon the phytoplankton absorption coefficients, because it reflects mainly the differences in the spectral shape [*Torrecila et al*., 2011]. No previous normalization of the $a_{ph}(\lambda)$ spectra is required, as the cosine similarity computation treats both vectors as unit vectors by normalizing them, yielding a measure of the angle between the two vectors. It therefore provides an accurate measure of similarity but with no regard to magnitude.

The HCA method is suitable for our study because two dendrograms obtained from differenc datasets, e.g. diagnostic pigments and CHEMTAX data, can be compared [*Torrecilla et al.*, 2011]. This is done by computation of the Cophenetic index, which represents the correlation between two cophenetic matrices (or matrices of similarity) associated with each dendrogram [*Sokal and Rohlf*, 1962].

For a given type of data, the input to the cluster analysis consisted of 136 numerical data vectors, each representing one of the 136 samples. For the input data representing the ratio of diagnostic pigments, the consecutive elements represent the ratio of each of the 10 diagnostic pigment concentrations to the sum of diagnostic pigment concentrations. Another type of data vector used in the cluster analysis is of the form where the consecutive elements represent the relative contribution of the 6 (for the cruises PATEX 5 and 6) and 7 (for the cruises PATEX 4 and 7) taxonomic groups to total phytoplankton biomass in terms of TChl*a*, as estimated from the CHEMTAX software. The input characterizing the hyperspectral absorption of phytoplankton for any given sample was used in the form of the following data vector $\{a_{ph}(400), a_{ph}(401), a_{ph}(402), \ldots, a_{ph}(700)\}$, where the consecutive elements represent the values of $a_{ph}(\lambda)$ at successive light wavelengths over the spectral range from 400 to 700 nm. In order to visualize the differences in spectral shapes detected by the HCA method, all absorption spectra of phytoplankton will be presented in the form of $\int a_{ph}(\lambda)$.

3. Results

TChl*a* varied from 0.13 to 22.15 mg m^{-3} at near-surface and depths of maximum chlorophyll fluorescence. Briefly, the highest concentrations were measured during PATEX 4 (0.95 to 22.15, average of 7.58 mg m^{-3}) along an intense bloom at the Patagonian shelf break. PATEX 5 was carried out over a patch of high reflectance in association with a coccolithophoride bloom in the southern continental shelf [*Garcia et al*., 2011; *de Souza et al.,* 2012] and moderate TChl*a* (0.20 to 1.48, average of 0.56 mg m^{-3}). PATEX 6 sampled waters of the Brazil-Malvinas Confluence, with TChl*a* spanned between 0.15 and 2.20 mg m^{-3} (average of 0.99 mg m^{-3}) [*Gonçalves-Araújo et al.,* 2012]. During the PATEX 7 cruise, the observations were made at southern of the Malvinas Island (Figure 1) and measured the lowest TChl*a* in the range of 0.15 to 1.19 mg m^{-3} (average of 0.41 mg m^{-3}). A more detailed description of the phytoplankton biomass including size fractionation for these cruises can be found in *Ferreira et al*. [in press].

Because our specific objective is to investigate the coherence between the phytoplankton composition and features in their absorption spectra, the

pigment/CHEMTAX data will be shown according to the HCA classification and subsequently compared to the classification of the absorption optical data.

3.1. Cluster analysis based on the diagnostic pigment ratios of phytoplankton

The optimal partitioning of the ratios of each diagnostic pigment concentration to the sum of diagnostic pigment concentrations derived from the dendrogram of linkage distances (not shown) was suggested to be into 4 clusters, denominated hereafter as $C1_{diag}$ through $C4_{diag}$ (Figure 2). $C1_{diag}$ grouped 38 samples, whereas 28 and 10 corresponded to PATEX 4 and 6, respectively. Those samples were largely predominated by Fuco (Figure 2a) with average ratios of the main diagnostic pigments as 0.78, 0.06 and 0.06 for Fuco, Chl*c1*, and Chl*c3*, respectively, which indicates the dominance of diatoms, as confirmed by microscopy analysis.

$C2_{diag}$ (Figure 2b) contained 29 samples (15 and 14 of PATEX 5 and 7 cruises, respectively) with Hex as the dominant diagnostic pigment (average ratio of 0.45) and in association with a considerable importance of Chl*c3* (0.18) and Fuco (0.14). This cluster was also characterized by the highest ratios of Buta (average of 0.08), an unequivocal marker for the haptophyte *Phaeocystis antarctica* [*Zapata et al.,* 2004]. Peri contributed to some extent in several samples, whereas Hex remained as the dominant diagnostic pigment (Figure 2b). Microscopy data were coherent with the pigment features, confirming the presence of the haptophyte *Emiliania huxleyi* (coccolithophoride) in all samples of PATEX 5. During this cruise, *E. huxleyi* showed an average contribution of 38% and dominated the algal biomass (contribution greater than 50%) in 6 samples. *P. antarctica* was present in all PATEX 7 samples, also contributing on average with 38% of the algal biomass for this cruise.

Most of the samples (N=63) were included in $C3_{diag}$, with Fuco (average ratio of 0.31) and Hex (0.21) as the principal and second most important diagnostic pigments, respectively (Figure 2c), while Chl*c3* strongly correlated with both these pigments. The pronounced contribution of Chl*b* and Pras in all $C3_{diag}$ samples evidences the presence of prasinophytes. This cluster thus classified samples with substantial and mixed importance of diatoms, haptophytes, and prasinophytes, whereas no single group was dominant (Figure 2c). $C3_{diag}$ included 7, 30, and 26 samples from the PATEX 5, 6, and 7 cruises, respectively.

Six samples (5 from the PATEX 5 and 1 from the PATEX 7 cruise) with Peri as the dominant diagnostic pigment (average ratio of 0.38) were ended up in a separate cluster ($C4_{diag}$), indicating unequivocally the abundance of dinoflagellates (Figure 2d). Haptophytes also contributed to the algal biomass to some extent in $C4_{diag}$ samples, with an average ratio of Hex of 0.25.

3.2. Cluster analysis based on the taxonomic composition of phytoplankton

The CHEMTAX technique refines the information yielded by the diagnostic pigment ratios, as it provides the relative contribution of phytoplankton taxonomic classes to total biomass in terms of chlorophyll-*a* concentration. Similarly to the cluster results obtained with the diagnostic pigment ratios as input, 4 clusters ($C1_{CHEM}$ through $C4_{CHEM}$) were adequate to cluster the CHEMTAX dataset in a satisfactory fashion (Figure 3). Not surprisingly, the results of this cluster analysis are quite consistent with the preliminary classification obtained for input data as the diagnostic pigment ratios

(Figure 2), with a cophenetic index of 0.69. The first three CHEMTAX-based clusters identified 35 samples dominated by diatoms ($C1_{CHEM}$), 39 by haptophytes ($C2_{CHEM}$), and with significant contributions of both these groups and prasinophytes, but no single group dominated the assemblages ($C3_{CHEM}$, N=49).

Although Chl*c1*-diatoms dominated all samples of $C1_{CHEM}$, Chl*c3*-diatoms showed significant contribution in many samples of this cluster (Figure 3a). Haptophytes dominated all samples of $C2_{CHEM}$, but dinoflagellates and Chl*c1*-diatoms were also representative (about 20-30% of contribution) (Figure 3b). The occurrence of prasinophytes in the $C3_{CHEM}$ samples previously suggested by detection of Pras (Figure 2c) was confirmed by a significant contribution of this group based on the CHEMTAX data, although strictly dominant (relative abundance higher than 50%) only in 3 samples (Figure 3c). Differently to the previous HCA that created $C4_{diag}$ as characterized by abundance of dinoflagellates (Figure 2d), $C4_{CHEM}$ grouped 13 samples with notable presence of Chl*c3*-diatoms with an average contribution of 44% (Figure 3d).

3.3. Classification of samples based on the dominant taxonomic group of phytoplankton

The previous sections showed the classification of the phytoplankton pigment data through cluster techniques with their own assumptions of similarities within a dataset. We have also utilized an independent approach to classify the phytoplankton assemblages using an objective criterion of dominance. The dominant taxonomic group was defined on the basis of the relative contribution of each group to the total phytoplankton biomass provided by CHEMTAX. Specifically, we assumed that a contribution greater than 50% defines the dominance.

For 136 samples, 38 were dominated by diatoms, of which 34 were dominated by Chl*c1*-diatoms and 3 by Chl*c3*-diatoms (see Figure 3d). A single sample was ended up as diatom-dominated by summing up the contributions of Chl*c1*-diatoms (49.2%) and Chl*c3*-diatoms (33.3%). Although the differentiation among these diatom types would be reasonable from a cell size aspect, which largely impacts the absorption properties, only three samples was dominated by Chl*c3*-diatoms. Any relevant feature in the absorption spectra associated with this group will be informed. Haptophytes were predominant in 40 samples, including all samples clustered in $C2_{CHEM}$ and one sample of $C4_{CHEM}$ (Figure 3). Three samples showed dominance of cryptophytes (1 sample), dinoflagellates (1), and prasinophytes (1), and all of these cases were comprised by $C3_{CHEM}$ (Figure 3c). 55 samples did not satisfy our 50% criterion for dominance. Therefore, 58 samples were not dominated neither by diatoms or haptophytes.

Our results show that although 6 main taxonomic groups occurred in our samples (Figures 2 and 3), the phytoplankton blooms at the Patagonian shelf break waters are typically dominated by diatoms and haptophytes. *Phaeocystis antarctica* is the main species of haptophyte present in these waters, unless specific environmental constraints allow the occurrence of blooms of the coccolithophorid *Emiliania huxleyi* (e.g. PATEX 5) [*Garcia et al*., 2011; *de Souza et al*., 2012]. As the second step of this study is focused on discriminating algal dominance on the basis of features in the phytoplankton absorption spectra, we classified each sample as (1) diatom-dominated (N=38), Dia-D, (2) haptophyte-dominated (N=40), Hap-D, or (3) not dominated by any of both these groups (N=58), Not-D. Thus, Not-D also includes those few samples not dominated by

diatoms or haptophytes, but dominated by any other taxonomic group (see Figure 3). The visual inspection of the normalized absorption spectra of phytoplankton, $\int a_{ph}(\lambda)$, for these samples revealed spectral shapes very similar to those with no dominance of any algal class (Figure 4c). This suggests that an attempt to discriminate samples dominated by other group besides diatoms or haptophytes from the $\int a_{ph}(\lambda)$ spectra would be more challenging, at least with the method proposed in this study.

3.4. Cluster analysis based on the phytoplankton absorption spectra

Figure 4a illustrates results from the HCA method performed on the absorption spectra of phytoplankton, which are shown for the normalized form of $\int a_{ph}(\lambda)$. Differently to the previous cluster analyses applied to the dataset of diagnostic pigment ratios and taxonomic contributions of phytoplankton (Figures 2 and 3), a dendrogram (not shown) indicated an optical partitioning of the phytoplankton absorption dataset into 3 clusters instead of 4, referred to as $C1_{aph}$ through $C3_{aph}$.

$C1_{aph}$ clustered the flattest absorption spectra with the lower blue to red ratios, i.e., stronger package effects (N=38). $C2_{aph}$ comprised the majority of the spectra (N=71) that were characterized by a shoulder around the 450-470 nm spectral range in addition to the usual spectral location of the absorption peak close to 440 nm, and higher blue to red ratios (Figure 4a). The spectra that resembled those of $C2_{aph}$ in normalized values at the first part of the blue spectral region but with lower normalized values around 460 nm and intermediate values from about 550 nm to higher wavelengths, compared to the $C1_{aph}$ and $C2_{aph}$ spectra were grouped in $C3_{aph}$ (N=27, Figure 4a).

Figures 4b through 4d depict the $\int a_{ph}(\lambda)$ spectra that correspond to the classification through the HCA method applied to the b) diagnostic pigment ratios and c) CHEMTAX datasets, and d) 50% dominance criterion. The similarity between the partitions based on the phytoplankton absorption spectra and those obtained using the diagnostic pigment ratios and CHEMTAX datasets is reflected by cophenetic indexes of 0.67 and 0.66, respectively.

As expected, the $\int a_{ph}(\lambda)$ spectra included in $C1_{aph}$ are associated with the predominance of diatoms. This cluster grouped 35 Dia-D samples, and 33 and 35 samples selected by $C1_{diag}$ and $C1_{CHEM}$, respectively. All spectra of $C2_{diag}$ and $C2_{CHEM}$ and Hap-D cases were grouped within $C2_{aph}$, which indicates that the second absorption maximum in the blue region close to 460 nm is related to Hex [*Jeffrey et al.,* 1997; *Siegel et al*., 2007]. The differences between the Dia-D and Hap-D spectra observed at the blue portion also agree with an important absorption at 467 nm due to Chl*c3* present in *Phaeocystis* sp [*Astoreca et al.,* 2009]. $C2_{aph}$ also assorted those few samples of $C1_{diag}$ and $C1_{CHEM}$ not assorted by $C1_{aph}$ and many samples of the $C3_{diag}$, $C4_{diag}$, $C3_{CHEM}$ clusters and Not-D cases. Therefore, $C2_{aph}$ did not discriminate Hap-D and Not-D spectra suitably, essentially because of the resemblance between many of these two classes of spectra at the locations of absorption peaks around 460 nm and 676 nm (Figures 4a and 4d).

$C3_{aph}$ clustered those Not-D spectra with $\int a_{ph}(\lambda)$ values comparatively lower and higher at about 460 and 676 nm, respectively (see Figures 4a and 4d), i.e., less flat spectra. This cluster also included all the $C4_{CHEM}$ spectra, i.e., those with important contribution of Chl*c3*-diatoms. Thus, the three samples dominated by this taxonomic group (see Figure 3d) showed spectral shape of absorption similar to that of the Not-D spectra. These cases indicate that the Chl*c3*-diatoms present in our samples have different

spectral shape of absorption compared to the Chl*c1*-diatoms, likely because their cell sizes are smaller (less package effect) than for Chl*c1*-diatoms.

With regard to the comparison of classification through cluster analysis for input data as the $a_{ph}(\lambda)$ spectra and that based on the 50% criterion of taxonomic dominance, 93 of 136 samples (about 68%) showed coherence among the classification based on the two different datasets. Specifically, the clusters $C1_{aph}$, $C2_{aph}$, and $C3_{aph}$ grouped 34, 36 and 23 samples that were classified as Dia-D (38 samples), Hap-D (40), and Not-D (58), respectively.

The few samples with noticeable importance of dinoflagellates that were grouped in a separate cluster on the basis of diagnostic pigment ratios ($C4_{diag}$) did not exhibit any important signature in their $\int a_{ph}(\lambda)$ spectra. Actually, the spectra included in $C4_{diag}$ were also similar to those spectra associated with lack of taxonomic dominance (Not-D). Therefore, the HCA method based on the pigment information, which includes diagnostic pigment ratios and taxonomic structure provided by CHEMTAX, and the phytoplankton spectra primarily classified the samples as dominated by i) Chl*c1*-diatoms ($C1_{diag}$, $C1_{CHEM}$, $C1_{aph}$), ii) haptophytes ($C2_{diag}$, $C2_{CHEM}$, $C2_{aph}$), iii) not dominated by any of both these taxonomic groups ($C3_{diag}$, $C4_{diag}$, $C3_{CHEM}$, $C4_{CHEM}$, $C3_{aph}$).

3.5. Features in the phytoplankton absorption spectra according to taxonomic dominance

In this section we investigated features in the phytoplankton absorption spectra as a means for assessing differences in terms of taxonomic contribution. Specifically, we considered as a reference the classification of samples as Dia-D, Hap-D or Not-D. We sought exclusive constraints on the $\int a_{ph}(\lambda)$ spectra as a basis for discriminating between these three main cases of phytoplankton taxonomic dominance found in our samples.

From the visual inspection of the spectral shape of the $\int a_{ph}(\lambda)$ spectra is clear that the vast majority of the Dia-D spectra, which are relatively flatter, can be discriminated based only on the blue spectral region by a single wavelength (Figure 4d). This is illustrated in Figure 5, which reveals an inverse dependence of $\int a_{ph}(443)$ on the relative contribution of diatoms (in percentage) to total biomass by considering all samples. Dia-D, Hap-D, and Not-D samples are represented as asterisks, squares, and stars, respectively. Specifically, 31 of 38 Dia-D spectra showed $\int a_{ph}(443)$ lower than 0.0075 (Figure 5).

Figure 5 is divided in four panels (I, II, III, and IV) delimited by the values of 0.0075 in the $\int a_{ph}(443)$ axis and 50% in the axis of relative contribution of diatoms (i.e. the threshold that defines Dia-D). The Dia-D samples with $\int a_{ph}(443)$ lower than 0.0075 are represented in Panel IV (31 of 38 samples). Seven Dia-D samples that showed $\int a_{ph}(443)$ higher than 0.0075 and therefore resembling the Not-D spectra (Figure 4d) are shown in Panel I. Most of the samples, which includes Hap-D and Not-D cases with $\int a_{ph}(443)$ higher than 0.0075, appear in Panel II. A single Not-D sample, with a diatom contribution of 38%, was ended up in Panel III.

Figure 5 also depicts the agreement among the $\int a_{ph}(443)$ values and the cell size parameter S_f. In general, the lower and higher S_f values correspond to the stronger and weaker package effects, respectively [*Ciotti et al.,* 2002]. Consequently, S_f has also a potential to discriminate the Dia-D spectra. The samples positioned in Panel IV were associated with the lowest S_f values (0.05 to 0.37, average of 0.18). The Dia-D cases

shown in Panel I were associated with S_f between 0.42 and 0.54 (average of 0.47). S_f ranged from 0.37 and 0.72 (average of 0.56) for the Not-D spectra and from 0.42 to 0.82 (average of 0.68) for the Hap-D spectra, nearly out of the range for the Dia-D spectra (0.05 to 0.54). This is consistent with large package effect for large diatoms cells.

Figure 5 illustrates that 31 of 32 phytoplankton absorption spectra (or 97% of these spectra) with $\int a_{ph}(443)$ lower than 0.0075 (i.e., placed in Panels III and IV) were associated with diatoms dominance. In other words, we could assume that the probability that the phytoplankton community of a sample with $\int a_{ph}(443)$ lower than 0.0075 is dominated by diatoms is 97%.

The distinction between the Hap-D and Not-D spectra is not as clear as for Dia-D from the others, mainly because of their resemblance in the $\int a_{ph}(\lambda)$ shapes along the whole visible spectra (Figure 4d). A second maximum absorption at the blue spectral region (close to 463 nm) that is attributed to Hex, assigns the majority of the Hap-D spectra. However, many Not-D spectra showed similar $\int a_{ph}(\lambda)$ values to those for Hap-D spectra around this spectral region (Figure 4d). Figure 6 is divided in four panels (I, II, III, and IV) as for Figure 5, delimited by the value of 0.0079 in the $\int a_{ph}(463)$ axis and 50% in the axis of relative contribution of haptophytes. The $\int a_{ph}(463)$ value of 0.0082 is also represented as a line.

A clear trend of increase in the $\int a_{ph}(463)$ values with an increase in the relative contribution of haptophytes is shown in Figure 6. The majority of the Hap-D spectra (30 of 40) showed $\int a_{ph}(463)$ higher than 0.0079 (Panel I). Four of the Hap-D spectra departed considerably from the general resembling for the majority of the Hap-D spectra, showing $\int a_{ph}(463)$ lower than 0.0079 (Panel IV). The Not-D spectra that showed $\int a_{ph}(463)$ higher than 0.0079 are represented in Panel II. Panel III contains the remaining cases that include all the Dia-D and most of Not-D samples. Contrary to what observed for the relative contribution of diatoms, a clear increase in the relative contribution of haptophytes is accompanied by an increase in S_f. As already seen, this parameter varied from 0.42 to 0.82 (average of 0.68) for the Hap-D samples and from 0.37 to 0.72 (average of 0.56) for the Not-D spectra. Higher S_f values are consistent with the smaller cell diameters for haptophytes, generally between 2 and 6 μm. Despite some overlapping for S_f values of the Hap-D and Not-D spectra, all S_f higher than 0.72 were associated with Hap-D spectra.

Figure 6 shows that 30 of 37 (or 81%) phytoplankton absorption spectra with $\int a_{ph}(463)$ higher than 0.0079 (i.e., encompassed by Panels I and II) were associated with haptophytes dominance. When this value is higher than 0.0082, all samples were predominated by haptophytes. Therefore, we could assume that the probability that the phytoplankton community of a sample with $\int a_{ph}(463)$ higher than 0.0079 is dominated by haptophytes is 81%. This probability reaches 100% if $\int a_{ph}(463)$ is higher than 0.0082.

4. Discussion

Torrecilla et al. [2011] applied cluster analysis to pigment data and spectra of the absorption coefficients of phytoplankton and remote sensing reflectance to investigate the potential to discriminate different phytoplankton assemblages in open ocean environments under non-bloom conditions. Specifically, the authors selected nine samples with significant differences in the ratios of diagnostic accessory pigments to chlorophyll-*a*. *Taylor et al.* [2011] applied the same approach to a larger dataset (48

samples) founding similar results from the former work, in addition to compare their classification with ecological provinces. Following these previous approaches of clustering to investigate coherence between algal pigments and optical data, we classified a dataset of 136 samples of diagnostic pigment ratios, CHEMTAX data, and phytoplankton absorption spectra of the blooms that occur along the Patagonia shelf break region.

The partitioning of our samples obtained on the basis of diagnostic pigment ratios is very similar to the partitioning based on the taxonomic information provided by the CHEMTAX method. Samples predominated by diatoms (and Fuco), haptophytes (and Hex), and with mixed taxonomic contributions represented separate clusters, with few disagreements (Figures 2 and 3). The main discrepancy between both partitions consisted on the fourth cluster formed in each case ($C4_{diag}$ and $C4_{CHEM}$). The clustering based on pigments separated samples with great importance of Peri ($C4_{diag}$), a biomarker for dinoflagellates. This taxonomic group, however, was not taxonomically dominant (i.e., contribution lower than 50%) but in one sample, as estimated by the CHEMTAX approach. The $C4_{diag}$ samples were grouped within the clusters $C2_{CHEM}$ and $C3_{CHEM}$ (Figure 3). The fourth cluster formed on the basis of relative taxonomic contributions ($C4_{CHEM}$) discriminated samples with the main contribution of Chl*c3*-containing diatoms, but this diatom type dominated only 3 samples. Eleven of 13 $C4_{CHEM}$ samples were ended up within $C3_{diag}$ (Figure 2).

The CHEMTAX approach estimates the algal class abundances based on accessory pigment to chlorophyll-*a* ratios, yielding the concentration of chlorophyll-*a* attributed to each class. The quality of these estimates is related to some limitations of the method, which are beyond of discussion in this study. Briefly, fluctuations in pigment ratios between species of the same group and/or within the cell itself may occur under influence of various environmental parameters such as light and availability of nutrients [e.g., *Wright and Jeffrey*, 2006; *DiTullio et al.,* 2007]. The quality of the CHEMTAX estimates depends mainly on how the initial pigment ratios are representative of the phytoplankton assemblages investigated [*Mackey et al.,* 1996]. Particularly, a quite good agreement was observed between microscopy analysis and CHEMTAX outputs for the dataset utilized in our study [*Gonçalves-Araújo et al.,* 2012; *de Souza et al.,* 2012].

The differences between the partitioning of samples based on the diagnostic pigment ratios and the CHEMTAX approach can be partially attributed to differences between the initial ratios and real ratios in our samples. Also, differences in the pigmentation may not be directly revealed in terms of taxonomic abundance because pigment composition depends also on adjustments for the environment conditions [e.g. *Schlüter et al.,* 2000]. Furthermore, distinct methods for computation of the distances between pairs of objects and to build clusters may yield variations in the partition of a given dataset. In this way, the choice of other methods for this computation could cause variations in the partitioning provided between both the datasets.

The good agreement between the partition based on the phytoplankton absorption spectra and the partitions obtained using the diagnostic pigment ratios and CHEMTAX datasets is reflected by cophenetic indexes of 0.67 and 0.66, respectively. This suggests that there is a certain degree of equivalence in using a dataset of diagnostic pigment ratios or taxonomic contributions as a basis for investigation of coherence between pigment information and optical properties in Patagonian waters. This is of particular interest

because the CHEMTAX software demands previous identification of the main taxa present in the samples examined, pigment to chlorophyll-*a* ratios representative of the studied region, and computation time consuming. Conversely, determination of the taxonomic composition from pigment data would be less straightforward than from CHEMTAX data. As expected, a better agreement was observed between the clusters formed on the basis of taxonomic contributions (Figure 4c) than for the diagnostic pigment ratios (Figure 4b) and the objective criterion of dominance of 50% (Figure 4d).

The degree of similarity between the pigment/CHEMTAX and phytoplankton absorption datasets was not improved by performing the clustering on the second derivative of phytoplankton absorption spectra [e.g. *Torrecilla et al.,* 2011]. We computed cophenetic indexes of 0.71 and 0.55 between the dendrogram for this new partition and those for the diagnostic pigment ratios and CHEMTAX data, respectively. Also in disagreement with other studies [*Torrecilla et al.*, 2011; *Taylor et al.,* 2011], lower degrees of similarity between these cluster trees were obtained when the $a_{ph}(\lambda)$ spectra was considered over the spectral range of 435 to 520 nm, where the most relevant pigments show their main absorption characteristics. This comparison provided cophenetic indexes of 0.35 and 0.32 for diagnostic pigment ratios and CHEMTAX data, respectively.

Our results support the notion of utilization of the clustering approach as a way to discriminate phytoplankton assemblages from optical data as suggested by *Torrecilla et al.* [2011]. One possible scenario is to consider the data analyzed in our study as a reference dataset of phytoplankton absorption and pigment data. Then, phytoplankton absorption spectra measured in further surveys in the region can be classified in relation to the pigment-based clusters on the basis of similarity with optical data from the reference subsets. The achievement of good results surely depends on the acquisition and analysis of data to be added to the original clustering routines. As we observed important differences between the optimal forms of the input optical data comparing with other studies (poorer agreements using optimal spectral ranges instead of the whole spectra and spectral derivative analysis), we believe that specificities of the phytoplankton absorption spectra for our study region may not be assumed for other regions. This is also supported by results obtained by our previous work with the dataset analyzed in this study [*Ferreira et al.,* in press]. For instance, important differences were found in the magnitudes of the phytoplankton absorption coefficients for a given chlorophyll-*a* concentration comparing to other regions, which were attributed to peculiarities in the size structure of the forming blooms in Patagonian waters [*Ferreira et al.,* in press]. The same study suggested photoprotection processes in the phytoplankton communities in the Patagonian shelf break and the surrounding waters, which may result in specific pigment composition that is reflected in the phytoplankton absorption properties.

A reasonable correspondence between the pigment data and the whole visible spectra of phytoplankton absorption is still observed when applying the clustering method to multispectral absorption data that correspond to satellite ocean color measurements at 412, 443, 490, 510, 555, and 670 nm. Cophenetic indexes of 0.57 and 0.52 were computed by comparing the dendrograms for the multispectral data and for diagnostic pigment ratios and CHEMTAX data, respectively. This indicates a potential to discriminate phytoplankton assemblages from multispectral absorption coefficients of phytoplankton retrieved from satellite. One possible investigation of the potential

usefulness to discriminate the phytoplankton assemblages of Patagonian waters from remote sensing is to test whether the satellite reflectance spectra can be clustered coherently with concurrent *in situ* pigment data [e.g., *Alvain et al.,* 2004; *Alvain et al.,* 2008].

As we have seen in this study, a clustering approach classified the absorption coefficients of phytoplankton according to their spectral shapes coherently with the main cases of taxonomic dominance found in our samples. The samples were separated into three broad groups comprising mostly diatoms or mostly haptophytes or with no dominance of any of these groups (Figures 4a and 4d). These two types of communities (diatoms and haptophytes) represent different key functional groups of phytoplankton [e.g., *Doney,* 1999] and therefore play different roles in the food web structure and in the air–sea CO_2 exchange dynamics. Diatoms are normally associated with high production rates and elevated carbon export flux [*Sarthou et al.,* 2005 and references therein]. *Phaeocystis* sp (the genus of haptophyte mostly representative in our samples) is of strong interest for climate studies since its blooms can be as effective as diatoms blooms in exporting carbon toward the deep ocean [*DiTullio et al.,* 2000]. They are also important producers of Dimethyl Sulfide (DMS), the precursor of secondary sulfate aerosols [*Belviso et al.,* 2004]. The coccolithophorids (bloom-forming during our PATEX 5 cruise) can have an impact on CO_2 partial pressure in surface waters, by increasing this gas during $CaCO_3$ plate formation [*Rost and Riebesell,* 2004]. Therefore, the alternation of dominance between diatoms and haptophytes may result in significant changes in the CO_2 exchange dynamics in the Patagonian waters [*Garcia et al.,* 2008].

The differences among spectral signatures of phytoplankton absorption under dominance conditions of diatoms or haptophytes as observed in our dataset have been already reported [*Stuart et al.,* 2000; *Astoreca et al.,* 2005; *Lubac et al.,* 2008; *Astoreca et al.,* 2009]. These differences are mainly related to signatures of diagnostic pigments (fucoxanthin for diatoms and 19'-hexanoyloxyfucoxanthin for haptophytes) and the package effect. Differences in the performance of the standard ocean color algorithms to estimate chlorophyll-*a* concentration from satellite have been attributed, for instance, to changes in the optical characteristics of these two groups [e.g., *Stuart et al.,* 2000; *Sathyendranath et al.,* 2001].

We have showed that the main three cases of algal taxonomic structure found in our dataset may be satisfactorily identified on the basis of *in situ* $\int a_{ph}(\lambda)$ spectra at one single wavelength. Diatoms dominance can be assigned by values of $\int a_{ph}(443)$ lower than 0.0075. With a certain degree of uncertainty, haptophytes dominance can be identified through values of $\int a_{ph}(463)$ higher than 0.0079, whereas values of $\int a_{ph}(463)$ higher than 0.0082 can be certainly attributed to a dominance of this group. The greater the relative contribution of diatoms or haptophytes, the higher is the success for detection of taxonomic dominance (Figures 5 and 6). Samples of which spectra do not satisfy any of these cases can be classified as not dominated by either diatoms or haptophytes.

It is noteworthy that these constraint values can be utilized only on the basis of the absorption spectra of phytoplankton in the normalized form of $\int a_{ph}(\lambda)$. This is because the computation of $\int a_{ph}(\lambda)$ is performed by dividing all $a_{ph}(\lambda)$ values of each spectrum by the sum of all $a_{ph}(\lambda)$ values of each spectrum, where λ varies from 400 to 700 nm. Therefore, any variation in the spectral range or resolution considered will change the spectral-based values to be used as a threshold to identify the taxonomic dominance in a sample.

The application of our approaches of clusters and based at one single wavelength for taxon-specific detection from phytoplankton absorption would be subject to several interferences through satellite data. Atmospheric correction errors [*International Ocean Colour Coordinating Group*, 2010] and the assumptions of semi-analytical models [*International Ocean Colour Coordinating Group,* 2006] have been still sources of uncertainties in the estimates of phytoplankton absorption coefficients from satellite remote sensing. Because the differences that were observed in the absorption signatures related to taxonomic dominance are spectrally dependent (the phytoplankton spectra were normalized by the sum of all spectral coefficient values), one would be appropriate the use of a semi-analytical model that does not assume the spectral shape of $a_{ph}(\lambda)$ to retrieve phytoplankton absorption coefficients from satellite [e.g., *Lee et al.,* 2002]. The investigation of coherence between field pigment information and phytoplankton absorption spectra as conducted in this study should be then performed on the multispectral coefficients as estimated from the current satellite spectral resolution.

With regard to current operating techniques for remote sensing and our results, a positive feature is the possibility to discriminate diatoms and haptophytes dominance in Patagonian waters from the assessment of the cell size parameter S_f from satellite [*Ciotti and Bricaud*, 2006]. The greater relative contributions of diatoms and haptophytes were linked to the lower (0.05 to 0.35) and higher (greater than 0.72) S_f values, respectively. This can be presumably attributed to a much greater pigment packaging effect (lower S_f) for diatoms than for smaller haptophytes cells (higher S_f). At least the extreme values of the S_f variation range can be suitably assigned to a dominance of both these phytoplankton groups mostly present at the Patagonian shelf break waters.

5. Conclusions

Through application of a hierarchical cluster analysis on the basis of diagnostic pigment/CHEMTAX data and hyperspectral phytoplankton absorption coefficients, we demonstrated that three main situations of phytoplankton taxonomic structure occur during the blooms at the Patagonian shelf break waters: dominance of 1) diatoms, 2) haptophytes, or 3) mixed contributions of these and other groups with no taxonomic predominance. These main situations are coherently reflected in features of the hyperspectral absorption spectra of phytoplankton, which indicates the usefulness of data of absorption coefficient for discriminating phytoplankton assemblages in Patagonian waters under bloom conditions. Specifically, our results support the notion of utilization of the clustering approach as a way to discriminate phytoplankton assemblages from optical data.

We also showed that the main three cases of algal taxonomic structure may be identified, with a small uncertainty associated, on the basis of the normalized absorption spectra, $\int a_{ph}(\lambda)$, at one single wavelength. The greater the relative contribution of diatoms or haptophytes, the higher is the success for detection of taxonomic dominance.

Although the proposed methodologies are generally applicable to other data sets, we believe that the specificities of the phytoplankton absorption spectra for our studied region may not be assumed for other regions. Application of the clustering methodology for other regions may require the establishment of regional reference subsets. The one wavelength-based approach for a given region demand local investigation of the dominant phytoplankton groups and a certain wavelength that can be useful to define a

normalized value of absorption as a threshold to identify a taxonomic dominance.

Further work is needed with satellite-based databases of phytoplankton absorption and concurrent *in situ* pigment data from Patagonian waters to examine the applicability of our approaches for identifying diatoms or haptophytes dominance in that region through multispectral resolution of satellite remote sensing. With regard to the current remote sensing approach that estimates the size parameter of phytoplankton, S_f, the extreme values of the S_f variation range can be suitably assigned to dominance of diatoms and haptophytes during bloom conditions at the Patagonian shelf break waters.

Acknowledgements

The PATagonian EXperiment (PATEX) is a multidisciplinary project conducted by the Group of High Latitude Oceanography (GOAL) in the Brazilian Antarctic Program. We are grateful to the crew of the Brazilian Navy *R/V Ary Rongel* for their assistance during field experiments. We also acknowledge Servicio de Hidrografia Naval (Argentina) for their cooperation in obtaining clearance for carrying out the fieldwork within the Argentinean EEZ. The PATEX 5, 6 and 7 cruises were conducted as part of the Southern Ocean Studies for Understanding Climate Changes Issues (SOS-CLIMATE) project, a Brazilian contribution to the International Polar Year. The SOS-Climate project was funded by the Ministry of Science and Technology (MCT) and Brazilian National Council on Research and Development (CNPq, grant 520189/2006-0). This work was also partly supported by GSFC/NASA through the project OCEANS/04123400362 and by the NASA Biodiversity Program (Grant NNX09AK17G awarded to D.S.). A. Ferreira was funded by CNPq with a graduate scholarship (Proc. No. 143234/2008-0) and the Brazilian agency CAPES (Coordenação de Aperfeiçoamento de Pessoal de Ensino Superior) with a doctoral student grant (Proc. No 6999/10-7). Part of the work was done during a 1-year research visit of A. Ferreira to the Marine Physical Laboratory, Scripps Institution of Oceanography in San Diego, California. The Center of Oceanography of FCUL (Lisbon, Portugal) provided the facilities for the HPLC analysis.

References

Aiken, J., et al. (2006), Validation of MERIS reflectance and chlorophyll during the BENCAL cruise October, 2002: preliminary validation of new demonstration products for phytoplankton functional types and photosynthetic parameters, *Int. J. Remote Sens., 28,* 497-516, doi:10.1080/01431160600821036.

Alvain S., C. Moulin, Y. Dandonneau, and H. Loisel (2008), Seasonal distribution and succession of dominant phytoplankton groups in the global ocean: a satellite view, *Global Biogeochem. Cy., 22,* GB3001, doi:10.1029/2007GB003154.

Alvain, S., C. Moulin, Y. Dandonneau, and F. M. Bréon (2005), Remote sensing of phytoplankton groups in case 1 waters from global SeaWiFS imagery, *Deep Sea Res. I, 52,* 1989-2004.

Antajan, E., et al. (2004), 19'hexanoyloxyfucoxanthin may not be the appropriate pigment to trace occurrence and fate of Phaeocystis: the case of *P. globosa* in Belgian coastal waters, *J. Sea Res., 52,* 165-177.

Astoreca, R., V. Rousseau, K. Ruddick, C. Knechciak, B. Van Mol, J.-Y. Parent, C. Lancelot (2009), Development and application of an algorithm for

detecting *Phaeocystis globosa* blooms in the Case 2 Southern North Sea waters, *J. Plankton Res., 31*, 287-300, doi:dx.doi.org/10.1093/plankt/fbn116.

Astoreca, R., V. Rousseau, K. Ruddick, B. Van Mol, J. Y. Parent, and C. Lancelot (2005), Optical properties of algal blooms in an eutrophicated coastal area and its relevance to remote sensing, *Proc. SPIE Int. Soc. Opt. Eng., 5885,* 245-255.

Belviso, S., C. Moulin, L. Bopp, and J. Stefels (2004), Assessment of a global climatology of oceanic dimethylsulfide (DMS) concentrations based on SeaWiFS imagery (1998 – 2001), *Canadian, J. Fish. Aquat. Sci., 61*, 804-816.

Bianchi, A. A., D. R. Pino, H. G. I. Perlender, A. P. Osiroff, V. Segura, V. Lutz, M. L. Clara, C. F. Balestrini, and A. R. Piola (2009), Annual balance and seasonal variability of sea-air CO_2 fluxes in the Patagonia Sea: Their relationship with fronts and chlorophyll distribution, *J. Geophys. Res., 114,* C03018, doi:10.1029/2008JC004854.

Bracher, A., M. Vountas, T. Dinter, J. P. Burrows, R. Röttgers, and I. Peeken (2009), Quantitative observation of cyanobacteria and diatoms from space using PhytoDOAS on SCIAMACHY data, *Biogeosciences*, *6,* 751-764.

Brewin, R. J. W., S. J. Lavender, N. J. Hardman-Mountford, T. Hirata (2010), A spectral response approach for detecting dominant phytoplankton size class from satellite remote sensing, *Acta Oceanol. Sin., 29*, 14-32, doi:10.1007/s13131-010-0018-y.

Bricaud, A., C. Mejia, D. Blondeau-Patissier, H. Claustre, M. Crepon, and S. Thiria (2007), Retrieval of pigment concentrations and size structure of algal populations from their absorption spectra using multilayered perceptrons, *Appl. Opt., 46,* 1251-1260, doi:10.1364/AO.46.001251.

Bricaud, A., H. Claustre, J. Ras, and K. Oubelkheir (2004), Natural variability of phytoplankton absorption in oceanic waters: influence of the size structure of algal populations, *J. Geophys. Res., 109,* C11010, doi:10.1029/2004JC002419.

Carreto, J. I., N. Montoya, R. Akselman, M. O. Carignan, R. I. Silva, and A. D. Cucchi Colleoni (2008), Algal pigment patterns and phytoplankton assemblages in different water masses of the Río de la Plata maritime front, *Cont. Shelf Res., 28,* 1589-1606, doi:10.1016/j.csr.2007.02.012.

Carreto, J. I., N. G. Montoya, H. R. Benavides, R. Guerrero, and M. O. Carignan (2003), Characterization of spring phytoplankton communities in the Río de La Plata maritime front using pigment signatures and cell microscopy, *Mar. Biol., 143,* 1013–1027.

Carreto, J. I., V. A. Lutz, M. O. Carignan, A. D. Cucchi Coleoni, and S. G. De Marco (1995), Hydrography and chlorophyll a in a transect from the coast to the shelf break in the Argentinian Sea, *Cont. Shelf Res., 15,* 315–336, doi:10.1016/0278-4343(94)E0001-3.

Chazottes, A., M. Crepon, A. Bricaud, J. Ras, and S. Thiria (2007), Statistical analysis of absorption spectra of phytoplankton and of pigment concentrations observed during three POMME cruises using a neural network clustering method*, Appl. Opt., 46*, 3790-3799, doi:10.1364/AO.46.003790.

Chazottes, A., A. Bricaud, M. Crepon, and S. Thiria (2006), Statistical analysis of a data base of absorption spectra of phytoplankton and pigment concentrations using Self-Organizing Maps, *Appl. Opt., 45,* 8102-8115.

Ciotti, A.M., and A. Bricaud (2006), Retrievals of a size parameter for phytoplankton and spectral light absorption by Colored Detrital Matter from water-leaving radiances at SeaWiFS channels in a continental shelf region off Brazil, *Limnol. Oceanogr. Methods*, *4,* 237–253.

Ciotti, A. M., M. R. Lewis, and J. J. Cullen (2002), Assessment of the relationships between dominant cell size in natural phytoplankton communities and the spectral shape of the absorption coefficient, *Limnol. Oceanogr., 47,* 404-417.

Ciotti, A. M., J. J. Cullen, and M. R. Lewis, (1999), A semi-analytical model of the influence of phytoplankton community structure on the relationship between light attenuation and ocean color, *J. Geophys. Res., 104,* 1559-1578.

Claustre, H. et al. (1990), A biochemical investigation of a Phaeocystis sp. bloom in the Irish Sea, *J. Mar. Biol. Assoc. UK, 70,* 197-207.

Claustre, H. (1994), The trophic status of various oceanic provinces as revealed by phytoplankton pigment signatures, *Limnol. Oceanogr., 39*, 1206-1210.

Craig, S. E., S. E. Lohrenz, Z. Lee, K. L. Mahoney, G. J. Kirkpatrick, O. M. Schofield, and R. G. Steward (2006), Use of hyperspectral remote sensing reflectance for detection and assessment of the harmful alga, Karenia brevis, *Appl. Opt., 45,* 5414-5425.

de Souza, M. S., C. R. B. Mendes, V. M. T. Garcia, R. Pollery, and V. Brotas (2012), Phytoplankton community during a coccolithophorid bloom in the Patagonian Shelf: microscopic and HPLC pigment analyzes, *J. Mar. Biol. Assoc. UK, 92*, 13-27, doi:10.1017/S0025315411000439.

Devred, E., S. Sathyendranath, V. Stuart, and T. Platt, (2011), Absorption-derived phytoplankton cell size: application to satellite ocean-colour data in the Northwest Atlantic, *Remote Sens. Environ.,115,* 2255-2266.

DiTullio, G. R., N. Garcia, S. F. Riseman, and P. N. Sedwick (2007), Effects of iron concentration on pigment composition in *Phaeocystis antarctica* grown at low irradiance, *Biogeochemistry, 83,* 71-81.

Doney, S. C. (1999), Major challenges confronting marine biogeochemical modeling, *Global Biogeochem. Cy., 13,* 705-714.

Eisner, L. B., M. S. Twardowski, and T. J. Cowles (2003), Resolving phytoplankton photoprotective: photosynthetic carotenoid ratios on fine scales using in situ spectral absorption measurements, *Limnol. Oceanogr., 48,* 632–646.

Feldman, G. C., N. A. Kuring, C. Ng, W. Esaias, C. McClain, J. Elrod, N. Maynard, D. Endres, R. Evans, J. Brown, S. Walsh, M. Carle, and G. Podesta (1989), Ocean color: availability of the global data set, *Eos Trans. AGU, 70,* 634-641.

Ferreira, A., D. Stramski, C. A. E. Garcia, V. M. Tavano, A. M. Ciotti, and C. R. B. Mendes, Variability in light absorption and scattering of phytoplankton in Patagonian waters: Role of community size structure and pigment composition, *J. Geophy. Res.,* in press.

Ferreira, A., V. M. T. Garcia, and C. A. E. Garcia (2009), Light absorption by phytoplankton, non-algal particles and dissolved organic matter at the Patagonia shelf break in spring and summer, *Deep Sea Res. Part I, 56,* 2162-2174, doi:10.1016/ j.dsr.2009.08.002.

Garcia, C. A. E., V. M. T. Garcia, A. I. Dogliotti, A. Ferreira, S. I. Romero, A. Mannino, M. S. Souza, and M. M. Mata (2011), Environmental conditions and bio-optical

signature of a coccolithophorid bloom in the Patagonian shelf, *J. Geophys. Res.*, *116,* C03025, doi:10.1029/2010JC006595.
Garcia, V. M. T., C. A. E. Garcia, M. M. Mata, R. C. Pollery, A. R. Piola, S. R. Signorini, C. R. McClain, and M. D. Iglesias-Rodriguez (2008), Environmental factors controlling the phytoplankton blooms at the Patagonia shelf break in spring, *Deep Sea Res. Part I, 55*, 1150-1166, doi:10.1016/j.dsr.2008.04.011.
Garcia, C. A. E., Y. V. B. Sarma, M. M. Mata, and V. M. T. Garcia (2004), Chlorophyll variability and eddies in the Brazil-Malvinas Confluence region, *Deep Sea Res. Part II, 51*, 159– 172, doi:10.1016/j.dsr2.2003.07.016.
Gonçalves-Araújo, R., M. S. de Souza, C. R. B. Mendes, V. M. Tavano, R. C. Pollery, and C. A. E. Garcia (2012), Brazil-Malvinas confluence: effects of environmental variability on phytoplankton community structure, *J. Plankton Res., 34*, 399-416, doi:10.1093/plankt/fbs013.
Gregg, W. W., N. W. Casey, and C. R. McClain (2005), Recent trends in global ocean chlorophyll, *Geophys. Res. Lett.*, *32,* L03606, doi:10.1029/2004GL021808.
Hirata, J. A., J. Aiken, N. J. Hardman-Mountford, T. J. Smyth, and R. Barlow (2008), An absorption model to derive phytoplankton size classes from satellite ocean color, *Remote Sens. Environ., 112,* 3153–3159, doi:10.1016/j.rse.2008.03.011.
Hoepffner, N. and S. Sathyendranath (1993), Determination of the major groups of phytoplankton pigments from the absorption spectra of total particulate matter, *J. Geophys. Res., 98,* 22789–22803.
International Ocean Colour Coordinating Group (IOCCG) (2010), Atmospheric Correction for Remotely-Sensed Ocean-Colour Products, edited by M. Wang, *IOCCG Rep. 10*, Dartmouth, N. S., Canada.
International Ocean Colour Coordinating Group (IOCCG) (2006), Remote sensing of inherent optical properties: Fundamentals, tests of algorithms, and applications, edited by Z. P. Lee, *IOCCG Rep. 5*, Dartmouth, N. S., Canada.
Jeffrey, S. W., R. F. C. Mantoura, and S. W. Wright (1997), Phytoplankton Pigments in Oceanography, 661 pp., U.N. Educ., Sci., and Cult. Org., Paris.
Kirk, J. T. O. (1975), A theoretical analysis of the contribution of algal cells to the attenuation of light within waters, II, Spherical cells, *New Phytol., 75,* 21–36.
Kishino M, N. Takahashi, N. Okami, and S. Ichimura (1985), Estimation of the spectral absorption coefficients of phytoplankton in the sea, *Bull. Mar. Sci., 37*, 634–642.
Kostadinov, T. S., D. A. Siegel, and S. Maritorena (2009), Retrieval of the particle size distribution from satellite ocean color observations, *J. Geophys. Res., 114,* C09015, doi:10.1029/2009JC005303.
Le Quéré, C., et al. (2005), Ecosystem dynamics based on plankton functional types for global ocean biogeochemistry models, *Global Change Biol., 11,* 2016–2040, doi:10.1111/j.1365-2468.2005.01004.x.
Lee, Z. P., K. L. Carder, and R. A. Arnone (2002), Deriving inherent optical properties from water color: a multiband quasi-analytical algorithm for optically deep waters, *Appl. Opt*., *41,* 5755-5772, doi:10.1364/AO.41.005755.
Lohrenz, S. E., A. D. Weidemann, and M. Tuel (2003), Phytoplankton spectral absorption as influenced by community size structure and pigment composition, *J. Plankton Res., 25*, 35–61, doi:10.1093/plankt/25.1.35.
Lubac, B., H. Loisel, N. Guiselin, R. Astoreca, L. Felipe Artigas, and X. Mériaux (2008),

Hyperspectral and multispectral ocean color inversions to detect Phaeocystis globosa blooms in coastal waters, *J. Geophys. Res., 113,* C06026, doi:10.1029/2007JC004451.

Lutz, V. A., V. Segura, A. I. Dogliotti, D. A. Gagliardini, A. A. Bianchi, and C. F. Balestrini (2010), Primary Production in the Argentine Sea during Spring Estimated by Field and Satellite Models, *J. Plankton Res., 32,* 181-195, doi:10.1093/plankt/fbp117.

Lutz, V. A., S. Sathyendranath, E. J. H. Head, and W. K. W. Li (2003), Variability in pigment composition and optical characteristics of phytoplankton in the Labrador Sea and the Central North Atlantic, *Mar. Ecol. Prog. Ser., 260*, 1–18, doi:10.3354/meps260001.

Mackey, M. D., D. J. Mackey, H. W. Higgins, and S. W. Wright (1996), CHEMTAX – a program for estimating class abundances from chemical markers: application to HPLC measurements of phytoplankton, *Mar. Ecol. Prog. Ser., 144,* 265–283, doi:10.3354/meps144265.

Mao, Z., V. Stuart, D. Pan, J. Chen, F. Gong, H. Huang, and Q. Zhu (2010), Effects of phytoplankton species composition on absorption spectra and modeled hyperspectral reflectance, *Ecol. Inform., 5,* 359-366, doi:10.1016/j.ecoinf.2010.04.004.

Mendes, C. R., P. Cataxana, and V. Brotas (2007), HPLC determination of phytoplankton and microphytobenthos pigments: comparing resolution and sensitivity of a C-18 and a C-8 method*, Limnol. Oceanogr. Meth., 5,* 362-370, doi:10.4319/lom.2007.5.363.

Millie, D. F., O. M. Schofield, G. J. Kirkpatrick, G. Hohnsen, P. A. Tester, and B. T. Vinyard, (1997), Detection of harmful algal blooms using photopigments and absorption signatures: a case study of the Florida red tide dinoflagellate, Gymnodinium breve. Gymnodinium breve, *Limnol. Oceanogr., 42,* 1240-1251.

Mitchell, B. G., et al. (2000), Determination of spectral absorption coefficients of particles, dissolved material and phytoplankton for discrete water samples, in *Ocean Optics Protocols For Satellite Ocean Color Sensor Validation, Tech. Memo. 2000-209966*, pp. 125-153, NASA, Greenbelt, Md.

Moisan, J. R., T. A. H. Moisan, and M. A. Linkswiler (2011), An inverse modeling approach to estimating phytoplankton pigment concentrations from phytoplankton absorption spectra, *J. Geophys. Res., 116,* C09018, doi:10.1029/2010JC006786.

Morel, A., and A. Bricaud (1981), Theoretical results concerning light absorption in a discrete medium, and application to specific absorption of phytoplankton, *Deep Sea Res., 28,* 1375-1393, doi:10.1016/0198-0149(81)90039-X.

Morel, A., and L. Prieur (1977), Analysis of variations in ocean color, *Limnol. Oceanogr., 22,* 709-722.

Mouw, C.B., and J. A. Yoder (2010), Optical determination of phytoplankton size composition from global SeaWiFS imagery, *J. Geophys. Res., 115,* C12018. doi:10.1029/2010JC006337.

Nair, N., S. Sathyendranath, T. Platt, J. Morales, V. Stuart, M.-H. Forget, E. Devred, and H. Bouman (2008), Remote sensing of phytoplankton functional types, *Remote Sens. Environ.*, *112*, 3366–3375, doi:10.1016/j.rse.2008.01.021.

Platt, T., S. Sathyendranath, and V. Stuart (2006), Why study biological oceanography? *Aquabiology, 28,* 542−557.

Rivas, A. L., A. I. Dogliotti, and D. A. Gagliardini (2006), Seasonal variability in satellite measured surface chlorophyll in the Patagonian Shelf, *Cont. Shelf Res., 26,* 703- 720, doi:10.1016/j.csr.2006.01.013.

Romero, S. I., A. R. Piola, M. Charo, and C. A. E. Garcia (2006), Chlorophyll-a variability off Patagonia based on SeaWiFS data, *J. Geophys. Res., 111,* C05021, doi:10.1029/ 2005JC003244.

Rost, B., and U. Riebesell (2004), Coccolithophores and the biological pump: responses to environmental changes, in Coccolithophores: From Molecular Processes to Global Impact, edited by Thierstein, H.R. and J. R. Young, pp. 99–125, Springer, Berlin.

Rudorff, N. M., and M. Kampel (2011), Orbital remote sensing of phytoplankton functional types: a new review, *Int. J. Remote Sens., 33,* 1967-1990, doi:10.1080/01431161.2011.601343.

Sarthou, G., K. R. Timmermans, S. Blain, and P. Treguer, (2005), Growth physiology and fate of diatoms in the ocean: a review, *J. Sea Res., 53*, 25-42, doi:10.1016/j.seares.2004.01.007.

Sathyendranath, S., L. Watts, E. Devred, T. Platt, C. Caverhill, and H. Maass (2004), Discrimination of diatoms from other phytoplankton using ocean colour data, *Mar. Ecol. Prog. Ser.,* 272, 59–68, doi:10.3354/meps272059.

Sathyendranath, S., G. Cota, V. Stuart, H. Maas, and T. Platt (2001), Remote sensing of phytoplankton pigments: a comparison of empirical and theoretical approaches, *Int. J. Remote Sens., 22,* 249–273, doi:10.1080/014311601449925.

Sathyendranath, S., D. V. Subba Rao, Z. Chen, V. Stuart, T. Platt, G. L. Bugden, W. Jones, and P. Vass (1997), Aircraft remote sensing of toxic phytoplankton blooms: a case study from Cardigan River, Prince Edward Island, *Can. J. Remote Sens., 23,* 15-23.

Sathyendranath, S., and T. Platt (1989), Remote sensing of ocean chlorophyll: consequence of non-uniform pigment profile, *Appl. Opt., 28,* 490–495.

Schlüter L, F. Møhlenberg, H. Havskum, S. Larsen (2000), The use of phytoplankton pigments for identifying and quantifying phytoplankton groups in coastal areas: testing the influence of light and nutrients on pigment/chlorophyll a ratios, *Mar. Ecol. Prog. Ser., 192,* 49-63.

Signorini, S., V. M. T. Garcia, A. R. Piola, C. A. E. Garcia, M. M. Mata, and C. R. McClain (2006), Seasonal and interannual variability of calcite in the vicinity of the Patagonian Shelf Break (38°S–52°S), *Geophys. Res. Lett., 33,* L16610, doi:10.1029/2006GL026592.

Siegel, H., T. Ohde, M. Gerth, G. Lavik, and T. Leipe (2007), Identification of coccolithophore blooms in the SE Atlantic Ocean off Namibia by satellites and in situ methods, *Cont. Shelf Res., 27,* 258–274, doi:10.1016/j.csr.2006.10.003.

Sokal, R. R., and F. J. Rohlf (1962), The comparison of dendrograms by objective methods. *Taxonomy, 11*, 33–40.

Stæhr, P. A. and J. J. Cullen (2003), Detection of *Karenia mikimotoi* by spectral absorption signatures, *J. Plankton Res., 25,* 1237-1249, doi:10.1093/plankt/fbg083.

Stauber, J. L., and S. W. Jeffrey (1988), Photosynthetic pigments in fifty-one species of marine diatoms, *J. Phycol., 24,* 158–172.

Stuart, V., S. Sathyendranath, E. J. H. Head, T. Platt, B. Irwin, and H. Mass (2000), Bio-optical characteristics of diatom and prymnesiophyte populations in the

Labrador Sea, *Mar. Ecol. Prog. Ser., 201,* 91–106.
Stuart, V., S. Sathyendranath, T. Platt, H. Maass and B. D. Irwin (1998), Pigments and species composition of natural phytoplankton populations: effect on the absorption spectra, *J. Plankton Res., 20,* 187-217.
Subramaniam, A., E. J. Carpenter, and P. G. Falkowski (1999), Optical properties of the marine diazotrophic cyanobacteria Trichodesmium spp.; II - a reflectance model for remote-sensing, *Limnol. Oceanogr., 44,* 618–627.
Takahashi, T., S. Sutherland, C. Sweeney, A. Poisson, N. Metzl, B. Tilbrook, N. Bates, R. Wanninkhof, R. Feely, and C. Sabine (2002), Global sea-air CO2 flux based on climatological surface ocean pCO2 and seasonal biological and temperature effects, *Deep Sea Res. Part II, 49,* 1601–1622, doi:10.1016/S0967- 0645(02)00003-6.
Tassan, S., and G. M. Ferrari (1995), An alternative approach to absorption measurements of aquatic particles retained on filters, *Limnol. Oceanogr., 40,* 1358–1368.
Taylor, B. B., E. Torrecilla, A. Bernhardt, M. H. Taylor, I. Peeken, R. Röttgers, J. Piera, and A. Bracher (2011), Bio-optical provinces in the eastern Atlantic Ocean and their biogeographical relevance, *Biogeosciences, 8,* 3609-3629.
Torrecilla, E., D. Stramski, R. A. Reynolds, E. Millán-Núñez, and J. Piera (2011), Cluster analysis of hyperspectral optical data for discriminating phytoplankton pigment assemblages in the open ocean, *Remote Sens. Environ.*, *115,* 2578-2593, doi:10.1016/j.rse.2011.05.014.
Uitz, J., H. Claustre, A. Morel, and S. B. Hooker (2006), Vertical distribution of phytoplankton communities in open ocean: An assessment based on surface chlorophyll, *J. Geophys. Res., 111,* C08005, doi:10.1029/2005JC003207.
Vidussi, F., H. Claustre, B. B. Manca, A. Luchetta, and J. C. Marty (2001), Phytoplankton pigment distribution in relation to upper thermocline circulation in the eastern Mediterranean Sea during winter, *J. Geophys. Res., 106,* 19939–19956, doi: 10.1029/1999JC000308.
Westberry, T. K., G. Dall'Olmo, E. Boss, M. J. Behrenfeld, and T. Moutin (2010), Coherence of particulate beam attenuation and backscattering coefficients in diverse open ocean environments, *Opt. Express, 18*, 15419-15425, doi:10.1364/OE.18.015419.
Wright, S.W., and Jeffrey, S.W. (2006), Pigment markers for phytoplankton production, in Marine Organic Matter: Biomarkers, Isotopes and DNA, edited by J. K. Volkmann, pp. 71-104, Spring-Verlag, Berlin.
Yentsch, C. S., and D. A. Phinney, (1989), A bridge between ocean optics and microbial ecology., *Limnol. Oceanogr., 34,* 1694-1705.
Zapata, M., F. Rodríguez and J. L. Garrido (2000), Separation of chlorophylls and carotenoids from marine phytoplankton: a new HPLC method using a reversed phase C8 column and pyridine-containing mobile phases, *Mar. Ecol. Prog. Ser., 195,* 29-45.

Figure Captions

Figure 1. Locations of the 120 oceanographic stations where measurements and sample collections were taken during the PATEX cruises within the Patagonian shelf break and adjacent areas.

Figure 2. Results of cluster analysis applied to 10 ratios of diagnostic pigments of phytoplankton to the sum of the 10 diagnostic pigment concentrations (diag). Each bar represents a sample. The pannels illustrate the 4 clusters formed: (a) $C1_{diag}$; (b) $C2_{diag}$; (c) $C3_{diag}$; (d) $C4_{diag}$.

Figure 3. Results of cluster analysis applied to the relative contributions of taxomic groups of phytoplankton (%) estimated from the CHEMTAX method (CHEM). Each bar represents a sample. The pannels illustrate the 4 clusters formed: (a) $C1_{CHEM}$; (b) $C2_{CHEM}$; (c) $C3_{CHEM}$; (d) $C4_{CHEM}$.

Figure 4. Spectra of phytoplankton absorption coefficient normalized by the sum of absorption between 400 and 700 nm, $\int a_{ph}(\lambda)$, no unit. The spectra are showed according to (a) the clusters created on the basis of phytoplankton absorption spectra (aph), $C1_{aph}$ through $C3_{aph}$; (b) the clusters created on the basis of dataset of 10 diagnostic pigments (diag), $C1_{diag}$ through $C4_{diag}$; (c) the clusters created on the basis of dataset of the relative contributions of taxomic groups of phytoplankton estimated from the CHEMTAX method (CHEM), $C1_{CHEM}$ through $C4_{CHEM}$; (d) the 50% dominance criterion of the phytoplankton taxonomic composition.

Figure 5. The values of $\int a_{ph}(443)$, no unit, plotted as a function of the diatom contribution to total phytoplankton biomass (%) for all samples. Asterisks represent the samples with diatom contribution greater than 50%. Squares represent samples with haptophyte contribution greater than 50%. Stars represent the samples not dominated by diatoms or haptophytes. The data are shown according to the parameter S_f, which varies in a

continuum of cell sizes, as indicated by the gray scale. The solid lines delimit vertically the diatom contribution of 50% and horizontally the $\int a_{ph}(443)$ value of 0.0075 (see text in section 3.5), and divide the plot in 4 panels (I, II, III, and IV). The statistics for the linear regression on $\int a_{ph}(443)$ vs. diatom contribution are: R^2=0.70, p<0.0001, N=136.

Figure 6. The values of $\int a_{ph}(463)$, no unit, plotted as a function of the haptophyte contribution to total phytoplankton biomass, in percentage, for all samples. Asterisks represent the samples with diatom contribution greater than 50%. Squares represent the samples with haptophyte contribution greater than 50%. Stars represent the samples not dominated by diatoms or haptophytes. The data are shown according to the parameter S_f, which varies in a continuum of cell sizes, as indicated by the gray scale. The solid lines delimit vertically the haptophyte contribution of 50% and horizontally the $\int a_{ph}(463)$ value of 0.0079, and divide the plot in 4 panels (I, II, III, and IV). The dashed line delimits horizontally the $\int a_{ph}(463)$ value of 0.0082 (see text in section 3.5). The statistics for the linear regression on $\int a_{ph}(463)$ vs. haptophyte contribution are: R^2=0.69, p<0.0001, N=136.

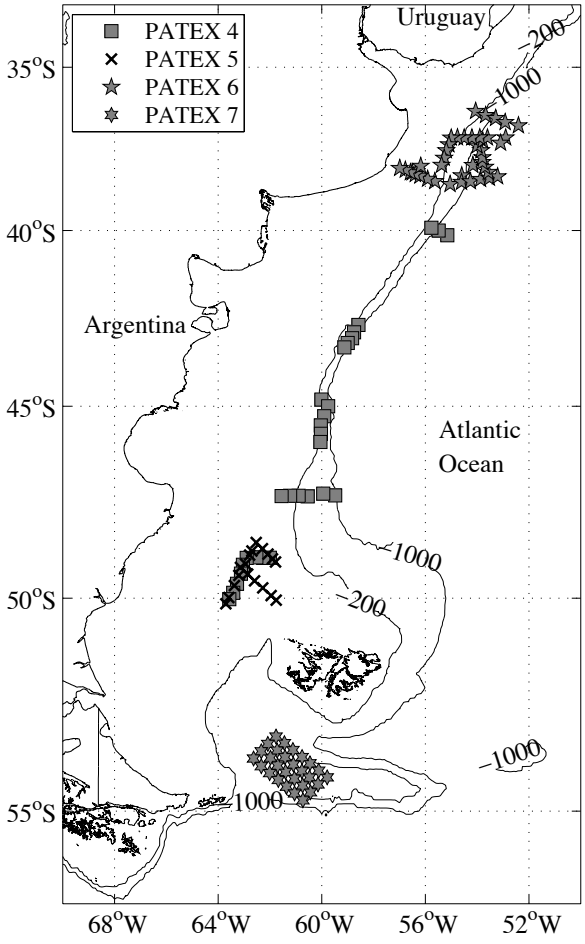

Figure 1. Locations of the 120 oceanographic stations where measurements and sample collections were taken during the PATEX cruises within the Patagonian shelf break and adjacent areas.

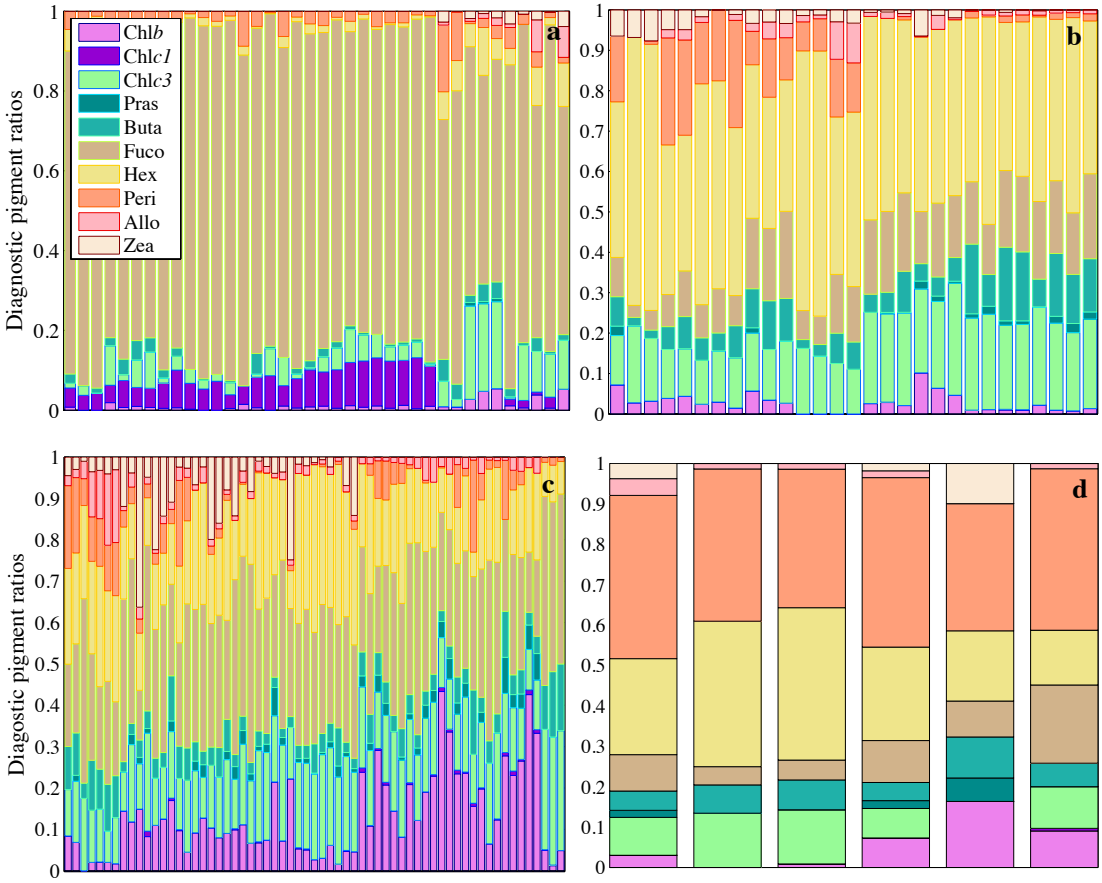

Figure 2. Results of cluster analysis applied to 10 ratios of diagnostic pigments of phytoplankton to the sum of the 10 diagnostic pigment concentrations (diag). Each bar represents a sample. The pannels illustrate the 4 clusters formed: (a) $C1_{diag}$; (b) $C2_{diag}$; (c) $C3_{diag}$; (d) $C4_{diag}$.

Figure 3. Results of cluster analysis applied to the relative contributions of taxomic groups of phytoplankton (%) estimated from the CHEMTAX method (CHEM). Each bar represents a sample. The pannels illustrate the 4 clusters formed: (a) $C1_{CHEM}$; (b) $C2_{CHEM}$; (c) $C3_{CHEM}$; (d) $C4_{CHEM}$.

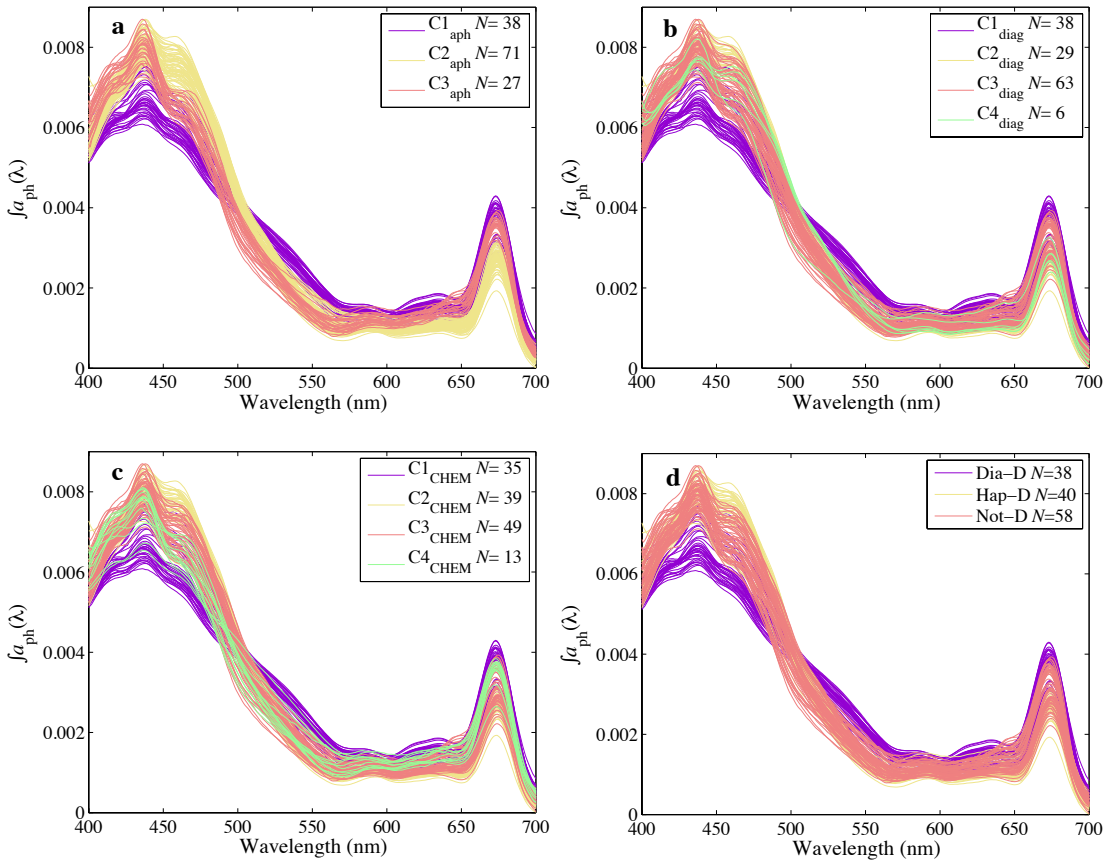

Figure 4. Spectra of phytoplankton absorption coefficient normalized by the sum of absorption between 400 and 700 nm, $\int a_{ph}(\lambda)$, no unit. The spectra are showed according to (a) the clusters created on the basis of phytoplankton absorption spectra (aph), $C1_{aph}$ through $C3_{aph}$; (b) the clusters created on the basis of dataset of 10 diagnostic pigments (diag), $C1_{diag}$ through $C4_{diag}$; (c) the clusters created on the basis of dataset of the relative contributions of taxomic groups of phytoplankton estimated from the CHEMTAX method (CHEM), $C1_{CHEM}$ through $C4_{CHEM}$; (d) the 50% dominance criterion of the phytoplankton taxonomic composition.

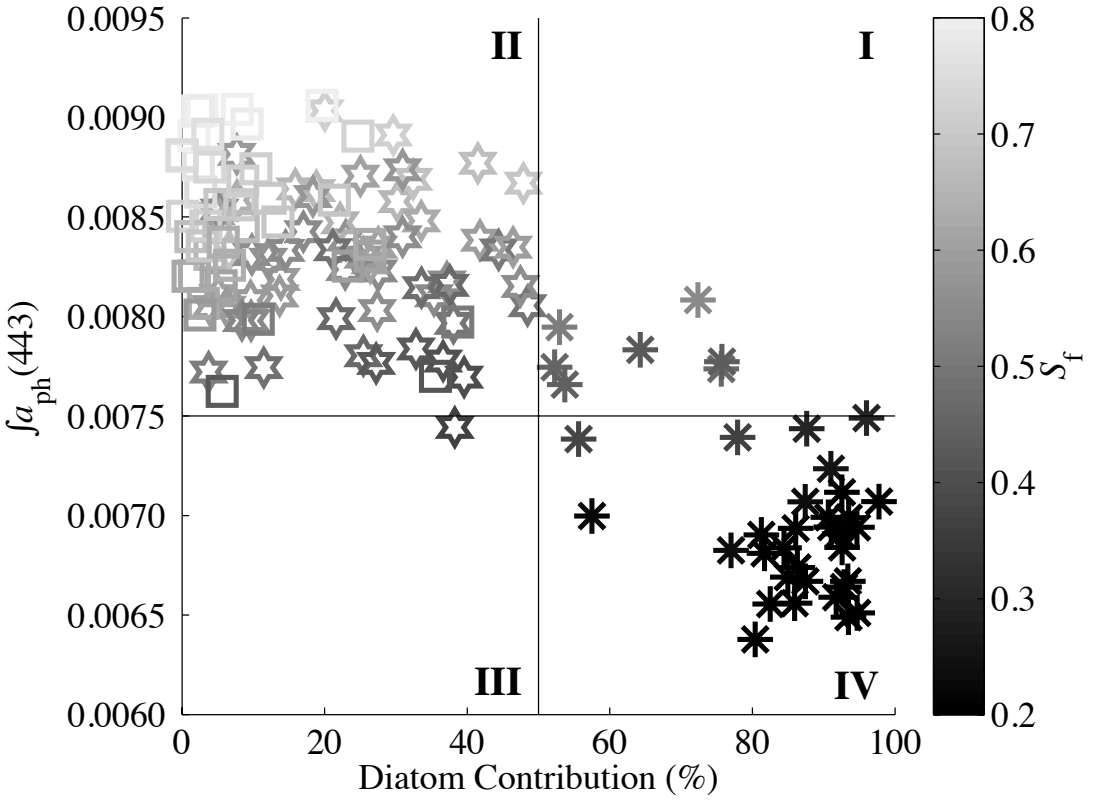

Figure 5. The values of $\int a_{ph}(443)$, no unit, plotted as a function of the diatom contribution to total phytoplankton biomass (%) for all samples. Asterisks represent the samples with diatom contribution greater than 50%. Squares represent samples with haptophyte contribution greater than 50%. Stars represent the samples not dominated by diatoms or haptophytes. The data are shown according to the parameter S_f, which varies in a continuum of cell sizes, as indicated by the gray scale. The solid lines delimit vertically the diatom contribution of 50% and horizontally the $\int a_{ph}(443)$ value of 0.0075 (see text in section 3.5), and divide the plot in 4 panels (I, II, III, and IV). The statistics for the linear regression on $\int a_{ph}(443)$ vs. diatom contribution are: R^2=0.70, p<0.0001, N=136.

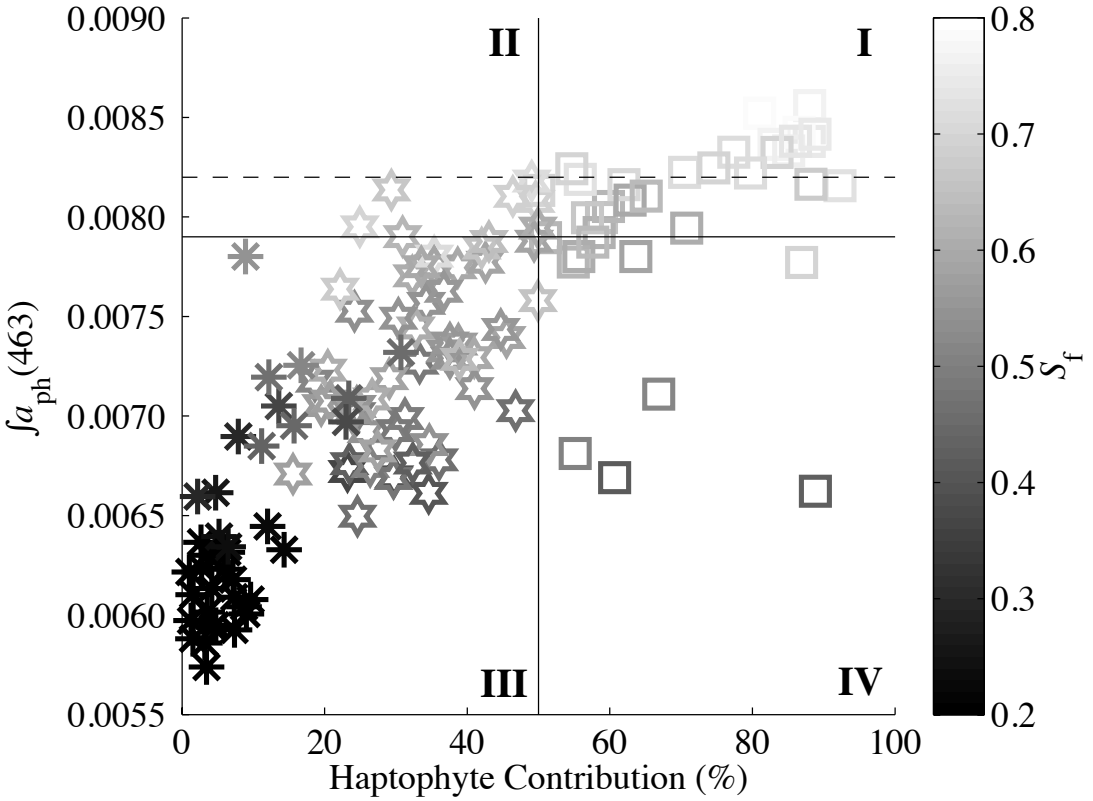

Figure 6. The values of $\int a_{ph}(463)$, no unit, plotted as a function of the haptophyte contribution to total phytoplankton biomass, in percentage, for all samples. Asterisks represent the samples with diatom contribution greater than 50%. Squares represent the samples with haptophyte contribution greater than 50%. Stars represent the samples not dominated by diatoms or haptophytes. The data are shown according to the parameter S_f, which varies in a continuum of cell sizes, as indicated by the gray scale. The solid lines delimit vertically the haptophyte contribution of 50% and horizontally the $\int a_{ph}(463)$ value of 0.0079, and divide the plot in 4 panels (I, II, III, and IV). The dashed line delimits horizontally the $\int a_{ph}(463)$ value of 0.0082 (see text in section 3.5). The statistics for the linear regression on $\int a_{ph}(463)$ vs. haptophyte contribution are: R^2=0.69, p<0.0001, N=136.